University of Liège

Laboratory of Neurophysiology and GIGA Neurosciences
Faculty of Medicine

Systems and Modeling Research Unit
Department of Electrical Engineering and Computer Science
Faculty of Applied Sciences

Regulation of Excitability, Pacemaking, and Bursting: Insights from Dopamine Neuron Electrophysiology

PhD Thesis by **Guillaume Drion** | January 2013

Supervised by Prof. Vincent Seutin
Prof. Rodolphe Sepulchre

Jury members:

Prof. Pierre Maquet	(President)	Professor, University of Liège
Prof. Rodolphe Sepulchre	(Advisor)	Professor, University of Liège
Prof. Vincent Seutin	(Advisor)	Professor, University of Liège
Dr. Jacqueline Scuvée-Moreau		Assistant Professor, University of Liège
Dr. Eric Bullinger		Francqui Assistant Professor, University of Liège
Dr. Dominique Engel		FNRS Research Associate, University of Liège
Dr. David Gall		Assistant Professor, Université Libre de Bruxelles
Dr. Boris Gutkin		Group Director, École Normale Supérieure, Paris

Abstract

The present thesis attempts to extract the dynamical mechanisms underlying neuronal excitability and its regulation, through the use of experimental and mathematical techniques. In particular, tools of dynamical system theory are used to extract physiologically relevant key players in the firing activity of various neuron types.

The main contribution of the thesis highlights the role of voltage-gated calcium-permeable channels in neuron excitability and firing patterns. Calcium channels are shown to induce a novel type of excitability that correlates to the electrophysiological properties of many neuron types, including midbrain dopamine-releasing cells, the neurons that initially motivated our study. In particular, calcium channels play a critical role in the generation and regulation of burst firing activity, a firing pattern that is important for the signaling of many cells.

The first part of the dissertation is dedicated to the mechanisms underlying dopaminergic (DA) neuron excitability (Part II). It identifies key players in the regulation of DA neuron firing patterns both *in vitro* and *in vivo*, including voltage-gated calcium channels and calcium-activated potassium channels. In particular, it shows that these channels are key regulators of DA neuron excitability.

The second part further investigates the dynamical phenomena extracted from dopaminergic neuron electrophysiology and generalizes these concepts to other neuronal populations (Part III). It incorporates the role of voltage-gated calcium channels in the current global picture of neuronal excitability proposed by FitzHugh in 1961. The inclusion of calcium channels in reduced models leads to a revised picture that uncovers two novel types of excitability, whose electrophysiological signatures are shared by many neuronal populations. This analysis is further extended to conductance-based models of arbitrary dimension, highlighting the impact of the balance between restorative and regenerative ion channels on neuron excitability. The regulation of this balance is shown to provide a physiologically plausible route to neuronal bursting.

The last part of the thesis illustrates a potential systemic consequence of the previous insights for Parkinson's disease (PD) (Part IV). It spotlights the systemic role of small conductance calcium-activated potassium channels in the regulation of many neuron types, many of these neurons being affected in PD.

Acknowlegments

My first words go to my "groovy" supervisors. Being part of their fruitful collaboration has been a priceless opportunity to develop my personal and professional skills, both from a mathematical and physiological viewpoint. They provided me a subtile mix of supervision and autonomy that I believe has been ideal for my scientific improvement. I heartily thanks Vincent for being so available, especially during the first part of my thesis. It has been a pleasure to share his passion for research, particularly during our journeys to SfN Annual Meetings. I also deeply acknowledge Rodolphe, whose shared enthusiasm has been essential for the accomplishment of this work. I admire his overwhelming open-mindedness, which has brought us to unexpected outcomes.

I secondly thank Pierre Sacré, with whom I really enjoyed sharing conversations and opinions on diverse subjects since the very beginning of my PhD. He is among those who played an important role during the course of this journey, both personally and professionally.

I also acknowledge Alessio Franci for the great time we had during the progress of this work. I enjoyed our energetic yet productive debates, as well as the amazing time spent in Toronto and New Orleans. "C'était génial!" I hope we will keep collaborating for many years.

My former and present colleagues at University of Liège are also greatly acknowledged. They established an ideal working environment, both at GIGA Neurosciences and Montefiore Institute. I also thank Prof. Peter Wellstead (Hamilton Institute, National University of Ireland, Maynooth, County Kildare, Ireland) and Dr. Mathieu Cloutier (GERAD and Ecole Polytechnique de Montreal, Montreal, QC, Canada) to have been involved in their project on the systems biology of Parkinson's disease.

I would also like to thank all members of the jury for devoting time and interest to the reading and evaluation of this manuscript, as well as all members of the thesis committee, who gave me important advices during the progress of this work.

I gratefully acknowledge the financial support from the Belgian Networks DYSCO (Dynamical Systems, Control, and Optimization, P7/19) and "Molecular and cellular mechanisms of electrical excitability" (P7/10), both funded by the Interuniversity Attraction Poles Program, initiated by the Belgian State, Science Policy Office. I also warmly thank the "Fonds Léon Fredericq" for their precious support.

I offer my regards to my family and friends. I express my greatest gratitude to my parents, who allowed me to evolve in an ideal environment and who are always present when I need them.

I finally dedicate this work to Elodie, whose mesmerizing liveliness thrills my everyday life.

Contents

Chapter 1

Introduction

This thesis combines experimental *in vitro* and *in vivo* recordings and mathematical reduction of conductance-based biophysical models to advance the systems electrophysiology of dopaminergic (DA) neurons. It highlights the role of specific ion channels - L-type calcium channels, small conductance calcium-activated (SK) potassium channels and KCNQ potassium channels - in excitability, pacemaking and burst firing activity of DA cells.

The critical role of calcium channels in DA neuron signaling is captured by reduced models that differ from the classical reductions of the Hodgkin-Huxley (HH) model in that they account for the specific regenerative nature of such channels in excitability and bursting. The newly proposed reduced models apply to arbitrary conductance-based models and address important and poorly understood issues such as the physiological route to bursting.

Current Challenges in DA Neuron Electrophysiology

Midbrain dopaminergic neurons are continuously active excitable cells that sustain important functions in everyday actions. Located at the basis of neuronal loops that involve numerous heterogenous populations, they act as real conductors of cellular rhythms that underly concrete behavioral properties. Notably, switches in their spiking activity correlate to switches in human behavior. For instance, a brief increase in excitability of substantia nigra pars compacta (SNc) DA neurons induces rhythmic changes in the basal ganglia loop, underlying the initiation of movement [97].

The complexity of DA neuron electrophysiology arises from this signaling property. These cells are indeed capable of switching between three different firing patterns: regular (pacemaker) firing, irregular single-spike firing, and bursting. Each firing pattern is governed by different ion channels and involves different mechanisms. Because of the diversity of involved ion channels, the challenge is to identify the key players in the different firing patterns.

The present thesis originated from a collaboration between the neurophysiology lab of the GIGA Neuroscience and the research unit in system and modeling at the University of Liege. Our master thesis investigated through a detailed computational model the role of a specific potassium channel on DA neuron signaling. The use of a state-of-the-art complex biophysical model of DA neurons (13 compartments accounting for soma and dendrites, more than 160 variables and thousands of parameters) allowed to make analyses and predictions that were successfully verified experimentally, extracting the selective influence of this ion channel on bursting activity (see Chapter 7).

We quickly faced the obstacle, however, of making qualitative predictions and extracting core mechanisms of firing patterns in a high-dimensional nonlinear model with many parameters. This motivated the development of reduced models to advance the understanding of DA neuron electrophysiology and, more generally, to propose new hypotheses on the generation of bursting patterns as the core contribution of this thesis.

The Importance of Reduced Modeling

Since the early days of neurophysiological modeling, reduced modeling has been essential to extract basic mechanisms underlying neuron firing. The need of reduced modeling is even stronger in modern conductance-based models of neurons that successfully reproduce neuronal firing and provide interesting hypotheses on the role of different ion channels, at the cost of including many different ion channels in the model. The resulting complexity, which rises with the complexity of the neuron under consideration, makes complex models impractical for qualitative mathematical analyses of the underlying firing mechanisms. This limitation was already clear in the very beginning of neurophysiological modeling, with the analysis of the first biophysical model of excitable membranes proposed by Alan Hodgkin and Andrew Huxley in 1952 [81], whose critical parameters were not easily extractable, even though the model was very basic.

The strategy of Richard FitzHugh in 1961 [50] was to reduce the complexity of the original Hodgkin-Huxley (HH) model via the aggregation of variables and the exploitation of timescale separations. Thanks to this reduction, the author proposed a simple two dimensional model which qualitatively reproduces the behavior of the original one. Its simplicity enabled the use of the tools of dynamical system theory in the analyses of action potential generation, such as phase portrait analyses, for instance, and he was able to extract critical conditions for neuronal spiking, such as strong timescale separation and bistability of the fast subsystem. Importantly, these qualitative features have been shown to be shared by almost all neurons regardless of their diversity, highlighting the power of this approach. To date, this reduced modeling strategy is widely used and has given rise to neurodynamics, a field of computational neuroscience focused on the understanding of the dynamical phenomena underlying neuronal excitability.

In the present dissertation, we mimic this reduced modeling strategy in order to extract the basic mechanisms of DA neuron signaling. Firstly, on the basis of the state-of-the-art complex model we used in our master thesis as well as experimental evidences, we develop a basic conductance-based model of DA neuron signaling endowed with the minimal set of ion channels that are critical to reproduce DA neuron firing patterns and the switches between them, while omitting the channels that solely affect quantitative properties (see Chapter 4). The resulting five dimensional model is used to extract the key players in the firing patterns of these cells both *in vitro* (Chapter 5) and *in vivo* as well as the switch between them (Chapter 6), using tools of dynamical system theory such as bifurcation analyses, among others. In addition, some of these phenomenological results are validated by the use of experimental protocols.

Secondly, we further reduce this conductance-based model to a two-dimensional model, following the original strategy of FitzHugh (Chapter 9). The proposed reduction is novel and differs from FitzHugh reduction of HH model. It is motivated by the observation that most of the dynamical mechanisms observed on the five dimensional DA neuron model are not captured by existing reduced models (Chapter 8). In particular, our analyses of DA neuron signaling highlight the prominent role of calcium channels in all firing patterns, both *in vitro* and *in vivo*, these calcium channels being absent from the original HH model and all reduced models that derive from it.

The reduction of the HH model augmented with calcium channels leads to a novel global picture of neuronal excitability that differs from the one originally proposed by FitzHugh. This novel picture is able to mechanistically explain the origin of the dynamical mechanisms extracted in the minimal conductance-based model of the DA neuron. In particular, it uncovers two novel types of excitability that differ from the three commonly described ones (see Chapter 10), and whose electrophysiological signatures are observed in a large amount of neurons, including DA cells. Specifically, most of these neurons are able to switch from a classical type of excitability towards a newly described one and conversely, through the dynamical regulation of particular ion channels, which we term "regenerative ion channels".

The Role of Regenerative Ion Channels in Neuronal Dynamics

In the two-dimensional models analyzed in Chapters 9 and 10, modeled neurons are able to switch between different excitability types via the regulation of one single parameter, reproducing switches of firing patterns observed physiologically. One illustration is the switch of firing observed in thalamocortical relay neurons during wakefulness and sleep, which can be reproduced in our proposed two-dimensional model through the change of a single parameter.

In order to shed light on the physiological meaning of this parameter, we extend our approach to conductance-based models of arbitrary dimensions. Generalizing the analyses of our two-dimensional models to high-dimensional conductance-based models leads to a simple mathematical condition that determines the type of excitability (see Chapter 11). This condition expresses a balance between ion channels that provide a slow negative feedback to membrane potential variations, called "restorative channels", and ion channels that provide a slow positive feedback to membrane potential variations, called "regenerative channels", regardless of their particular molecular nature.

The role of restorative ion channels has been widely investigated in neurodynamics to date. Their main representatives are voltage-gated potassium channels, a critical component of action potential generation. In general, restorative channels are merged in a single "recovery" variable in existing two dimensional models, and their dominance leads to one of the three commonly described excitability types, which we term "restorative excitability".

In contrast, the role of regenerative ion channels seems to have been disregarded to date in low-dimensional models, perhaps for historical reasons. Indeed, regenerative ion channels, whose main representative are voltage-gated calcium channels, are absent from the original HH model, and therefore from the Fitzhugh phase portrait. We show that these channels are the main generators of the newly described types of excitability, called "regen-

erative excitability". Namely, conductance-based models of arbitrary dimension are able to express these excitability types, provided that the role of regenerative ion channels is dominant at rest.

In addition, most of regenerative ion channels can be physiologically regulated, allowing a dynamical switch from restorative to regenerative excitability and conversely, as shown in Chapter 11. One simple example is the case of T-type calcium channels, which are regenerative channels that inactivate at low threshold. When these channels are present, the resting state of the neuron determines the amount of them which are activable, and thus indirectly determines neuron excitability type. For instance, an hyperpolarization of thalamic reticular and relay cell membrane generates a switch from restorative to regenerative excitability, strongly affecting cell response to external stimulations, as observed experimentally. In that sense, regenerative ion channels, and particularly voltage-gated calcium channels, are therefore key players in neuron excitability and firing pattern regulation.

Impact of Reduced Models on Experimental Electrophysiology

In the last part of the dissertation, we return to the original motivation of the thesis, that is, we investigate the physiological implication of the mathematical insights gained from reduced modeling. In particular, we analyze the physiological impact of a switch from restorative to regenerative excitability on neuronal firing.

We show that switching from restorative to regenerative excitability generates a switch from robust single-spike firing to robust burt firing both in two-dimensional models and in conductance-based models of arbitrary dimensions (Chapter 12). This switch is due to the appearance of a robust bistable zone in regenerative excitability, this bistable zone being fragile or even absent in restorative excitability. Knowing that excitability type is determined by the balance between restorative and regenerative ion channels, any regulation of this balance provides a potential physiological route to bursting. As an illustration, a deinactivation of T-type calcium channels by membrane hyperpolarization in thalamic reticular and relay neurons, which generates a switch from restorative to regenerative excitability, is responsible for the switch from single-spike firing to bursting in these cells. Similarly, an heterogeneity in DA neuron L-type calcium channel density is proposed to explain the heterogenous firing pattern that is observed *in vitro* when their SK channels are blocked.

In addition, we investigate whether such a simple mechanism can produce the great bursting diversity observed in neurons. We observe that the quality of bursting is given by the combination of two parameters, that is the balance weight and the adaptation gain, different couples of parameters generating different bursting types such as parabolic bursting, square-wave bursting or triangular bursting, even though the underlying mechanism is similar. This observation contrasts with the common view of neuronal bursting, where each bursting type is viewed as arising from a different underlying mechanism.

Taken together, these results show how reduced modeling can help experimental electrophysiology. Understanding the dynamical mechanisms underlying spiking behaviors allows the extraction of key players in the regulation of neuronal activities, which can apply to many different neuronal types regardless of their specificities. In the last part of the dissertation, we exploit this system viewpoint on neurodynamics to propose a potential origin for the selective neurodegeneration in Parkinson's disease (Chapter 13). We emphasize the systemic role of SK channels as main regulators of the adaptation gain of many neurons affected in the disease, which suggests that a global dysregulation of the channels might affect these neurons in a similar way. In particular, such dysregulation would increase neuron entrainability and burstiness, strongly affecting calcium homeostasis, a potential source of neurodegeneration.

Publications

The main results of the thesis can be found in the following publications (* highlights the equal contributors).

Drion G*, Bonjean M*, Waroux O*, Scuvée-Moreau J, Liégeois JF, Sejnowski J, Sepulchre R, Seutin V (2010) M-type channels selectively control bursting in rat dopaminergic neurons. Eur J Neurosci. 31:827-35.
(*This publication constitutes the core of Chapter 7*).

Drion G, Massotte L, Sepulchre R, Seutin V (2011) How modeling can reconcile apparently discrepant experimental results: The case of pacemaking in dopaminergic neurons. PLoS Comput. Biol. 7, e1002050.
(*This publication constitutes the core of Chapter 5*).

Drion G, Sepulchre R and Seutin V (2012) Mitochondrion- and endoplasmic reticulum-induced SK channel disregulation as a potential origin of the selective neurodegeneration in Parkinson's disease. The Systems Biology of Parkinson's Disease, Genetics and Systems Biology, Springer.
(*This publication is partly reproduced in Chapters 6 and 13*).

Drion G*, Franci A*, Seutin V and Sepulchre R (2012) A novel phase portrait for neuronal excitability. PLoS One. 7:e41806.
(*This publication constitutes the core of Chapter 9*).

Franci A*, Drion G* and Sepulchre R (2012) An organizing center in a planar model of neuronal excitability. SIAM J. Appl. Dyn. Syst., 11:16981722.
(*This publication is partly reproduced in Chapter 10*).

Franci A*, Drion G*, Seutin V and Sepulchre R (2013) The Balance between Competitive and Cooperative Ion Channels Determines Neuronal Excitability. PLoS Comput. Biol. Under Revision.
(*This publication constitutes the core of Chapter 11*).

Part I

Introduction to Experimental and Computational Electrophysiology

Introduction

The human body is composed of trillions of cells, the functional basic units of life. These units form distinct compartments, functionally isolated from each others and the extracellular medium by selectively permeable membranes. Small molecules such as oxygen, carbon dioxide and water can freely cross this membrane, while larger molecules and ions can enter/leave the cell only through specific "gates". The specific exchanges of large molecules and ions occurring through the membrane of a cell are closely correlated to its functions.

There exist about 210 distinct human cell types, each carrying out particular functions. However, despite this great variability, cells share many common structures, as sketched in Fig. I.I. Almost all animal cells are composed of two main components: the nucleus, a membrane bound structure that contains cell's hereditary information; surrounded by the cytoplasm, consisting of all of the intracellular elements. The latter is isolated from the extracellular space by the plasma membrane and contains organelles, specialized subunits that have specific functions and are usually enclosed within their own membrane.

The functions of the different organelles are highly conserved from cell to cell, and even from species to species. Some are specialized in protein manufacturing (rough endoplasmic reticulum, ribosomes), packaging and secretion (Golgi apparatus), others in cellular digestion (lysosomes) or cell morphology (cytoskeleton). Similarly, mitochondria are involved in cellular respiration in every eukaryotic cells and, together with the endoplasmic reticulum (ER), have an important role in intracellular calcium homeostasis. This highlights an important fact frequently observed in nature: *the great diversity and richness in biological architecture arises from the interconnection of simple basic structures.*

In the present study, we do not focus on particular organelles, these intracellular compartments being barely involved in the mechanisms under consideration. We better consider the cell as a compartment which tightly regulates the exchanges of substances between the intracellular and extracellular spaces. This regulation mechanism involves an important component of the cell: the plasma membrane.

The Plasma Membrane

The cell membrane, or plasma membrane, is a biological membrane that separates the cytoplasm from the extracellular medium. As mentioned above, it is selectively permeable to ions and large organic molecules and regulates the exchanges of substances between the intracellular and the extracellular spaces.

A scheme of the plasma membrane is given at the bottom of Fig. I.I. It is composed of a phospholipid bilayer, which is permeable to small molecules and water but almost fully impermeable to ions and large molecules, such as glucose. This part of the membrane can be seen as a passive element, through which the diffusion of small molecules occurs, following their concentration gradient. It is also the place of an osmotic flow for water, which emerges from a concentration gradient of non diffusible molecules across the membrane. This highlights the importance for a tight regulation of this concentration gradient, any disturbance in the balance resulting in a massive flow of water that might affect the integrity of the cell.

The flow of large molecules and ions, which do not diffuse through the phospholipid bilayer, is allowed by the presence of proteins embedded in the plasma membrane and crossing it from side to side (transmembrane proteins). These proteins act as gateways to regulate the transport of specific substances in and out of the cell. There exist many types of transmembrane proteins, selectively permeable to one or few particular substances and whose gating is regulated by various mechanisms. These proteins may assist in the movement of substances by facilitated diffusion or active transport. Among the great diversity in these transmembrane proteins, two families are particularly relevant in the context of this report: ion channels and active transporters.

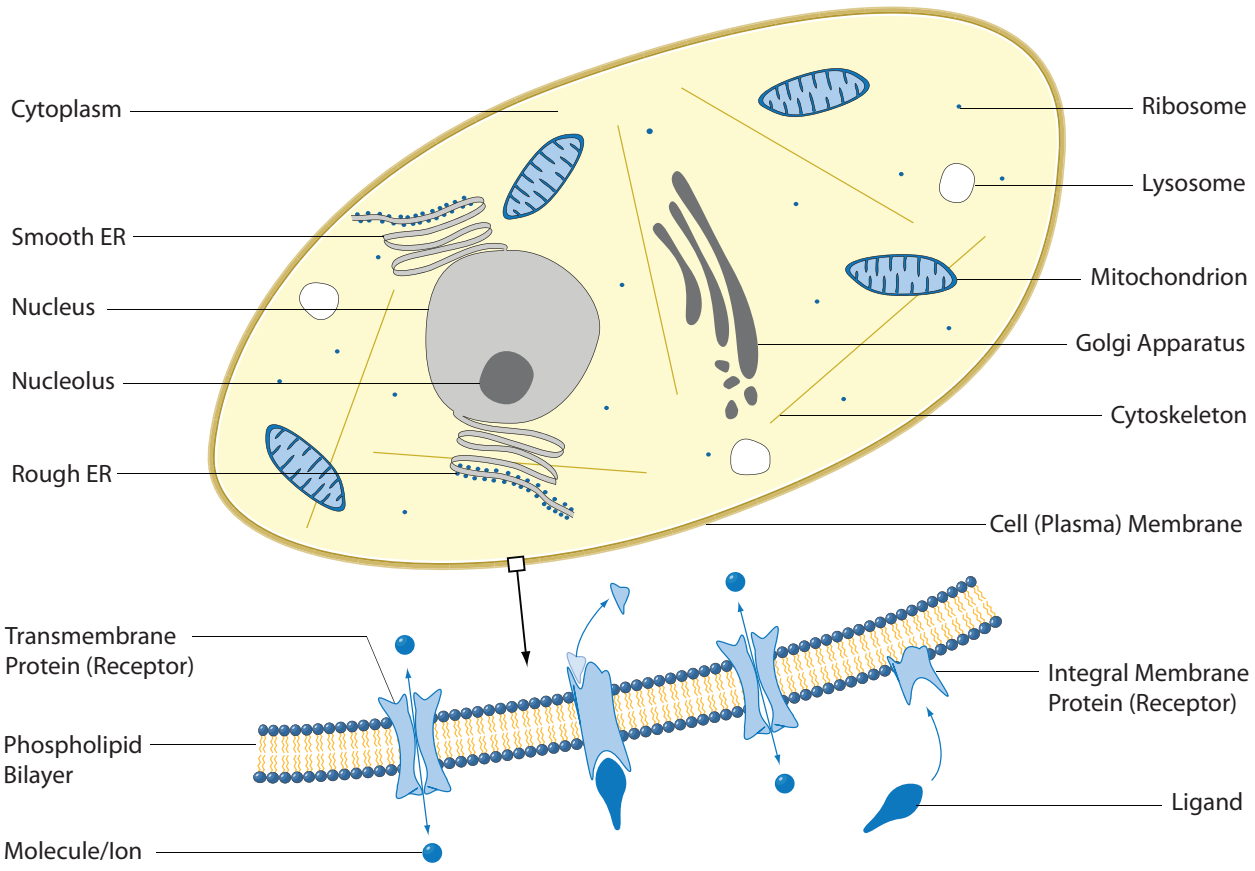

Figure I.1 – Besides diverse morphological, physiological and functional peculiarities, cells share many common structures. Roughly, cells are composed of a nucleus and a cytoplasm, which is delimited by the plasma membrane and contains many specialized organelles, such as mitochondria. The figure represents a typical eukaryotic (animal) cell. Please note that the list of components represented in the figure is not exhaustive. ER=endoplasmic reticulum.

Ion channels

Ion channels are macromolecular pore-forming proteins which allow the flow of specific ions through the plasma membrane, following their concentration gradient. They are generally highly selective to one particular ion that is strongly involved in cell signaling, such as sodium Na^+, potassium K^+, calcium Ca^{2+} and chloride ions Cl^-, and their gating is regulated by various mechanisms. Ion channels that are selective for Na^+ are named *sodium channels*, and similarly for other ions.

One has to realize the dual role of such channels in cell homeostasis. In addition to regulating the concentration of ions inside and outside the cell, they critically impact the charge repartition across the cell membrane, ions being charged molecules. This has an important role in cells that are highly involved in signaling, and more precisely in excitable cells, as extensively discussed below.

Active transporters

Active transporters allow the movement of a substance across the cell membrane against its concentration gradient, using chemical energy provided by adenosine triphosphate (ATP) for instance. They are critical to maintain unbalanced concentrations of substances inside and outside the cell, this concentration gradient being involved in many cellular functions.

An essential active transporter in human cells is the $Na^+/K^+ATPase$, also called the sodium pump. This transporter, which pumps K^+ inside and Na^+ outside, is responsible for cells containing relatively high concentrations of K^+ but low concentrations of Na^+. This is of critical importance in many cellular behaviors, such as transport or control of cell volume. It consumes up to 85% of produced ATP in the kidney and the nervous system, where Na^+ and K^+ concentration gradients are essential for cell function.

Note that the plasma membrane also contains other types of proteins, such as integral membrane proteins, which are embedded to the cell surface, as well as many other molecules such as carbohydrates, glycoproteins, or glycolipids. These molecules play many different roles in cell signaling. In addition, the activity/gating of many proteins is regulated through the action of external molecules, called ligands, acting as authentic receptors of specific external stimuli. Finally, the quantitative repartition of these proteins is not static but dynamic. Namely, the viscosity of the lipid bilayer confers an important fluidity to the plasma membrane, and molecules such as transmembrane proteins are dynamically added to and removed from the membrane.

These facts highlight the importance of the plasma membrane in cell integrity and communication with the external environment. In several categories of cells, such as excitable cells, this membrane is even the key player in the achievement of their function.

Excitable Cells

To ensure an harmonious management of the whole organism, each cell is devoted to a particular function. For instance, many cells form tissues that line the cavities and surfaces of structures throughout the body, for which they are designed to maintain robust and impermeable cohesions. Other cell types are devoted to the signalization between cells, and between the organism and the environment, and regulate the responses to stimuli. This is for instance the case of hormone releasing cells, such as pancreatic β-cells, which respond quickly to spikes in blood glucose by releasing insulin. Another example are myocytes, or muscle cells, in which external stimuli induce contraction.

Cells that are actively involved in information processing share a common property: they are *excitable*. Namely, they can be stimulated by external electrical or chemical stimuli to create an electric current, through a dynamical regulation of ion flow across their membrane. These responses can be very different from cells to cells, and even in the same cell depending on environmental conditions. The present thesis focuses on the mechanisms underlying these responses in highly excitable cells composing the nervous system: the neurons.

Neurons

Neurons are excitable cells that constitute the functional units of the nervous system. They receive, integrate and transmit informations that come from the organism or the environment and organize the responses to these stimuli.

The different types of neurons can be very different from one to the others and sustain very particular functions, as illustrated in Fig. I.II. However, almost all neurons share a common typical structure (Fig. I.III). Typical neurons possess a cell body, usually called soma, from which emerge a variable number of thin extensions, called dendrites. These dendrites often extend for hundreds of micrometers and branch multiple times, giving rise to what is called a "dendritic tree". In addition, neurons possess a single axon, specialized structure that arises from the soma or a primary dendrite and makes synapses with a set of distant neurons, up to 1 meter far from the soma in humans.

Typically, informations coming to the neuron are collected by the dendrites and integrated in the soma. An electrical signal, called *action potential* or *spike*, is thus

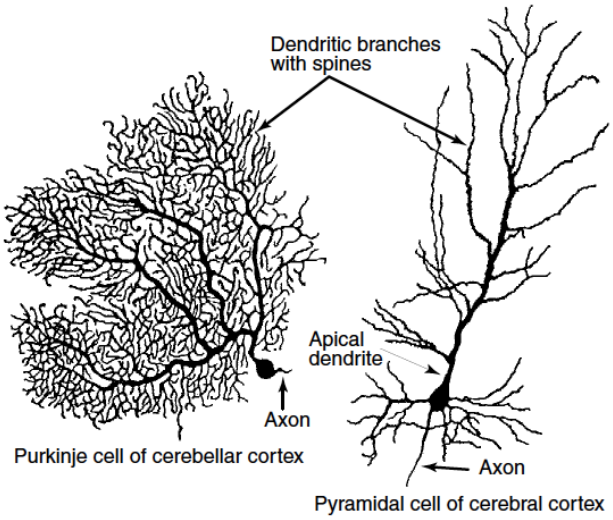

Figure I.II – Neurons have various sizes and shapes. The figure compares a Purkinje cell of the cerebellar cortex (left) to a pyramidal cell of the cerebral cortex (right). Neurons are highly polarized cells. Taken from [21].

generated in the axon initial segment (AIS), then propagated along the axon and back-propagated to the dendrites (the neuron is said to fire). When this electrical signal arrives at the synapses, it is directly transmitted to the target neurons (electrical synapses), or, more generally, it induces the release of a chemical compound called *neurotransmitter*, which is transmitted to the target neuron (chemical synapses, Fig. I.IV).

A chemical synapse is composed of a presynaptic terminal, which ends the axon of the transmitting (afferent) neuron, and a postsynaptic terminal, which arises from a dendrite of the receiving (efferent) neuron (Fig. I.IV). These two terminals are separated by the synaptic cleft. After their release by the afferent neuron, neurotransmitters diffuse into the synaptic cleft and eventually bind to receptors present at the surface of the postsynaptic terminal, which generates an electrical signal in the efferent neuron. In addition, some of the released neurotransmitters are recaptured by the afferent neuron itself, through the action of specific transporters located at the surface of the presynaptic terminal. Non-neuronal brain cells, called astrocytes, can also help in the regulation of neurotransmitter concentration and diffusion in the synaptic cleft.

There exist many different types of neurotransmitters, some of the most known being noradrenaline (NA, or norepinephrine), acetylcholine (ACh), serotonin (5-HT), dopamine (DA),glutamate (Glu) and GABA. A neuron that release dopamine is called "dopaminergic", an "adrenergic" neuron releases adrenaline, and so on.

Each neurotransmitter acts as a ligand to specific

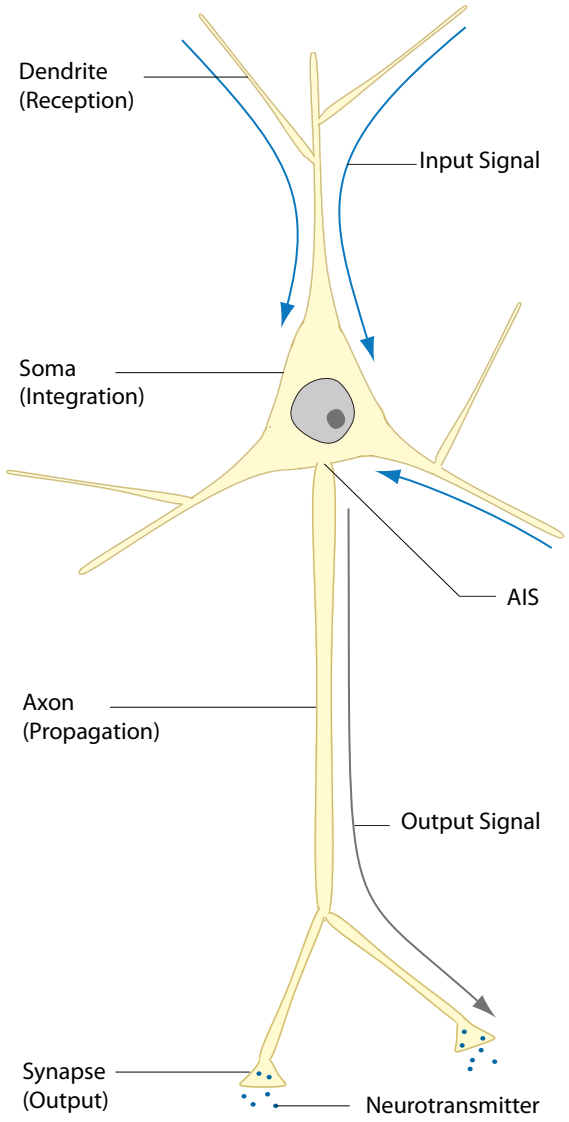

Figure I.III – Typical structure of a neuron. A typical neuron is composed of a cell body, called soma, from which emerge dendrites and an axon. The dendrites make connections with afferent neurons, where they receive external stimulations. These informations are integrated in the soma and the resulting signal is transmitted through the axon, which makes synapses with the dendrites/soma of efferent neurons.

receptors, and has different effects on target cells, depending on the type of receptor it activates. As an illustration, dopamine has an overall inhibitory effect while stimulating D2 receptors, and an excitatory effect while stimulating D1 receptors. In addition, for each kind of receptor, the response to a neurotransmitter depends on its concentration in the synaptic cleft, the receptor having a particular *affinity* for this neurotransmitter (for a given neurotransmitter concentration, the higher the

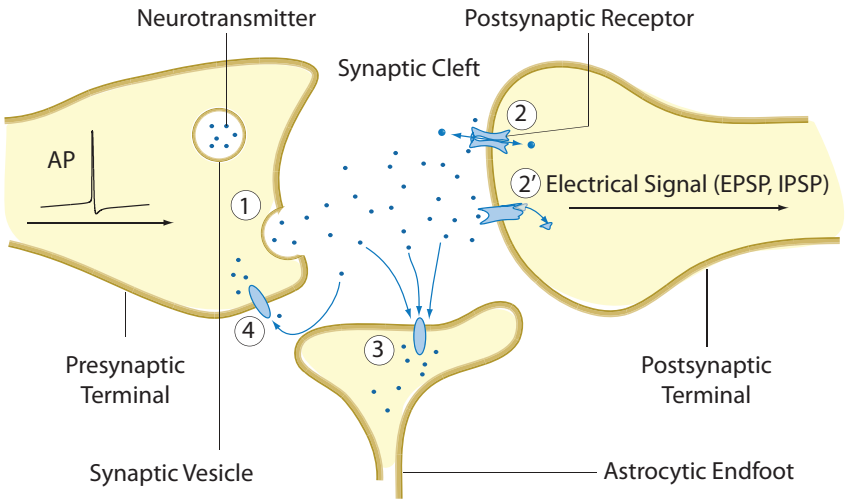

Figure I.IV – Typical structure and function of a chemical synapse. The synapse is composed of a presynaptic terminal arising from the afferent neuron and a postsynaptic terminal arising from the efferent neuron, both separated by the synaptic cleft. The occurrence of an action potential (AP) induces the release of neurotransmitters in the synaptic cleft (1). These neurotransmitters bind to postsynaptic receptors (2 and 2'), inducing an electrical signal in the efferent neuron, either excitatory (excitatory postsynaptic potential, EPSP) or inhibitory (inhibitory postsynaptic potential, IPSP). Some neurotransmitters are recaptured by astrocytes (3) or by the presynaptic neuron itself (4).

affinity, the stronger the response). As a consequence, although a single neuron solely releases one type of neurotransmitter, it can transmit a rich amount of specific informations through chemical synapses. Namely, various firing dynamics induce various neurotransmitter diffusion dynamics, and result in various postsynaptic receptor activations. The information is thus mainly coded by the way action potentials are generated in the soma, which is called the *firing pattern*. Note that some neurons can also release several types of neurotransmitters, further enriching their signaling possibilities.

The present thesis focuses on the mechanisms underlying the generation of different firing patterns in neurons. As a starting point, the following chapters summarize the state of the art in single-cell neurodynamics, the study of rhythmic neural activity from a mathematical framework (Chapter 2), and give an overview of available experimental techniques in the field (Chapter 3). In particular, an effort is made to connect mathematical analyses with physiological observations, this connection being a guiding thread of the present work.

Chapter 2

Elements of Single-Cell Electrophysiology

In the early fifties, Alan Lloyd Hodgkin and Andrew Fielding Huxley made an invaluable advance in physiology: they proposed a biophysical model that explains the ionic mechanisms underlying the initiation and propagation of action potentials in a nerve cell (the squid giant axon) [81]. This work, for which they shared the 1963 Nobel Prize in Physiology or Medicine, was remarkable from several points of view.

Firstly, their experimental technique was a real trapeze act. They manually recorded the membrane potential of a five hundred micrometers tick axon using an intracellular electrode (Fig. 2.1, left), performing a technique called *voltage clamp*, which is still widely used to date.

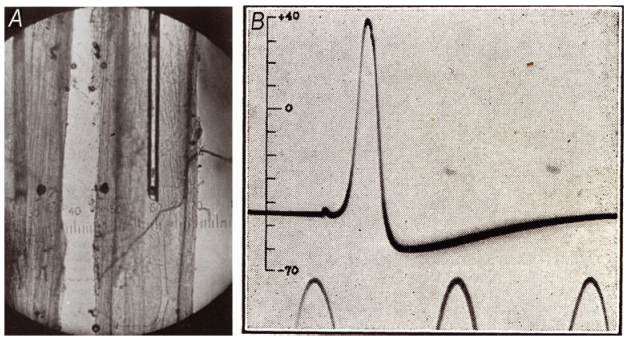

Figure 2.1 – Intracellular recording of the squid giant axon action potential. A Picture a squid giant axon with the intracellular electrode inside. Image taken from Hodgkin and Huxley (1945). **B** Intracellular recording of an action potential.

Secondly, they were the first to quantitatively record an action potential (Fig. 2.1, right), and to show the involvement of sodium ions in its regenerative upstroke. In addition, they uncovered the role of voltage gated ion channels in the initiation and propagation of spikes, and made a quantitative analysis of their kinetics, using simple experimental artifices.

Finally, they completed their study by a mathematical modeling of action potential generation. Fitting equations to their experimental data, they developed a model of the squid giant axon excitable membrane which was able to reproduce its excitability behavior. This model, known as the Hodgkin-Huxley (HH) model, is the basis of modern single-cell electrophysiology and is still widely used to date. Note that simulating this model in the fifties was a serious labor, and it took three weeks to Huxley to complete the simulation of the propagated action potential.

This pioneering work gave rise to modern electrophysiology. From an experimental point of view, state-of-the-art electrophysiological techniques such as intracellular recordings and patch-clamp can be seen as extensions of the technique developed by Hodgkin and Huxley. In addition, their mathematical modeling strategy is still predominant today. On the one hand, the exact same modeling principles are used to generate high-dimensional quantitative models of specific neurons, these models being used to predict effects of pharmacological compounds on cellular behavior, for instance. On the other hand, dynamical analyses of the HH model, initiated by the work of Richard FitzHugh in 1961 [50], permit to uncover the mechanisms underlying neuronal excitability, giving rise to what is now called neurodynamics.

The present chapter contains a summary of these important concepts, in order to make this thesis self-contained. More complete descriptions are available in many textbooks focused on neurodynamics [21, 46, 89, 101].

The Membrane Model

Signaling of excitable cells relies on the movement of unequally distributed charges across the plasma membrane. These charges are carried by ions, each ion being asymmetrically distributed in the intracellular and the extracellular spaces. As an illustration, Fig. 2.2 shows the relative concentrations of important ions across the plasma membrane of mammalian excitable cells. These asymmetric concentrations are generated by active trans-

porters, or pumps, which use cellular energy to move specific ions against their concentration gradient. Among others, the $Na^+K^+ATPase$ is responsible for cells containing relatively high concentrations of K^+ but low concentrations of Na^+, as mentioned above.

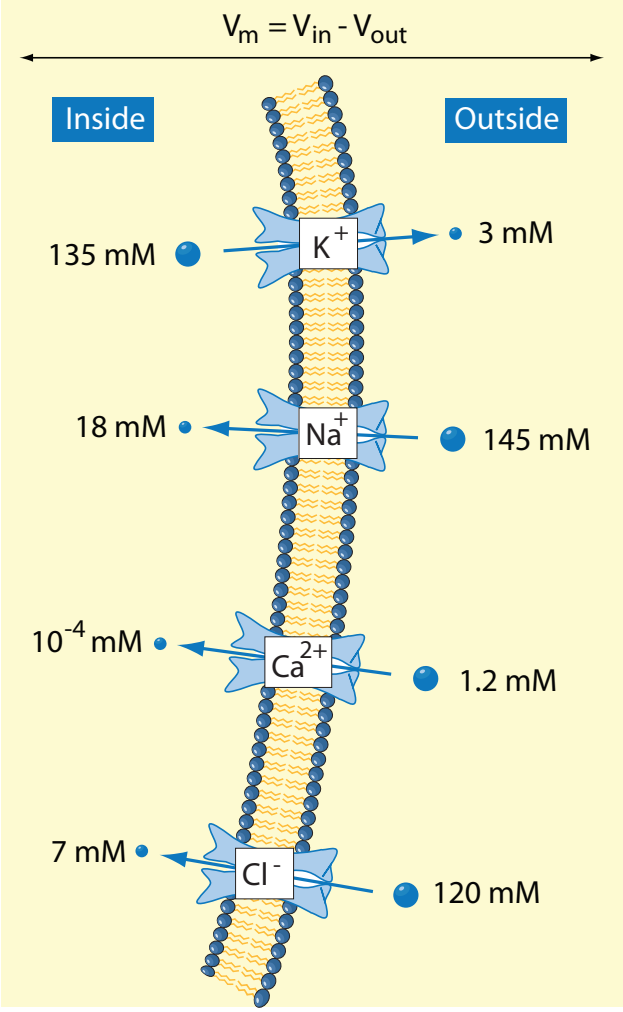

Figure 2.2 – Ions have a differential concentration across the membrane of a neuron. Neuron membrane possesses several ion channels that are selectively permeable to one or several ions. The four main ones involved in cell signaling are sodium Na^+, potassium K^+, calcium Ca^{2+} and chloride Cl^- ions (the concentrations shown in the figure are typical for a mammalian neuron). These concentration gradients are responsible for a voltage gradient across the membrane, giving rise to a membrane potential V_m.

The flow of ions following their concentration gradient, or passive diffusion, is finely regulated by the particular structure of the plasma membrane: ions can only cross the membrane through highly selective ion channels, the other channels and the phospholipid bilayer being impermeable to them. The permeability of the membrane to a specific ion is therefore a dynamical variable which is defined by the density of ion channels selective to this ion as well as their opening state.

The distribution of ions across the cell membrane and the permeability of the membrane to these ions result in an electrical potential gradient across the membrane, called the *membrane potential* (V_m). Typical values of resting membrane potentials are around -70 mV in neurons, but it can rise up to 40 mV during action potential upstroke. These membrane potential fluctuations are the basis of excitable cell signaling.

Concentration and voltage gradients both play a role in ion diffusion through ion channels

Ion channel opening leads to the flow of specific ions through the plasma membrane, following their concentration gradient. However, ions are charge molecules, and their asymmetric distribution generates a voltage gradient across the membrane, which also impacts ion diffusion. The diffusion therefore occurs until the chemical and electrical driving forces are exactly balanced, i.e. when the *electrochemical equilibrium* is reached.

Away from the equilibrium, the system possesses a non-zero Gibbs free energy, which is due to the electrochemical gradient

$$\Delta G = -RT \ln \frac{[ion]_{out}}{[ion]_{in}} + \Delta V z F \tag{2.1}$$

where R and F are the gas constant and the Faraday's constant, respectively, T is the temperature in Kelvin, and z the valence of the considered ion ($z = 1$ for Na^+ and K^+, $z = 2$ for Ca^{2+} and $z = -1$ for Cl^-). By convention, a negative free energy allows a spontaneous diffusion from the extracellular to the intracellular spaces, and conversely.

The first part of Eq. 2.1 represents the free energy brought by the concentration gradient ΔG_{conc}: when the extracellular concentration $[ion]_{out}$ is larger than the intracellular concentration $[ion]_{in}$, ΔG_{conc} is negative and ions diffuse into the cell. Similarly, the second part of the equation represents the free energy brought by the voltage gradient ΔG_{volt}: when the membrane potential ΔV is negative, there are more positive charges in the extracellular space, and positively (resp. negative) charged ions diffuse into (resp. outside) of the cell. Indeed, for positively charged ions, z is positive, and ΔG_{volt} has the sign of ΔV.

At the electrochemical equilibrium, the Gibbs free energy is zero by definition, and the chemical and voltage driving forces are exactly balanced

$$\Delta V z F = RT \ln \frac{[ion]_{out}}{[ion]_{in}} \tag{2.2}$$

which gives

$$\Delta V = V_{Nernst} = V_{ion} = \frac{RT}{zF} \ln \frac{[ion]_{out}}{[ion]_{in}} \quad (2.3)$$

The potential V_{Nernst} defined in Eq. 2.3 is the membrane potential at which the voltage driving force exactly balance the chemical driving force brought by the asymmetric distribution of the considered ion. This potential is usually called the *Nernst potential*, or the *reversal potential*. It is specific for each particular ion.

Based on the concentration values given in Fig. 2.2, we can compute the typical reversal potentials of Na^+, K^+, Ca^{2+} and Cl^-, which gives $V_{Na} = 56$ mV, $V_K = -102$ mV, $V_{Ca} = 125$ mV and $V_{Cl} = -76$ mV, respectively.

Ionic currents can either depolarize or hyperpolarize the membrane

At rest, the plasma membrane of an excitable cell has a low and stable permeability to the different ions which, together with the stable asymmetric distribution of these ions across the membrane, generates a stable resting membrane potential. This resting potential is always negative, and typically range from -50 mV to -100 mV in neurons. In the case of monovalent ions ($z = 1$) such as Na^+ and K^+, this resting potential is defined by the Goldman-Hodgkin-Katz (GHK) equation

$$V_m = \frac{RT}{F} \ln \left(\frac{P_{Na^+}[Na^+]_{out} + P_{K^+}[K^+]_{out}}{P_{Na^+}[Na^+]_{in} + P_{K^+}[K^+]_{in}} \right) \quad (2.4)$$

which is a generalization of the Nernst equation 2.3. Indeed, if we consider a plasma membrane only permeable to potassium ions ($P_{Na^+} = 0$ in Eq. 2.4), the GHK equation becomes

$$V_m = \frac{RT}{F} \ln \left(\frac{[K^+]_{out}}{[K^+]_{in}} \right) \quad (2.5)$$

which is equivalent to the Nernst equation that defines the reversal potential of potassium ions.

This result shows that the resting potential V_m of an excitable cell whose plasma membrane is solely permeable to K^+ is equal to the K^+ reversal potential V_K, which is very negative. In that configuration, the cell is said to be *hyperpolarized*. Similarly, if the plasma membrane is solely permeable to Na^+, we have $V_m = V_{Na}$, V_{Na} being very positive, and the cell is said to be *depolarized*.

This phenomenon in illustrated in Fig. 2.3, which shows the evolution of the membrane potential with variations of K^+ and Na^+ permeabilities as predicted by the GHK equation. At resting state, the plasma membrane is slightly permeable to both K^+ and Na^+, and the resting state is somewhere between both reversal potentials V_K and V_{Na} (the permeability to K^+ being larger than to Na^+, the resting potential is hyperpolarized). As K^+ plasma membrane permeability increases, the resting potential tends to approach the K^+ reversal potential. This phenomenon, which generally relies on potassium channel opening, generates a hyperpolarization of the membrane. On the other hand, an increase in Na^+ permeability depolarizes the cell, following the same mechanism.

In summary, any modification of plasma membrane permeability to ions significantly affects the membrane potential of the cell, some ions hyperpolarizing the cell, other depolarizing it. In excitable cells, this permeability is dynamically regulated, which is at the origin of action potential generation and cell signaling.

The Mechanisms of Action Potential Generation

The plasma membrane can be modeled as an electrical circuit

The particular structure of excitable cell plasma membrane makes it particularly suitable for mathematical modeling. Indeed, it can be easily assimilated to a classical electrical circuit, as illustrated in Fig. 2.4.

Each ion channel lets ions flow through the membrane, following their concentration gradient, until the membrane potential V_m reaches the ion reversal potential V_{ion}. These ion channels can therefore be assimilated as resistors, whose conductance g_{ion} is dynamically regulated as the channels regulate their opening state. The flow of ion therefore define an ionic current I_{ion}, which, following the Ohm's law, depends on the conductivity of the channel g_{ion} and the difference between the membrane potential and ion reversal potential:

$$I_{ion} = g_{ion}(V_m - V_{ion}). \quad (2.6)$$

The term $(V_m - V_{ion})$ accounts for the fact that, the smaller the difference between the membrane potential and ion reversal potential, the weaker the electrochemical force (2.1), and thus the smaller the ionic current. Ion channels generate an ionic current that tends to approach the membrane potential to their specific reversal potential, as predicted by the GHK equation (2.4). By convention, an inward (resp. outward) current has negative (resp. positive) sign.

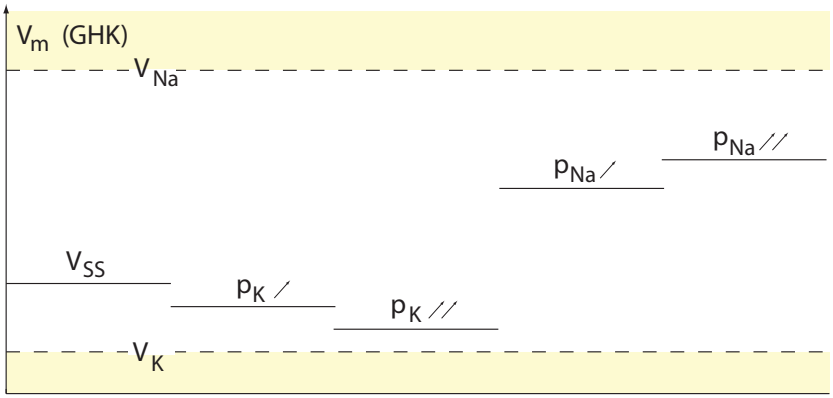

Figure 2.3 – Variations of K^+ and Na^+ plasma membrane permeabilities oppositely affect neuron membrane potential. Values are computed from the Goldman-Hodgkin-Katz (GHK) equation, considering K^+ and $Na+$ ions only. Ion concentrations are as in Fig. 2.2. An increase in K^+ permeability induces an hyperpolarization of the cell (V_m decreases), whereas an increase in Na^+ permeability depolarizes the cell (V_m increases). Note that the membrane potential is always contained in the range $V_K \leq V_m \leq V_{Na}$.

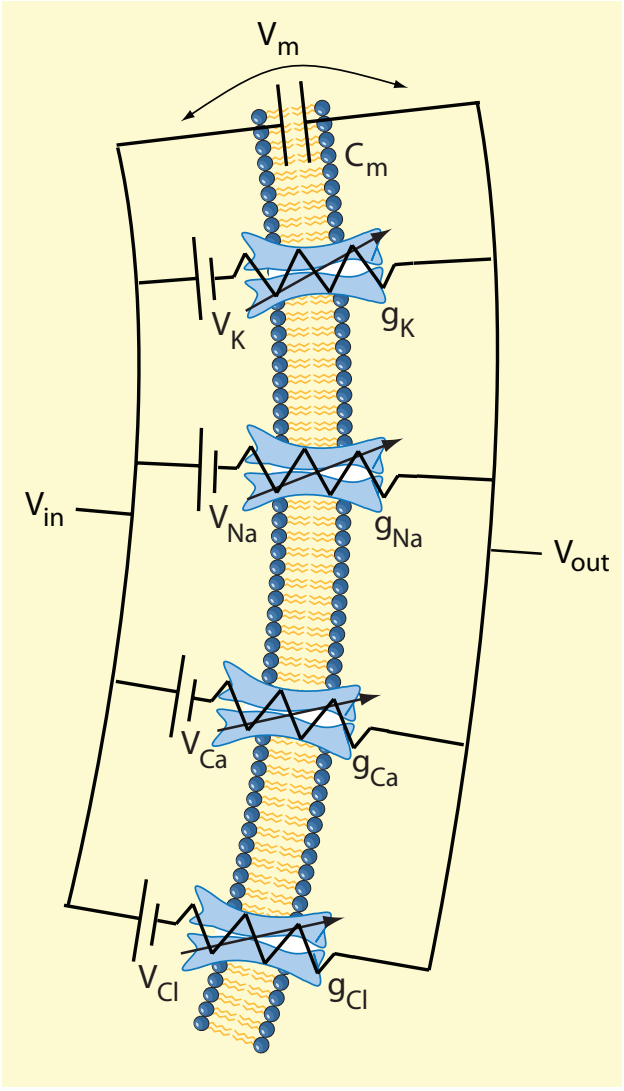

Figure 2.4 – The plasma membrane can be modeled as an electrical circuit. Each ion channel can be assimilated as a resistor of variable conductance g_{ion} (spring-shaped line) associated to the reversal potential of its specific ion V_{ion}. The phospholipid bilayer can be assimilated as a capacitor of capacitance C_m.

The membrane is also mainly composed of a phospholipid bilayer, which is impermeable to ions. This part of the membrane accumulates ions to its intracellular and extracellular sides, acting as an authentic capacitor. Its capacitance C_m is fixed by the structure of the membrane as well as the morphology of the cell. Any changes in the distribution of charges across this membrane capacitance can be assimilated as a capacitive current I_C, which can be defined as usual:

$$I_C = C_m \frac{dV_m}{dt} \tag{2.7}$$

where dV_m/dt represents the variations of the membrane potential per unit of time.

Considering the case of the four ion channels represented in Fig. 2.4, the application of Kirchhoff's current law gives

$$I_C + I_K + I_{Na} + I_{Ca} + I_{Cl} = 0 \tag{2.8}$$

where each ionic current is defined as in Eq. 2.6 and the capacitive current as in Eq. 2.7, which gives

$$C_m \frac{dV_m}{dt} = -g_K(V_m - V_K) - g_{Na}(V_m - V_{Na}) - g_{Ca}(V_m - V_{Ca}) - g_{Cl}(V_m - V_{Cl}) \tag{2.9}$$

If we generalize Eq. 2.9 to an arbitrary set of n different ionic currents and add an applied current I_{app} representing external stimulations, we have

$$C_m \frac{dV_m}{dt} = -\sum_n g_{ion}(V_m - V_{ion}) + I_{app} \tag{2.10}$$

This equation models the variations of membrane potential induced by variations of ion channel permeability. It is at the basis of electrophysiological modeling and neurodynamics.

Ion channels involved in action potential generation are voltage-gated

Neuronal signaling relies on a tight regulation of membrane potential variations, these variations being induced

by variations of ion channel permeability. Neuronal signaling therefore indirectly relies on the tight regulation of ion channel opening states.

In their early work on the squid giant axon, Hodgkin and Huxley experimentally observed that the amplitude of specific ionic currents was directly dependent upon the membrane potential itself. This voltage-dependent regulation is the basic mechanism underlying excitability and axon potential generation. In particular, they identified that the underlying channels were voltage-gated, which was at the origin of this regulation mechanism. Their observation has been extensively confirmed in later works, showing that this voltage-gating is strongly widespread in mammalian neurons as well, through a great richness in voltage-gated channel family.

An easy way to model the voltage-gating of ion channels is to consider that they possess gates that can open or close the channel, these gates being controlled by membrane potential variations. In that configuration, plasma membrane permeability to a particular ion can dynamically oscillate between a zero value, where all ion channels are closed, to a maximal value $\bar{g}_{ion}$, where all ion channels are opened. The maximal conductance $\bar{g}_{ion}$ depends on ion channel density present in the plasma membrane. As mentioned in the introduction, the dynamical property of the plasma membrane makes this density strongly regulable.

The dynamical variations of membrane permeability between these two extreme values can be modeled following the law of mass action. Considering the kinetic diagram

$$C \underset{\beta_n(V_m)}{\overset{\alpha_n(V_m)}{\rightleftharpoons}} O$$

where O corresponds to channel open state, C to its close state, and $\alpha_n(V_m)$, $\beta_n(V_m)$ are the voltage-dependent rate constants ; variations in the fraction of open channels (n) over time is expressed by

$$\dot{n} = \alpha_n(V_m)(1-n) - \beta_n(V_m)n \tag{2.11}$$

where $n \in [0,1]$. Defining

$$n_\infty(V_m) = \frac{\alpha_n(V_m)}{\alpha_n(V_m)+\beta_n(V_m)} \tag{2.12}$$

$$\tau_n(V_m) = \frac{1}{\alpha_n(V_m)+\beta_n(V_m)}, \tag{2.13}$$

we have

$$\tau_n(V_m)\dot{n} = (n_\infty(V_m) - n) \tag{2.14}$$

where $n_\infty(V_m)$ is the fraction of open channels at steady-state and $\tau_n(V_m)$ the channel time constant. These functions are specific for each ion channel type and can be extracted from experimental recordings, as detailed below.

Following these assumptions, an ionic current I_{ion} can be defined by

$$I_{ion} = \bar{g}_{ion} n_{ion} (V - V_{ion}). \tag{2.15}$$

Ion channel voltage-gating is generally monotonic. Channel gates that open with a depolarization of the membrane are called *activation gates*, whereas gates that close with a depolarization of the membrane are called *inactivation gates*. Note that one channel can possess both an activation and an inactivation gate, the kinetics of the latter being generally several times slower than that of the former. Transient sodium channels provide the most famous example of this kind. They are key players in action potential generation.

Action potential generation involves sodium and potassium channels

At rest, excitable cell membrane is hyperpolarized (around -70 mV), as predicted by the GHK equation, the cell being slightly more permeable to potassium than to sodium in that state. As an external excitatory stimulation occurs, it induces a modest depolarization of the cell, from which two scenarii are possible: either the stimulation is not strong enough to activate the endogenous machinery of the cell, which recovers its resting potential as soon as the stimulation is relaxed (the stimulation is said to be "subthreshold", and the information is not transmitted by the neuron) ; or stimulation amplitude is sufficiently high ("suprathreshold") to generate a cascade of membrane permeability changes to sodium and potassium ions, which are at the origin of the action potential generation. These permeability changes rely of the particular kinetics of sodium and potassium channels inserted in the membrane, as sketched in Fig. 2.5.

Cell membrane of most excitable cells contains transient sodium channels and delayed-rectifier potassium channels. Transient sodium channels are voltage-gated ion channels that are selectively permeable to sodium. As mentioned above, their gating shows a bidirectional sensitivity to membrane potential variations: they are rapidly activated but slowly inactivated by membrane depolarization. Delayed-rectifier potassium channels are solely activated by membrane depolarization, activation kinetics being in a similar time-scale of transient sodium channel inactivation, therefore several times slower than sodium channel activation. This configuration is illustrated in Fig. 2.5, activation (resp. inactivation) channel properties being illustrated by activation (resp. inactivation) gates.

At rest, the membrane potential is hyperpolarized; sodium and potassium channel activation gates are both closed and sodium channel inactivation gate is open, which makes cell membrane barely permeable to these

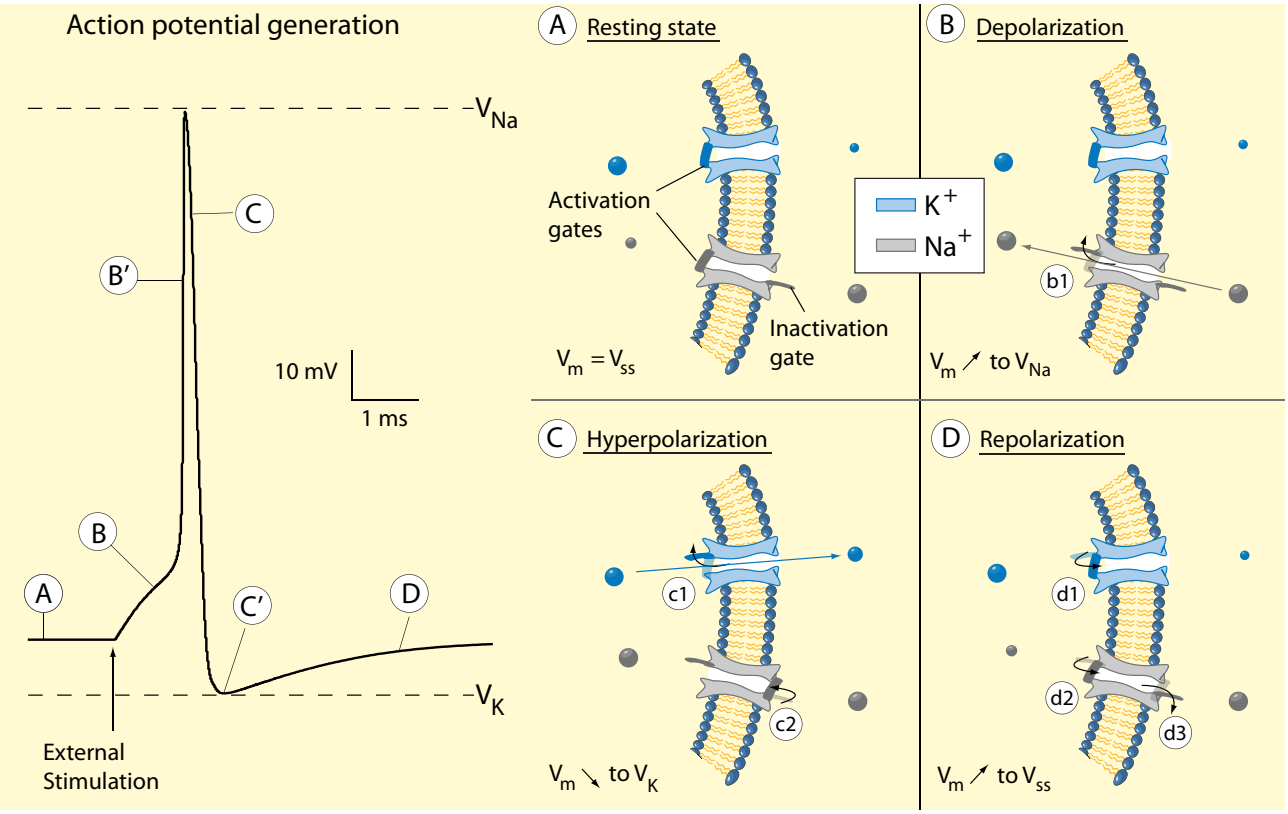

Figure 2.5 – Mechanisms of action potential generation. The figure shows the time-course of a typical action potential (left) as well as an illustration of the intracellular mechanisms at the origin of its generation (right). **A**. At rest, membrane potential being hyperpolarized ($V_m \simeq -70$ mV), sodium and potassium channel activation gates are both closed and sodium channel inactivation gate is open, which makes cell membrane barely permeable to these ions. **B**. The depolarization induced by the excitatory stimulus promotes the rapid opening of sodium channel activation gate (b1), whereas sodium inactivation gate and potassium activation gate do not move, due to their slower kinetics. This induces a massive flow of sodium ions into the cell, generating a strong membrane depolarization, membrane potential converging toward sodium reversal potential ($V_m \nearrow V_{Na} \simeq +40$ mV). **C**. After several hundreds of microseconds, potassium channel activation gate starts to open (c1) and sodium channel inactivation gate start to close (c2), due to the strong membrane potential depolarization. This both disrupts the flow of sodium across the cell membrane and allows potassium to flow out of the cell, generating a strong membrane hyperpolarization, membrane potential now converging toward potassium reversal potential ($V_m \searrow V_K \simeq -90$ mV). **D**. Cell hyperpolarization first promotes the closing of sodium channel activation gate (d2), and than the closing of potassium channel activation gate (d1) and the opening of sodium channel inactivation gate (d3). The membrane recovers its initial permeability to sodium and potassium ions together with its initial resting potential.

ions (phase **A** in Fig. 2.5). The occurrence of a suprathreshold stimulation induces the generation of an action potential, whose mechanisms rely on the following cascade of ion channel gating variations:

i. The depolarization induced by the excitatory stimulus promotes the rapid opening of sodium channel activation gates, whereas sodium inactivation gate and potassium activation gate do not move, due to their slower kinetics. This induces a massive flow of sodium ions into the cell, generating a strong membrane depolarization, membrane potential converging toward sodium reversal potential ($V_m \nearrow V_{Na} \simeq +40$ mV) (phase **B** in Fig. 2.5). Here, the rising phase of the action potential shows a slow initial phase (**B**) followed by a rapid phase (**B'**). This comes from the voltage-dependence of sodium channel activation time constant, this constant decreasing as the membrane depolarizes.

ii. After several hundreds of microseconds, potassium channel activation gates start to open and sodium channel inactivation gates start to close, due to the strong membrane potential depolarization. This both disrupts the flow of sodium across the cell membrane and allows potassium to flow out of the cell, generating a strong membrane hyperpolarization, membrane potential now converging toward potassium reversal potential ($V_m \searrow V_K \simeq -90$ mV) (phase **C** in Fig. 2.5).

iii. Cell hyperpolarization first promotes the closing of sodium channel activation gates, and than the closing of potassium channel activation gates and the opening of sodium channel inactivation gates. The membrane recovers its initial permeability to sodium and potassium ions together with its initial resting potential (phase **D** in Fig. 2.5).

Note that ion concentrations across the cell membrane are here considered constant during action potential generation. Indeed, ion concentration variations are very small and their asymmetric distribution across cell membrane is ensured by active transporters such as the $Na^+/K^+ATPase$, as mentioned above. However, this parameter can be important for neuron excitability in specific cases.

These physiological events can be mathematically modeled, following the mathematical steps described above. Namely, if we solely consider the case of transient sodium channels and delayed-rectifier potassium channels, Eq. 2.10 becomes

$$\begin{aligned} C_m\dot{V}_m = & - \bar{g}_{Na} m_{Na} h_{Na} (V_m - V_{Na}) \\ & - \bar{g}_K m_K (V_m - V_K) \\ & - g_{leak}(V_m - V_{leak}) + I_{app}, \end{aligned} \quad (2.16)$$

where the term $g_{leak}(V_m - V_{leak})$ accounts for the passive diffusion occurring through the membrane independently of voltage-gated channels.

The variables m_{Na} and h_{Na} are the activation and inactivation variables of sodium channels, respectively, and m_K the activation variable of potassium channels. In the remaining of this disseration, the term m_x (resp. h_x) will always refer to the activation (resp. inactivation) variable of the current I_x. Following the formalism of Eq. 2.14, the kinetics of these variables are given by

$$\tau_{m_{Na}}(V_m)\dot{m}_{Na} = (m_{Na} - m_{Na,\infty}(V_m)) \quad (2.17)$$

$$\tau_{h_{Na}}(V_m)\dot{h}_{Na} = (h_{Na} - h_{Na,\infty}(V_m)) \quad (2.18)$$

$$\tau_{m_K}(V_m)\dot{m}_K = (m_K - m_{K,\infty}(V_m)). \quad (2.19)$$

A negative $\dot{m}_x$ means that the activation gate m_x is closing, and conversely.

Equations 2.16, 2.17, 2.18 and 2.19 define a model of neuronal membrane potential variations, composed of transient sodium channels and delayed-rectifier potassium channels. This model is therefore potentially capable of generating action potentials in response to external excitatory stimuli, according to the kinetics of the included channels.

The voltage-clamp technique

Ion channel kinetics can be measured experimentally using the "Voltage-clamp" technique. This method consists in fixing the membrane potential to particular constant values and recording the ionic currents flowing through the membrane at these potentials. Indeed, if V_m is fixed, $\dot{V}_m = 0$ and Eq. 2.16 becomes

$$\begin{aligned} I_{app} = & + \bar{g}_{Na} m_{Na} h_{Na} (V_m - V_{Na}) \\ & + \bar{g}_K m_K (V_m - V_K) \\ & + g_{leak}(V_m - V_{leak}), \end{aligned} \quad (2.20)$$

which shows that the applied current needed to maintain V_m at a target value is a direct image of the ionic currents, the amplitude of these ionic currents being therefore indirectly measured. Moreover, specific ion channels can be isolated from the others, either pharmacologically or via changes in the experimental protocol. For instance, Hodgkin and Huxley extracted the potassium current by removing all sodium ions from the extracellular medium, which made the presence of a sodium current improbable.

Two key parameters of ion channel kinetics can be extracted from these recordings: its voltage-dependence

$(X_\infty(V_m))$, which can be measured for each value of membrane potential when the current has reached its steady-state, and its time constant $(\tau_X(V_m))$, which can be extracted from the transient phase occurring in reaction to an abrupt change in V_m. These experimental traces can be fitted by a mathematical expression. For instance, fitting experimental results obtained on the squid giant axon to the HH model proposed the following equations

$$\begin{aligned} C_m\dot{V_m} = & - \bar{g}_{Na}m_{Na}^3h_{Na}(V_m - V_{Na}) \\ & - \bar{g}_K m_K^4(V_m - V_K) \\ & - g_{leak}(V_m - V_{leak}) + I_{app}, \end{aligned}$$

with

$$\begin{aligned} \tau_{m_{Na}}(V_m)\dot{m_{Na}} &= -(m_{Na} - m_{Na,\infty}(V_m)) \\ \tau_{h_{Na}}(V_m)\dot{h_{Na}} &= -(h_{Na} - h_{Na,\infty}(V_m)) \\ \tau_{m_K}(V_m)\dot{m_K} &= -(m_K - m_{K,\infty}(V_m)), \end{aligned}$$

where

$$\begin{aligned} \tau_X(V_m) &= \frac{1}{\alpha_X(V_m) + \beta_X(V_m)} \\ X_\infty(V_m) &= \frac{\alpha_X(V_m)}{\alpha_X(V_m) + \beta_X(V_m)}, \end{aligned}$$

and

$$\begin{aligned} \alpha_{m_{Na}}(V_m) &= \frac{V_m + 35}{10\left[1 - e^{-(V_m+35)/10}\right]} \\ \beta_{m_{Na}}(V_m) &= 4e^{-(V_m+60)/18} \\ \alpha_{h_{Na}}(V_m) &= 0.07e^{-(V_m+60)/20} \\ \beta_{h_{Na}}(V_m) &= \frac{1}{1 + e^{-(V_m+30)/10}} \\ \alpha_{m_K}(V_m) &= \frac{V_m + 50}{100\left[1 - e^{-(V_m+50)/10}\right]} \\ \beta_{m_K}(V_m) &= 0.125e^{-(V_m+60)/80}. \end{aligned}$$

Fig. 2.6 shows a simulation of the effect of subthreshold and suprathreshold excitatory inputs on the behavior of the model, which demonstrate that model behavior is very close to experimental observations. This model can therefore be used to investigate the evolution of an excitable cell plasma membrane in different conditions.

A constant depolarizing current can induce sustained membrane potential oscillations

Fig. 2.7 shows the response of the HH model to two step inputs of excitatory current. In response to a subthreshold step input, the modeled neuron generates a transient action potential before reaching a new stable steady-state (Fig. 2.7A). In contrast, in response to a suprathreshold step input, the neuron membrane potential starts to oscillate (Fig. 2.7B). Physiologically speaking, these oscillations can be assimilated to a periodic opening and closing of the Na^+ voltage-gated channels and conversely for the K^+ voltage-gated channels.

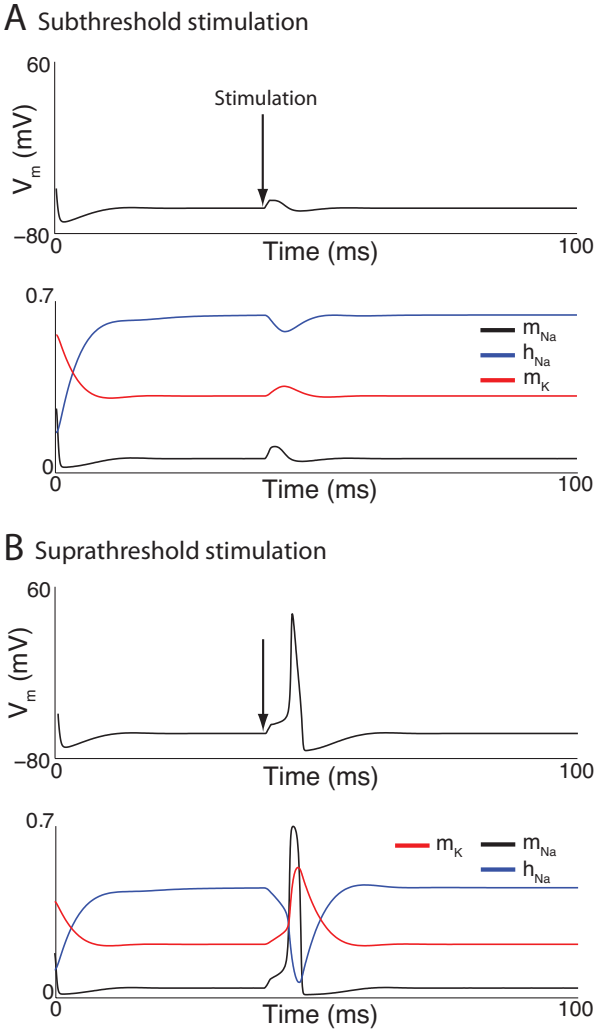

Figure 2.6 – Effect of subthreshold (A) and suprathreshold (B) inputs on HH model behavior. A and **B**. Variations of membrane potential (top) and gating variables (bottom) over time.

From a system theory point of view, such a change in system behavior relies on an abrupt change in its intrinsic dynamical properties: the system undergoes a *bifurcation*. These qualitative changes are generally analyzed via the construction of a *bifurcation diagram*, which shows the behavior of the model according to the value of a chosen parameter, called the *bifurcation parameter*.

Fig. 2.8 shows the bifurcation diagram of the HH model, where the amplitude of the applied current I_{app} is the bifurcation parameter. Indeed, the change in be-

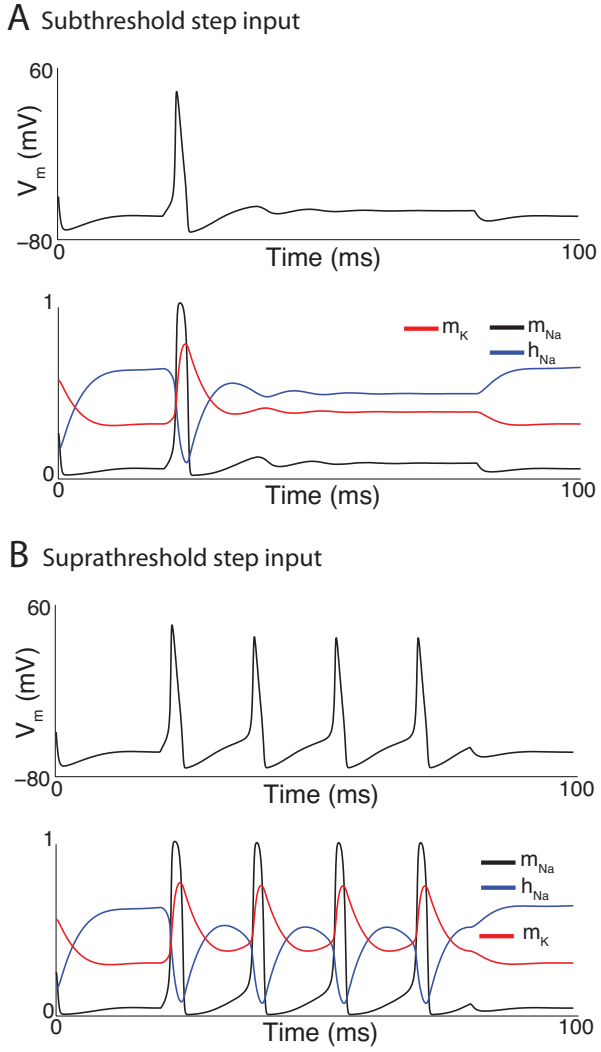

Figure 2.7 – Effect of subthreshold (A) and suprathreshold (B) step inputs on HH model behavior. A and **B**. Variations of membrane potential (top) and gating variables (bottom) over time.

havior that occurs in Fig. 2.7 is due to the application of a step input of excitatory current of sufficient amplitude, which justifies the choice of this parameter as the bifurcation parameter. This diagram shows three qualitatively different zones, delimited by two bifurcations (HB_{low} and HB_{high}, HB for Hopf bifurcation). Below HB_{low}, the system has one stable steady-state V_{ss} corresponding to the hyperpolarized resting potential (black full line). This configuration corresponds to Fig. 2.7A, where the neuron returns to its resting state after generating one transient action potential. Between HB_{low} and HB_{high}, the stable steady-state corresponding to the hyperpolarized resting potential becomes unstable (black dashed line), whereas a stable limit cycle appears, whose minimum and maximum values are depicted by the blue curves (V_{min} and V_{max}, respectively). This configuration corresponds to Fig. 2.7B, where the neuron exhibits sustained oscillations as a response to the step input of excitatory current. Finally, the stable limit cycle vanishes and the steady-state becomes stable again above HB_{high}, which corresponds to a stable depolarized resting potential, often called "depolarization block" in experimental electrophysiology.

These analyses show how bifurcation theory can help understanding dynamical phenomena observed in neurons. It is widely used in the investigation of neuronal excitability (see [46, 90, 101], among others). In particular, the three different types of excitability originally described by Hodgkin [80] have been shown to originate from different bifurcation types [46, 90], leading to the concept of Type I, Type II and Type II excitability. Indeed, many bifurcation types exist, from which originate specific dynamical properties. These concepts are further analyzed and discussed in Part II and Part III of the dissertation.

A two-dimensional reduction of the Hodgkin Huxley model uncovers the dynamics of action potential generation

Conductance-based models of neurons are high-dimensional models whose complexity makes their dynamical analyses complicated. In particular, although HH model has given strong insights on the mechanisms of action potential generation, the key parameters are not easy to extract from this model.

In the early sixties, Richard FitzHugh proposed a strategy to reduce HH model complexity [50]. Taking advantage of timescale separation, he reduced the four dimensional HH model to a two-dimensional model that qualitatively reproduces the behavior of the original one. In particular, he realized that transient sodium channel activation m_{Na} is one order of magnitude faster than all other gating variables, whereas sodium channel inactivation h_{Na} and potassium channel activation m_K evolve on a similar timescale. As a consequence, he considered sodium channel activation as instantaneous ($m_{Na} \approx m_{Na,\infty}(V_m)$), and combined h_{Na} and m_K in one slow variable w ($m_K = w$, $h_{Na} = 0.8 - w$). FitzHugh reduction of HH model reads

$$\begin{aligned} C_m \dot{V}_m = & - \bar{g}_{Na} m_{Na,\infty}^3(V_m)(0.8-w)(V_m - V_{Na}) \\ & - \bar{g}_K w^4 (V_m - V_K) \\ & - g_{leak}(V_m - V_{leak}) + I_{app}, \\ \tau_w(V_m)\dot{w} = & - (w - w_\infty(V_m)). \end{aligned}$$

The interest of reducing HH model complexity to a two-dimensional model is to allow the use of phase por-

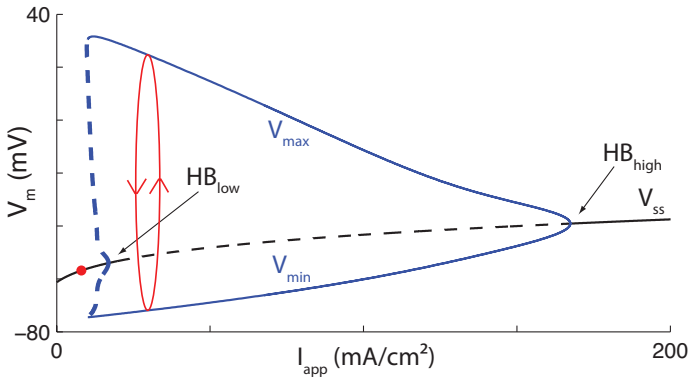

Figure 2.8 – Bifurcation diagram of the HH model with the applied current I_{app} as the bifurcation parameter. The black line corresponds to the steady-state V_{ss} (full line=stable, dashed line=unstable). Blue lines correspond to limit cycles (full line=stable, dashed line=unstable). HB denotes an Hopf Bifurcation. Applying a step input of excitatory current of sufficient amplitude induces a bifurcation in the HH model, switching from a stable resting potential (red dot) to sustained oscillations (red oriented lines).

trait analyses to uncover the dynamics of action potential generation, as shown in Fig. 2.9. A phase portrait is a visual display of system characteristics, each axe displaying one state variable. The blue and red curves represent nullclines, i.e. the locus of points where the derivative is null. The V-nullcline corresponds to all (V_m, w) for which $\dot{V}_m = 0$ (red curve in Fig. 2.9). Similarly, the w-nullcline corresponds to all (V_m, w) for which $\dot{w} = 0$ (blue curve in Fig. 2.9). The intersection between the two nullclines, where both $\dot{V}_m = 0$ and $\dot{w} = 0$, corresponds to a fixed point of the system. This fixed point can be stable or unstable, depending on the local properties of the vector field at this point.

Fig. 2.9A illustrates the excitability of the HH model in the phase portrait. For subthreshold stimulus, the voltage increases only sightly before it decreases monotonically to its steady-state value. For suprathreshold stimulus, the neuron produces an action potential. Firstly, the membrane potential quickly increases, whereas w barely varies, and the trajectory is almost horizontal until it reaches the sodium resting potential (Phase 1 in Fig. 2.9A). Secondly, w slowly increases. It corresponds to the inactivation of sodium channels and the activation of the potassium channels (Phase 2 in Fig. 2.9A). Thirdly, w becomes large and V_m starts to decrease quickly, reaching the potassium resting potential (Phase 3 in Fig. 2.9A). Finally, w decreases slowly and the neuron reaches its initial resting potential (Phase 4 in Fig. 2.9A). This is the typical geometry of action potential generation.

Phase portrait analysis is useful to extract key parameters of neuronal excitability. It shows that a growth of potential for suprathreshold simulations is solely possible if the voltage dynamics are much faster than the recovery dynamics, allowing the horizontal trajectory of phase 1 in Fig. 2.9A. Likewise, the inverted N shape of the V-nullcline is also essential. Namely, an action potential is generated if the stimulation puts the trajectory below both the V-nullcline and the w-nullcline, which defines the excitability threshold (further explanations on these properties are provided in [46, 90, 101], among others).

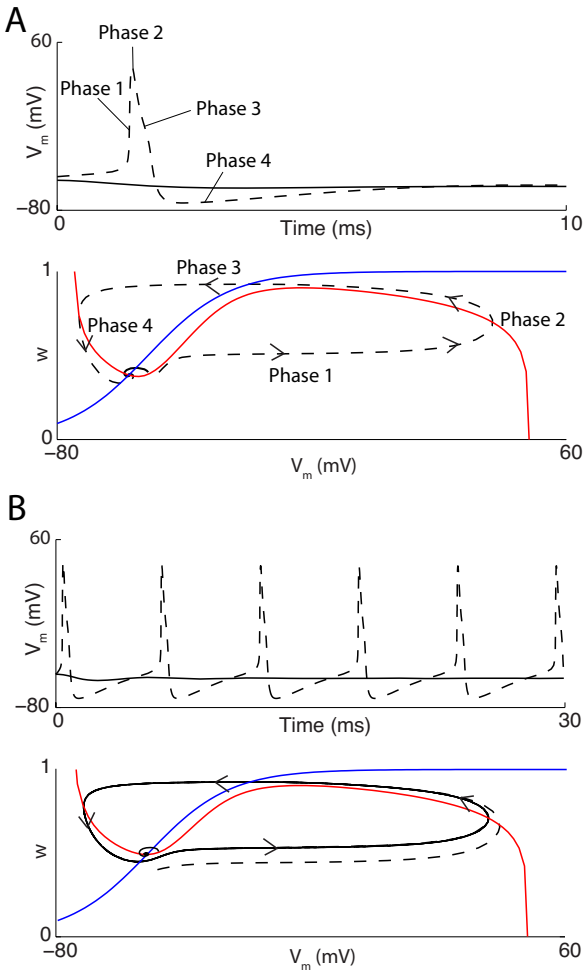

Figure 2.9 – Phase portrait analyses of the reduced HH model for two different values of I_{app}. A and **B**. Top: Variations of the membrane potential over time for two different initial conditions (full line and dashed line). Bottom: phase portrait of the reduced model, showing the V-nullcline (red), the w-nullcline (blue) and the trajectories corresponding to the time-courses of the top panel (full and dashed black curves).

These dynamical properties are shared by most neuron types.

Fig. 2.9B shows membrane potential response to the application of a constant current. As it is the case for the original HH model, the application of a sufficiently large constant current generates oscillations. With the phase plane analysis, we can now investigate the dynamical origin of these oscillations. Applying a constant current translates the V-nullcline vertically. The intersection between the two nullclines is moved to the right, and when this intersection passes the local minimum of the V nullcline, the fixed point becomes unstable and a stable limit cycle appears in the phase plane, resulting in sustained oscillations (dashed black line). This phenomenon corresponds to the bifurcation we extracted from the original HH model in Fig. 2.8.

To summary, bifurcation analyses of conductance-based models and phase portrait analyses of reduced models give important insights on the mechanisms underlying neuronal excitability and action potential generation. These tools are extensively used in the forthcoming chapters.

The Richness of Neuronal Excitability

Neurons exhibit a wide variety of electrophysiological properties

The mechanisms of action potential generation described above are common to almost all neurons. However, there exist many different neuron types that sustain various functions within the nervous system. These neurons build their diversity on their morphology, interconnections, electrochemistry, etc. ; but also on the particular way they generate action potentials over time. That is, each neuron is able to exhibit one or several specific *firing pattern*, this firing pattern being a key component of its signaling.

Fig. 2.10 shows different firing patterns exhibited by different neuron types of the mammalian brain. Its shows that the firing rate and pattern can be highly different from one neuronal population to the other, but also in a same population, as illustrated for cortical pyramidal and thalamic relay cells. Two important firing patterns are often described: single-spike firing and burst firing. Burst firing corresponds to the generation of relatively high frequency spiking periods separated by quiescent periods. Many cell types are able to switch between these two modes, as illustrated in the figure. The mechanisms underlying this switch of firing pattern represent one main investigation of the present dissertation.

Neurodynamical richness relies on ion channel diversity

Action potential generation in the squid giant axon solely relies on one transient voltage-gated sodium channel and one delayed-rectifier voltage-gated potassium channels, as shown above. However, a large amount of different ion channels exists. Namely, ion channels can be permeable to different ion types, the more frequent being sodium, potassium, calcium and chloride. These channels can be voltage-gated, ligand-gated, molecule-gated, etc., and even channels whose permeability and gating properties are similar can strongly differ in their properties, such as gating kinetics for instance, as illustrated in Fig. 2.11 for voltage-gated potassium channels.

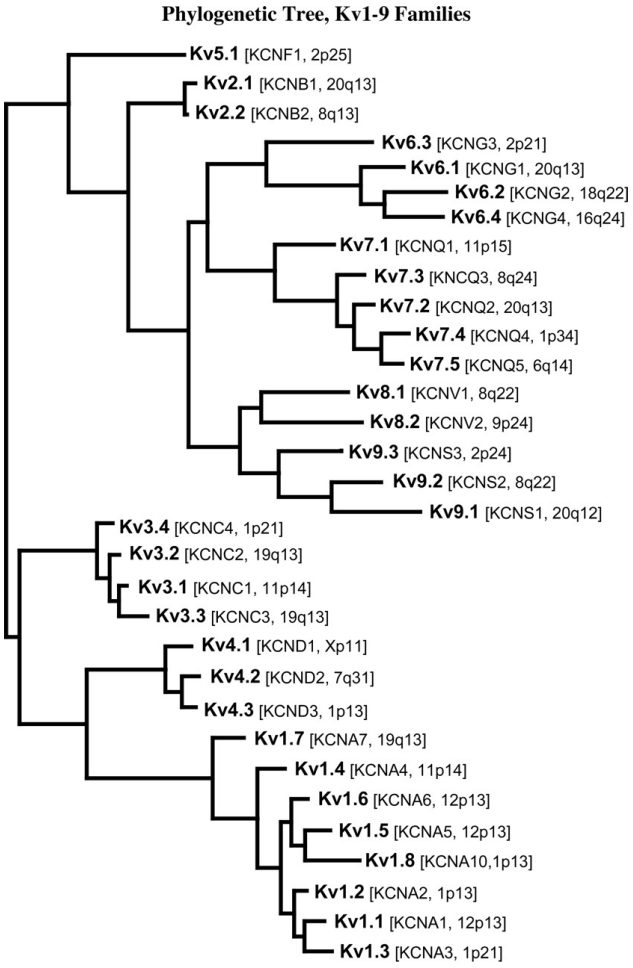

Figure 2.11 – Phylogenic tree of voltage-gated potassium channels. Taken from [69]

The great diversity in neuronal excitability arises form this diversity in ion channel subtypes. A main challenge in modern electrophysiology is therefore to extract the key players of the firing patterns of the different neuron types, which is the main motivation of the present dissertation.

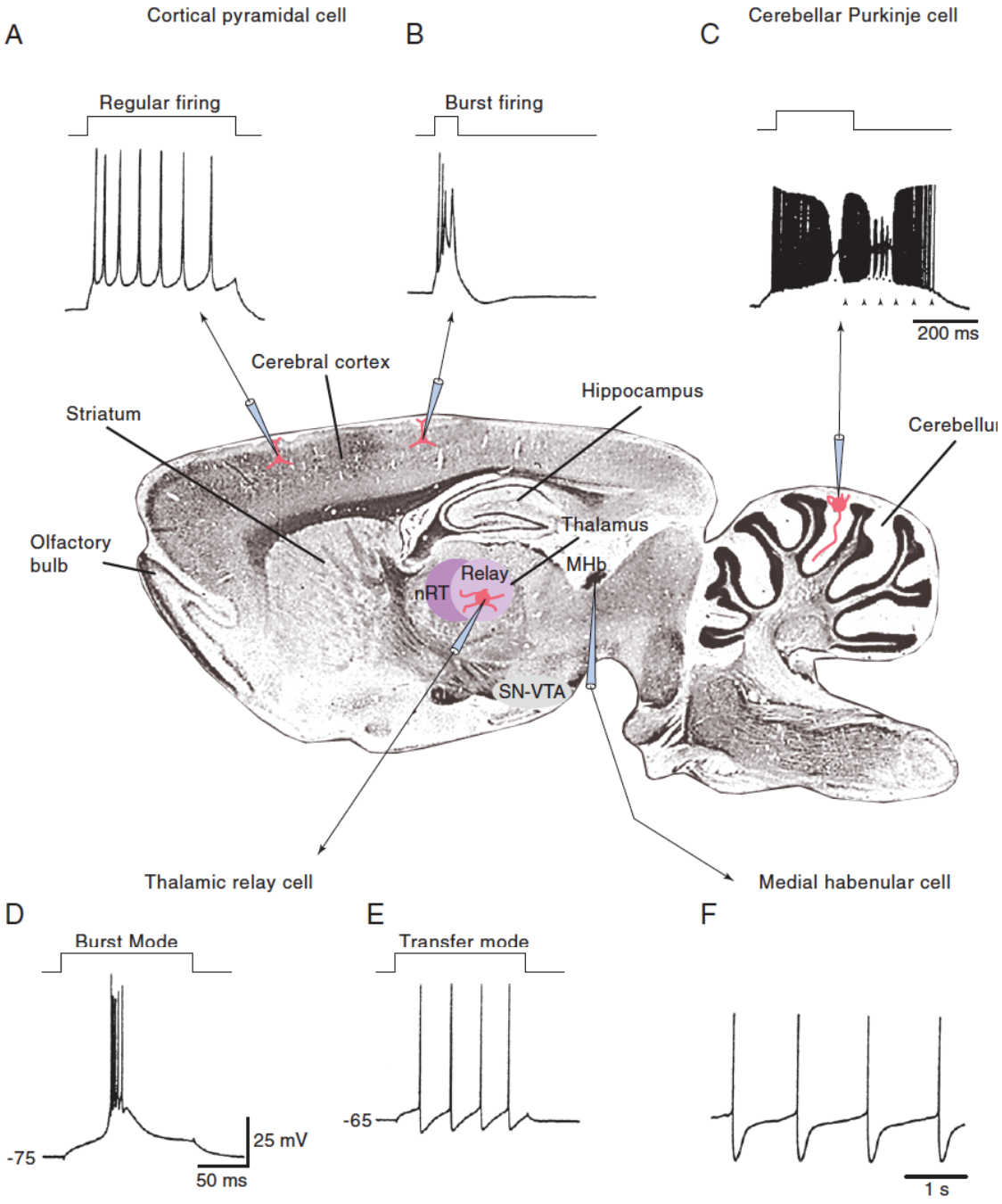

Figure 2.10 – Neurons exhibit various electrophysiological properties. The figures show different firing patterns exhibited by different neuron types of the mammalian brain. Taken from [21]

Chapter 3

Experimental Techniques

This chapter attempts to give a brief overview of several experimental techniques available for single-cell electrophysiology. Its main goal is to familiarize the reader with the different techniques used in this thesis.

Single-cell recordings on brain slices

In vitro recordings are generally performed on brain slices or cell cultures. Brain cells are kept alive artificially, via the continuous perfusion of an oxygenated artificial cerebrospinal fluid (ACSF) in the recording chamber. The ACSF shares most properties of the physiological cerebrospinal fluid, such as its pH (around 7.4), its osmolarity (around 300 mOsm), its ionic composition (high sodium concentration, low potassium concentration), etc. There exists three main types of *in vitro* recordings, that is extracellular recordings, intracellular recordings and patch-clamp recordings (Fig. 3.1).

Extracellular recordings

It is possible to record neuron electrical activity from the extracellular medium with a rather thick electrode. With this technique, only abrupt changes in target cell membrane potential can be recorded, not the membrane potential itself (Fig. 3.1, left). This technique is therefore widely used to record neuron firing pattern and analyze its response to pharmacological compounds, for instance. As for all *in vitro* recordings, these compounds are perfused in the recording chamber together with the ACSF, so all neurons of the brain slice are affected.

One main advantage of this recording technique is that it does not affect the integrity of the cell, the electrode staying in the extracellular space, in contrast with the other techniques. On the other hand, it is not possible to directly record the membrane potential or ionic currents, as mentioned above. In addition, it is not possible to apply any current to the neuron.

Intracellular recordings

Intracellular recordings allow a direct recording of neuron membrane potential (Fig. 3.1, middle). In this case, a very thin electrode is inserted into the cytoplasm through the plasma membrane. This technique is therefore rather invasive, but the cell generally tolerates it thanks to the thinness of the electrode and the fluidity of the plasma membrane.

Current clamp is possible during intracellular recordings. Namely, it is possible to inject either excitatory or inhibitory currents to the recorded cell to investigate its excitability properties. This technique is well suited for current clamp recordings because it barely affects the composition of the intracellular medium, electrode thinness limiting the diffusion of its internal solution.

Patch clamp recordings

Patch-clamp recording is the most advanced technique used in single-cell electrophysiology. It has been developed by Erwin Neher and Bert Sakmann in the late 1970s and early 1980s, for which they received the Nobel Prize in Physiology or Medicine in 1991.

In this case, the electrode is sealed onto the surface of the cell membrane, rather than inserted through it (Fig. 3.1, right). Similarly to intracellular recording, it allows a direct recording of neuron membrane potential, but greatly extends the analysis possibilities. It allows to record neuron activity both in current-clamp or voltage-clamp mode. The latter mode is used to measure the ion currents through the membrane of the recorded cell while holding the membrane voltage at a target value. This technique also makes single-channel recordings possible. There indeed exists many different patch-clamp configurations, such as cell-attached, whole-cell, inside-out, outside-out and nucleated patch, among others. Each of these configurations permits to extract particular parameters.

One main peculiarity of the patch clamp technique is the existence of a continuum between the internal pipette

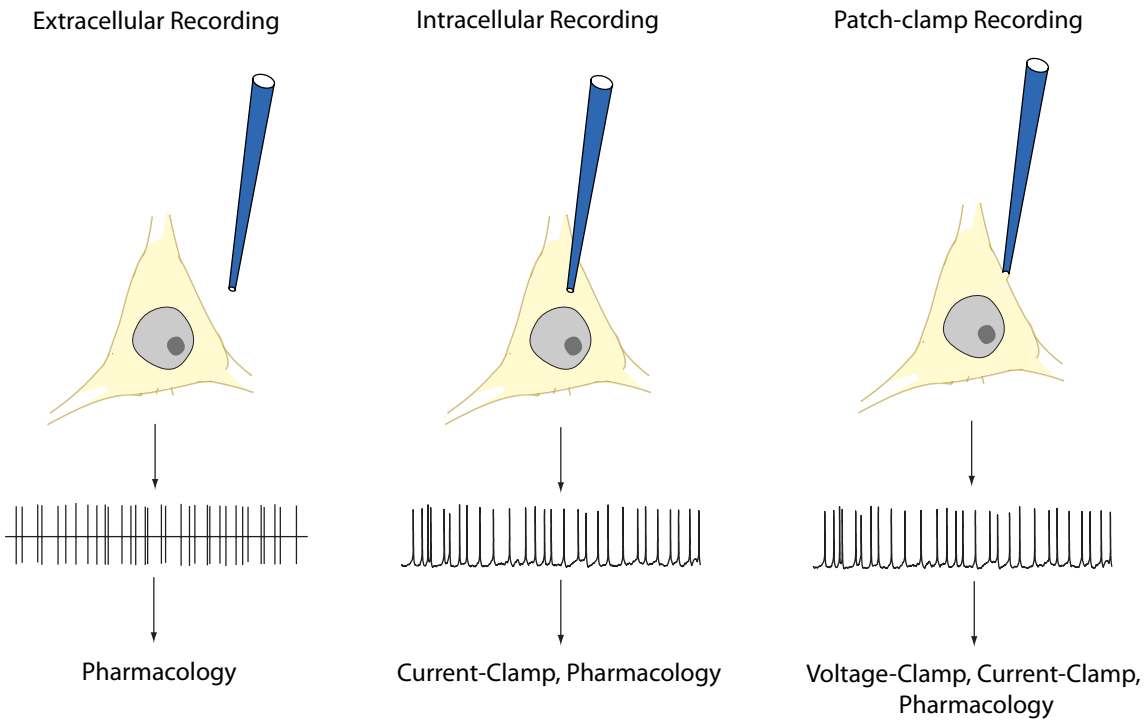

Figure 3.1 – Neuron electrical activity can be recorded using different techniques.

solution and the cytoplasm in whole-cell configuration. It induces the diffusion of the different molecules from the intracellular space to the pipette and conversely, which can be a good and a bad thing. Firstly, this property can be used to diffuse a specific dye or pharmacological compound into the cytoplasm of the sole recorded cell. This technique is often used to permit the post localization of the recorded neuron in the slice, via the diffusion of a fluorescent dye. On the other hand, diffusion of the internal pipette solution into the cytoplasm can induce the dilution of the cell intracellular space, potentially affecting its integrity. As a consequence, we keep using extracellular and intracellular recordings when we need to record neuronal activity in endogenous or current-clamp configurations.

Single-cell extracellular recordings in vivo

It is also possible to record neurons in *in vivo* conditions, both on anesthetized or awake animals.

Theoretically, the three methods described for *in vitro* recordings might be used *in vivo*. However, extracellular recordings are most widely used, because of their relative simplicity and because neuron firing pattern is generally the signal of interest. Some laboratories start nevertheless to perform patch clamp recordings *in vivo*, but mainly in neurons that are close to the brain surface, such as cortical neurons.

There are three main ways of applying pharmacological compounds during *in vivo* recordings: Intraperitoneal (i.p.) injection, intravenous (i.v.) injection and microiontophoresis. The injection methods are systemic. In that sense, they spread the compound into the whole organism, which potentially affects all cells. They can therefore act indirectly on the recorded neuron via changes in the firing of their afferents. This limitation can nevertheless be overcome by the use of synaptic blockers. This technique is usually used for the application of uncharged pharmacological compounds that can cross the blood brain barrier.

Microiontophoresis can be very local. This technique involves a microiontophoresis pipette located very close to the recording electrode, in which are stored one or several pharmacological compounds. For instance, the pipettes we use in the laboratory of neurophysiology are composed of six channels, five of them being potentially filled by one specific drug (the sixth one is the reference). As a consequence, the applied compound specifically affects the recorded neuron, and have little systemic effects. Only charged drugs can be applied using this technique. Indeed, the retention or extrusion of the drug is performed via the application of a small current in the corresponding channel. The amount of extruded compound depends on the intensity of the applied current, which makes a dose/response analysis possible.

Part II

Dopaminergic Neuron Electrophysiology

Main collaborators on this part were

- *Ms. Anne Collard, who contributed to the unicellular stochastic analyses of Chapter 6,*
- *Mrs. Scuvée-Moreau, who made the in vitro intracellular recordings of Chapter 7,*
- *Mr. Laurent Massotte, who made the in vitro extracellular recordings of Chapter 5,*
- *Dr. Olivier Waroux, who developed the in vivo extracellular recording protocol of Chapter 7,*
- *Dr. Maxime Bonjean, who incorporated the M-current analyzed in Chapter 7 in the model of [23].*

Introduction

Midbrain dopaminergic (DA, i.e. dopamine releasing) neurons sustain important physiological functions such as control of movement [97] and signaling of positive error in reward prediction in the mesolimbic system [158]. A dysfunction of the DA system is implicated in the pathophysiology of Parkinson's disease, schizophrenia, and drug abuse [87].

Under physiological conditions, DA neurons can switch between three distinct firing modes: tonic (pacemaker), irregular [62], and burst firing [17, 63] (Fig. II.I), and the firing pattern of these cells strongly affects behavioral parameters, because this pattern has a strong influence on postsynaptic DA receptor activation. For instance, disruption of burst firing in the mesolimbic system, which is known to blunt increases in dopamine concentrations [27], has been shown to affect cue-dependent reward learning [206].

Many studies have focused on the factors controlling the switch of firing pattern in DA neurons. It is generally agreed that bursting requires an external glutamatergic excitatory input stimulating N-methyl-D-aspartate (NMDA) receptors [98, 137] . This has been further demonstrated recently by the observation that selective genetic inactivation of NMDA receptors in these neurons strongly disrupts burst firing, with many important behavioral consequences [206]. On the other hand, activation of $GABA_A$ inhibitory receptors inhibits bursting because of their shunting effect on the oscillatory behavior [181]. Finally, both *in vitro* and *in vivo* experiments show that a reduction of a potassium conductance mediated by small conductance Ca^{2+}-activated K^+ (SK) channels greatly potentiates irregularity and/or bursting [95, 133, 164, 167, 168, 191]. Although these studies have brought important insights in firing pattern regulation of DA neurons, the mechanisms underlying this regulation remain unclear to date.

In the following chapter, we analyze the ionic mechanisms underlying these firing activities, via the combination of mathematical modeling, *in vitro* recordings on brain slices and *in vivo* recordings on anesthetized rats. In Chapter 4, we develop a minimal model of a DA neuron that contains the minimal set of conductances that is necessary to reproduce the firing patterns of these cells. This qualitative model is sufficiently simple to allow deep mathematical analyses, in opposition to existing detailed models that focus on quantitative phenomena.

Using this simple model, we analyze the mechanisms underlying DA neuron pacemaking *in vitro* in Chapter 5. In particular, we discuss the cooperative role of sodium and L-type calcium channels in the spontaneous generation of spikes and slow oscillatory potentials (SOPs), and we highlight this cooperation as the origin of discrepancies observed in the experimental literature regarding the role of these channels.

In vivo entrainability mechanisms are discussed in Chapter 6. This chapter mainly focuses on the role of SK channels as regulators of synaptically-induced bursting and synchrony of DA neurons. It suggests that physiological regulations of these channels, through G-protein coupled receptors (GPCR) for instance, might be at the basis of the switches in firing patterns and synchrony observed in DA neurons *in vivo*. This physiological switch is critical for the generation of motor action [97], for instance.

Finally, we analyze a potential origin of selective modulation of bursting in DA neurons, via regulation of KCNQ K^+ channels. These potassium channels have been recently detected in DA neurons, but they do not affect the pacemaking behavior *in vitro* [75]. Using a published detailed mathematical model [23] and *in vivo* extracellular recordings on anesthetized rats, we show that the role of this current is overcomed by SK channels in single-spike firing, but strongly affects the quantity of SK channel blockade-induced bursting *in vivo*.

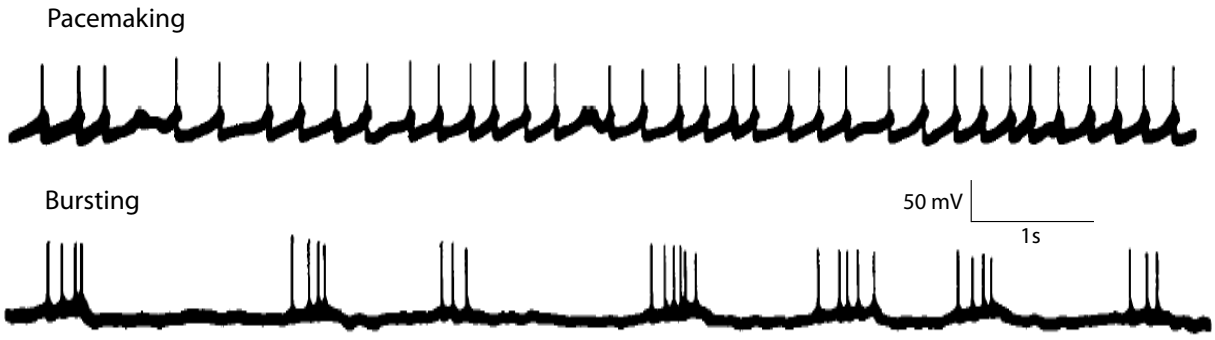

Figure II.1 – Pacemaker and burst firing of midbrain dopaminergic neurons (adapted from [62, 63])

Chapter 4

A Simple Qualitative Model of a Dopaminergic Neuron

DA neuron electrophysiology has been modeled by several groups [3, 23, 24, 105, 111, 113, 196]. Most of these models were elaborated in order to reproduce experimental observations. Although they clearly succeed at making detailed predictions, their complexity may prevent a detailed analysis of the mechanisms underlying the firing patterns of these neurons.

In order to extract the essential mechanisms of firing of DA neurons, we develop a minimal model endowed with the minimal set of conductances which is necessary to reproduce the firing patterns of these cells. The model follows a scheme based on the Hodgkin-Huxley (HH) model [81]. An equivalent circuit of the model is shown in Fig. 4.1. It is composed of voltage-gated sodium channels I_{Na} and delayed-rectifiers potassium channels $I_{K,DR}$, which are responsible for the rising and the falling phases of action potentials, respectively. The equations for these currents are identical for those of the HH model, where time constants are tuned to fit DA neuron specifics ($\tau_{DA} = 0.25\tau_{HH}$, see [40] for detailed equations).

Because the endogenous rhythm of SNc DA neurons strongly relies on variations of intracellular calcium concentration [70], we added calcium dynamics to the HH model:

$$\begin{aligned}\frac{d[Ca^{2+}]_{in}}{dt} = & - k_1(I_{Ca,L} + I_{Ca,pump}) \\ & - k_C[Ca^{2+}]_{in} - k_2 I_{Na}.\end{aligned}$$

Calcium enters through L-type calcium channels endowed with calcium dependent inactivation (CDI) [78, 201], whereas calcium extrusion is carried out by calcium pumps. We choose a particular category of calcium channels; called L-type calcium channels, because they have been shown to play an important role in the pacemaking of SNc DA neurons [70, 143, 144]. The kinetics of these channels are given as follows:

$$I_{Ca,L} = \bar{g}_{Ca,L} d_L f_L (V_m - V_{Ca})$$

where

$$\begin{aligned}\tau_{d_L}\frac{dd_L}{dt} &= d_{L,inf} - d_L, \\ d_{L,inf} &= \frac{1}{1+\exp\left(-(V_m+55)/3\right)}, \\ \tau_{d_L} &= 72\exp\left(-(V_m+45)^2/400\right) + 6\end{aligned}$$

accounts for the voltage-activation of the channels, and

$$f_L = \frac{K_{M,L}}{K_{M,L} + [Ca^{2+}]_{in}}$$

accounts for the calcium-inactivation of the channels [78]. The current of the calcium pump is given by:

$$I_{Ca,pump} = I_{Ca,pump,max}\left(1 + \frac{K_{M,P}}{[Ca^{2+}]_{in}}\right)^{-1}$$

In addition, the model contains a SK-type calcium-activated potassium current, which has been shown to regulate the electrophysiological behavior of these neurons:

$$I_{K,Ca} = \bar{g}_{K,Ca}\left(\frac{[Ca^{2+}]_{in}}{K_D + [Ca^{2+}]_{in}}\right)^2 (V_m - V_K)$$

In agreement with experimental results, this current is calcium-activated but not voltage-gated.

Finally, a depolarizing current activated by an external input was added to mimic synaptic inputs:

$$I_{syn} = R_{syn}\bar{g}_{syn}(V_m - 0).$$

The external input R_{syn} can have different shapes: deterministic shapes, such as step or square wave inputs; or a stochastic shape. The latter is designed to mimic physiological synaptic inputs, which can be modeled through a Poisson stochastic process (small amplitude noise to mimic *in vitro*-like conditions and high amplitude noise to mimic *in vivo*-like conditions). The chosen rate for the stimulations is about fifty events per seconds. For the j^{th}

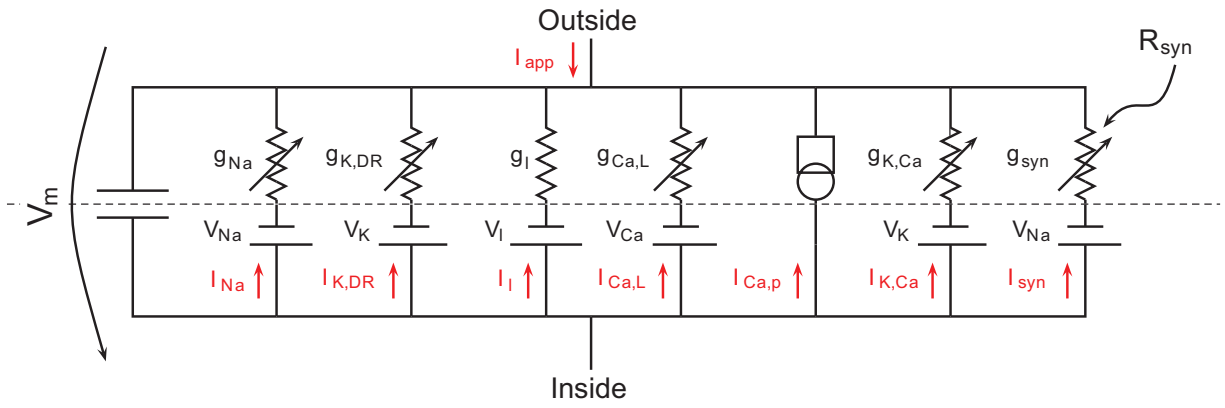

Figure 4.1 – Equivalent circuit diagram of the model. The model is composed of one compartment containing the conductances shown, in parallel with a membrane capacitance.

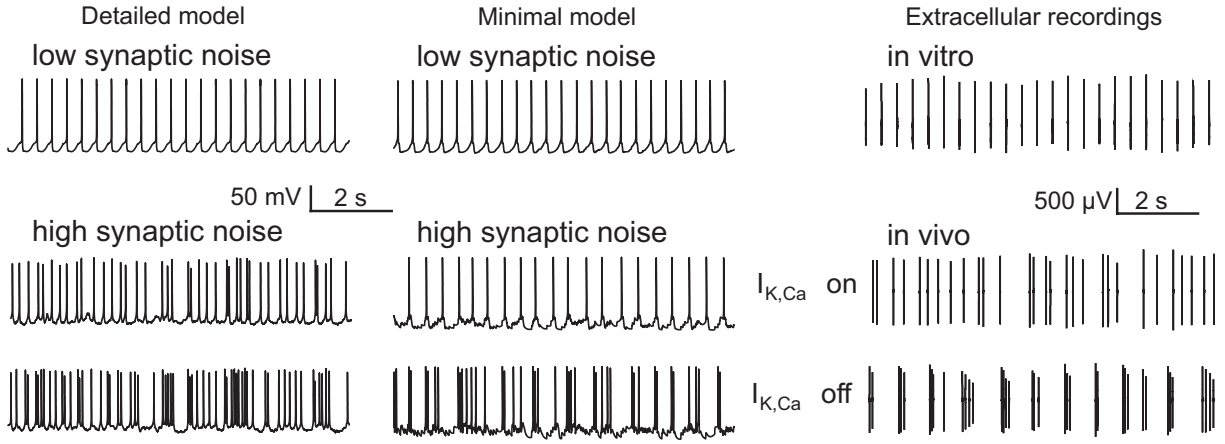

Figure 4.2 – Comparison of the behavior of the detailed model of [23] (left) and of the minimal model (middle) in in vitro and in vivo-like conditions with experimental data obtained from dopaminergic neurons (right). In each case, the neuron fires regularly in single spikes *in vitro*, and an inhibition of calcium-activated potassium channels induces burst firing *in vivo*. Experimental data are from Seutin (unpublished)(upper panel) and Drion (unpublished)(lower panel).

event that occurs at time t_j, the marginal activation r_j is given by

$$\begin{aligned} r_j(t) &= 0 & t < t_j \\ r_j(t) &= p_{syn} \exp\left((t_j - t)/\tau_{syn}\right) & t \geq t_j. \end{aligned}$$

The global synaptic input R_{syn} is given by the sum of the n $r(t)$ corresponding to the n events of the Poisson stochastic process:

$$R_{syn}(t) = \sum_{j=1}^{n} r_j(t).$$

The values of the parameters used for these currents are given in Supplementary Tab. S4.1.

The proposed minimal model is able to reproduce the firing patterns exhibited by DA neurons, namely pacemaker firing *in vitro*, irregular single-spike and burst firing *in vivo*, or be in a hyperpolarized state (Fig. 4.2). As it has been shown experimentally, the switch between irregular single-spike firing and bursting can be induced by a blockade of small conductance calcium-activated potassium (SK) channels [96, 191].

This model serves as a basis for the analyses of DA neuron firing patterns *in vitro* and *in vivo* proposed in Chapter 5 and Chapter 6, respectively.

Chapter 5

Mechanisms of Spontaneous Firing *in vitro*

The nature of the channels involved in the low frequency pacemaking of DA neurons is still strongly discussed. Indeed, whereas many studies have shown that L-type calcium channels are critical for this spontaneous activity, others, including ours, have observed little effect of a blockade of these channels on this firing pattern (see Tab. 5.1). Therefore, the respective contribution of calcium and sodium channels in pacemaking remains unclear. On the other hand, it is commonly accepted that low-frequency spontaneous firing requires oscillations in the cytoplasmic free calcium concentration [102, 143].

In the presence of the sodium channel blocker tetrodotoxin (TTX), DA neurons also exhibit slow oscillatory potentials (SOPs) [133, 139], which have been shown to be sustained by L-type calcium channels [70]. Guzman et al. recently observed that SOPs and spikes are not correlated in rate and regularity, from what they concluded that pacemaking and SOPs are driven by different mechanisms [70]. This conclusion is used to support the hypothesis that L-type calcium channels would not strongly contribute to pacemaking in DA neurons, which is in opposition with many experimental results [143, 144] (Table 1). An additional controversy results from the fact that the block of SK channels prolongs depolarizing plateaus under sodium channel inhibition, whereas it only slightly affects the firing rate when the neurons fire action potentials.

In this chapter, we use a mathematical analysis to extract the mechanisms underlying the spontaneous activity of DA neurons. The main conclusion of our analysis is that pacemaker firing in DA neurons is sustained by the cooperation of sodium and L-type calcium channels (and more modestly N-type or P/Q-type calcium channels [143]), whereas variations of the intracellular calcium concentration play a major role in the rate of this spontaneous firing pattern. On the basis of this mechanism, we identify potential causes for the experimental discrepancies mentioned above, using our minimal model, as well as the detailed model. We observe that neurons only differing by less than 1% in their maximal sodium conductance react oppositely to a blockade of L-type calcium channels. Experiments performed in rat brain slices confirm that L-type calcium and sodium channels cooperate to generate pacemaking in these neurons.

As a secondary conclusion, our model shows that, even though the initiation of SOPs and spikes is sustained by the same mechanism, these oscillatory patterns are not correlated, which is in agreement with experimental results [70]. We show that this absence of correlation is due to different mechanisms of depolarizing phase termination in the two oscillatory behaviors, as well as different kinetics of calcium entry (resp. exit) during depolarizing phases (resp. hyperpolarizing phases). These results show that the lack of correlation between pacemaking and SOPs does not exclude a shared initiation mechanism.

Results

Experiments on neurons with very similar channel build-ups may lead to contradictory observations.

In the absence of synaptic inputs, DA neurons fire spontaneously in a very regular manner [164, 200]. The mechanisms underlying this pacemaker activity are still strongly discussed, experimental results being contradictory (Table I). However, it is commonly accepted that pacemaking of DA neurons requires calcium oscillations and that SK channels are not critical to sustain this firing pattern [200]. Fig. 5.1 illustrates the mechanisms involved in pacemaker firing in the minimal model. As it has been demonstrated experimentally [70], the spontaneous activity is synchronized with calcium oscillations. Namely, each action potential is generated when the intracellular calcium concentration reaches a constant minimal value (Fig. 5.1A). This is consistent with experimental results [70, 139].

The mechanisms involved in the pacemaker activity of the minimal model can be fully understood using bifurcation analysis. The bifurcation diagram shown in Fig.

Reference	Nature of the preperation	Agent used	Observed effect
Nedergaard et al., 1993	Slices from adult guinea-pigs, SNc, intracellular recordings.	nifedipine ($1 - 20\ \mu M$)	Cessation of firing at undisclosed concentration.
Mercuri et al., 1994	Slices from adult Wistar rats, SNc and lateral VTA, intracellular recordings.	nifedipine and nimodipine ($0.3 - 30\ \mu M$)	Decrease in the firing rate of about 50% with $1\ \mu M$ of both drugs. Cessation of firing with $20 - 30\ \mu M$ of both drugs.
Puopolo et al., 2007	Acutely dissociated neurons from the SNc of juvenile (16 day-old) mice, whole cell recordings.	$1.8\ mM\ \ Co^{2+}$ in replacement of Ca^{2+} nimodipine ($1\ \mu M$) ω-aga-IVA ($200\ nM$)	Cessation of firing in all neurons (17/17). Firing rate decreased in 9/17 neurons. Firing rate decreased in 10/14 neurons.
Chan et al., 2007	Slices from juvenile mice (younger than P21), SNc, cell-attached and whole-cell recordings. Slices from young adult mice (older than P28), SNc, cell-attached and whole cell recordings.	isradipine ($20\ \mu M$) and nimodipine ($20\ \mu M$) isradipine ($20\ \mu M$) and nimodipine ($20\ \mu M$)	"Firing largely unaffected" (but firing reduced by an I_H blocker). Cessation of firing in all neurons (15/15): "plastic" phenomenon in "several" neurons (firing resumes during block > 1 hour in some neurons).
Guzman et al., 2009	Slices from both juvenile and young adult mice, SNc, cell-attached and whole cell recordings	isradipine ($5\ \mu M$)	Firing unaffected.
Putzier et al., 2009	Slices from juvenile rats (younger than P21), SNc, whole cell recordings	nimodipine ($10\ \mu M$)	Cessation of firing.
Khaliq and Bean, 2010	Slices from both juvenile and young adult mice, medial VTA, whole cell recordings	$0\ Ca^{2+}$, $3\ mM Mg^{2+}$	Firing increased three-fold.
Seutin et al., unpublished	Slices from adult ($>$ 6 week-old) rats, SNc, extracellular recordings)	nifedipine ($20 - 50\ \mu M$) nimodipine ($5 - 20\ \mu M$)	Firing unaffected (N = 5). Variable effects, no clear trend (N = 5).

SNc: substantia nigra, pars compacta; VTA : ventral tegmental area. Rodents are classified as juvenile ($<$ P21), young adults ($>$ P28) or adult ($>$ 6 weeks)

Table 5.1 – Effect of manipulations that block voltage-dependent Ca^{2+} channels on the pacemaking of midbrain DA neurons ex vivo or in vitro.

5.1B illustrates how the spike generation is governed by the intracellular calcium concentration, the latter being the bifurcation parameter. The diagram defines three distinct ranges of intracellular calcium concentration : a low range where the only stable steady-state is depolarization block ($[Ca^{2+}]_{in} \leq [Ca^{2+}]_{in,low}$) ; a high range where the only stable steady-state is hyperpolarization ($[Ca^{2+}]_{in} \geq [Ca^{2+}]_{in,high}$) ; and an intermediate bistable range where a limit cycle may coexist with the two stable steady-states ($[Ca^{2+}]_{in,low} \leq [Ca^{2+}]_{in} \leq [Ca^{2+}]_{in,high}$). The thresholds separating these zones are mainly dependent on the regulation of calcium channels and calcium pumps by the intracellular calcium concentration. Thus, a rise of the intracellular calcium concentration induces an inactivation of the L-type calcium channels [78, 201], which reduces the amount of inward (i.e. depolarizing) current, and an activation of calcium pumps, which increases the amount of outward (i.e. repolarizing) current [153]. As a consequence, the excitability of the cell decreases with the intracellular calcium concentration. A variation of the intracellular calcium concentration that exceeds the high threshold will induce a switch from firing to a hyperpolarized state. Therefore, the high threshold, which is defined as the value of $[Ca^{2+}]_{in}$ at which the stable limit cycle disappears, defines the maximal possible intracellular calcium concentration which is compatible with firing.

The low threshold in Fig. 5.1 defines the value of intracellular calcium concentration at which an action potential is spontaneously generated. As a consequence, the current which initiates the depolarization at this point is the critical one for pacemaking. For instance, for the set of parameter values used in Fig. 5.1, action potentials are generated by an opening of L-type calcium channels, and a complete blockade of these channels prevents firing. But if we use other sets of values for the conductance of sodium and L-type calcium channels, the mechanism of spontaneous initiation of spikes can vary. This sug-

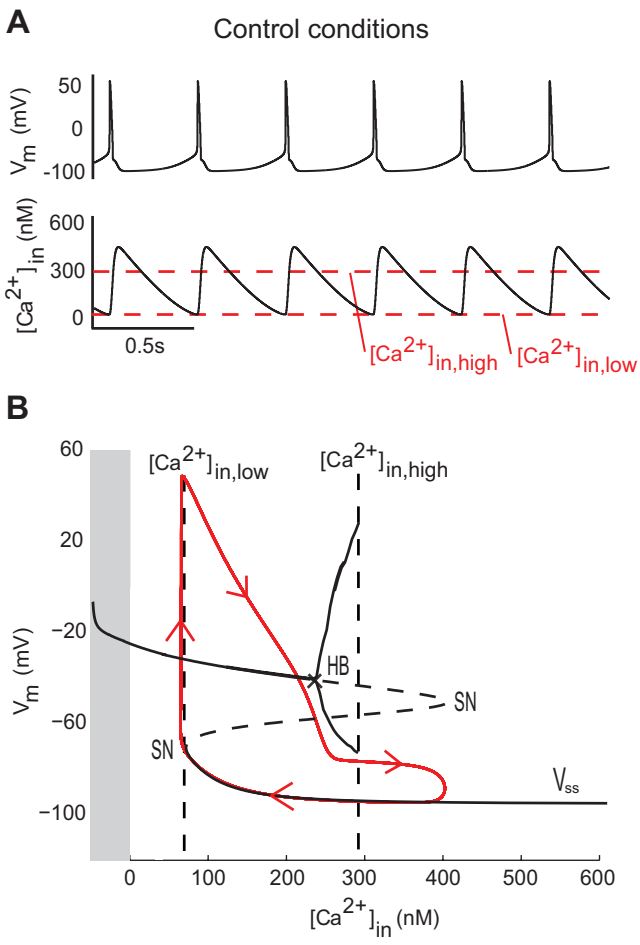

Figure 5.1 – Analysis of the spontaneous activity of the minimal model. A. Variations of the membrane potential (top) and the intracellular calcium concentration (bottom) over time. **B.** Sketch of the bifurcation diagram of the minimal model, with $[Ca^{2+}]_{in}$ as the bifurcation parameter. The gray part corresponds to negative values of $[Ca^{2+}]_{in}$, which is non physiological. V_{ss} denotes the steady-state curve for each value of the bifurcation parameters. The dotted part of V_{ss} shows its unstable part. HB denotes a Hopf bifurcation and SN a saddle-node bifurcation. The trajectory of the membrane potential is plotted in red.

gests a strong cooperation between sodium and L-type calcium channels to drive the pacemaker activity of DA neurons, as suggested by Guzman et. al [70].

The important consequences of this cooperation are illustrated in Fig. 5.2. The threshold separating a hyperpolarized state (white) from pacemaking (blue) is defined by an almost linear combination of the L-type calcium conductance $\bar{g}_{Ca,L}$ and the sodium conductance $\bar{g}_{Na}$. Moreover, when the conductance of one channel type is above a threshold value, these channels are sufficient to drive a spontaneous activity during blockade of the others. As a consequence, very similar neurons which would have minimal differences in their sodium or L-type calcium channel density may exhibit very different responses to experimental manipulations that shut off one of the two conductances, as illustrated in the various inserts of Fig. 5.2.

Panels **A** to **D** of Fig. 5.2 show the behavior of the minimal model in control conditions and during blockade of L-type calcium channels or sodium channels for a particular set of conductances. The blockade is modeled by setting the conductance to zero. Only the sodium and L-type calcium conductances slightly differ in the four represented situations. Note that the electrical behavior of each modeled neuron in control conditions is almost similar: the differences in parameter values are very small, and the mechanisms that underly their spontaneous activity are similar. However, these neurons react very differently to the blockade of one conductance. In the case of neuron **D** ($\bar{g}_{Na} = 240mS/cm^2, \bar{g}_{Ca,L} = 2.3mS/cm^2$), L-type calcium current inhibition completely inhibits the spontaneous activity of the cell, whereas an oscillatory behavior remains after a sodium current inhibition. On the basis of these experimental-like scenarii, we would conclude that the pacemaker activity of neuron **D** is driven by L-type calcium channels. If we examine neuron **A** ($\bar{g}_{Na} = 250mS/cm^2, \bar{g}_{Ca,L} = 2.2mS/cm^2$), L-type calcium current inhibition barely affects the firing rate and pattern of the cell, whereas a sodium current inhibition induces a hyperpolarization of the membrane. These observations would therefore lead to the opposite conclusion, namely that the pacemaker activity of neuron **A** is driven by sodium channels. As a consequence, the results of the two experiments would be contradictory, despite the great similarity of the neurons. More generally, Fig. 5.2 illustrates the fact that very similar neurons may produce drastically different responses to the same experimental manipulation. Remarkably, the four distinct behaviors exhibited by almost identical neurons in the minimal model can be exactly reproduced in the detailed model (see details in Supplementary Fig. S5.1).

Experimental confirmation that sodium and L-type calcium channels cooperate to generate spontaneous pacemaking in SNc DA neurons.

In order to confirm that the spontaneous initiation of spikes in DA neurons is mainly sustained by the cooperation between sodium and L-type calcium channels, we performed extracellular recordings (additional to those reported in Tab. 1) of these neurons in slices from adult rats containing the substantia nigra pars compacta. A potential advantage of this recording method is that it does not disrupt the contents of the neuron, contrary to

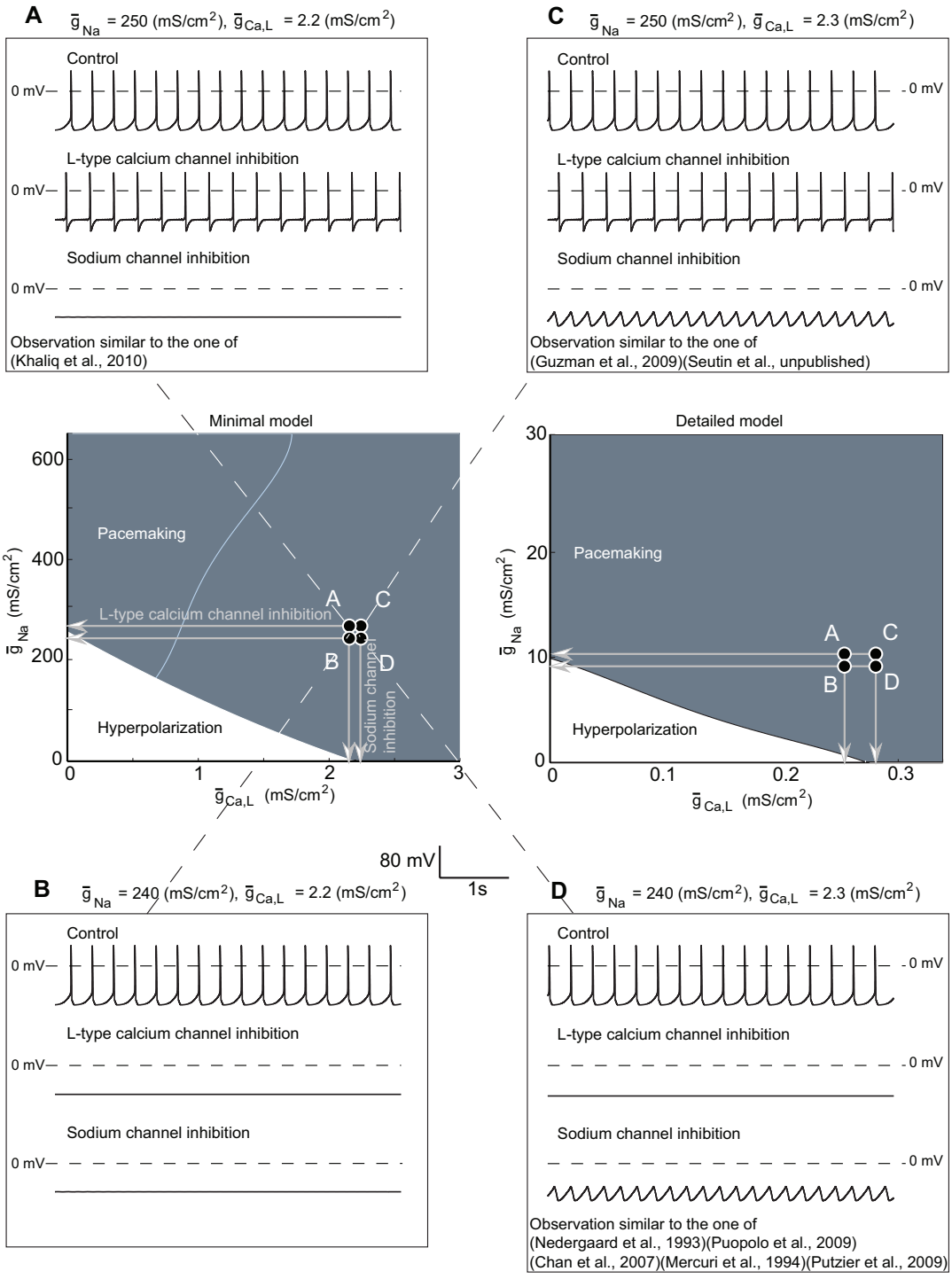

Figure 5.2 – Cooperation between sodium and calcium channels in the generation of spontaneous activity in the minimal model and in the detailed model. The center panels show the type of pacemaker activity according to the value of sodium and L-type calcium conductances. The white zone represents the couples of conductances which result in a hyperpolarized state of the cell and the dark blue zone accounts for pacemaking. Each insert shows the behavior of the model in control condition and during a blockade of L-type calcium channels or sodium channels for a particular set of conductances. The pacemaker behavior of the model strongly relies on the values of both the sodium and the L-type calcium conductances.

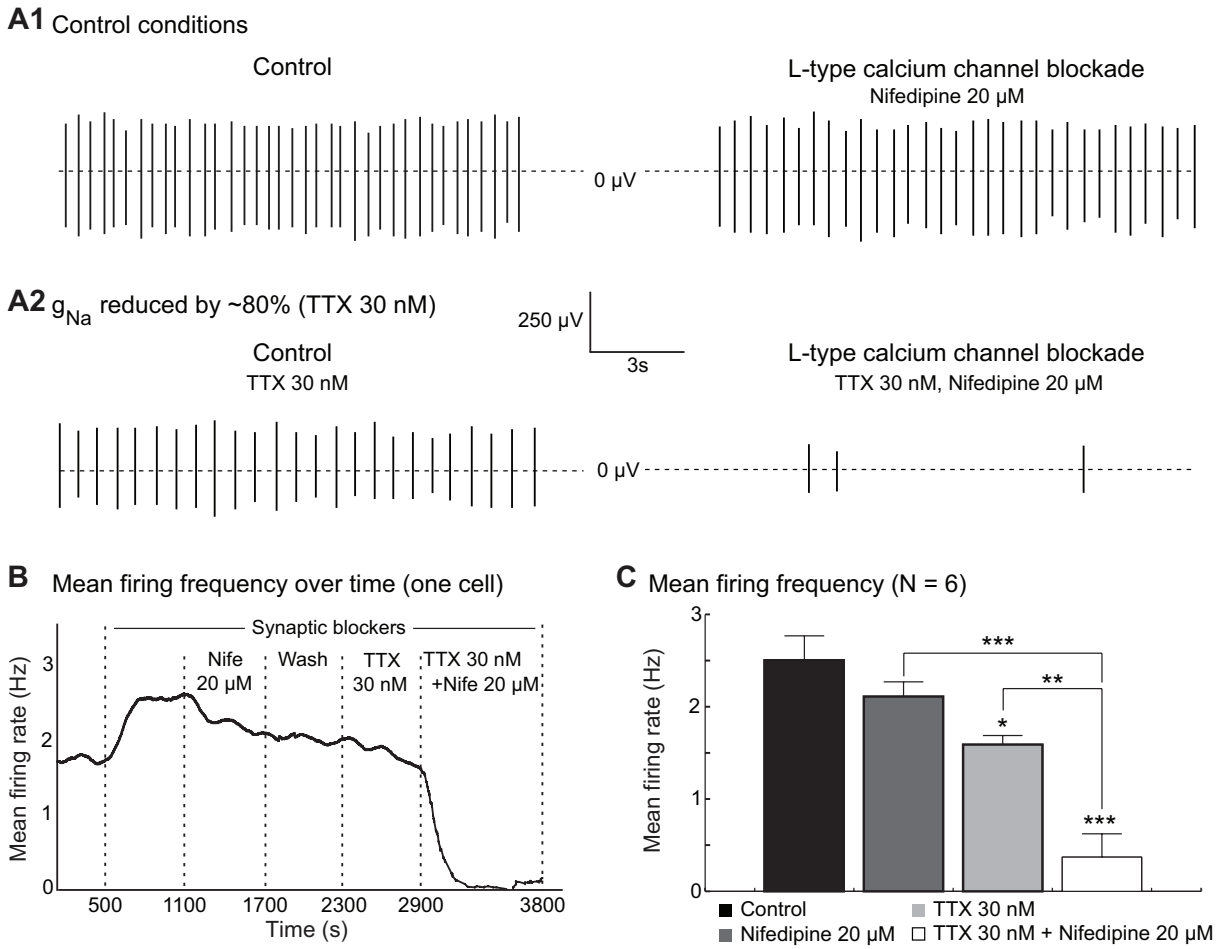

Figure 5.3 – Effect of sodium and L-type calcium channel blockade on the firing of SNc dopaminergic neurons in vitro. **A1.** Extracellular recording of a DA cell in control conditions (left) and after application of 20 μM nifedipine (right). **A2.** Same as **A1.** after a 80% reduction of the sodium conductance by the superfusion of 30 nM TTX. **B.** Evolution of the mean firing rate (samples of 2 minutes) of a DA cell over time. **C.** Mean firing frequency (N = 6) for each condition (mean $\pm$ sem). A simultaneous application of TTX and nifedipine affects the firing of the cells more strongly, as compared to the application of either of the two compounds alone. All experiments were performed in the presence of blockers of synaptic transmission. Note that the superfusion of the blockers produces an excitation of the neurons, which can be attributed to the block of inhibitory D2 autoreceptors. *P $<$ 0.05, **P $<$ 0.01, ***P $<$ 0.001.

conventional patch-clamp recordings. For these experiments, we superfused the slices with blockers of synaptic transmission (10 μM CNQX, 1 μM MK801, 10 μM SR95531, 1 μM sulpiride and 1 μM CGP55845, which block AMPA, NMDA, $GABA_A$, D2 and $GABA_B$ receptors, respectively), in order to isolate the neurons from their afferences. Control experiments showed that application of the synaptic blockers alone induced a small increase in firing rate which was stable for at least one hour (n=4, Supplementary Fig. S5.2).

We next tested the effect of 20 μM nifedipine (a L-type calcium channel blocker), 30 nM TTX (a sodium channel blocker), as well as their simultaneous application on the firing rate of DA cells, respectively. This concentration of TTX was used because it had been shown to block a major fraction (about 80%) of the somatic sodium conductance [165], but did not abolish action potentials. The precise experimental protocol is shown graphically in Fig. 5.3B and is described in detail in the Methods section.

These recordings were performed on eleven neurons. In one case, nifedipine completely inhibited the spontaneous activity of the cell. In four other cells, nifedipine produced little effect, whereas TTX completely suppressed the firing (not shown). In the six other neurons, coapplication of nifedipine and TTX inhibited the

firing to a greater extent than either agent alone. Indeed, an ANOVA test showed that the firing rate of the neurons was different in the four experimental conditions (synaptic blockers alone, +nifedipine, +TTX, +TTX and nifedipine, F[3,20] = 21.12, p =0.000002). The application of nifedipine alone did not significantly affect the firing rate of these cells (from 2.51 $\pm$ 0.26 Hz to 2.11 $\pm$ 0.16 Hz, mean $\pm$ s.e.m., p = 0.52, Tukey's post hoc test) (Fig. 5.3). The application of TTX alone significantly but only partially decreased the firing rate of the cells to 1.59 $\pm$ 0.10 Hz ($p < 0.05$), and reduced the amplitude of spikes. The latter effect is in agreement with the fact that the maximal sodium conductance is quite reduced. The simultaneous application of TTX and nifedipine reduced the firing rate of the cells to 0.37 $\pm$ 0.25 Hz ($p < 0.001$), and this reduction was significantly larger than the effect of either agent alone ($p < 0.001$ vs nifedipine, $p < 0.01$ vs TTX). Moreover, the simultaneous pharmacological block of sodium (80%) and L-type calcium channels almost completely eliminated the spontaneous firing in 5 of these 6 cells (frequency $\leq$ 0.4 Hz). In summary, our experiments confirm that the degree of cooperation between the two currents is highly variable from neuron to neuron, even in a fixed experimental protocol.

Pacemaking can be driven by different cooperating currents.

The fact that L-type calcium channels and sodium channels can cooperatively drive the pacemaker activity of DA neurons can be explained by comparing the I-V curves of the two currents (Supplementary Fig. S5.3A). Indeed, Putzier et al. recently showed that the only critical parameter of the L-type calcium current for pacemaking is the value of its half-activation potential ($V_{\frac{1}{2}}$), which should not be too negative [144]. Moreover, they showed that artificial NMDA receptors that would have a similar half-activation potential would also induce sustained firing. The half-activation potentials of sodium and L-type calcium channels are very similar (Supplementary Fig. S5.3A), which explains why they can cooperate in the pacemaking generation.

This similarity is observed in the detailed model as well (Supplementary Fig. S5.3B). If we compare the I-V curves of the other calcium currents, it is clear that, in this model, N-type calcium channels have a $V_{\frac{1}{2}}$ similar to the one of sodium and L-type calcium channels, whereas $V_{\frac{1}{2}}$ of T-type calcium channels is much more negative. On the basis of these observations, the previous analysis suggests that N-type calcium channels should be able to induce pacemaking if their density is high enough whereas T-type channels, which have a significant more negative $V_{\frac{1}{2}}$, should not. We test this hypothesis in Fig. 5.4 (where we reduce the sodium conductance to reduce the contribution of sodium channels to the pacemaking) using the detailed model. As predicted, a N-type calcium current of sufficient amplitude is able to drive a low-frequency pacemaker activity, whereas a T-type calcium current is not, even with a very high maximal conductance value. Moreover, N-type channels are able to induce SOPs when sodium channels are blocked, as L-type channels do (Fig. 5.2C and D). These simulations are therefore in agreement with the prediction that whatever the nature of the depolarizing current, the only parameter which is critical is its voltage dependence, and more precisely its half-activation potential [144].

The common mechanism of pacemaking and slow oscillatory potentials does not imply that these oscillatory activities are correlated or are affected in the same way by the same experimental manipulation.

Our minimal model also sheds light on the mechanisms of, and related controversies on, slow oscillatory potentials (SOPs). Indeed, it has experimentally been shown that SNc DA neurons exhibit SOPs during application of TTX *in vitro* [133, 139], and that these SOPs are driven by L-type calcium channels [70]. Recently, it has been shown that pacemaking and SOPs are uncorrelated [70], which led to the conclusion that these two oscillatory behaviors are driven by different mechanisms, thus rejecting L-type calcium channels for pacemaking.

In addition, it has been reported that block of the SK current on TTX-treated DA neurons strongly affects the shape of SOPs. Namely, this manipulation significantly increases the duration of the depolarizing and hyperpolarizing phases [139]. This observation led to the hypothesis that, in control condition, this inhibition might induce burst firing in DA neurons. However, experiments have invalidated this intuitive suggestion, SK channel blockade only inducing irregularities in the firing of these cells, but not bursting (at least not reproducibly) [200]. These contradictory observations can be explained through an analysis of the behavior of the minimal model in configurations that mimic these experiments.

For a sufficiently high value of $\bar{g}_{Ca,L}$ (compare Fig. 5.2C,D and Fig. 5.2A,B), SOPs are also observed after blockade of the sodium current in the minimal model (Fig. 5.5C). As in the case of pacemaking, these SOPs are synchronized with the calcium oscillations (Supplementary Fig. S5.4). Fig. 5.5 shows how sodium channel blockade affects the bifurcation diagram in the presence and in the absence of SK channels. As illustrated in the figure, sodium channel blockade has no effect on the low threshold, which implies that a same mechanism initiates both spikes and SOPs in the minimal model.

In contrast, sodium channel blockade has a critical impact on the high threshold. Indeed, the Hopf bifurcation

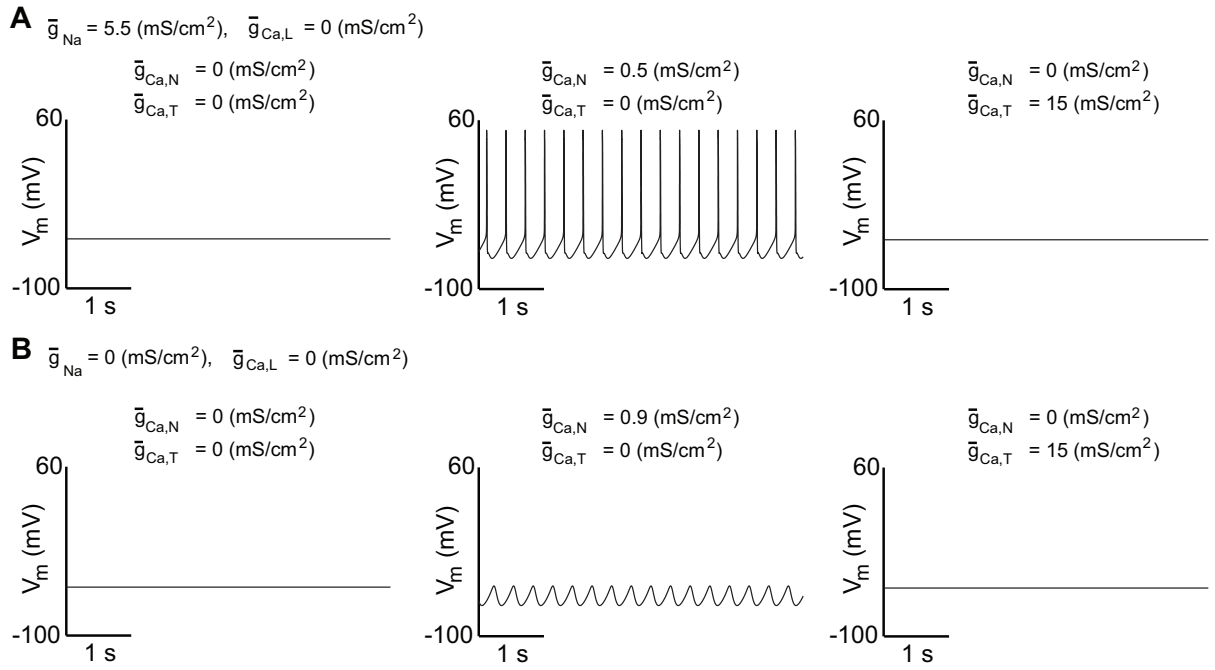

Figure 5.4 – Ability of a N-type, but not of a T-type calcium current, to drive pacemaker activity in the absence of all other calcium channels in the detailed model. A. Variations of the membrane potential of the modeled neuron over time when all calcium currents are blocked, in the presence of N-type calcium channels and in the presence of T-type calcium channels, from left to right, respectively. **B.** Same as **A.**, but during an inhibition of sodium channels. N-type calcium channels in sufficient density are able to generate an oscillatory behavior, contrary to T-type calcium channels.

which defines the high threshold in pacemaking vanishes when sodium channels are blocked. As a consequence, the high threshold of SOPs is defined at the right saddle-node bifurcation, which is masked by the Hopf bifurcation in control conditions. This implies that, whereas the depolarization mechanism is identical in spikes and SOPs, the repolarization mechanisms are different.

This difference has significant consequences on the model behavior, all consistent with experimental data:

(i) SK channel blockade has little effect on the left saddle-node bifurcation but a dramatic effect on the right one (compare Fig. 5.5A,C and Fig. 5.5B,D). This effect is masked in normal conditions because of the Hopf bifurcation. As a consequence, inhibition of the SK current barely affects the pacemaker firing in normal conditions (Fig. 5.5A,B) but strongly affects SOP frequency when sodium channels are blocked (Fig. 5.5C,D). These predictions are in agreement with experimental data [139, 200].

(ii) There is no reason to expect a strong correlation between spikes and SOPs.

Fig. 5.6A shows that the interevent interval histograms of pacemaking (in light blue) and SOPs (in dark blue) do not match either in the presence (Fig. 5.6A, left) or in the absence (Fig. 5.6A, right) of SK channels. Moreover, depending on the parameters of the model, spike rate can be lower or higher than SOP oscillation rate (Fig. 5.6B), as observed experimentally [70]. In Fig. 5.6, the parameters that are varied are the conductances of L-type calcium channels and SK channels. The main origin of this lack of correlation is that the quantity and kinetics of calcium entry taking place during an action potential strongly differs from the one taking place during the depolarized phase of SOPs. This affects the rate of their respective oscillations (Supplementary Fig. S5.5).

In addition, Guzman et. al recently showed that spikes are much more regular than SOPs in DA neurons [70]. In its low-noise configuration (representing the *in vitro* condition), our model exhibits similar results (Fig. 5.6C, which can be compared to Fig. 3e of [70]). Indeed, we found that SOPs are much more sensitive to noise than spikes in the presence of SK channels, mainly because SOP oscillations induce less calcium entry than spikes and because the kinetics of calcium entry is slower (Supplementary Fig. S5.5).

These results show that a lack of correlation between spikes and SOPs does not necessarily imply that the gen-

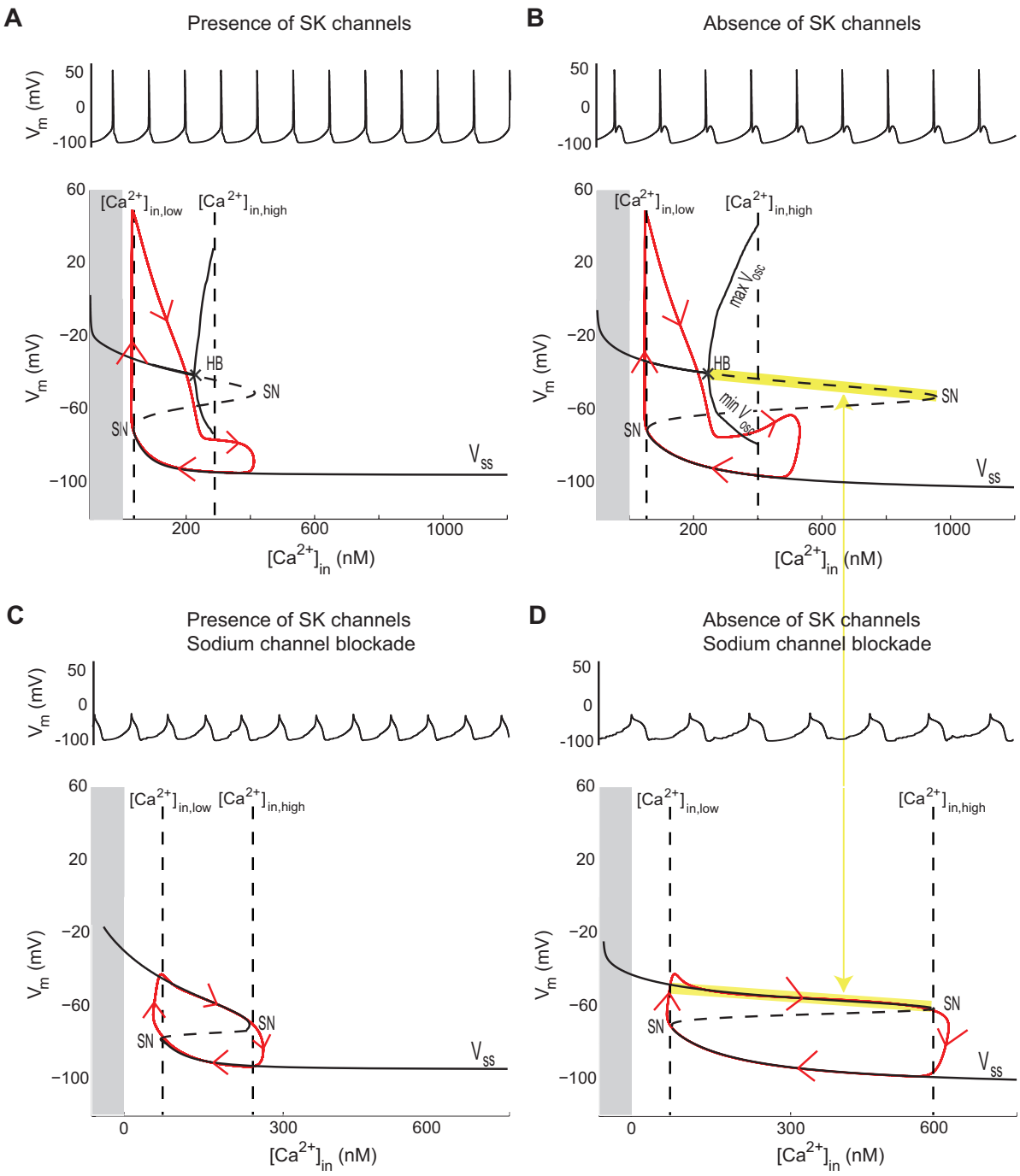

Figure 5.5 – Analysis of the effect of SK channel blockade on the spontaneous activity of the minimal model. A. and **B.** Variations of the membrane potential over time (top) and sketch of the bifurcation diagram of the minimal model (bottom, with $[Ca^{2+}]_{in}$ as the bifurcation parameter) in the presence and in the absence of SK channels. The grey part corresponds to negative values of $[Ca^{2+}]_{in}$, which are non physiological. V_{ss} denotes the steady-state curve for each value of the bifurcation parameters. The dotted part of V_{ss} shows its unstable part. HB denotes a Hopf bifurcation and SN denotes a saddle-node bifurcation. Trajectories of the membrane potential are plotted in red. **C.** and **D.** Same as **A.** and **B.** but when sodium channels are blocked. The frequency of SOPs is almost halved, whereas the frequency of spikes is barely affected. This simulations were performed in the absence of noise, which would induce irregularities in the absence of SK channels.

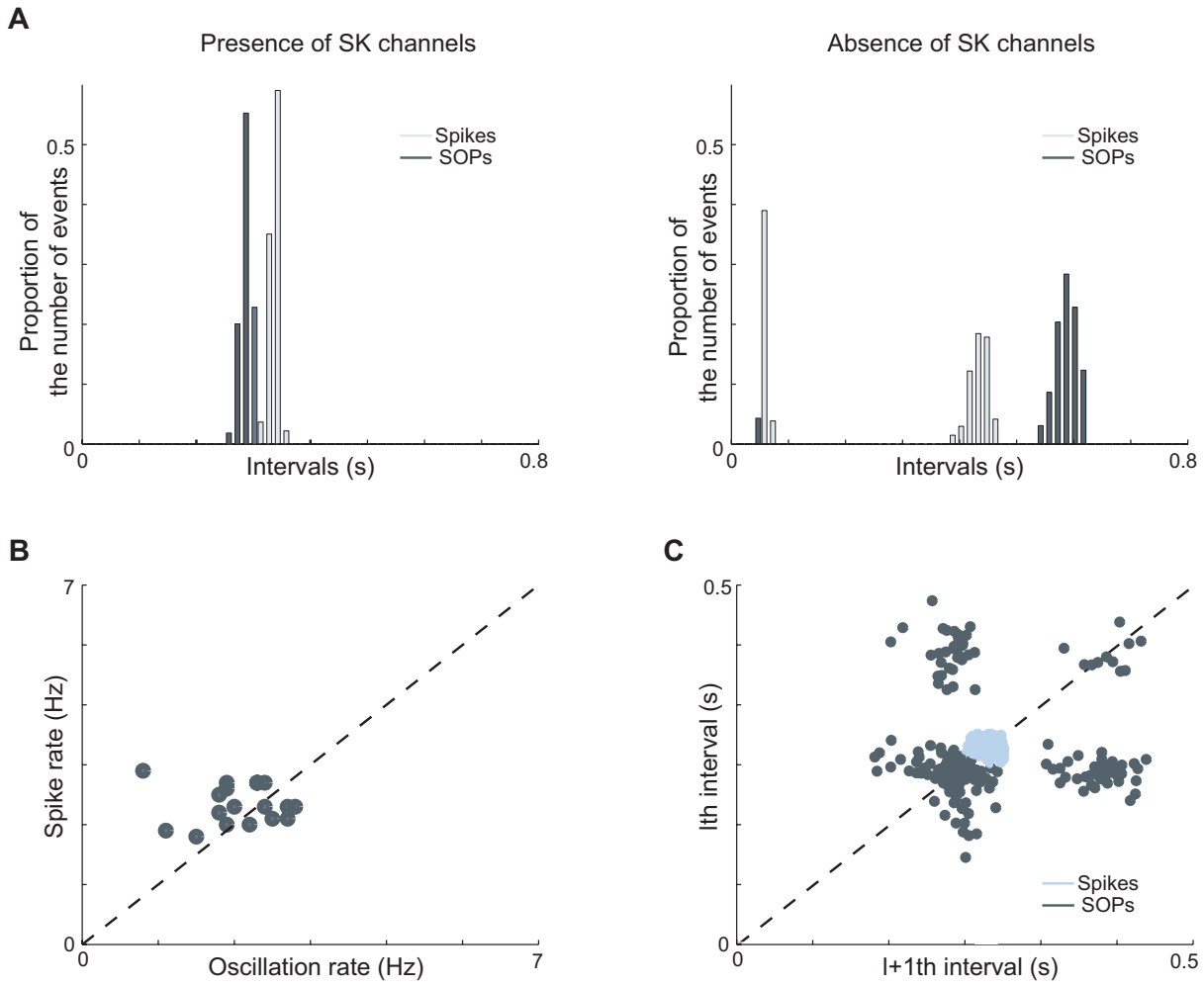

Figure 5.6 – Comparison of the pacemaking ("spikes") and slow oscillatory potentials ("SOPs") in the minimal model. Note that the simulations have been performed using *in vitro*-like conditions (low amplitude noise). **A.** Interspike interval histograms (ISIh's) of a set of modeled cells in the presence (left) and in the absence (right) of SK channels. The light blue bars account for spikes in control conditions and the dark blue bars for SOP oscillations during sodium channel blockade. **B.** Comparison of the rate of spikes and SOPs for different values of $\bar{g}_{Ca,L}$ and $\bar{g}_{K,Ca}$. **C.** Plot of successive spike intervals (light blue) or successive SOP intervals (dark blue) of a set of modeled cells. Although they are driven by the same mechanisms, spikes and SOPs are not correlated. Moreover, SOPs are more sensitive to the noise.

erating mechanism of these two oscillatory behaviors is different. Therefore, this experimental observation may not be used to dismiss a role of L-type calcium channels in the generation of spikes in DA neurons.

Discussion

The generation of spikes during low-frequency pacemaker firing mainly relies on the cooperation between sodium and L-type calcium channels, whereas its rhythm follows the variations in $[Ca^{2+}_{in}]$.

In spite of many experimental studies, the precise mechanisms underlying the spontaneous initiation of spikes in DA neurons are still largely debated in the literature. Using our minimal model as well as a detailed model of a DA neuron, we extracted two critical parameters for the low frequency spontaneous firing.

Firstly, low-frequency single-spike firing and high-frequency intra-bursts firing have to be sustained by two dynamics operating on different time scales. Fast firing is limited by the refractory period of action potentials, which is fixed by the kinetics of voltage-gated channels. On the other hand, the dynamics that are the most likely to limit the rate of low-frequency firing are the variations of the intracellular calcium concentration. Indeed, an accumulation of calcium in the cytoplasm strongly reduces the excitability of the cells, through the inactivation of depolarizing currents (i.e. L-type calcium currents) and the activation of hyperpolarizing currents (i.e. calcium pumps and SK channels). This is in agreement with experimental data, which show that replacement of calcium with either cobalt [143] or magnesium [102] strongly affects pacemaking.

Secondly, the spontaneous initiation of action potentials in DA neurons is the result of the cooperation between various depolarizing currents. In agreement with the experimental results of Putzier et al. [144], we found in the detailed model that any depolarizing current having a half-activation potential less negative than $-50mV$ (voltage-dependent sodium channels, L-type and N-type calcium channels) may play a role in this initiation. Their relative contribution, as well as the robustness of pacemaking, depend on the respective density of each channel type. Therefore, the fact that the selective blockade of a particular channel does not completely disrupt pacemaking does not mean that these channels are not involved in physiological pacemaking. This might be an important note of caution for experimentalists. Moreover, we confirmed experimentally that L-type calcium and sodium channels do indeed cooperate to generate pacemaking with a degree of cooperation that is highly variable. This precise observation has never been made previously.

Experimental protocols are not robust to physiologically plausible variability.

The most contradictory experimental results obtained on DA neurons are probably those concerning the role of L-type calcium channels in the spontaneous initiation of spikes *in vitro* (Table 1). Using very similar modeled neurons that differ by less than 1% in one conductance parameter (all remaining parameters being identical), we were able to reproduce these contradictory results both in our minimal model and in a detailed model of DA neurons.

Such subtle differences in conductance parameters are quite likely to occur in various experimental conditions. For example, it has recently been shown that there are quantitative differences between DA neurons from the SNc and the VTA in terms of density of these conductances [102, 143]. It was proposed that sodium channels play a major role in the spike generation of VTA DA cells, whereas calcium channels are predominant in SNc DA neurons. Among other findings, replacement of calcium with cobalt in SNc neurons completely inhibits the firing, whereas replacement of calcium with magnesium in VTA neurons increases the firing rate [102, 143]. Both these effects are also observed in the minimal and detailed models whit slightly different maximal sodium conductances (Supplementary Fig. S5.6).

A second source of contradictory experimental results might be the difference between the preparations that are used in different laboratories. For instance, in the case of DA neurons, in which the initial segment is often remote from the soma [13], it is clear that the total sodium current will be smaller in acutely dissociated neurons than in neurons recorded in the slice preparation. In terms of the model that we have developed, this probably means that the small conductance variations illustrated in Fig. 5.2 could result from minor experimental variations such as dissociated neurons vs neurons recorded in slices, as well as variable developmental stages of the animals.

The lack of correlation between spikes and slow oscillatory potentials is compatible with a same generating mechanism.

SOPs exhibited by DA neurons during blockade of sodium channels have been largely studied [70, 133, 139] and compared to the spontaneous spiking activity. Moreover, it has been recently shown that the two oscillatory patterns are not correlated [70], a phenomenon that is also observed in our model. It is tempting to conclude from this observation that their underlying mechanisms are different. However, our analysis shows that the generation mechanisms are actually the same. Moreover, Fig. 5.5 clearly illustrates that the different effect of SK channel blockade on pacemaking and SOPs simply arises from the fact that the high intracellular calcium concentration threshold only slightly changes when sodium channels are present, whereas a more than two fold change in this high threshold occurs when sodium channels are blocked.

Chapter 6

Entrainability Mechanisms *in vivo*

The present chapter focuses on the role of SK channels on the firing pattern of dopaminergic neurons *in vivo*. Remarkably, these channels are totally insensitive to the variations of membrane potential, which makes their activity an image of the intracellular calcium concentration. These channels are important and prevalent in a large set of neurons (for a recent review, see e.g. [187]). In hippocampal CA1 pyramidal cells, these channels are located close to NMDA receptors and mediate a negative feedback loop by hyperpolarizing the membrane when calcium flows through NMDA channels. This hyperpolarization in turn reduces the NMDA conductance and reduces the development of synaptic plasticity [134]. In dopaminergic neurons, it has been shown that the blockade of SK channels increases irregularity *in vitro* [200] and bursting *in vivo* [76, 96, 191].

Here, we extract the firing mechanisms of dopaminergic neurons in *in vivo*-like condition (i.e. submitted to synaptic inputs) through the mathematical analysis of the minimal model proposed above. We find that the main role of SK channels in dopaminergic neurons is to filter excitatory inputs, in order to protect the endogenous single-spike firing pattern (i.e. inactive mode) of the cell. On the other hand, when SK channels are blocked, the neuron is critically sensitive to these excitatory inputs, resulting in irregularities or bursting (i.e. active mode) depending on the amplitude of the excitatory noise. Moreover, the bursting mode is strongly entrained by synaptic currents. These results suggest that the information coded in the synaptic inputs is only transmitted to the neuron when SK channels are downregulated, these channels being key players in the control of the switch of firing pattern of dopaminergic neurons.

We also find that SK channels may control the synchrony of sub-populations of dopaminergic neurons submitted to a common excitatory input. Indeed, SK channels normally filter this common excitatory input, letting the neurons firing asynchronously in low-frequency single spike firing according to their respective endogenous rhythm. In contrast, when SK channels are downregulated, the neurons are strongly entrained by the common input, leading to synchronous bursting in the population. This switch of electrical activity is of critical importance for the relative activation of post-synaptic D1 and D2 receptors. Indeed, Dreyer and colleagues showed that, whereas D2 receptors are saturated during asynchronous single-spike firing, synchronized bursts significantly activates D1 receptors [38].

To summarize, we propose that SK channels, through their sensitivity to the intracellular calcium concentration, are regulators of synaptically-induced bursting and synchrony of dopaminergic neurons, whereas the shape of bursting mainly relies on the interaction between the endogenous rhythm of the cell and the synaptic afferents, where the information should be coded. Importantly, the control of firing pattern and synchrony being sustained by a same mechanism, their concomitance is ensured.

Results

SK channels regulate the synaptically-induced accumulation of calcium in the cell, balancing the rise in concentration that accompanies high frequency firing.

After having extracted the pacemaking mechanisms of the DA neuron model, we now analyze how this firing pattern is affected *in vivo*, starting by analyzing the effect of a step input of synaptic current (Fig. 6.1).

In the presence of SK channels, the firing pattern is barely affected, because the step input of excitatory current does not affect the low ($[Ca^{2+}]_{in,low}$) and high calcium thresholds ($[Ca^{2+}]_{in,high}$) that corresponds to the initiation and termination of spiking, respectively (Fig. 6.1,right). Physiologically, the opening of L-type calcium channels by supra-threshold synaptic inputs (or any other source of calcium), activates the SK channels through the rise of calcium concentration (see [117] for experimental evidences). The resulting outward current balances the inward current induced by synaptic inputs.

As illustrated in Fig. 6.2, the effect of a step input

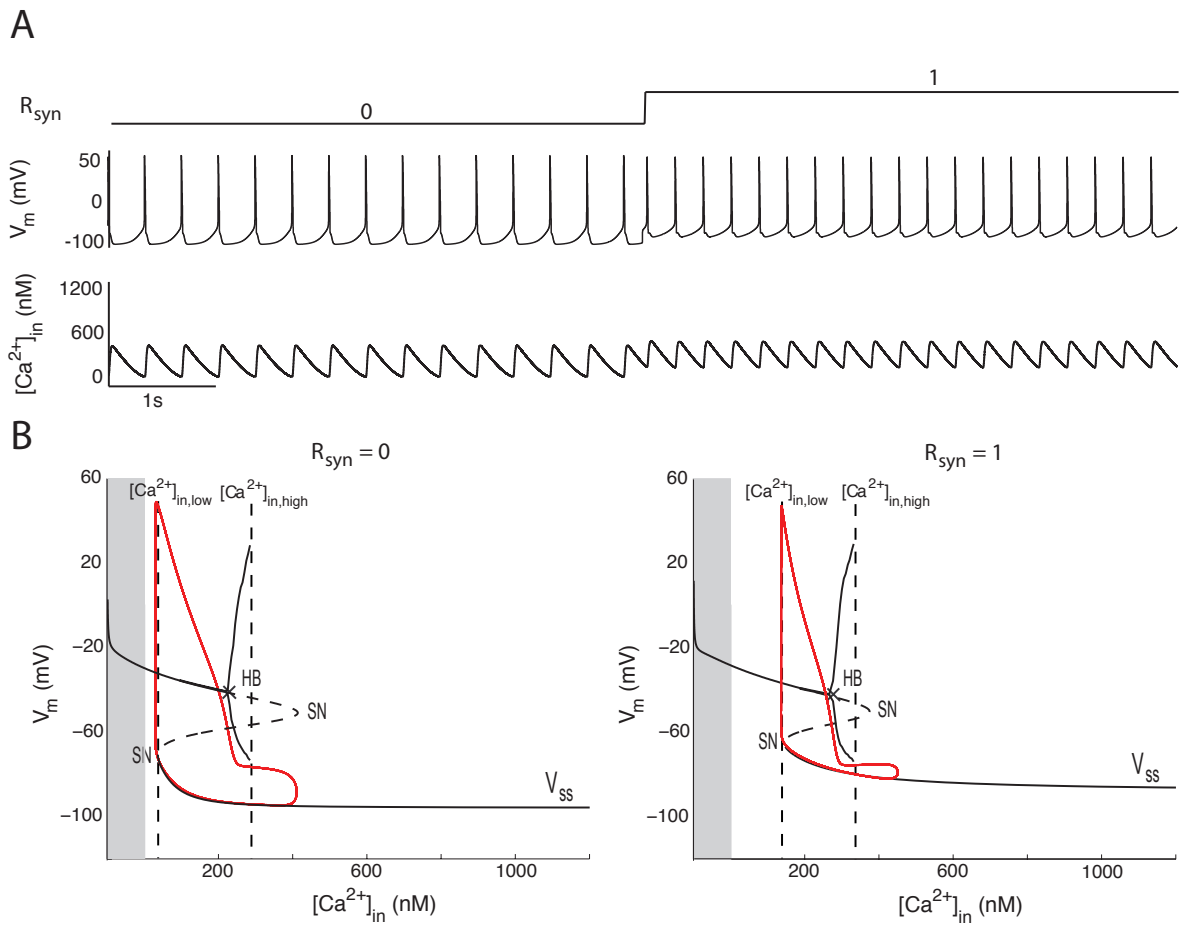

Figure 6.1 – Effect of a step input of synaptic current activation on the cell firing in the presence of SK channels. A. Variations of synaptic input activation (top), the membrane potential (middle) and the intracellular calcium concentration (bottom) over time. **B.** Trajectories of membrane potential time-courses in the bifurcation diagram in the absence (left) and during the application of an external stimulation (right). The application of a step input barely affects the firing of the cell in the presence of SK channels.

is dramatically different in the absence of SK channels. The step input now changes the current balance, dramatically increasing the low and high calcium thresholds. As a consequence, it takes many action potentials for the calcium to accumulate beyond the hyperpolarizing threshold. If the inward step current is large enough, the calcium balance may even stabilize the calcium concentration below the high threshold, resulting in sustained high frequency firing (Fig. 6.2, right). Similarly, the larger the previous synaptic activation, the more the cell has to evacuate calcium before firing again, and thus the longer the hyperpolarization period (Supplementary Fig. S1). Qualitatively similar electrophysiological responses to a step of depolarizing current in the presence and during blockade of SK channels have been observed in experiments on dopaminergic neurons [160].

Fig. 6.3 shows how the low and high calcium thresholds evolve with the level of input current. In the presence of SK channels (Fig. 6.3C), they are barely affected whereas both thresholds dramatically increase with the input current in the absence of SK channels (Fig. 6.3D). These statements can be easily interpreted physiologically. As previously mentioned, the accumulation of calcium into the cytoplasm reduces the excitability of the cell, through the inactivation of inward currents and the activation of outward currents. Therefore, the cell is solely able to fire spontaneously when $[Ca^{2+}]_{in}$ is lower than a particular value, which we called the high calcium threshold $[Ca^{2+}]_{in,high}$. This threshold, such as the low threshold, corresponds to a particular combination of the inward and the outward currents.

When synaptic inputs activate depolarizing channels, they change the combination of the ionic currents, and the cell becomes more excitable for the same value of

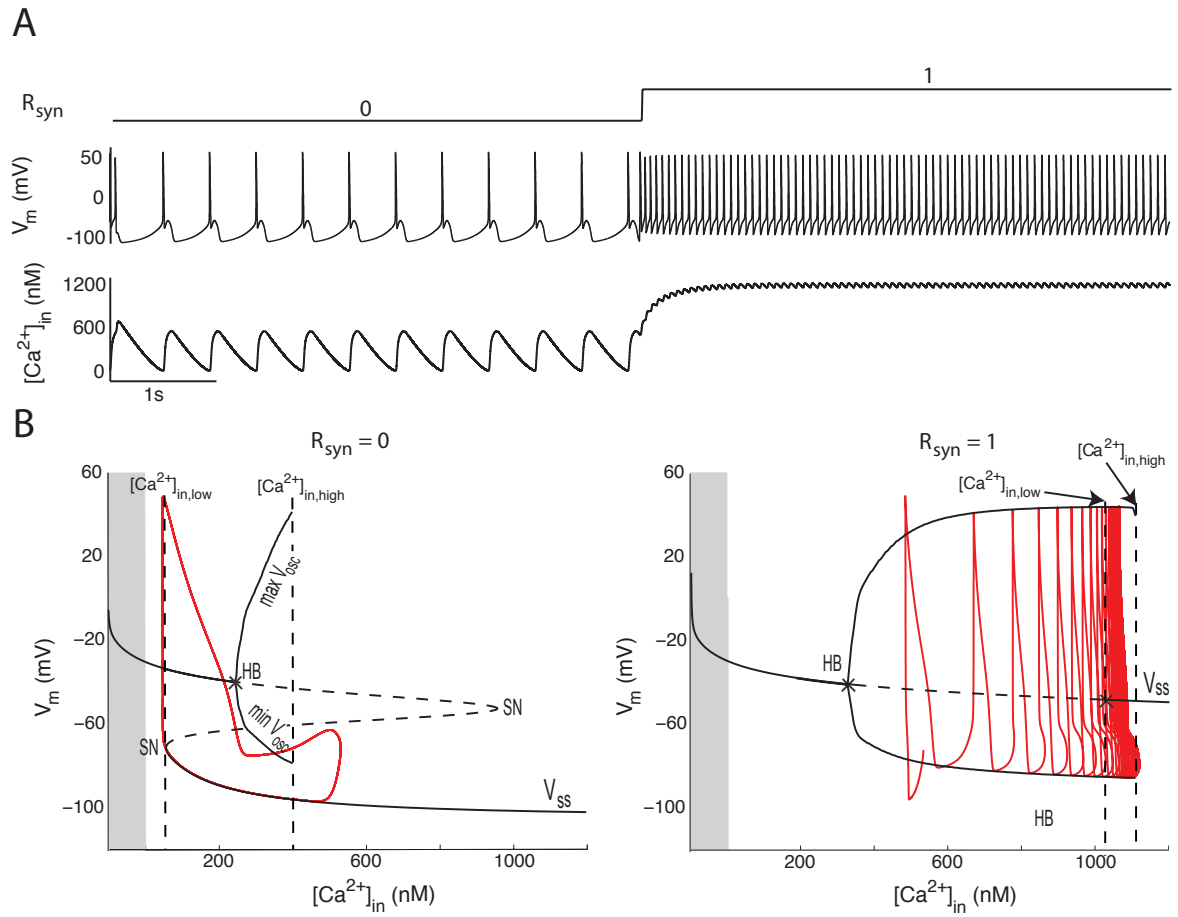

Figure 6.2 – Effect of a step input of synaptic current activation on the cell firing in the absence of SK channels. **A.** Variations of synaptic input activation (top), the membrane potential (middle) and the intracellular calcium concentration (bottom) over time. **B.** Trajectories of membrane potential time-courses in the bifurcation diagram in the absence (left) and during the application of an external stimulation (right). The application of a step input induces fast firing accompanied by intracellular calcium accumulation in the absence of SK channels.

cytoplasmic calcium. As a consequence, the neuron is able to fire, and thus accumulate calcium, to an extend at which the entry of calcium exactly opposes the excitation induced by the synaptic input. This value of cytoplasmic calcium defines the new $[Ca^{2+}]_{in,high}$.

When present, SK channels are very sensitive to variations of $[Ca^{2+}]_{in}$ and may generate high amplitude currents. Therefore, only small variations of calcium are needed for these channels to generate a hyperpolarizing current that fully offsets the excitatory depolarizing current (Fig. 6.4A,C). This explains why the calcium channels are barely sensitive to synaptic stimulation in the presence of SK channels. On the other hand, when SK channels are blocked, the effect of calcium accumulation on the excitability of the cell is dramatically reduced, this accumulation only mildly affecting the other calcium-regulated channels. A large calcium entry is therefore needed to counterbalance the synaptic stimulation, and the values of the calcium thresholds become significantly larger 6.4b,d. However, because the filtering mechanism of SK channels only offsets a depolarizing current smaller or equivalent to their maximal current, any depolarizing pulse larger than this current would strongly affect the firing, even in the presence of SK channels.

A similar behavior is observed in the detailed model, as shown in Fig. 6.3E,F. As in the case of the minimal model, the calcium thresholds are barely sensitive to the step input current in control conditions, whereas the latter strongly increases these thresholds when SK channels are blocked. The only difference between the detailed and the minimal model is the difference between the low and high calcium thresholds. In the detailed one, the two values almost coincide due to additional balancing currents, such as N-type and T-type calcium channels.

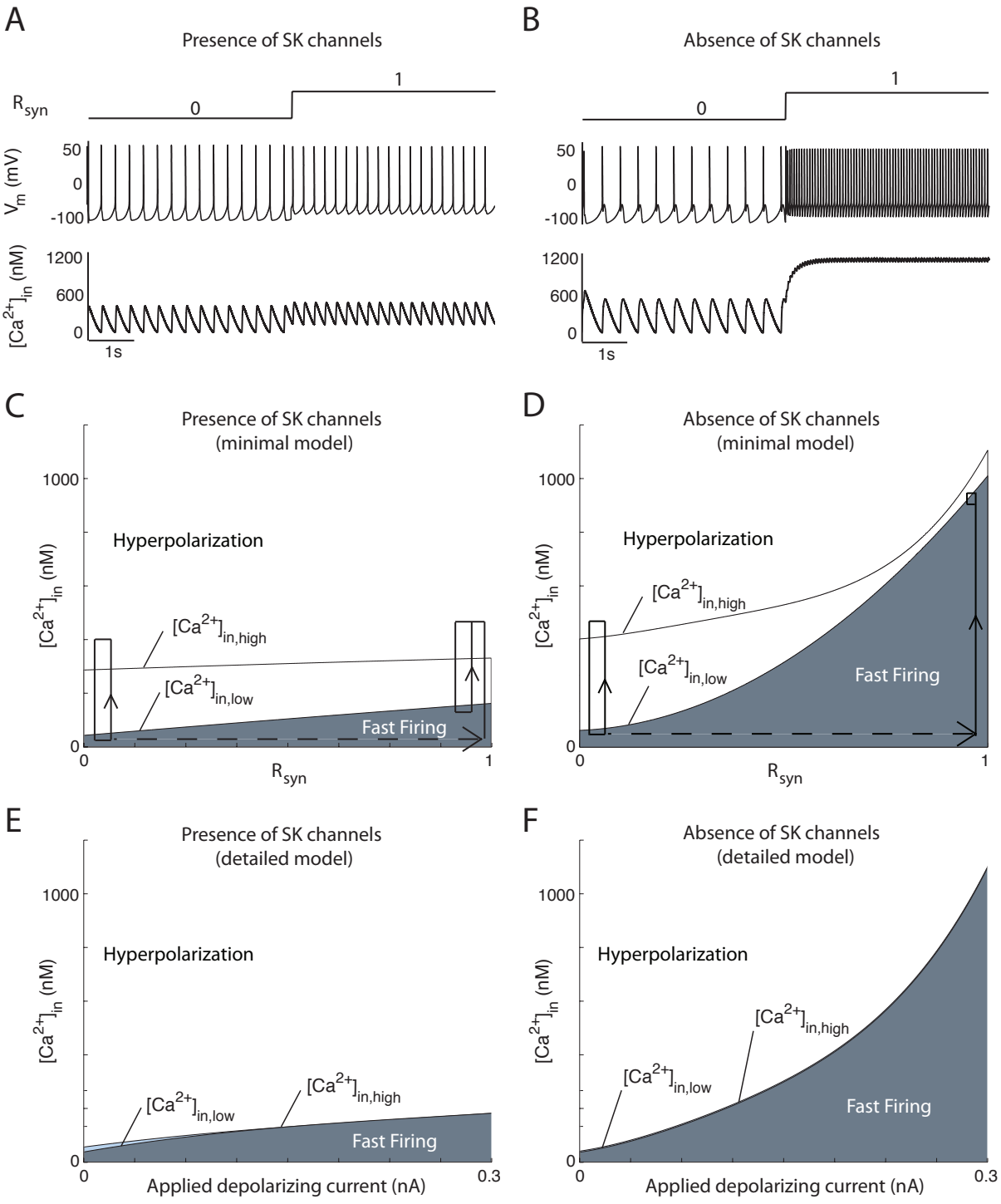

Figure 6.3 – Effect of a step input of synaptic current activation on the cell firing in the presence (left) and in the absence (right) of SK channels. A. and **B.** variations of synaptic input activation (top), the membrane potential (middle) and the intracellular calcium concentration (bottom) over time in the presence and in the absence of SK channels, respectively. **C.** and **D.** Variation of the calcium thresholds in the simple model according to synaptic current activation in the presence and in the absence of SK channels, respectively. **E.** and **F.** Variation of the calcium thresholds in the quantitative model according to synaptic current activation in the presence and in the absence of SK channels, respectively. The rise of the calcium thresholds with a rise of synaptic currents is strongly attenuated by the presence of SK channels. As a consequence, cell firing is highly sensitive to a step input of synaptic current activation only in the absence of SK channels.

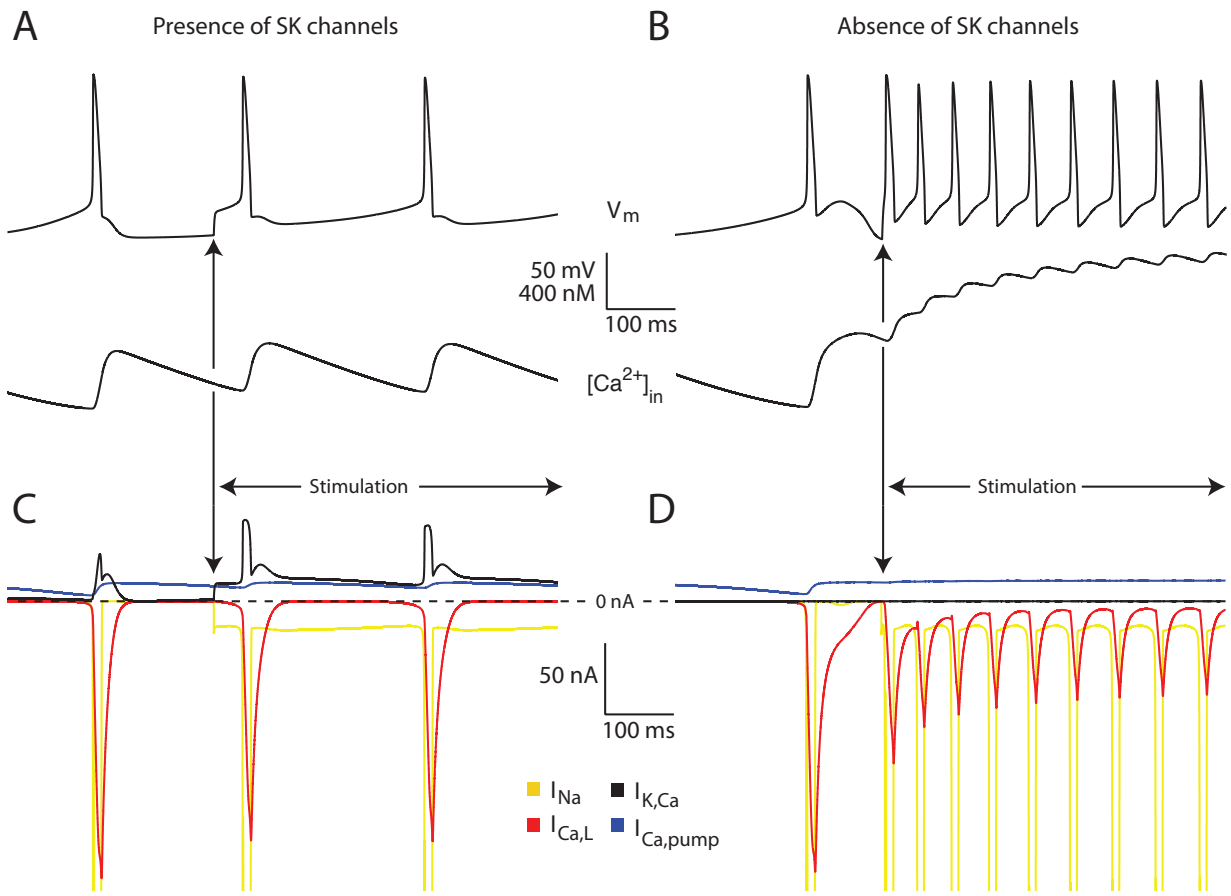

Figure 6.4 – Effect of a step input of synaptic current activation on the cell firing in the presence (left) and in the absence (right) of SK channels. A. and **B.** Variations of the membrane potential (top) and the intracellular calcium concentration (bottom) over time in the presence and in the absence of SK channels, respectively. **C.** and **D.** Variations of the ionic currents over time in the presence and in the absence of SK channels, respectively. Yellow:sodium+input currents, red: calcium current, black: calcium-activated potassium current, blue: calcium pump current. When present, SK channels counteract the increase of inward current generated by the synaptic input, no other outward current having a similar filtering effect. As a consequence, cell firing is highly sensitive to a step input of synaptic current activation only in the absence of SK channels.

A periodic activation of excitatory synaptic currents induces burst firing only in the absence of SK channels.

The analysis of a step input in the previous section is now extended to a (still not physiological) periodic input (Fig. 6.5). In the presence of SK channels, the periodic input only mildly affects the inter-spike intervals in the tonic firing mode (Fig. 6.5A). The high threshold being almost independent from the synaptic activation, the firing pattern is not significantly affected. A variation of synaptic currents only speeds up or delays the generation of the next action potential, hence the low frequency irregularities in the firing pattern of the cell. Note that, in that configuration, the firing is not time-locked with the variations of the input, which shows that the neuron preferentially follows its proper endogenous rhythm.

In the absence of SK channels, the modeled neuron fires in bursts, synchronized with the variations of synaptic activation (Fig. 6.5B). Two phases are clearly distinguished (Fig. 6.5D): high-frequency firing when the input is on (phase **1**), which causes a strong calcium accumulation ; followed by a silent phase when the input is off (phase **2**), allowing for evacuation of the calcium. When a stimulation occurs, the ability of the cell to accumulate calcium in the high-frequency firing mode is strongly increased, which results in the generation of several action potentials at a high frequency (period **1**). During this period, the intracellular calcium concentration critically increases. When the applied synaptic current is stopped, the neuron stops firing, which allows the evacuation of the accumulated calcium (period **2**). The phenomenon

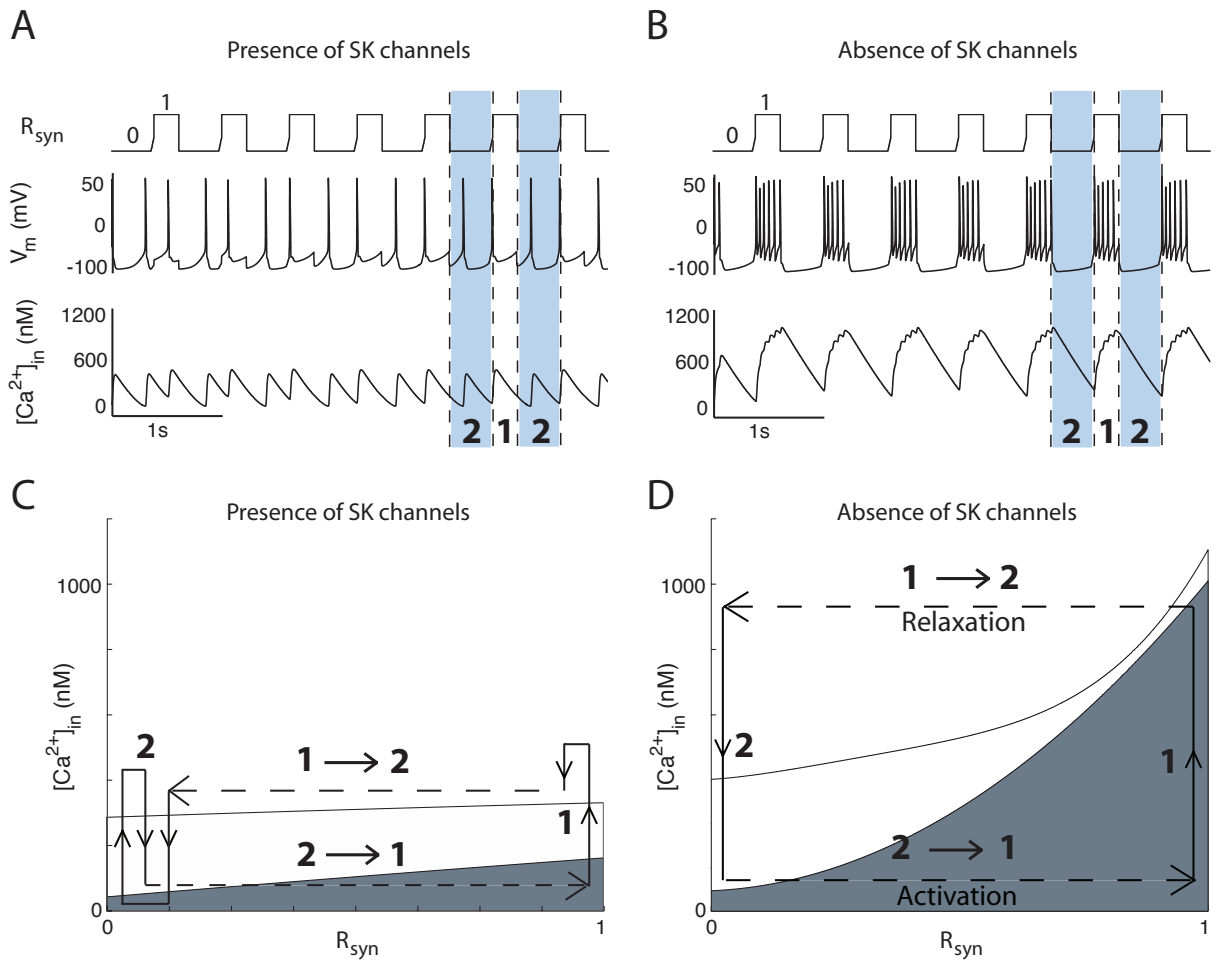

Figure 6.5 – Effect of periodic input of synaptic current activation on the cell firing in the presence (left) and in the absence (right) of SK channels. A. and B. Variations of R_{syn} (top), the membrane potential (middle) and the intracellular calcium concentration (bottom) over time in the presence and in the absence of SK channels, respectively. **C.** (resp. **D.**) Trajectories corresponding to **A.** (resp. **B.**) in the R_{syn}-$[Ca^{2+}]_{in}$ plane in the presence (resp. in the absence) of SK channels. Phasic variations of synaptic activation induce bursting only in the absence of the calcium-activated potassium current.

repeats itself periodically, resulting in a burst firing pattern.

It is thus the periodic variation of the synaptic input current that causes the bursting firing pattern. In that sense, the bursting is exogenous rather than endogenous, causing the rhythm of bursting to be correlated to the one of the synaptic input.

SK channels act as a protection against excitatory noise and reduce noise-induced firing irregularities

The deterministic analysis in the previous sections is useful to understand the regulation mechanism, but does not describe a physiological configuration. To gain realism, we now model the synaptic afferents through Poisson stochastic processes of different amplitudes, which crudely mimick *in vitro* and *in vivo*-like conditions.

In the absence of SK channels (Fig. 6.6B), the firing in the simple model is strongly sensitive to the excitatory inputs. A low level of noise (modeling *in vitro* conditions) induces irregularities in the firing rate, whereas a high level of noise (modeling *in vivo* conditions) induces bursting. For a low level of noise, interspike intervals (ISI's) are separated in two main groups (Fig. 6.6D, left) : a group of "long" intervals (around 100 ms), which account for the endogenous rythm of the cell ; and a group of "short" intervals (around 25 ms) representing doublets. For a high level of noise (Fig. 6.6D, right), the proportion of short intervals becomes more important, whereas the group of long intervals is distributed over a large number of intervals. This distribution is typical of

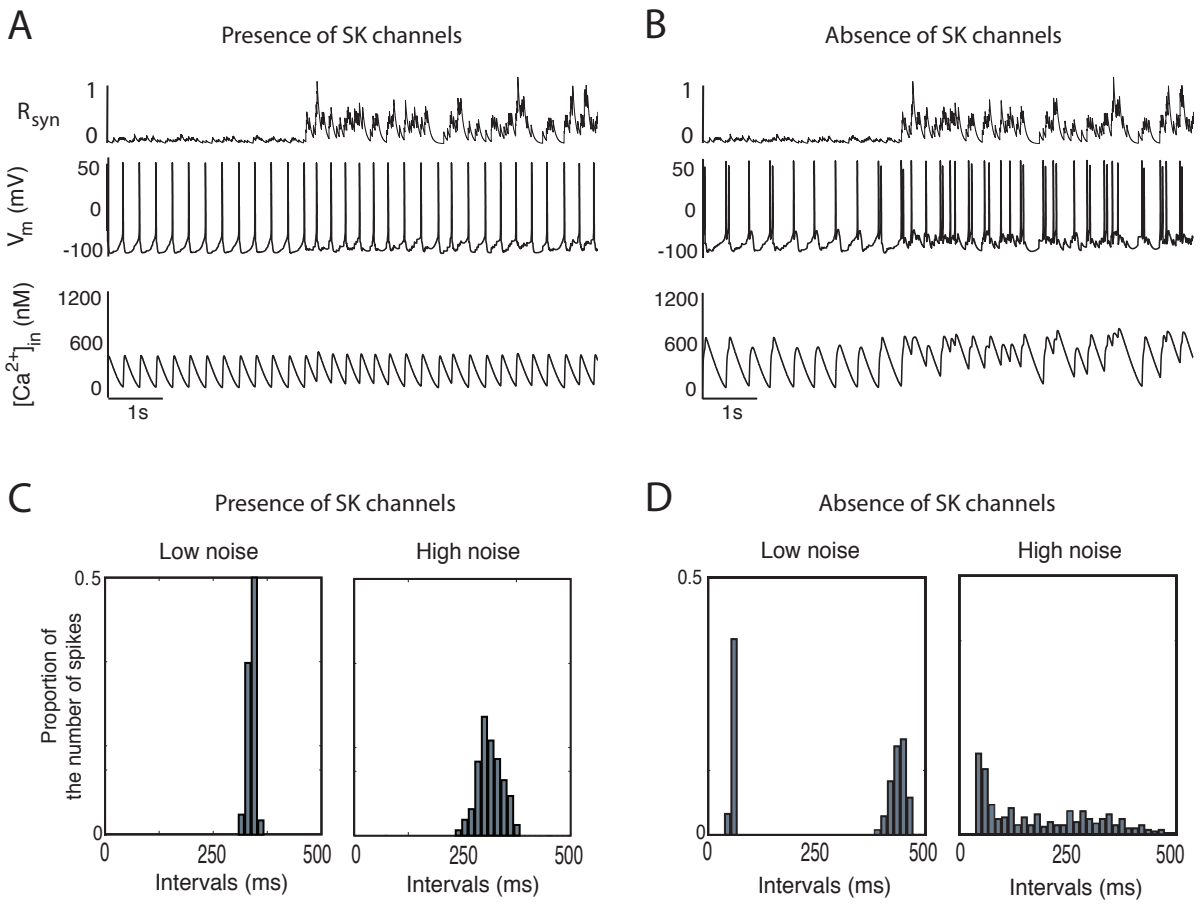

Figure 6.6 – Behavior of the model when some noise is injected, in the presence (left) and in the absence (right) of SK channels. A. and **B.** variations of synaptic input current activation (top), the membrane potential (middle) and the intracellular calcium concentration (bottom) over time in the presence and in the absence of SK channels, respectively. **C.** and **D.** Interspike interval histogram for a low (left) and a high (right) level of noise in the presence and in the absence of SK channels, respectively.

a burst firing pattern. Fig. 6.6A shows that the sensitivity of the cell to synaptic currents is strongly attenuated in the presence of SK channels. Indeed, the firing rate is hardly affected. Even a high level of noise only induces irregularities, without inducing high frequency firing. These behaviors are well captured by the interval interspike histograms (ISIH's) (Fig. 6.6C).

This stochastic analysis confirms that the SK current prevents the generation of noise-induced high frequency action potentials. In that sense, SK channels act as a switch between resting and excited states. Moreover, these results are supported by *in vivo* extracellular recordings in the anesthetized rat (Fig. 6.7, see methods). Indeed, SK channel blockade *in vivo* induces bursting in dopaminergic neurons [191]. This shows that, *in vivo*, the tone of synaptic input is almost always high enough to induce bursting in the absence of SK channels (Fig. 6.7, right and [191]). In contrast, SK channels filter the synaptic inputs in Fig. 6.7, left. Moreover, the figure clearly indicates that the shape of bursting can be qualitatively different from one DA neuron to the other, even if their single-spike firing is comparable (compare e.g. neuron 4 and neuron 7 in the figure, for instance). This reinforces the claim that the bursting is not endogenous but highly dependent on the shape of the excitatory input.

SK channels counteract synaptically-induced synchronization of neurons with different endogenous rhythms

In our model, SK channels strongly attenuate the entrainability of the cell by excitatory external inputs. This property has important implications at the population level. If a group of dopaminergic neurons are stimulated by a same set of glutamatergic inputs, SK channels could play

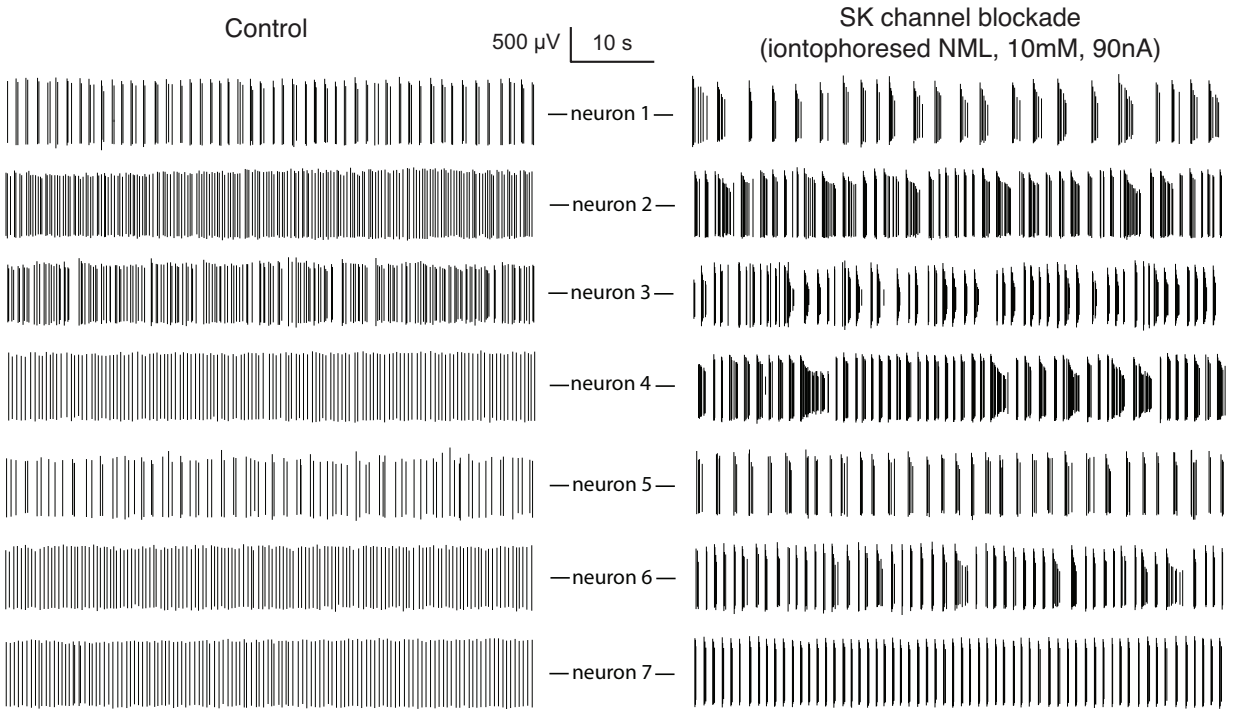

Figure 6.7 – Effect of a SK channel blockade on the firing of dopaminergic neurons in vivo. Extracellular recordings of 7 neurons before (left) and after (right) the local injection of a SK blocker are shown. SK channel blockade induces burst firing in these neurons, and the shape of the burst differs a lot qualitatively from one neuron to the other.

an important role in opposing the collective synchronization. This hypothesis is investigated in this section, by the simulation of modeled neurons with different endogenous firing rates, subjected to a same excitatory synaptic input over time.

Since the synchronization of interest is a synchronization of pattern rather than a synchronization of spikes, it is more appropriate to analyze the correlation of the most representative variable of this pattern, namely the intracellular calcium concentration. Fig. 6.8A shows the mean correlation coefficient of the variations of intracellular calcium concentration over time of each cell compared to a reference cell, according to their relative endogenous rhythm.

Not surprisingly, when subjected to the same external noise, identical neurons are fully synchronized in both conditions. Interestingly, in the presence of SK channels (black columns), a difference of three percent in the endogenous rhythm is sufficient to have poorly synchronized cells ($\rho < 0.4$), and even cells that are not synchronized at all for relative differences higher than ten percents ($\rho < 0.2$). This observation supports the hypothesis that, in the presence of a calcium-activated potassium currents, the neurons follow their endogenous rhythm rather than the external excitatory inputs, the latter being filtered by the potassium current.

In the absence of SK channels (grey columns), the synchronization is much more robust to differences in the endogenous firing rate. Indeed, the neurons mainly follow the time variations of the synaptic activation, being only slightly influenced by their endogenous rhythm. The result is that these neurons are all entrained by the synaptic inputs, and thus synchronized. Therefore, a set of neurons differing only by their endogenous rhythm and subjected to the same external excitatory inputs would be synchronized only in the absence of SK channels (Fig. 6.8B), and consequently only in bursting mode. Fig. 6.9 illustrates the resulting significant impact on the mean potential of such a neural network. Moreover, this figure illustrates the fact that this synaptically-induced synchrony is reversed as soon as SK channels are up-regulated.

The analyses above suggest a potential regulation mechanism at the population level: in the presence of SK channels, the neurons fire tonically and are not synchronous. Considering that the main goal of this firing pattern is to maintain a constant low level of neurotransmitter, the asynchronism of the neurons in that state ensures a constant low level of global release in the network. In contrast, when SK channels are down-regulated, the

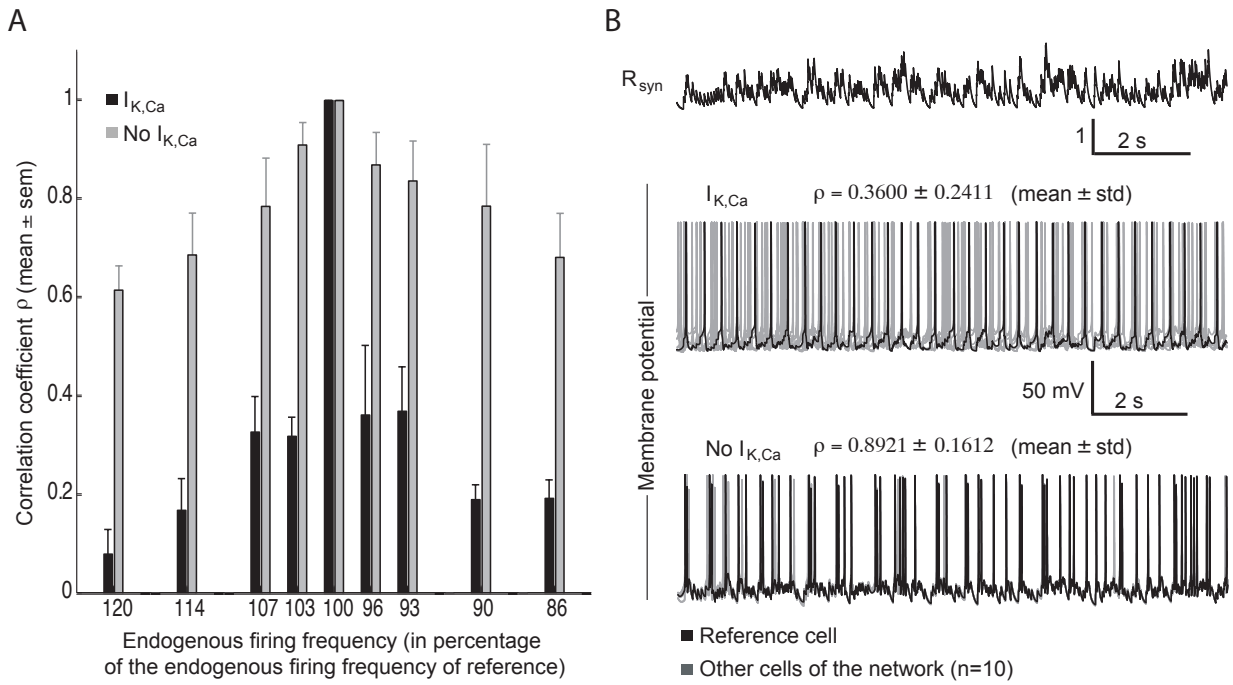

Figure 6.8 – Synchronization of cells of different endogenous firing rate subjected to the same excitatory inputs. A. Correlation coefficient ρ (mean $\pm$ SEM) between the $[Ca^{2+}]_{in}$ variations over time of one cell and the reference cell according to their relative endogenous rhythm, in the presence (black) and in the absence (gray) of SK channels. **B.** Variations of $R_{Na,syn}$ (top) and the membrane potential of the neurons of the network in the presence (middle) and in the absence (bottom) of SK channels. When SK channels are inhibited, the neurons fire in bursts synchronously, whereas they fire irregularly in single spikes in the presence of SK channels, following their respective endogenous rhythm.

neurons fire simultaneously in bursts and synchronize to the synaptic afferents. Therefore, in that state, the release of neurotransmitter by the network is much larger (because of the high intra-burst firing frequency), and correlated to the excitatory inputs (Supplementary Fig. S2). In other words, the network is in its excited state and faithfully integrates and transmits the information provided by the synaptic afferents.

This regulation mechanism might be of particular interest regarding post-synaptic receptors activation. Indeed, the relation between the firing patterns of DA neurons and the relative activation of D1 and D2 receptors has recently been investigated [38]. In this study, Dreyer and colleagues showed that asynchronous irregular firing preferentially activates D2 inhibitory receptors, these receptors being more sensitive to dopamine. On the other hand, D1 excitatory receptors are preferentially activated by bursting DA cells, at the condition that these bursts are synchronous, which is ensured in our proposed regulation mechanism.

Discussion

The switch between single-spike firing and bursting In Vivo *can be induced via a modulation of the SK channel conductance.*

In the absence of SK channels, stochastic excitatory inputs of sufficiently high amplitude induce burst firing. In this configuration, the lengths of the bursts and of the hyperpolarization periods are mainly determined by the variations of the synaptic inputs, and the endogenous rhythm of the cell plays a minor role. Namely, the initiation and termination of bursts do not depend on an additional ionic current. This is in agreement with the fact that bursts can be of highly variable length and highly variably spaced in a same cell (Fig. 6.7). Physiologically, the interest of this mechanism is that bursting strongly follows the shape of the excitatory inputs, where the information can be easily coded.

However, the enhancement of cell excitability by synaptic afferents is accompanied by an increase in the intracellular calcium concentration. As a consequence, SK channels, when present, are indirectly activated by these excitatory inputs, and generate an outward current

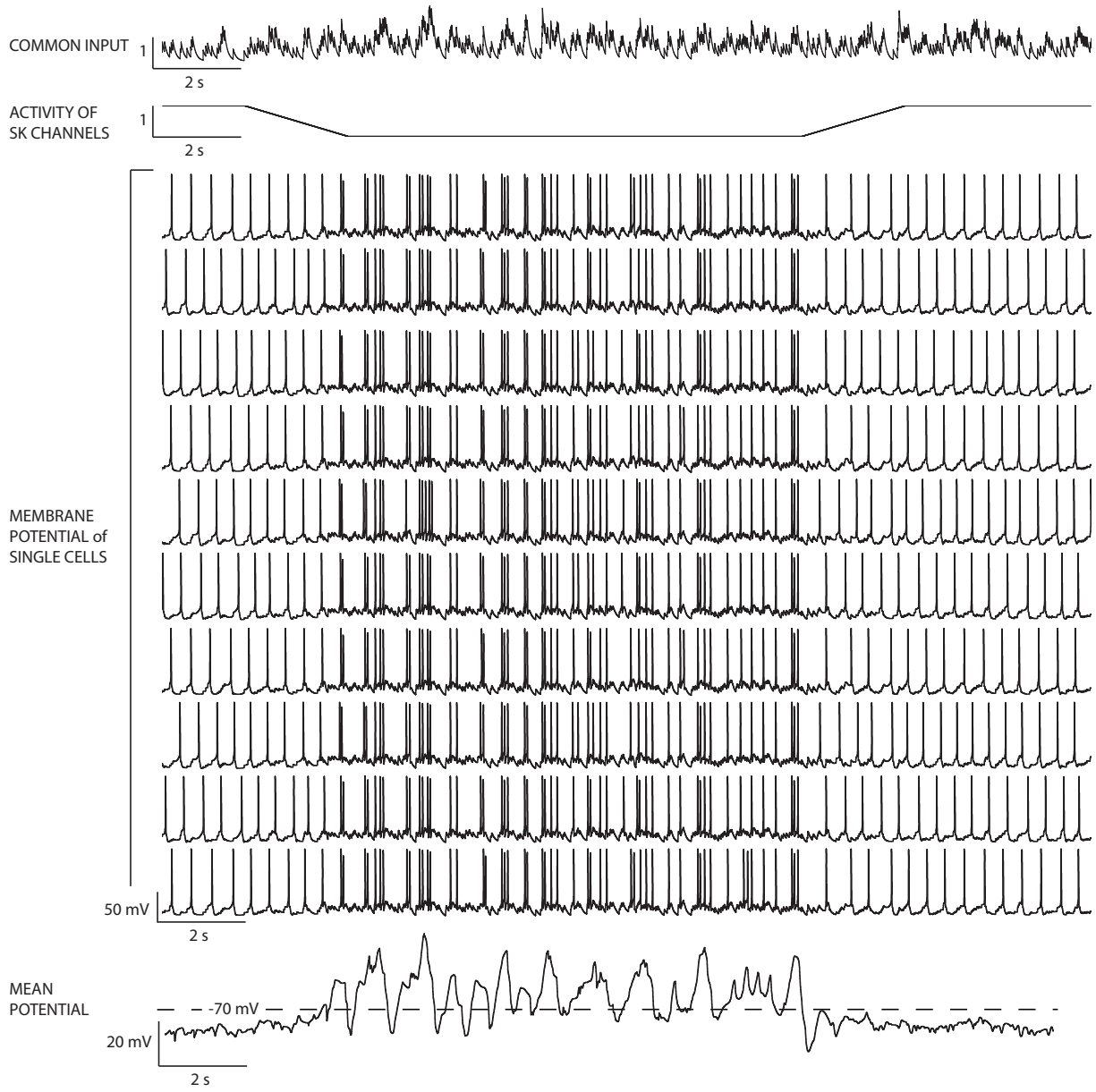

Figure 6.9 – Variations of neuronal firing pattern and synchrony during a down-regulation of SK channels. From top to bottom : common activation of excitatory inputs, variations of SK channels activity over time, variations of membrane potential of each cells of the network (n=10) over time and mean electrical activity of the network. A down-regulation of SK channels simultaneously induces bursting and synchrony in all cells of the network, resulting in a significant change in the global electrical activity of the population.

that counteracts this phenomenon. The result is that, in the presence of SK channels, the cell is barely excited by these excitatory inputs, and therefore fires in single spikes rather than in bursts. These observations are consistent with the observed effects of SK blockade in DA neurons [76, 96, 191].

The isolation mechanism performed by SK channels may be important for two reasons. On the one hand, it ensures a robust regular pacemaker firing, which is for instance critical for neurons which encode information in their firing rate. On the other hand, it acts as a switch of firing pattern in neurons subjected to high amplitude excitatory inputs. In that sense, the excitation state of neurons, regulated by SK channels, and the information

coding, carried by synaptic inputs, could be managed by two independent pathways, which can be modulated differentially.

A potential mechanism of synchrony of dopaminergic neurons

The mechanism of neural synchrony that we propose is based on the assumptions that populations of pacemaker neurons having different endogenous rates would be excited by common inputs (Fig. 6.10). In the absence of synaptic inputs, the neurons exhibit pacemaker firing, following their individual endogenous rhythm. In this state, the cells are not synchronized (Fig. 6.10A). In the presence of synaptic inputs, the firing and synchrony of cells will depend on the conductance of SK channels. This can be controlled e.g. by G-protein coupled receptors (GPCRs). For example, activation of norepinephrine receptors inhibits SK currents in dorsal root ganglion neurons [119]. When GPCRs are inactive, SK channels are not blocked and regulate the entrainability of the cells by the synaptic inputs. The result is that the cells fire asynchronously in single spikes, following their endogenous rhythm (Fig. 6.10B). The blockade of SK channels through GPCRs highly enhances the entrainability of the cells by synaptic afferents. The neurons in which SK channels are blocked fire in bursts, phased-locked to the excitatory inputs. The inputs being common to all neurons of the network, they are highly synchronized (Fig. 6.10C,D).

Different inputs (GPRC1,2) might differentially regulate the activity of the network, in order to suit specific needs. For instance, in Fig. 6.10, SK channels of neurons 1 and 3 are both regulated by the G protein-coupled receptor GPCR1, whereas GPCR2 regulates the SK channels of the three cells. As a consequence, SK channel regulation through GPCR1 will only induce synchronized burst firing in neuron 1 and 3, whereas SK channel regulation through GPCR2 will induce synchronized bursting in all cells of the network.

Note that, in this illustration, the regulation of SK channels by GPCRs is fully hypothetical, no physiological evidence for their regulation in DA cells being observed to date. However, it has recently been showed that SK channels are regulated by muscarinic M1 receptors in CA1 pyramidal cells of the hippocampus [60, 19].

In summary, the quality of the bursts is controlled by a glutamatergic input and the ability to switch to bursting is regulated by the SK channels regulators. Moreover, the switch of firing pattern and the synchronization being sustained by the same mechanisms, their concomitance is ensured ; and the synchronization does not rely on the synchronization of the afferent glutamatergic neurons. Another means of synchronizing neuronal activity could be electrical coupling. However, there is little evidence for dopaminergic neurons (at least in the adult) [185, 186]. Therefore, the mechanism that we describe may be more widespread.

Physiologically, we hypothesize that the asynchronism of these neurons in tonic firing is as important as the synchronism in bursting mode. Mainly, the main purpose of irregular firing being to sustain a constant low level of neurotransmitter, the asynchronism of the neurons in that state ensures a global constant release in the network. In contrast, when SK channels are down-regulated, the neurons fire simultaneously in bursts and synchronize to the synaptic afferents. Therefore, in this state, the release of neurotransmitter by the network is much larger and phase-locked to the excitatory inputs. This may be especially important in meso-accumbens dopaminergic neurons, whose synchronized bursting may be the mechanism of quick increases in dopamine concentrations induced by drug intake or positive error in reward prediction [4, 158]. Moreover, it is completely concordant with recent modeling results on how the pattern of dopamine release, which is correlated to the firing pattern, influence receptor activation [38]. Namely, Dreyer et. al showed that receptor occupancy is crucially dependent on synchrony and the balance between tonic and phasic firing modes, the synchrony being only critical in burst firing.

Implications for further experimental strategies

Our model suggests a number of predictions that could be tested experimentally. Namely, technical advances make the realization of such analyses possible *in vitro* or *in vivo*.

In vitro, simultaneous recordings of neurons using patch-clamp would give insightful data on how neighboring cells would react to a same synaptic activation (mimicked using the dynamic clamp technique) when SK channels are operating and when they are blocked.

Our synchronization hypothesis is based on the existence of common glutamatergic inputs to subpopulations of DA neurons. There is evidence for this in other neurons such as GnRH neurons [22] but not, to our knowledge, in DA neurons. Therefore, it would be of great interest to verify this hypothesis anatomically in dopaminergic neurons of the SNc and the VTA.

In more physiological conditions, simultaneous recordings performed *in vivo* on behaving animals would be of great interest as well. Namely, it would be interesting to compare the respective synchronizations of single-spike firing cells and of physiologically and/or SK blockade-induced bursting cells.

On the other hand, the understanding of these mechanisms allows to easily predict the effect of blockade of

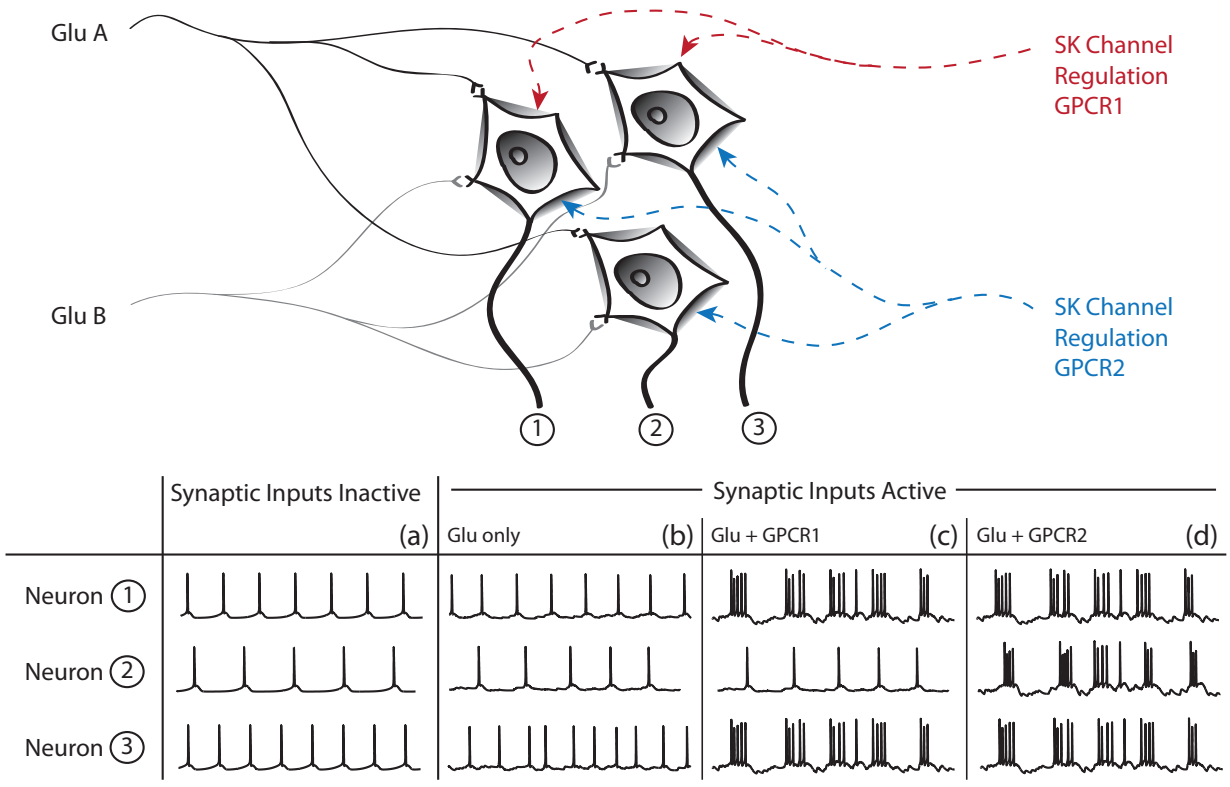

Figure 6.10 – Synchronization and firing mechanisms in dopaminergic neurons.

a particular channel on the firing of this type of neurons, or how to act on the neuron to change its behavior in a particular way. For instance, the modulation of a current that is regulated by the intracellular calcium concentration or that can regulate the calcium dynamics would act on the global shape of the firing pattern of the cell, whereas the modulation of a voltage-gated current would principally regulate the bursting quality, mainly the intra-burst firing frequency [39].

In summary, our model provides a mechanistic description of the control of firing of dopaminergic neurons, at the single cell level as well as at the population level. Moreover, it may provide a conceptual framework to better understand the mechanisms underlying firing patterns and synchronization of such pacemaker neurons.

Chapter 7

Selective Modulation of Firing Patterns *in vivo*

In the previous chapters, we analyzed the mechanisms underlying the pacemaker activity of DA neurons *in vitro*, as well as the role of SK channels in generating switches between single-spike firing and bursting activity *in vivo*. Although the coexistence and switch between these firing patterns is essential for DA neuron signaling, each of them has to be selectively regulated to modulate its information processing.

In this chapter, we investigate the role of one potential molecular source of such selective regulation, that is a K^+ recently described to be present in DA neurons [75, 106]. This current had the typical electrophysiological signature [18, 109] and pharmacology of the M current, being enhanced by retigabine and blocked by 10,10-bis(4-pyridinylmethyl)-9(10H)-anthracenone dihydrochloride (XE991) [180, 188]. Moreover, one of the subunits carrying M-currents (KCNQ4) was highly expressed in DA neurons [75].

Blockade of the M-current by XE991 had only minor effects on the spontaneous firing of DA neurons in rat brain slices and *in vivo* ([75], and see Results). Thus, the M-current does not appear to act as a brake on low frequency firing. We hypothesized that, given its voltage-dependence, its rather slow activation rate and lack of inactivation, the M-current could be specifically involved in controlling the bursting behavior in these cells. Indeed, depolarized plateaus are observed in DA neurons during bursting [63] and they are a priori sufficiently long-lasting (200-700 ms) to enable activation of M-channels.

We test this hypothesis using a combination of *in vivo* extracellular recordings of nigral DA neurons, intracellular recordings in a brain slice preparation, and computer modeling in which M-channels were added to the detailed computational model of [23]. In particular, we show that the M-current selectively gates the bursting behavior in DA neurons, their blockade selectively enhancing burst firing of DA neurons *in vivo* and increasing the proportion of short interspike intervals in bursts.

Results

Effect of systemic and local application of XE991 on the firing of DA neurons

In a first series of experiments, we studied the impact of intraperitoneally administered XE991 (3 mg/kg i.p.) on the firing of DA neurons. In previous *in vitro* experiments, we had demonstrated that this compound is a specific blocker of the M-current in these cells: thus, it had no effect on the shape of action potentials, on the resting membrane potential or on the medium-duration afterhyperpolarization induced by the opening of SK channels [75].

The effect of i.p. XE991 was variable, ranging from no change to a large inhibitory effect (n = 6) (Supplementary Fig. S7.1). This could be due to a mixture of direct and indirect factors, since KCNQ channels are also expressed by many neurons that project to DA neurons. The firing of rat DA neurons is under the inhibitory control of $GABA_A$ receptors [181]. The experiments were therefore repeated while iontophoresing a pharmacologically active (Supplementary Tab. S7.1) amount of the specific $GABA_A$ antagonist SR95531. Under these conditions, XE991 had no effect on the spontaneous firing rate or pattern (Fig. 7.1A) of DA neurons: firing rates were 2.9 $\pm$ 0.4 and 3.1 $\pm$ 0.4 spikes/s (mean $\pm$ SEM) (P = 0.25, Wilcoxon test, n = 6) in control conditions and in the presence of XE991, respectively. The percentage of spikes in bursts (see Methods) was 4.2 $\pm$ 2.3 and 3.7 $\pm$ 1.0 %, respectively (P = 0.89, Wilcoxon test, n = 6).

To evaluate the ability of the neurons to fire in bursts, we iontophoresed a reversibly acting blocker of small conductance Ca^{2+}-activated K^+ (SK) channels, N-methyllaudanosine (NML, 10 mM) [160]. This procedure facilitates bursting in these cells in an intensity-dependent manner [191]; that is, the percentage of spikes fired in bursts increases as a function of current intensity (30, 60 or 90 nA).

In order to assess the physiological relevance of our

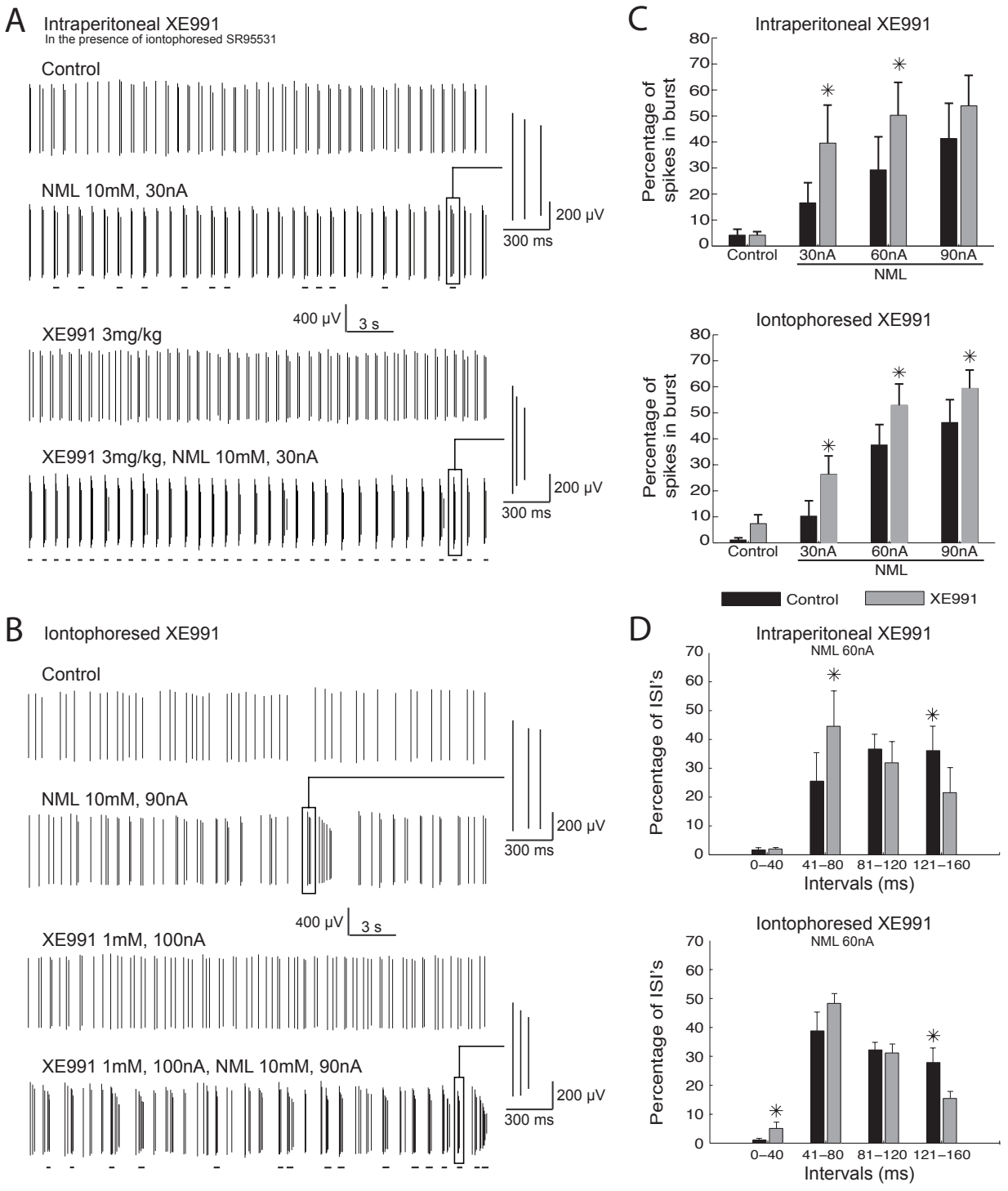

Figure 7.1 – XE991 selectively enhances burst firing of DA neurons in vivo, and increases the proportion of short interspike intervals in bursts. A. M-current blockade was induced by a systemic administration of XE991 (3 mg/kg i.p.). A $GABA_A$ antagonist (SR95531) was also iontophoresed (1mM, 100nA) during these recordings to block the most important inhibitory afferences. **B.** Local M-channel blockade was performed by iontophoresis of XE991 (1 mM, 100 nA). Events which are underlined correspond to bursts. **C.** Histogram showing a significant potentiation of bursting of DA neurons during M-current blockade (intraperitoneal XE991, n = 6; iontophoresed XE991, n = 8). **D.** Both i.p. and local XE991 applications induced a significant shift of ISIs toward the shorter intervals, as also illustrated by the insets in **A.** and **B.**. (*, $p < 0.05$).

model of bursting, we compared the characteristics of natural (i.e. spontaneous) and NML-induced bursts in the absence of any other pharmacological agent. They were found to be remarkably similar (Supplementary Fig. S7.2 and S7.3 see also [191]). Thus, the mean value of the interspike intervals (ISIs) was similar in both cases, as was the fact that the first ISI was shorter than the next ones, the values of which were close to 100 ms. Burst size histograms showed that the relative frequency of the bursts as a function of their number of spikes was similar in both conditions (Supplementary Fig. S7.3A). Importantly, a progressive decrease in the amplitude of the extracellularly recorded action potentials was observed in both natural and NML-induced bursts, and this decrease had a mean amplitude ($\tilde{2}0$ %, Supplementary Fig. S7.3B) that was similar in both conditions. The latter data strongly suggest that the membrane potential changes underlying both types of bursts are quantitatively similar, confirming the validity of our model. Moreover, all these parameters were similar to those described previously (e.g. [63]).

We next examined the influence of XE991 on NML-induced bursts. Fig. 7.1A shows that i.p. administered XE991 potentiated NML-induced bursting when $GABA_A$ receptors of DA neurons were blocked with SR95531. The amplitude of the effect of the M-channel blocker was dependent on the NML iontophoresis current intensity. Thus, during 30 nA NML, XE991 increased the percentage of spikes in bursts from 16 8 to 39 15 % ($P = 0.028$, Wilcoxon test, $n = 6$). A similar effect was seen during 60 nA (from 29 $\pm$ 13 to 50 $\pm$ 13%, $P = 0.028$, Wilcoxon test). At 90 nA, no significant effect was observed (from 41 $\pm$ 14 to 54 $\pm$ 12 %, $P = 0.17$, Wilcoxon test), probably because of a saturation effect. Control i.p. injections of the vehicle had no discernible effect ($n = 3$, Supplementary Fig. S7.4A).

In order to test whether XE991 acts directly on DA neurons, we next iontophoresed it onto the recorded neurons. For these experiments, we chose not to use a $GABA_A$ antagonist in order to mimic as closely as possible the physiological situation. Moreover, local application of XE991 made any indirect effect of the drug unlikely. As shown in Fig. 7.1B, the effects of the drug were quite similar to those observed after i.p. injection. Thus, XE991 (100 nA) had no effect on tonic firing (3.4 $\pm$ 0.6 and 3.5 $\pm$ 0.6 spikes/s in control conditions and in the presence of XE991, respectively, $P = 0.21$, Wilcoxon test, $n = 8$), but increased the percentage of spikes in bursts from 10 $\pm$ 8 to 26 $\pm$ 9 % during 30 nA NML ($P = 0.018$, Wilcoxon test) and from 37 $\pm$ 10 to 53 $\pm$ 11 % during 60 nA ($P = 0.018$, Wilcoxon test). At 90 nA, the increase (46 $\pm$ 12 to 59 $\pm$ 9 %) was also significant ($P = 0.049$, Wilcoxon test) (Fig. 7.1C, lower panel). Iontophoresis of the vehicle had no effect at any intensity of NML iontophoresis ($n = 5$, Supplementary Fig. S7.4B). A close inspection of the bursting behavior revealed that the M-channel blocker also modified it qualitatively. For example, Fig. 7.1D shows that, when administered either i.p. or by iontophoresis, it increased the proportion of short ISIs during 60 nA (other results are shown in Supplementary Fig. S7.5). This is also apparent in the insets of Fig. 7.1A and B.

XE99 facilitates fast firing induced by current injection in vitro

In order to confirm the ability of XE991 to facilitate the occurrence of short interspike intervals in DA neurons, we performed intracellular recordings of these neurons in slices containing the SNc. This recording mode was chosen because it is the least likely to disrupt intracellular pathways, which are critical in the control of M-channels [35]. For these experiments, we superfused the slices with blockers of synaptic transmission (10 μM CNQX, 50 μM APV, 10 μM SR95531 and 1 μM CGP55845) in order to exclude indirect effects. A supramaximal concentration of the SK blocker apamin (300 nM) was used to mimic our in vivo conditions. Neurons were hyperpolarized to -60 mV by negative current injection (-50 to -150 pA) and depolarizing pulses (50-150 pA, 800 ms) were given repeatedly to evoke spikes. In these conditions, 10 μM XE991 significantly increased the number of spikes from 3.2 $\pm$ 0.5 to 5.2 $\pm$ 0.9 after 10 minutes (Fig. 7.2) ($n = 4$) ($F = 17.1$, $P = 0.000$, repeated measures ANOVA; values after the 5th minute of XE991 application were significantly different from those of the control condition (Newman-Keuls test); see Fig. 7.2 for the various levels of significance). On the other hand, it had no effect on the baseline voltage. XE991 had no significant effect in the absence of apamin (not shown, data from [75]).

Computer modeling of the effect of the M-current

We next explored the mechanism underlying our in vivo observations in a model of a DA neuron [23], which included amongst others a SK current and a M-current. The activation of synaptic currents was modeled by a Poisson process. Many of the electrophysiological features observed in DA neurons, including low frequency pacemaker activity and burst firing were reproduced in the model, which confirmed that the absence of M-current potentiates SK blockade-induced bursting (Fig. 7.3A). Quantitative analysis of 6 different model neurons (using different synaptic input patterns) reproduced the experimental results (Fig. 7.3B, Supplementary Fig. S7.5D). This effect was robust when the M-conductance was 5 times that measured experimentally [106]. When the conductance value was identical to the measured one,

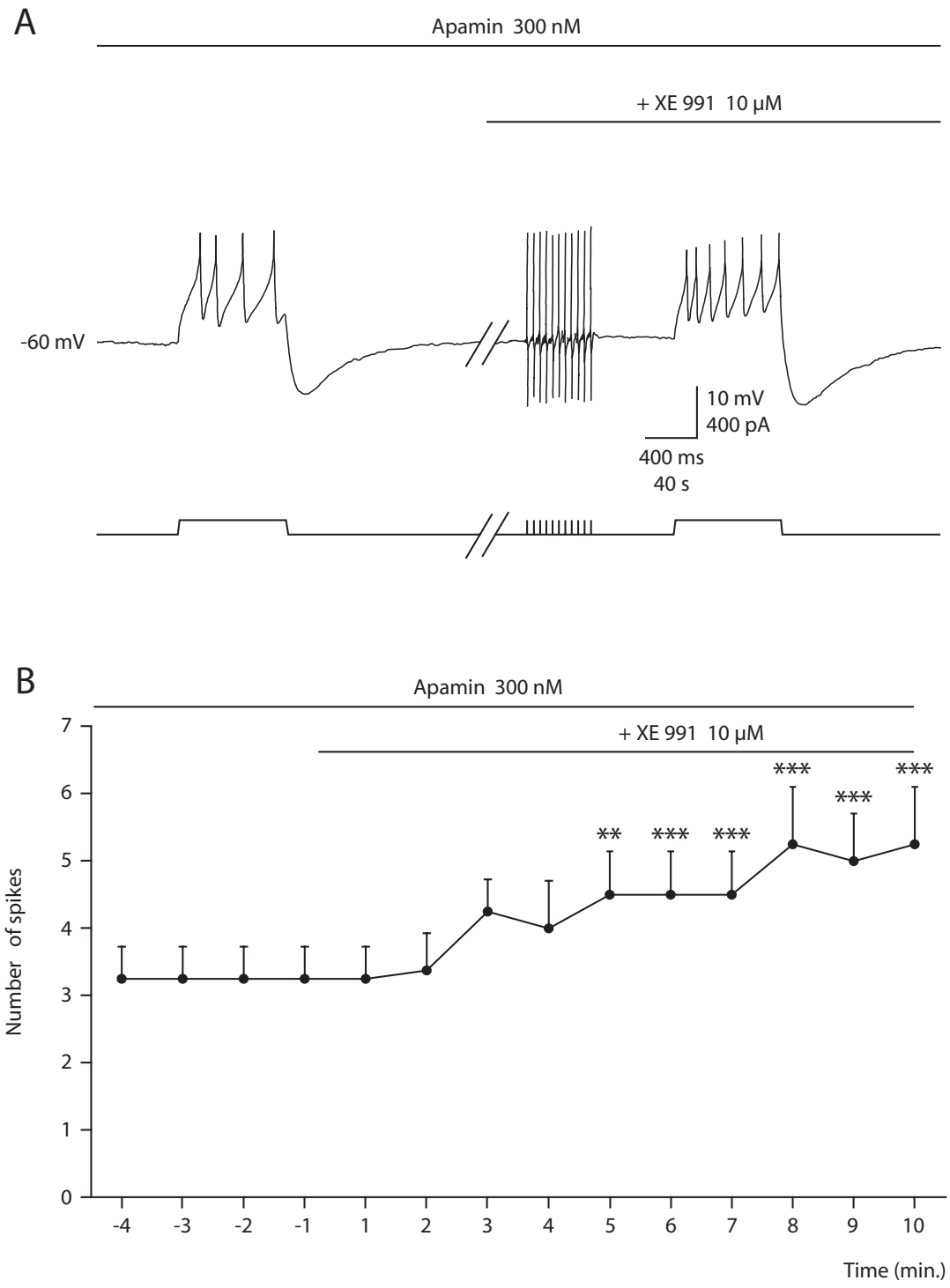

Figure 7.2 – XE991 increases fast firing in dopaminergic neurons in vitro. A. Intracellular recording showing that a given amount of current (+ 120 pA) elicits more spikes (truncated in the figure) in the presence of XE991. The experiment was performed in the presence of 300 nM apamin, 10 μM CNQX, 50 μM APV, 10 μM SR95531 and 1 μM CGP55845. Baseline membrane potential was set at -60 mV by a continuous injection of -100 pA. The speed of the recording was reduced 100 fold at the beginning of the superfusion of XE991. **B.** Summary plot showing the time-course of the effect of XE991 (n = 4). (**, $p < 0.01$; ***, $p < 0.001$ versus control)

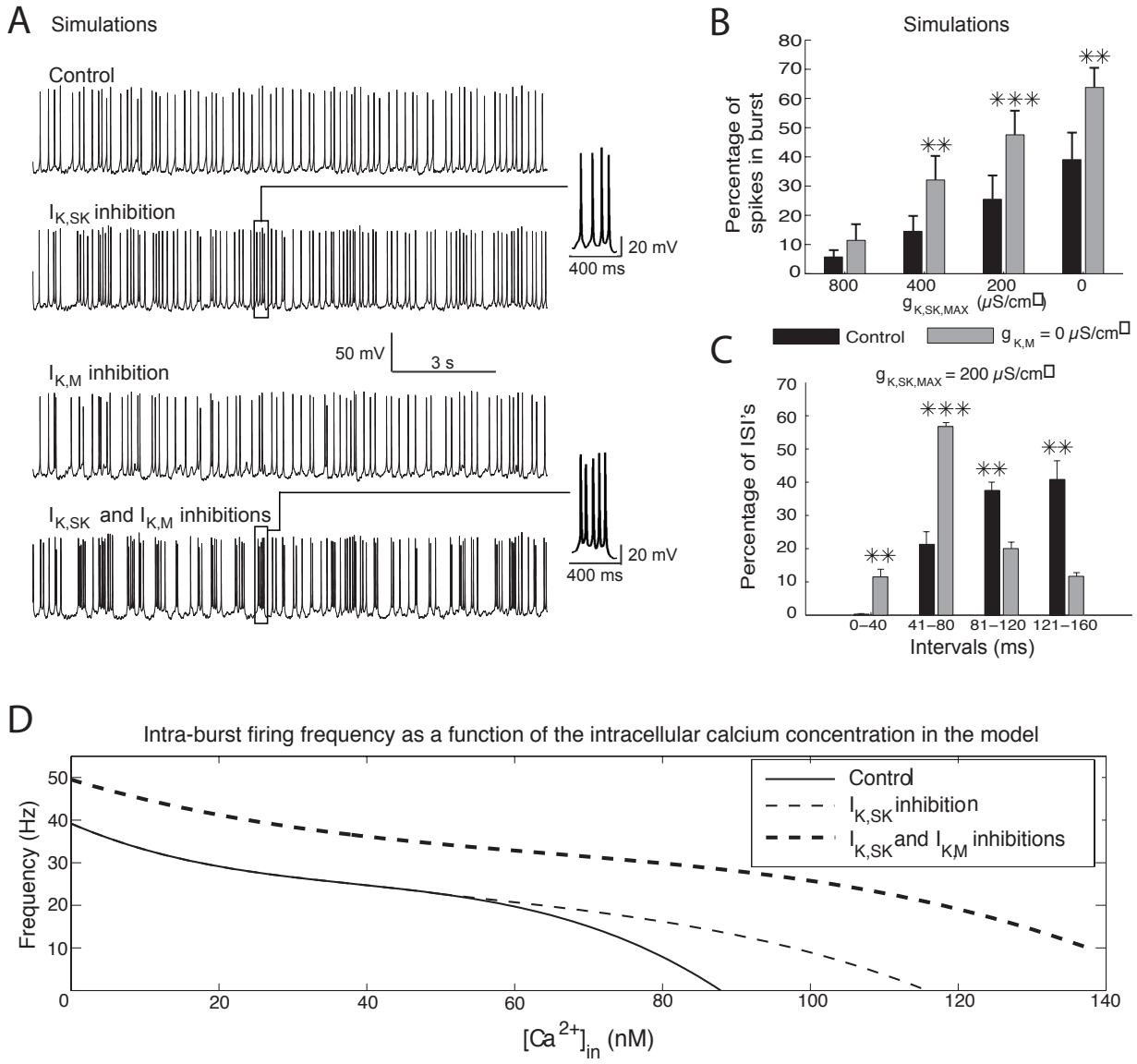

Figure 7.3 – Simulations of M-current blockade on a DA neuron model confirm its selective effects on burst firing. A. Example of a simulation. M-current inhibition was modeled by setting the M-current conductance to 0, while the effect of NML was modeled by reducing the $I_{K,SK}$ conductance (in this case to 0). The temporal pattern of synaptic inputs was exactly the same in the four traces. **B.** Simulations (n = 6) showed a significant potentiation of bursting of the model DA neuron during M-current inhibition. **C.** A significant shift of ISIs toward the shorter intervals is seen in the model, as also illustrated by the insets in **A.**. **D.** Effect of $I_{K,SK}$ and combined $I_{K,SK}$ and $I_{K,M}$ inhibitions on the relationship between $[Ca^{2+}]_{in}$ and intra-burst firing rate. (**, p < 0.01; ***, p < 0.001).

the effect was very modest (Supplementary Fig. S7.6).

The model also confirmed the ability of M-current blockade to increase the proportion of short ISIs within bursts (Fig. 7.3C). A plot of intra-burst firing frequency versus $[Ca^{2+}]_{in}$ (Fig. 7.3D) shows the predicted effect of the SK and M conductances on the firing behavior of the model neuron. As compared to the control condition, SK blockade allowed faster firing at intermediate $[Ca^{2+}]_{in}$ values. Additional block of M channels shifted the curve to even higher frequencies (as observed experimentally by a higher proportion of short ISIs).

We next analyzed the M-current quantitatively in the model, both when the SK conductance was maximal and when it was set to 0. The charge transfer through the M conductance was higher in the second condition (Fig. 7.4A,B). The difference was even more striking when con-

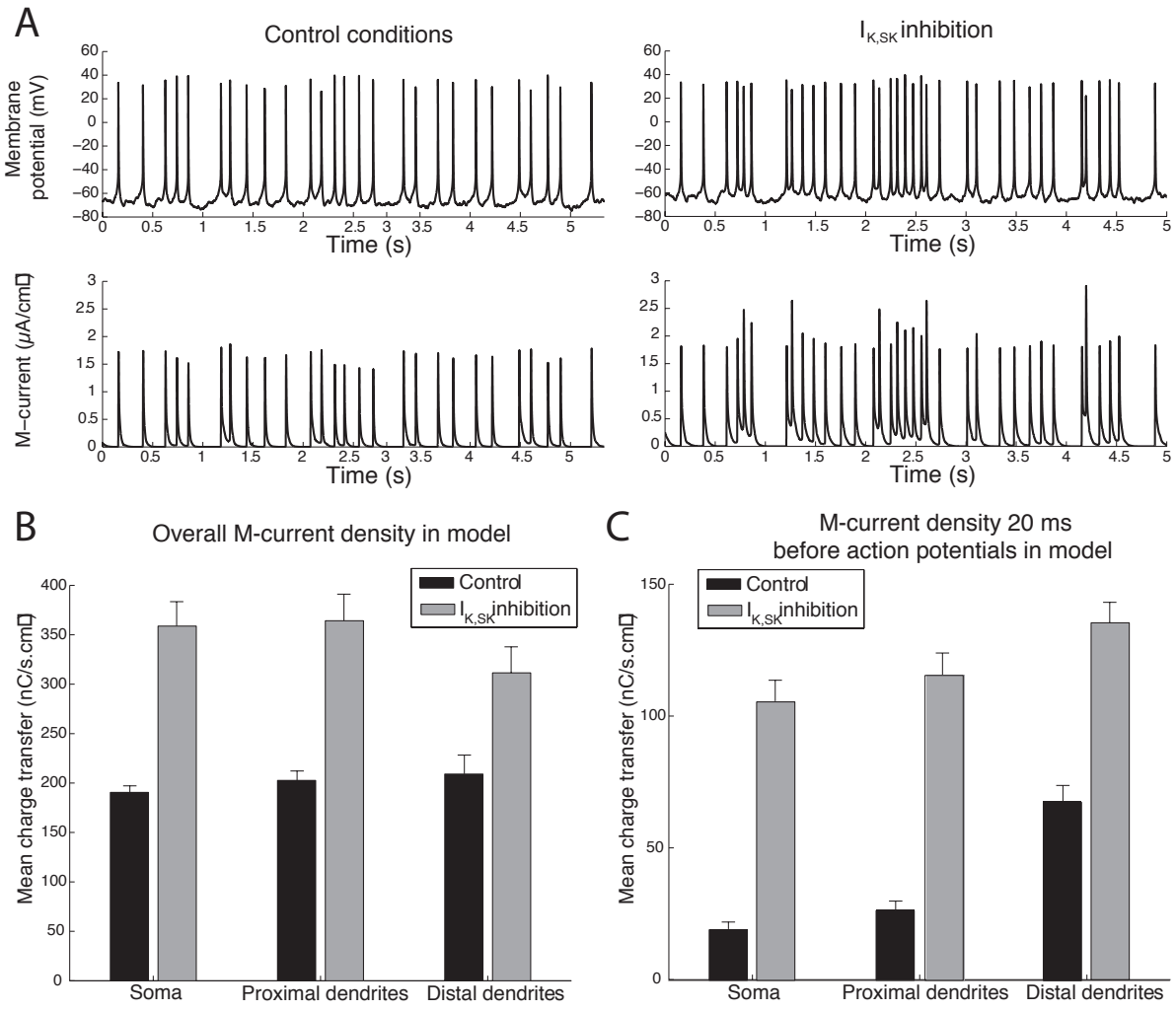

Figure 7.4 – Charge transfer through M channels in the model when SK channels are present or absent. A. Values of the membrane potential (top) and the amplitude of the M-current (bottom) in control conditions (left) and during a $I_{K,SK}$ inhibition (right). **B.** Overall M-current density in model. **C.** M-current density 20 ms before action potentials in model (n $>$ 200 events in 6 modeled cells). The overall M-current density during $I_{K,SK}$ inhibition is only twice that in control conditions. However, the amount of M-current that opposes the generation of action potentials is much larger during $I_{K,SK}$ inhibition. p < 0.001 between control and $I_{K,SK}$ inhibition (Students t-test for paired values **B.** and Students t-test for unpaired values **C.**).

sidering the mean charge transfer at 20 ms before the onset of action potentials in both conditions (Fig. 7.4C, see Methods). Clearly, the M-current completely deactivates between two successive action potentials during low frequency pacemaker or irregular firing, but not when the membrane potential is more depolarized during SK blockade (Fig. 7.4A).

Discussion

Taken together, the experimental and modeling data demonstrate that the M-current selectively gates the bursting behavior in DA neurons. The effect that we observe experimentally *in vivo* is most probably due to the blockade of somato-dendritic M channels, whose existence has been demonstrated experimentally. Indeed, the burst enhancing effect is observed when $GABA_A$ receptors (the major substrate of afferent inhibition in the rat [181]) are blocked. Furthermore, our slice experiments confirm that XE991 facilitates fast firing in these

neurons by a direct effect. Although the precise mechanism(s) underlying natural bursts in DA neurons in vivo is (are) not known, our demonstration that natural and NML-induced bursts have similar characteristics allows to generalize our findings to the physiological situation.

Our results show that low frequency pacemaker firing is largely unaffected by XE991, presumably because the membrane potential does not reach sufficiently depolarized levels for long enough for M-channels to become substantially activated (Fig. 7.4A). The M-channels activate during each action potential during this firing pattern, but quickly deactivate, so that no current is flowing through them at the onset of the next spike. On the contrary, during burst firing, complete deactivation is prevented by fast firing during depolarized plateaus and this allows the channels to exert their inhibitory effect under these circumstances.

Besides its quantitative enhancement of burst firing, suppression of the M-current also alters the quality of the bursts, with a relative enrichment of very short ISIs. This effect is likely to be biologically important because it will increase the saturation of dopamine transporters at the terminals and hence sharpen the increases in the concentration of dopamine. The effect of M-current blockade on the distribution of ISIs was more spectacular in the model than in the experiments (compare Supplementary Fig S7.5b and d). This is probably due to the fact that the dominant repolarizing currents (other than the SK current) after the action potential deactivate too quickly in the model. This leads to a high proportion of closely spaced action potentials.

Our results demonstrate a novel pathway for selectively altering the transient responses of DA neurons to excitatory inputs without changing their low frequency tonic activity. Given the variety of intracellular pathways that control M-current in CNS neurons [35], it may offer a powerful means by which various afferent neurotransmitters can fine tune DA transmission. One obvious candidate is acetylcholine, which blocks the M-current via M1/M3 receptors in many types of neurons. There is ample evidence for an excitatory and burst-enhancing effect of muscarinic agonists on midbrain DA neurons [65, 128]. However, acetylcholine obviously has multiple effects including inhibitory ones - on DA neuron excitability, depending on the concentration of synaptic acetylcholine and its duration of action [49]. Pharmacological modulation of the M-current should have a major impact on DA signaling that could be exploited therapeutically in the future (see [173] for further discussion).

More generally, our results demonstrate that M-channels do not reduce spontaneous low frequency firing in DA neurons. This is because of the parameters of their activation and deactivation relative to the voltage trajectory during pacemaking. However, their presence makes these neurons relatively insensitive to excitatory inputs. Therefore, modulation of this conductance may selectively control the excitability of these neurons when they are in bursting mode. This may be an advantage in some behavioral contexts.

Discussion

Summary of Results

Part II of the dissertation is devoted to the analysis of the qualitative mechanisms underlying dopaminergic neuron electrophysiology both *in vitro* and *in vivo*, via the use of mathematical modeling and experiments. It extracts key players in the different DA neuron firing patterns, as well as potential candidates for the important switch between them, via the use of the minimal biophysical model of DA neuron signaling proposed in Chapter 4.

Starting with *in vitro* conditions, we introduced the dynamical properties of the spontaneous activities of DA cells, namely pacemaker firing and slow oscillatory potentials (Chapter 5). We highlighted the robustness of pacemaking, which originates from a redundant cooperation between sodium and calcium channels in the spontaneous generation of spikes. This observation suggests an origin for the lack of robustness of certain experimental protocols, which may lead to conflicting conclusions although the underlying mechanisms are common.

Continuing with *in vivo* conditions, we discussed the exogenous origin of bursting activity and its regulation by calcium-activated small conductance potassium channels (Chapter 6). These channels were shown to act as filters against excitatory inputs, protecting the endogenous rhythm of the cell in the presence of external noise or stimulations. This analysis was extended at the population level, where a similar mechanism is shown to be able to regulate the synchrony of subpopulations submitted to common synaptic inputs.

Finally, a mechanism of selective regulation of bursting quantity was proposed (Chapter 7). It involves KCNQ potassium channels, generating a M-type outward current, in the regulation of short intraburst interspike intervals. These channels being commonly regulated by muscarinic receptors in excitable cells, this mechanism might occur physiologically, and might also provide a target for the pharmacological treatment of diseases whose symptoms correlate with a dysregulation of the dopamine system, such as Parkinson's disease.

Limitations and Open Questions

Although qualitative modeling provides insights on the mechanisms underlying DA neuron signaling, this strategy faces some limitations, particularly regarding quantitative properties.

Firstly, the proposed minimal model of DA neuron solely contains ion channels that are critical to reproduce the firing activities of these cells. However, many other ion channels have been shown to play quantitative roles in these spiking behavior, one example being the KCNQ channels discussed in Chapter 7, which are not included in the reduced conductance-based model. This simplification certainly has some impacts on the results. For instance, the role of the considered ion channels might be overestimated, because they have to compensate for the missing ones.

A second limitation is that, even if we attempted to verify several of the mathematical results experimentally, some of those still rely on unproved hypotheses. The main example is the potential existence of a physiological regulation of SK channels in dopaminergic cells, which is at the basis of the mechanisms underlying the switch between single-spike firing and bursting in *in vivo* conditions proposed in Chapter 6. Indeed, although such physiological regulation of SK channels has recently been observed in other neurons [60, 123], its existence still remains unclear in DA cells. Many experiments have therefore still to be performed in order to validate or exclude the existence of the mechanisms proposed on a mathematical basis in DA neuron signaling, as discussed in the "Conclusion and Prospects" section.

Finally, experimental protocols also face some limitations. Indeed, even if experiments allow direct recordings of real neuron activity, these recordings are never performed in a real physiological configuration. Therefore, one has to keep in mind that the conditions of the experiments might strongly affect the results, as shown concerning the effect of L-type calcium channel blockade on DA neuron pacemaking in brain slices, where even

a same experimental protocol leads to conflicting conclusions. A second example is our analysis on the role of KCNQ potassium channels on DA neuron bursting *in vivo*. In this study, bursting is induced through a blockade of SK channels, which might be different from what happens physiologically, even though we showed that bursts are very similar in both cases.

In addition to a need for several experimental validations, the results discussed in Part II also raise some general open questions concerning the dynamical mechanisms of neuronal excitability.

Firstly, even if the model we used to describe DA neuron signaling is minimal, it is still a five-dimensional conductance-based model for which the use of dynamical system tools such as phase portrait analysis is not possible. This motivates a further reduction to a planar model as usually done in neurodynamics, in order to compare its behavior with the available pictures of excitability originally proposed by FitzHugh. For instance, the bifurcation diagram shown in Fig. 5.1B is quite different from what is commonly described in neurodynamics, and DA neurons exhibit electrophysiological signatures that are not easily reproduced in current two-dimensional models, such as after-depolarization potentials (see Fig. 5.5B, for instance) and plateau oscillations.

Secondly, our analysis suggests a fundamental role of calcium channels in the firing patterns of DA neurons, both *in vitro* and *in vivo*. But, these calcium channels are rarely integrated in reduced models, their activation being generally approximated as instantaneous as it is the case for sodium channels. This contradicts the observation that calcium channel activation is one order of magnitude slower than activation of sodium channels [78], which makes this approximation inappropriate in many cases. This motivates an alternative reduction exploiting the fact that they activate on the timescale of potassium channels.

These theoretical open questions, raised by our analysis of DA neuron electrophysiology, are investigated in the following part.

Part III

Restorative and Regenerative Excitability

Main collaborators on this part were

- *Dr. Alessio Franci, who contributed equally to all the results presented in this part,*
- *Mr. Laurent Massotte, who made the in vitro extracellular recordings of Chapter 8,*
- *Ms. Julie Dethier, who provided the subthalamic nucleus neuron hybrid model used in Chapter 12.*

Introduction

Since the early days of electrophysiological modeling, neurodynamics has focused on the understanding of the dynamical phenomena underlying neuronal excitability. Tools of dynamical systems theory such as bifurcation and phase portrait analyses have been used to study the geometry of excitability over the years.

Many results in neurodynamical studies rely on the phase portrait originally proposed by FitzHugh in 1961, which comes from an empirical reduction of the Hodgkin-Huxley model (see Part I or [46, 90, 101], among others). This phase portrait helped explaining the mechanisms of action potential generation, and has established itself as the key dynamical structure of neuronal spiking to date.

Motivated by the analyses of the mechanisms underlying dopaminergic neuron signaling proposed in Part II, the purpose of this third part is to deepen the understanding of particular extracted dynamical phenomena and to contrast these phenomena to state-of-the-art neurodynamics. In particular, our effort will be to include the role of calcium channels in the global picture of neuronal excitability originally proposed by FitzHugh, these channels being key players of the firing behavior of DA neurons and many other cell types.

Bifurcation analyses on the five-dimensional conductance-based model of DA neuron developed in Chapter 4 with a high calcium channel maximal conductance highlight examples of dynamical properties that fail to be reproduced and explained by FitzHugh phase portrait (Chapter 8). To address this limitation, we mimic FitzHugh approach by empirically reducing the Hodgkin-Huxley model augmented with a calcium channel of physiologically relevant kinetics (Chapter 9). This reduction leads to a revised picture of neuronal excitability that is able to explain the dynamical properties observed in the DA neuron models. In particular, it uncovers two novel types of excitability in addition to the three generally described. Their electrophysiological signatures are shared by many neurons including DA cells (Chapter 10).

A similar qualitative picture is extracted in conductance-based models of arbitrary dimensions (Chapter 11). It shows that the three commonly described types of excitability, merged into the term "restorative excitability", rely on the dominant role of slowly activating ion channels that generate a negative feedback to membrane potential variations, such as voltage-gated potassium channels. In contrast, the two novel types of excitability, merged into the term "regenerative excitability", rely on the dominant role of slowly activating ion channels that generate a positive feedback to membrane potential variations, such as voltage-gated calcium channels. Moreover, the balance between restorative and regenerative ion channels can be modulated through the regulation of particular channel properties, leading to a robust regulation mechanism of neuronal excitability.

The major difference between restorative and regenerative excitability is the presence of robust bistability in the latter. We view this robust bistability as a key component of neuronal bursting, and we show that the switch from restorative to regenerative excitability provides a robust physiological route to bursting in the presence of ion channels that activate on an ultraslow timescale, such as small conductance calcium activated potassium channels (Chapter 12). The proposed mechanism is simple. Yet, it is shown to account for many different bursting qualities, via the regulation of two key parameters, called "balance weight" and "adaptation gain". As a result, we propose a novel transcritical hybrid model of neuronal bursting that is able to reproduce switches in firing patterns observed in many neurons through the sole (physiologically relevant) regulation of these two parameters.

Chapter 8

Varying L-type Calcium Channel Density Affects DA Neuron Excitability, not Pacemaking

In Chapter 5, we have discussed the mechanisms underlying pacemaker firing in dopaminergic neurons. In particular, we showed that sodium and L-type calcium channels cooperate to generate this spontaneous activity, and that it is very robust against an heterogeneity in these channels. Indeed, whether sodium or calcium channel is the dominating channel barely affects the nature of pacemaking. Calcium and sodium channels are in this sense redundant in pacemaking generation.

Because of this redundancy, a blockade of these channels has been suggested to protect DA neurons against neurodegeneration, without impacting the pacemaking behavior [86]. Indeed, calcium entering through L-type calcium channels during pacemaking is a source of metabolic stress, leading to an exacerbated vulnerability of these cells in neurodegenerative diseases such as Parkinson's disease [71]. However, the balance between sodium and calcium channels might have a strong effect on neuronal excitability, even if it does not affect pacemaking. Surprisingly, the effect of L-type calcium channel heterogeneity on DA neuron excitability has been barely investigated to date [99, 169].

In this Chapter, we investigate how changes in L-type calcium channel density affect DA neuron excitability. In particular, we show that increasing L-type calcium channel maximal conductance increases burstiness in the DA neuron model, both in *in vitro* and *in vivo* conditions. We experimentally validate this observation by showing that SNc DA neurons heterogeneously respond to SK channel blockade *in vitro*, this heterogenous response being abolished by an inhibition of the L-type calcium current.

Finally, we analyze the effect of varying the L-type calcium channel density on the dynamical mechanisms underlying the spontaneous generation of spikes in the simple DA neuron model. We show that increasing L-type calcium channel density induces a switch in the bifurcation mechanism at the origin of the spike initiation during pacemaking, leading to the concept of "sodium" and "calcium pacemaking". Whereas the mechanisms of sodium pacemaking are well known in neurodynamics, those of calcium pacemaking seems to differ from what have been described in the literature to date.

Results

An increase in L-type calcium channel density increases burstiness in DA neurons

We previously showed that DA neuron spontaneous firing is robust against physiologically plausible variability in L-type calcium channels (Chapter 5). Here, we test whether such a variability would affect neuron response against excitatory inputs, as it occurs *in vivo*. To this end, we submit our simple DA neuron model to a stochastic excitatory noise that follows a Poisson process (see Chapter 4 for details on the model and the synaptic noise).

Fig. 8.1A shows the electrophysiological behavior of the model under SK channel blockade in *in vivo* condition, for three different values of L-type calcium channels that have been shown to barely affect the pacemaker behavior. Note that the excitatory noise that defines the *in vivo* condition is exactly similar for the three cases. As illustrated on the figure, the response of the neuron to a same input strongly differs depending on its L-type calcium channel density. That is, the higher the L-type calcium channel density, the more the neuron exhibits synaptically-induced bursting. This observation suggests that calcium channels, while redundant for pacemaking, strongly affect the excitability of the neuron.

Interestingly, our model shows that a SK channel blockade would also induce bursting in DA neurons *in vitro*, as soon as L-type calcium channel density is sufficiently high (Fig. 8.1B). This observation is at first sight inconsistent with the current knowledge on DA neuron electrophysiology, because it is commonly accepted that

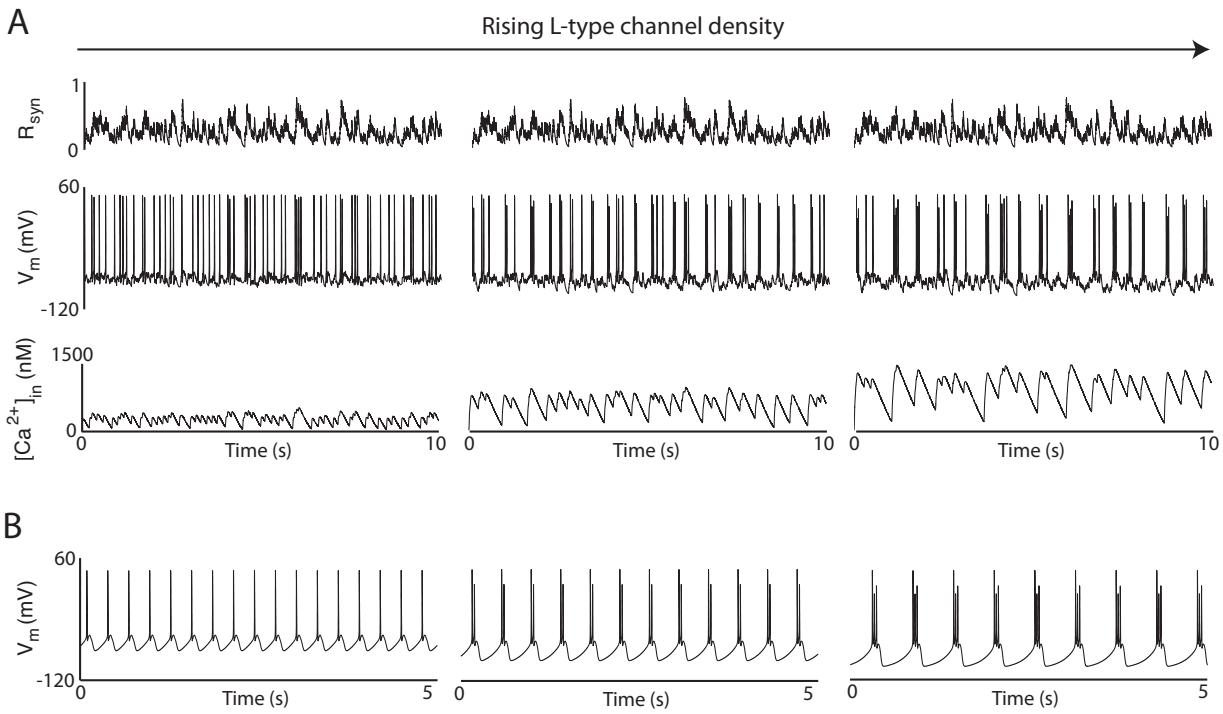

Figure 8.1 – Electrophysiological behavior of the simple DA neuron model in in vivo conditions for three different values of L-type calcium channel maximal conductance. The figure shows the evolution of the excitatory input (top), the membrane potential (middle) and the intracellular calcium concentration (bottom) over time. Each neuron is subjected to a SK channel blockade and to the same external excitatory input. An increase in L-type calcium channel density increases the burstiness of the neuron.

bursting necessitates the presence of NMDA excitatory inputs. On the other hand, this common view is not based on the fact that SK channel blockers do not affect DA neuron firing *in vitro*, but more on the fact that the effect is highly variable and therefore not statistically significant. One might therefore hypothesize that this variability comes from a variability in L-type calcium channel density between different DA neurons. Namely, neurons showing a high density of these calcium channels would switch from single-spike firing to bursting during SK channel blockade, whereas the others would be barely affected.

We verified this hypothesis on DA neuron extracellular recordings from the substantia nigra pars compacta (SNc) in the presence of synaptic blockers (10 mM CNQX, 1 mM MK801, 10 mM SR95531, 1 mM sulpiride and 1 mM CGP55845, which block AMPA, NMDA, $GABA_A$, D2 and $GABA_B$ receptors, respectively) (Fig. 8.2). Control experiments showed that application of the synaptic blockers alone induced a small increase in firing rate which was stable for at least one hour [40].

Consistent with the model prediction, the application of Apamin 300 nM, a SK channel blocker, has mixed effects on DA neuron signaling: whereas it barely affect firing rate and pattern in some neurons (Fig. 8.2A, left), it strongly increases irregularities and/or induces spontaneous bursting in others (Fig. 8.2A, right). This heterogenous effect was reversed by the application of a L-type calcium channel blocker (Nifedipine 20 μM), regularizing and homogenizing the firing pattern (Fig. 8.2B).

Consistent with our model predictions, these experimental observations suggest that L-type calcium channels play an important role in the SK channel blockade induced irregularities and bursting of DA cells. In particular, it shows that increasing L-type calcium channel density increases neuron burstiness under SK channel blockade both *in vitro* and *in vivo*. This heterogeneity might also be at the origin of the variability in the quality of SK channel-induced bursting observed in DA neurons *in vivo*, as reported in Chapter 6 (see Fig. 6.7).

To summarize, although DA neuron pacemaker activity is robust against heterogeneity in several ion channels, owing to the cooperativity of these channels, the nature of the dominant channel has nevertheless a strong impact on the excitability of the cell and its firing pattern under SK channel blockade. In particular, neurons whose dominant channels are L-type calcium channels, or "calcium pacemakers", would be proner to burst than "sodium

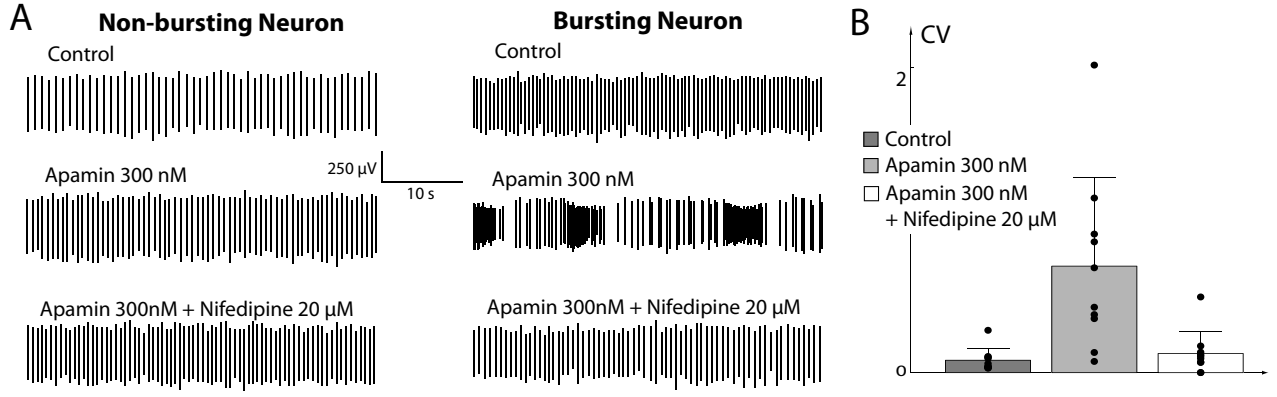

Figure 8.2 – The heterogeneity of dopaminergic (DA) neuron L-type calcium channel density is responsible for an heterogeneity in their firing pattern. A. Extracellular recordings of substantia nigra of two DA neurons from rat brain slices in control condition (top), during SK channel blockade (middle), and during concomitant blockade of SK channel and L-type calcium channel (bottom). **B.** Coefficient of variations of neuron firing patterns in each condition. Black point represents values for each neuron, bars represents the mean values and the standard deviation. Although DA neurons exhibit similar firing patterns in control conditions, SK channel blockade uncovers an heterogeneity, some DA neuron exhibiting electrophysiological signature of competitive excitability, namely single-spike firing, others of cooperative excitability, namely burst firing. A L-type calcium channel blockade solely affect the firing pattern of bursting neurons.

pacemakers", in which pacemaking is mostly sustained by sodium channels.

Sodium and calcium pacemaking

Fig. 8.3A,B shows the bifurcation diagram of the DA simple model of Chapter 4 for two configurations which differ in their maximal L-type calcium conductance ($\bar{g}_{Ca,L} = 1.5mS/cm^2$ for **A**, $\bar{g}_{Ca,L} = 0.5mS/cm^2$ for **B**). Several bifurcations show up for specific values of intracellular calcium concentrations, and these values are lower in configuration **B**. Indeed, we know that a rise of intracellular calcium concentrations reduces the excitability of the cell, through the inactivation (resp. activation) of an inward current exhibited by L-type calcium channels (resp. an outward current exhibited by calcium pumps). Moreover, calcium currents being excitatory, a reduction in their conductance results in a reduction of the excitability of the cell for a fixed value of $[Ca^{2+}]_{in}$. This explains why the curves move to the left when $\bar{g}_{Ca,L}$ is reduced.

Two types of bifurcations are observed: saddle-node bifurcations, which only occur in the presence of L-type calcium channels to be present (see Chapter 5) ; and Hopf bifurcations, which arises from sodium channels. Therefore, any event that occurs at a saddle node bifurcation (resp. Hopf bifurcation) relies on L-type calcium channels (resp. sodium channels). Among these events, one of particular interest is the initiation of action potentials. In Fig. 8.3A, the initiation of action potentials occurs at a saddle-node bifurcation, from what we may conclude that the early initiation of spikes in the simple model is induced by L-type calcium channels for that set of parameters, which refer to "calcium pacemaking".

On the other hand, when we reduce $\bar{g}_{Ca,L}$, this bifurcation moves to lower values of $[Ca^{2+}]_{in}$ (Fig. 8.3C). When this value of calcium becomes too low, a subcritical Hopf bifurcation appears and becomes the initiator of action potentials (configuration **B** in Fig. 8.3C) . In this configuration, the early initiation of spikes is induced by sodium channels, hence the name "sodium pacemaking".

These results show that, although sodium and calcium channels cooperate to sustain pacemaker firing in the simple DA neuron model, their relative proportion strongly affects the dynamical mechanisms of action potential initiation. In particular, there exists couples of conductance values at which the bifurcation responsible for the spike initiation switches from a subcritical Hopf bifurcation to a saddle-node bifurcation. Although Hopf bifurcation is a common mechanism for spiking in neurodynamics, the saddle node induced by a rise of $\bar{g}_{Ca,L}$ has never been described in neurodynamics to date (it even differ from the saddle-node not on invariant cycle bifurcation proposed in [90]). Moreover, further increases in L-type calcium channel maximal conductance increase the bistable range separating the low and high calcium thresholds (Supplementary Fig. S8.1), and his bistability is a key component of bursting. This might explains why a rise in L-type calcium channel density increases neuron burstiness.

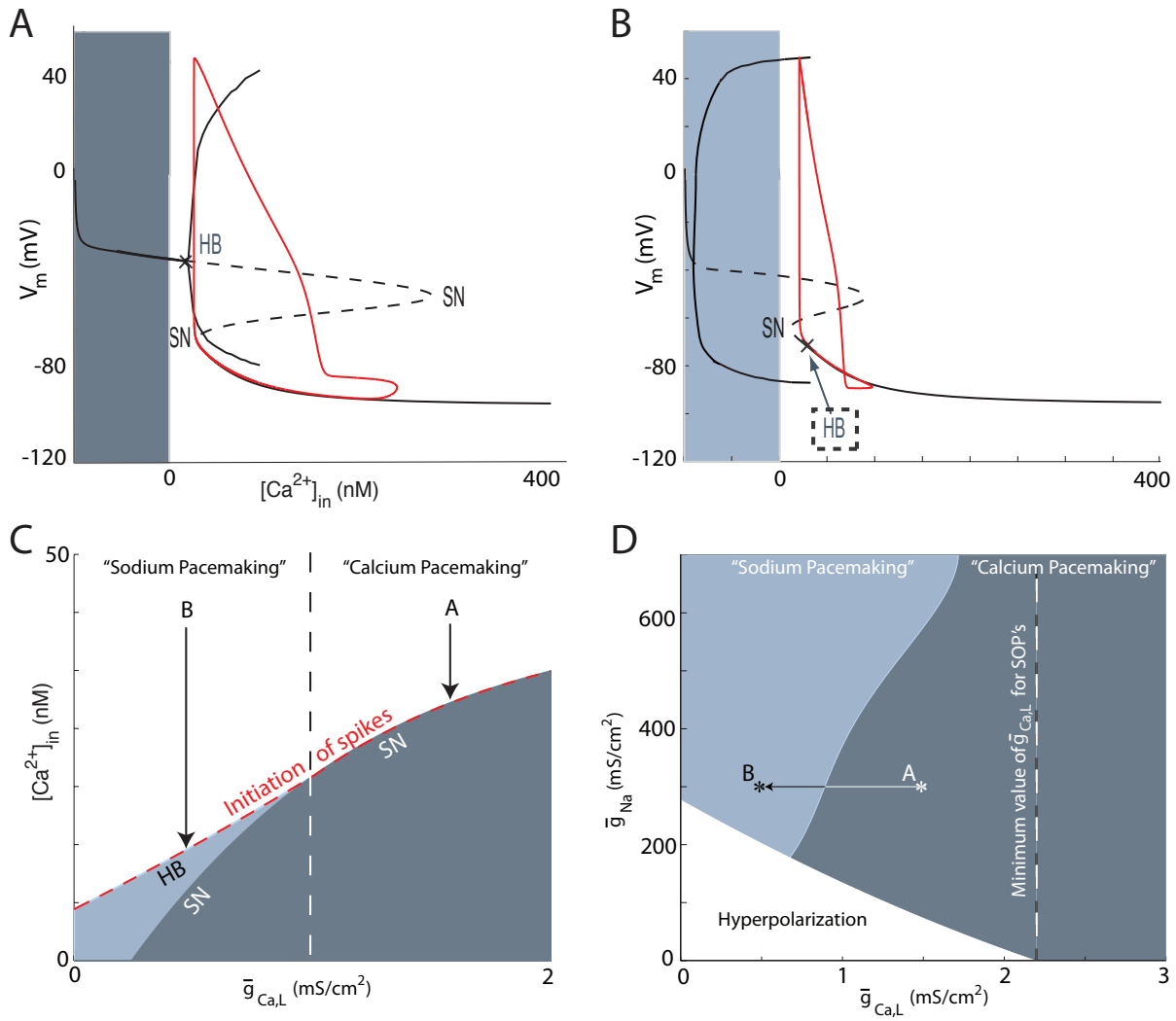

Figure 8.3 – Cooperation between sodium and calcium channels in the generation of spontaneous activity in the simple DA neuron model. A. Bifurcation diagram of the simple model in a relatively high L-type calcium conductance configuration ($\bar{g}_{Na} = 300mS/cm^2$, $\bar{g}_{Ca,L} = 1.5mS/cm^2$). **B.** Bifurcation diagram of the simple model in a relatively low L-type calcium conductance configuration ($\bar{g}_{Na} = 300mS/cm^2$, $\bar{g}_{Ca,L} = 0.5mS/cm^2$). **C.** Evolution of the value (in terms of $[Ca^{2+}]_{in}$) of the bifurcation responsible for the generation of spikes according to the L-type calcium channels maximal conductance. **D.** Type of pacemaker activity according to the sodium and L-type calcium conductances. The white zone represent the couples of conductances which results to a spontaneous hyperpolarization of the cell, the light blue zone account for "sodium pacemaking" and the dark blue zone for "calcium pacemaking". The pacemaker behavior of the model strongly rely on the values of both the sodium and the L-type calcium conductances.

Discussion

In this chapter, we analyzed the effect of L-type calcium channel density variations on the excitability of the DA neuron model and SNc DA neurons on brain slices. We saw that an increase in this density decrease neuron entrainability and burstiness. The dynamical origin of this increase in burstiness is the appearance and growth of a robust bistable zone as the calcium maximal conductance $\bar{g}_{Ca,L}$ increases. Moreover, the nature of the dominant channel during pacemaking determines different dynamical mechanisms of spike initiation, leading to the concept of sodium and calcium pacemaking. Although the bifurcation diagram of sodium pacemaking corresponds to the classical one of HH model, the bifurcation diagram of calcium pacemaking strongly differs from what has been described in the neurodynamics literature to date. It is therefore of interest to further investigate this uncommon spiking mechanism that seems to originate from calcium channels.

Chapter 9

A Novel Phase Portrait for Neuronal Excitability

Fifty years ago, FitzHugh introduced a phase portrait that became famous for a twofold reason: it captured in a physiological way the qualitative behavior of Hodgkin-Huxley model [81] and it revealed the power of simple dynamical models to unfold complex firing patterns [50]. To date, in spite of the enormous progresses in qualitative and quantitative neural modeling, this phase portrait has remained a core picture of neuronal excitability. Yet, FitzHugh analysis being based on the original Hodgkin-Huxley model [81], it only accounts for the role of sodium and potassium channels.

On the other hand, the prominent role of calcium channels in firing mechanisms has been highlighted in electrophysiology since then. In particular, calcium channels have an important role in the pacemaking behavior of DA neurons, as shown in Chapter 5, and the classical phase portrait fails to reproduce and explain the mechanisms underlying this firing pattern. Indeed, we saw in Chapter 8 that increasing L-type calcium channel maximal conductance in the simple DA neuron model induces a switch in the dynamical mechanisms underlying spike initiation, leading to a mechanisms that has not been described in neurodynamics to date.

In this chapter, we show that including a calcium current in Hodgkin-Huxley dynamics leads to a revision of FitzHugh-Nagumo phase portrait that affects in a fundamental way the reduced modeling of neural excitability. The revisited model considerably enlarges the modeling power of the original one. In particular, it captures essential electrophysiological signatures that otherwise require non-physiological alteration or considerable complexification of the classical model.

The results of these mathematical analyses lead to a novel simple model that further enriches the modeling power of the popular hybrid model of Izhikevich. A single parameter in the new model controls the neuron calcium conductance. In low calcium conductance mode, the model captures the standard behavior of earlier models. But in high calcium conductance mode, the same model captures the electrophysiological signature of neurons with a high density of calcium channels, in agreement with many experimental observations. For this reason, the novel reduced model is particularly relevant to understand the firing mechanisms of neurons that switch from a low calcium-conductance mode to a high calcium-conductance mode. Because thalamocortical (TC) neurons provide a prominent example of such neurons, they are chosen as a proof of concept of the present chapter, the benefits of which extend to a much broader class of neurons, as shown in Chapters 10, 11 and 12.

Results

Planar reduction of Hodgkin-Huxley model revisited in the light of calcium channels

Calcium channels participate in the spiking pattern by providing, together with sodium channels, a source of depolarizing currents. In contrast to sodium channels whose gating kinetics are fast, calcium channels activate on a slower time-scale, similar to that of potassium channels [78]. As a consequence, their activation opposes the hyperpolarizing effect of potassium current activation, resulting in bidirectional modulation capabilities of the post-spike refractory period. We model this important physiological feature by considering the HH model [81] with an additional non-inactivating voltage-gated calcium current I_{Ca} and a DC-current I_{pump} that accounts for hyperpolarizing calcium pump currents. The inactivation of calcium channels occurs in a slower time scale than the HH dynamics [189]. It can be modeled by a slower adaptation of the calcium conductance, which does not affect the single spike generation mechanism.

Figure 9.1A illustrates the spiking behavior induced by the action of an external square current I_{app} in the two different modes. As compared to the original HH model (Fig. 9.1A left), the presence of the calcium current is characterized by a triple electrophysiological signature (see Fig. 9.1A right):

- spike latency: the spike train (burst) is delayed with

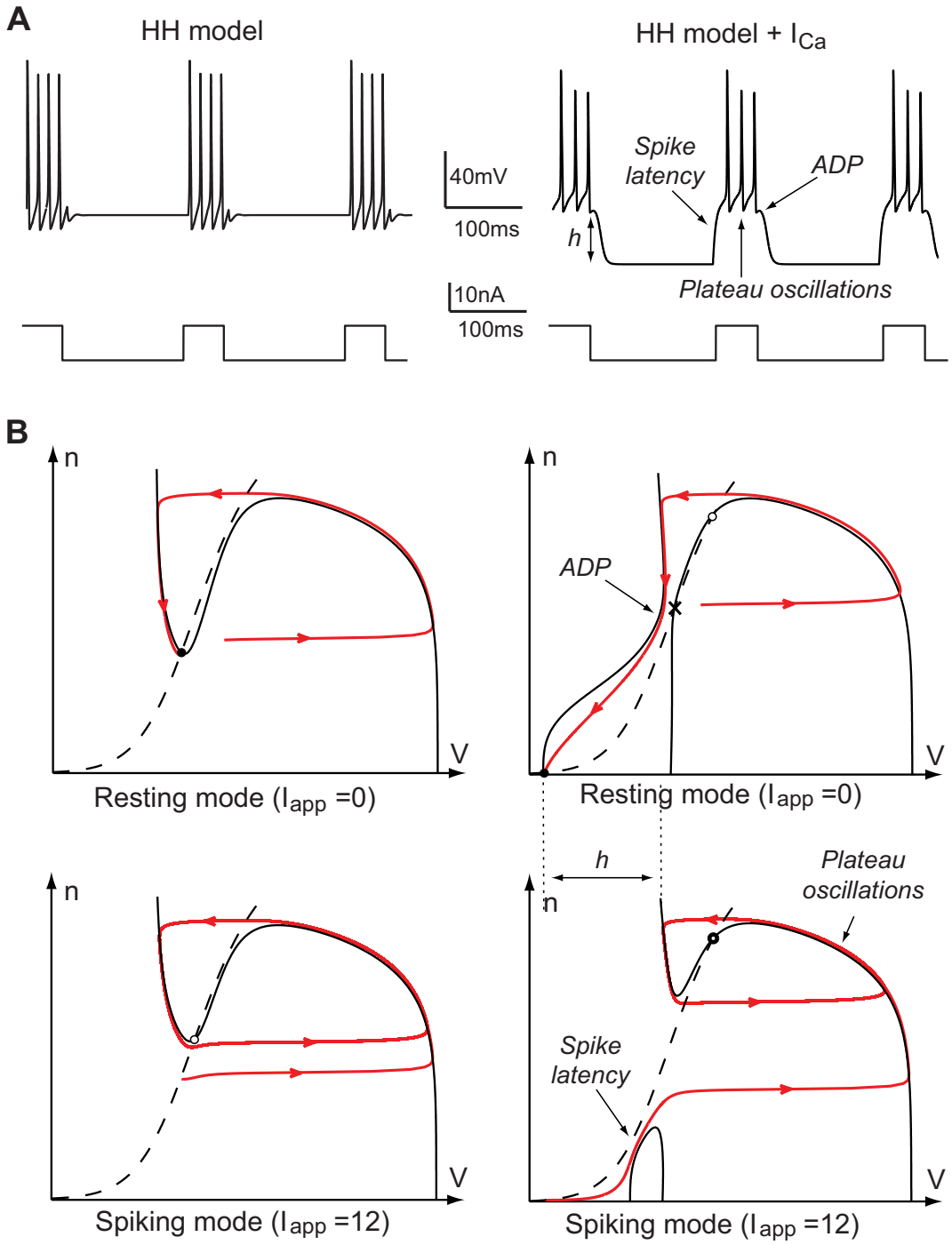

Figure 9.1 – Step responses of the HH model without (left) and with a calcium current (right). A. Time-evolution of the applied excitatory current (bottom) and of the corresponding membrane potential (top) in HH model (the reduced model leads to almost the same behavior (Supplementary Fig. S9.1)). **B**. Phase portraits of the reduced Hodgkin-Huxley model in resting (top) and spiking states (bottom). The V- and n-nullclines are drawn as a full and a dashed line, respectively. Trajectories are drawn as solid oriented red lines. Black circles denote stable fixed points, white circles unstable fixed points, and cross saddle points. The presence of calcium channels strongly affects the phase-portrait and the corresponding electrophysiological time-response of the neuron to excitatory inputs.

respect to the onset of the stimulation

- plateau oscillations: the spike train oscillations occur at a more depolarized potential than the hyperpolarized state
- after-depolarization potential (ADP): the burst terminates with a small depolarization

This electrophysiological signature is typical of neurons with sufficiently strong calcium currents. See for instance: spike latency [130, 146], plateau oscillations [9], ADPs [6, 26]. However, the mechanisms by which these behaviors occur have never been analyzed using reduced planar models to date.

Following the standard reduction of HH model [50], we concentrate on the voltage variable V (that accounts for the membrane potential) and on a recovery variable n (that accounts for the overall gating of the ion channels) as key variables governing excitability (see methods). The phase-portrait of the reduced HH model is shown in Fig. 9.1**B** (left). This phase portrait and the associated reduced dynamics are well studied in the literature (see [50] for the FitzHugh paper, and [46, 89] for a recent discussion and more references). We recall them for comparison purposes only. The resting state is a stable focus, which lies near the minimum of the familiar N-shaped V-nullcline. When the stimulation is turned on (spiking mode), this fixed point loses stability in a subcritical Andronov-Hopf bifurcation (see below), and the trajectory rapidly converges to the periodic spiking limit cycle attractor. As the stimulation is turned off (resting mode), the resting state recovers its global attractivity via a saddle-node of limit cycles (the unstable one being born in the subcritical Hopf bifurcation), and the burst terminates with small subthreshold oscillations (cf. Fig. 9.1**A** left).

In the presence of the calcium current, the phase-portrait changes drastically, as shown in Fig. 9.1B (right). In the resting mode, the hyperpolarized state is a stable node lying on the far left of the phase-plane. The V-nullcline exhibits a "hourglass" shape. Its left branch is attractive and guides the relaxation toward the resting state after a single spike generation. The sign of $\dot{V}$ changes from positive to negative approximately at the funnel of the hourglass, corresponding to the ADP apex. The right branch is repulsive and its two intersections with the n-nullcline are a saddle and an unstable focus.

When the stimulation is turned on, the V-nullcline breaks down in an upper and a lower branch. The upper branch exhibits the familiar N-shape and contains an unstable focus surrounded by a stable limit cycle, very much as in the reduced Hodgkin-Huxley model. In contrast, the lower branch of the V-nullcline, which is not physiological without the calcium currents, comes into play. While converging toward the spiking limit cycle attractor from the initial resting state, the trajectory must travel between the two nullclines where the vector field has smaller amplitude. As a consequence, the first spike is fired with a latency with respect to the onset of the stimulation, as observed in Fig. 9.1A (right) in the presence of the calcium current (see also Supplementary Fig. S9.1). In addition, a comparison of the relative position of the resting state and the spiking limit cycle in Fig. 9.1B (right) explains the presence of plateau oscillations. As the stimulation is turned off the spiking limit cycle disappears in a saddle-homoclinic bifurcation (see below), and the resting state recovers its attractivity.

The presence of the lower branch of the V-nullcline has a physiological interpretation. In the reduced HH model, the gating variable n accounts for the activation of potassium channels and the inactivation of sodium channels. Their synergy results in a total ionic current that is monotonically increasing with n for a fixed value of V (Fig. 9.2, left). In this situation, at most one value of n solves the equation $\dot{V} = 0$ and there can be only one branch for the voltage nullcline. In contrast, when calcium channels are present, the reduced gating variable must capture two antagonistic effects. As a result, the total ionic current is decreasing for low n (the gating variable is excitatory), and increasing for large n (the gating variable recovers its inhibitory nature) (Fig. 9.2, right). In this situation, two distinct values of n solve the equation $\dot{V} = 0$, which explains physiologically the second branch of the V-nullcline. To summarize, the lower branch of the voltage nullcline accounts for the existence of an excitatory effect of n, which is brought by calcium channel activation.

A bifurcation diagram with I_{app} as the bifurcation parameter sheds more light on the transition mechanism between the resting and spiking modes (Fig. 9.3). We use XPPAUT [45] for this numerical analysis. We draw the bifurcation diagram without (left) and with calcium channels (right) only for small I_{app}, corresponding to the transition from resting to limit cycle oscillations (Fig. 9.3) (for larger I_{app}, the stable limit cycle disappears in a supercritical Andronov-Hopf bifurcation in both cases, which leads to a stable depolarized, *i.e.* high-voltage, state).

Fig. 9.3 (left) illustrates the bifurcation diagram of the original reduced Hodgkin-Huxley model. For low values of I_{app}, the unique fixed point is a stable focus that loses stability in a subcritical Andronov-Hopf bifurcation at $I_{app} = I_{AH}$. Beyond the bifurcation, the trajectory converges to the stable spiking limit cycle. When I_{app} is lowered again below I_{SNLC}, the spiking limit cycle disappears in a saddle-node of limit cycles, the unstable one (not drawn) emanating from the subcritical Andronov-

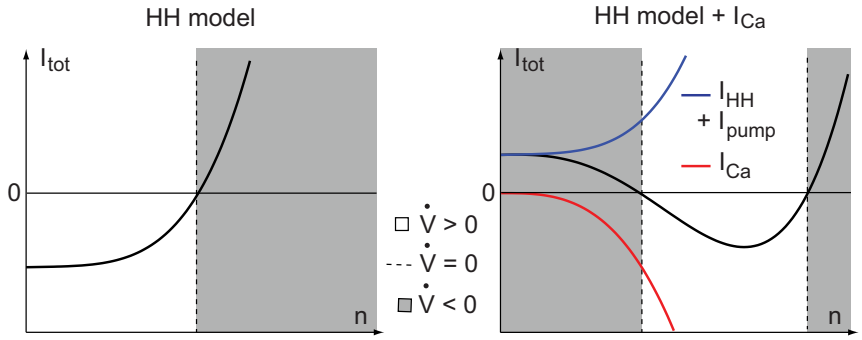

Figure 9.2 – Total ionic currents for V fixed as a function of n without (left) and with calcium channels (right). Blank portions corresponds to the values of n where $\dot{V} > 0$, shaded portions corresponds to the values of n where $\dot{V} < 0$, and the dashed lines correspond to the values of n where $\dot{V} = 0$. Note that the total ionic currents monotonically increase only in the absence of calcium channels (left).

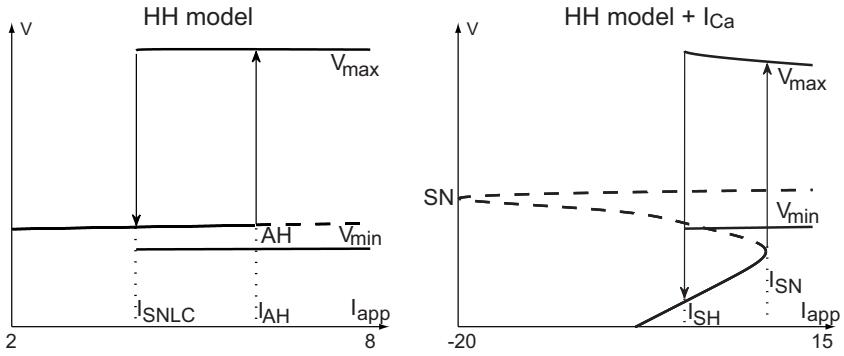

Figure 9.3 – One parameter bifurcation diagram of the reduced Hodgkin-Huxley model without (left) and with calcium channels (right). Thin solid lines represents stable fixed points, while dashed lines unstable fixed points or saddle points. The thick lines labeled V_{min} and V_{max} represent the minimum and the maximum voltage of stable limit cycles, respectively. I_x, with $x = SNLC, AH, SH, SN$, denotes the value of the input current for which the system undergoes the bifurcation x.

Hopf bifurcation, and the trajectory relaxes back to rest.

Fig. 9.3 (right) illustrates the bifurcation diagram of the reduced Hodgkin-Huxley model in the presence of calcium channels. For $I_{app} < I_{SN}$, a stable node (lower branch), a saddle (central branch), and an unstable focus (upper branch) are present, as in Fig. 9.1B(top right). The node and the saddle coalesce in a supercritical fold bifurcation at $I_{app} = I_{SN}$, and disappear for $I_{app} > I_{SN}$, letting the trajectory converge toward the stable limit cycle. The spike latency observed in the I_{Ca}-on configuration unmasks the ghost of this bifurcation. The stable limit cycle disappears in a saddle homoclinic bifurcation as I_{app} falls below I_{SH}, which lets the trajectory relax back to the hyperpolarized state. The homoclinic bifurcation exhibited by the Hodgkin-Huxley model with calcium channels is a key mathematical difference with respect to the standard HH model.

The central ruler of excitability is a transcritical bifurcation, not a fold one

The power of mathematical analysis of the reduced planar model is fully revealed by introducing two further simplifications.

- Time-scale separation: we exploit that the voltage dynamics are much faster than the recovery dynamics by assuming a small ratio $\dot{n} = O(\varepsilon)\dot{V}$ (the approximation holds away from the voltage nullcline) and by studying the singular limit $\varepsilon = 0$.

- Transcritical singularity: by comparing the shape of the voltage nullcline in Fig. 9.1B(right) for $(I = 0)$ and $(I = 12)$, one deduces from a continuity argument that a critical value $0 < I_c < 12$ exists at which the two branches of the voltage nullcline intersect.

The critical current I_c depends on ε. In the singular limit $(\varepsilon = 0)$ and for the corresponding critical current $I_c = I_c(0)$, one obtains the highly degenerate phase portrait in Fig. 9.4A (center). This particular phase portrait contains a transcritical bifurcation (red circle) which is the key ruler of excitability. This is because, as illustrated in Fig. 9.4B for $\epsilon > 0$, the convergence of solutions either to the resting point $(I < I_c)$ or to the spiking limit cycle $(I > I_c)$ is fully determined by the stable W_s and unstable W_u manifolds of the saddle point. In the singular limit shown in Fig. 9.4A, these hyberbolic objects degenerate to a critical manifold that coincides with the voltage nullcline near the transcritical bifurcation. It is in that sense that the X-shape of the voltage nullcline completely organizes the excitability, i.e. the transition from resting state to limit cycle.

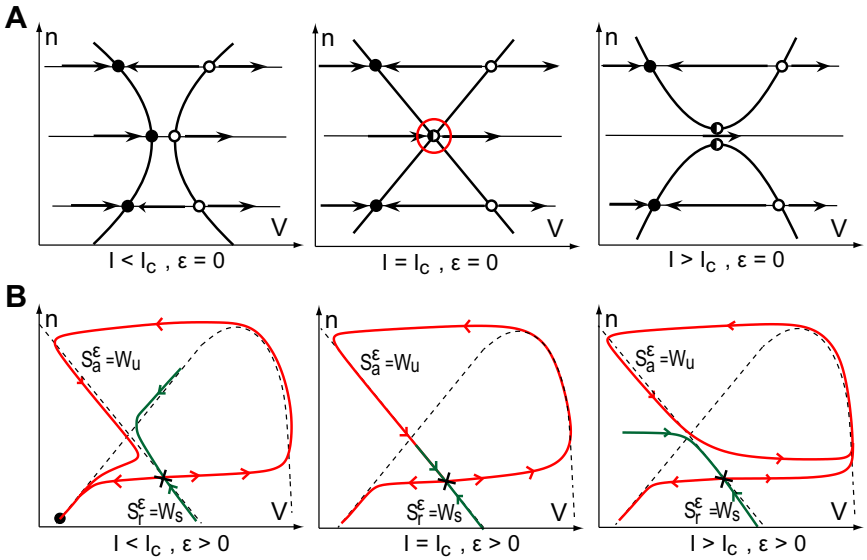

Figure 9.4 – Transcritical bifurcation as the main ruler of neuronal excitability. **A.** Cartoon of the V-nullcline transition through a singularly perturbed transcritical bifurcation. Black circles denote stable fixed points, white circles unstable fixed points. **B.** Continuation of the stable W_s (in green) and the unstable W_u (in red) manifolds of the saddle away from the singular limit (*i.e.* $\epsilon > 0$). They dictate the transition from the resting state ($I < I_c$) to the the spiking limit cycle ($I > I_c$) via a saddle-homoclinic bifurcation ($I = I_c$).

The persistence of the manifold W_s and W_u away from the singular limit can be rigorously established by geometric singular perturbation. The details of this analysis are available in the report [51]. The same analysis also establishes a normal form behavior in the neighborhood of the transcritical bifurcation: in a system of local coordinates centered at the bifurcation, the voltage dynamics take the simple form

$$\dot{v} \quad = \quad v^2 - w^2 + i + h.o.t.$$

where i is a re-scaled input current and with $h.o.t.$ referring to higher order terms in v, w, ε.

It should be emphasized that it is the same perturbation analysis that leads to the classical view of the Hodgkin-Huxley reduced dynamics: the transition from Fig. 9.1B left ($I = 0$) to Fig. 9.1B left ($I = 12$) involves a fold bifurcation that governs the excitability with a fold normal form

$$\dot{v} \quad = \quad v^2 - w + i + h.o.t.$$

It is of interest to realize that the addition of the calcium current in the HH model unmasks a global view of its phase portrait that has been disregarded to date for its lack of physiological relevance. Figure 9.5**A** shows the phase portrait of the classical reduced HH model for three different values of the hyperpolarizing current, revealing the transcritical singularity for the middle current value. The unshaded part of the first plot (and only this part of the plot) is familiar to most neuroscientists since the work of FitzHugh. Likewise, the conceptual sketch of the transcritical bifurcation will be familiar to all readers of basic textbooks in bifurcation analysis. For instance, the sketch is found in [166] as a prototypical example of non-generic bifurcation. It is symptomatic that this particular example is described at length but not connected to any concrete model in a texbook that puts much emphasis on the relevance of bifurcation analysis in neurodynamics applications. As shown in Fig. 9.5B, the missing connection is brought to life by calcium channels. Their particular kinetics renders the transcritical bifurcation of HH model physiological in the presence of a high-conductance calcium current.

Transcritical hybrid modeling of neurons

The singular limit of planar reduced models reveals that the excitability properties of spiking neurons are essentially determined by a local normal form of bifurcation of the resting equilibrium. This property is at the core of mathematical analysis of neuronal excitability (see [46, 89] and the rich literature therein).

In recent work, Izhikevich showed that, for computational purposes, the combination of the local normal form dynamics with a hybrid reset mechanism, mimicking the fast (almost discontinuous) spike down-stroke, is able to reproduce the behavior of a large family of neurons with a high degree of fidelity [88, 91]. Mimicking Izhikevich approach, we simplify the planar dynamics into the hybrid model:

$$\begin{aligned} \dot{v} &= v^2 - w^2 + I \qquad && \text{if } v \geq v_{th}, \text{then} \\ \dot{w} &= \epsilon(av - w + w_0) && v \leftarrow c, w \leftarrow d \end{aligned}$$

The proposed transcritical hybrid model is highly reminiscent of the hybrid model of Izhikevich, but it considerably enlarges its modeling power by including two features of importance:

- the transcritical normal form $\dot{v} = v^2 - w^2 + I$ replaces the fold normal form $\dot{v} = v^2 - w + I$, in

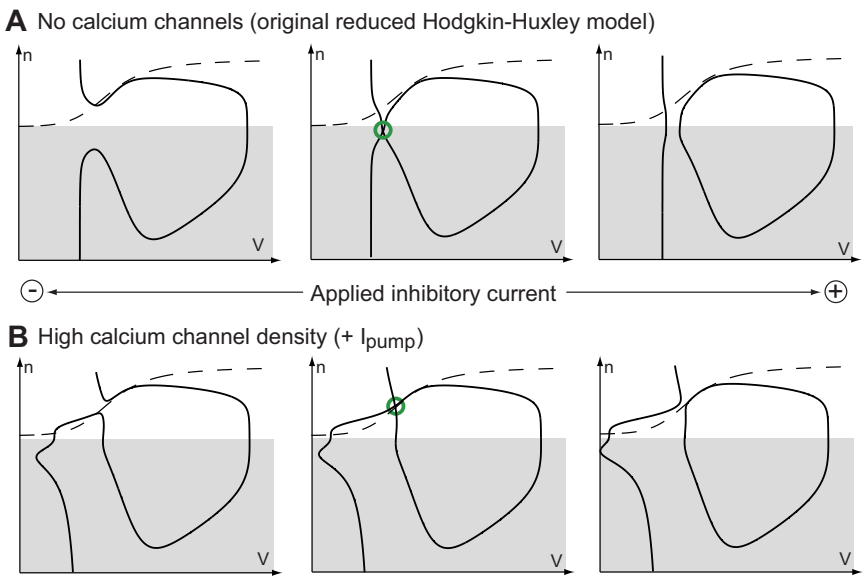

Figure 9.5 – Unfolding of the transcritical bifurcation in the global reduced Hodgkin-Huxley phase portrait. A. and **B.** Phase portraits or the original reduced HH model without (**A**) and with a calcium current (**B**). A constant inhibitory current of increasing amplitude (from left to right) is applied to the model. The transcritical bifurcation is non physiological in the classical reduced HH model (**A**) but plays an important physiological role in the presence of calcium channels (**B**).

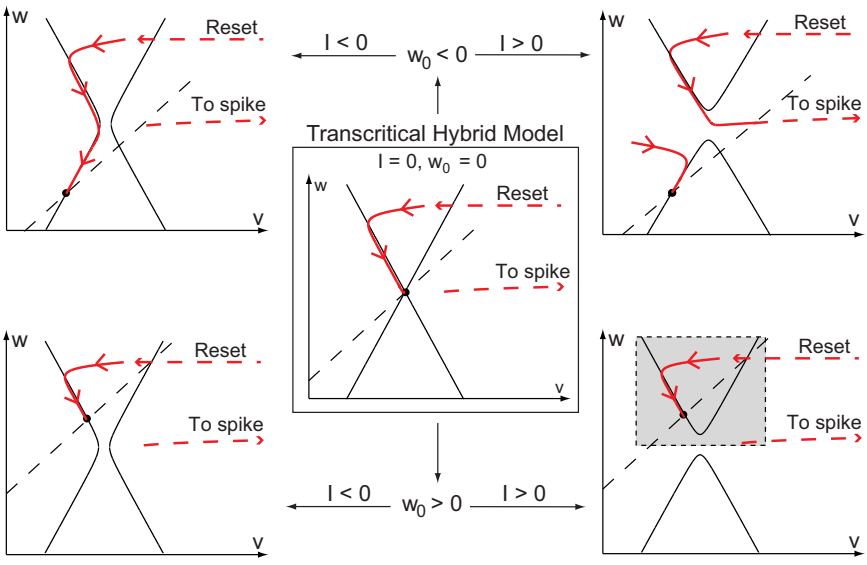

Figure 9.6 – Schematic phase-portraits of the transcritical hybrid model for different values of I and w_0. The v- and n-nullclines are drawn as full and dashed lines, respectively. The trajectories are drawn as red oriented lines. Many different phase-portraits derive from the transcritical hybrid model, including the one of the fold hybrid model, which only captures the shaded area.

accordance with the normal form analysis presented earlier.

- the new parameter w_0 determines whether the intersection of the voltage and recovery nullclines will take place above ($w_0 > 0$) or below ($w_0 < 0$) the transcritical singularity.

The parameter w_0 is a direct image of the calcium conductance: for small calcium conductances, the recovery variable nullcline only intersects the upper branch of the voltage nullcline (Supplementary Fig. S9.2) ; likewise in the hybrid model when $w_0 > 0$. For high calcium conductance, the recovery variable nullcline intersects the lower branch of the voltage nullcline (Supplementary Fig. S9.2) ; likewise in the hybrid model when $w_0 < 0$.

Fig. 9.6 summarizes the four different phase portraits that derive from the transcritical hybrid model for different values of I and w_0. For $w_0 > 0$, the model captures the classical view of the reduced HH model Fig. 9.6(bottom). For $w_0 < 0$, the model reveals the novel excitability properties associated to a high calcium conductance Fig. 9.6(top).The reader will notice the similarity between the phase portraits of Fig. 9.1 and of Fig. 9.6. The lower plots in Fig. 9.6 ($w_0 > 0$) correspond to the left plots in Fig. 9.1 (HH model, no calcium current). Likewise, the upper plots in Fig. 9.6 ($w_0 < 0$) correspond to the right plots in Fig. 9.1 (HH model + calcium current).

Reduced modeling of a thalamocortical relay neuron

Thalamocortical (TC) relay neurons are the input to sensory cortices. These neurons exhibit two distinct firing patterns: either a continuous regular spiking (Fig. 9.7A) or a plateau burst spiking (Fig. 9.7B) [83, 92, 93, 124]. The switch between the two modes is regulated by prominent T-type calcium currents that are deinactivated by hyperpolarization, thereby modulating the resting membrane potential [31, 83, 93, 124, 205]. These firing patterns have been observed during both *in vitro* and *in vivo* recordings [58, 66, 67, 68, 170], and have been shown to play an important role in thalamocortical relay [30, 125, 171, 175]. Among others, synchronous burst firing of TC relay cells is the key component of slow-wave sleep [125, 176], whereas the pathological generation of this firing pattern during wakefulness leads to absence epilepsy [84, 172, 203].

Because TC relay cells have an important role in physiology and pathology, they have been widely studied in the literature. In particular, their electrophysiological activity has been successfully reproduced in various conductance-based models [37, 83, 124, 189, 194, 204]. The two distinct spiking modes of TC neurons and their dependence on the activation of calcium channels make them

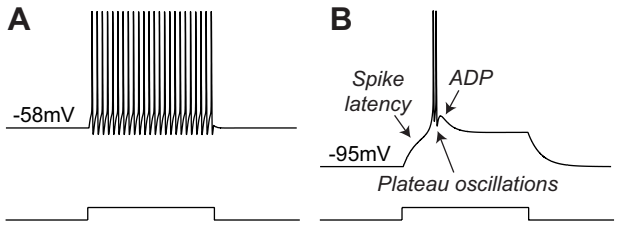

Figure 9.7 – Step responses of a conductance-based TC neuron model (adapted from [37]) in low (left) and high calcium conductance modes (right). (**A** and **B**): Membrane potential variations of the simulated TC neuron over time in both conditions. The model reproduces the firing patterns exhibited by TC relay cells, namely tonic and burst firing.

a good candidate to test the relevance of our qualitative reduced model against quantitative conductance-based models. In order to verify this hypothesis, we perform a classical two-dimension reduction of a state-of-the-art conductance based model proposed in [37] (see Methods for the reduction details).

Fig. 9.8 shows the phase portraits of the reduced TC model in the two different modes. When the neuron is initially depolarized, T-type calcium channels are inactivated, and the phase portrait is similar to the traditional FitzHugh-Nagumo model: the voltage nullcline has a simple (upper) branch, which breaks into a left and a right branches when the stimulation is off (Fig. 9.8A, black solid curves). The accompanying transcritical singularity appears at non-physiological values of the gating variable m_T. When the stimulation is turned on, the v-nullcline upper branch rises (Fig. 9.8A, light gray solid curve), the fixed point looses its stability to a limit cycle that relaxes to the resting state when the stimulation is switched off. Likewise, no plateau is observed and the repolarization phase is strictly monotonic (no ADP can be exhibited).

The situation is very different when the neuron is initially hyperpolarized, because T-type calcium channels are then deinactivated, critically affecting the phase portrait: a lower v-nullcline branch is now present for physiological values of m_T, and the hyperpolarized state belongs to this lower branch (Fig. 9.8B, upper-left, black gray solid curves). When a depolarizing current step is applied, this branch falls below the m_T-nullcline (Fig. 9.8B, upper-left, light gray solid curves). In order to generate the first spike, the state travels the narrow region between the two nullclines, resulting in a pronounced latency. This latency relies on the small level of I_T activation in this hyperpolarized state (the m_T-nullcline is almost horizontal), and is amplified by the dynamic inactivation of T-type calcium channels, which further narrows this funnel. This observation in agreement with previ-

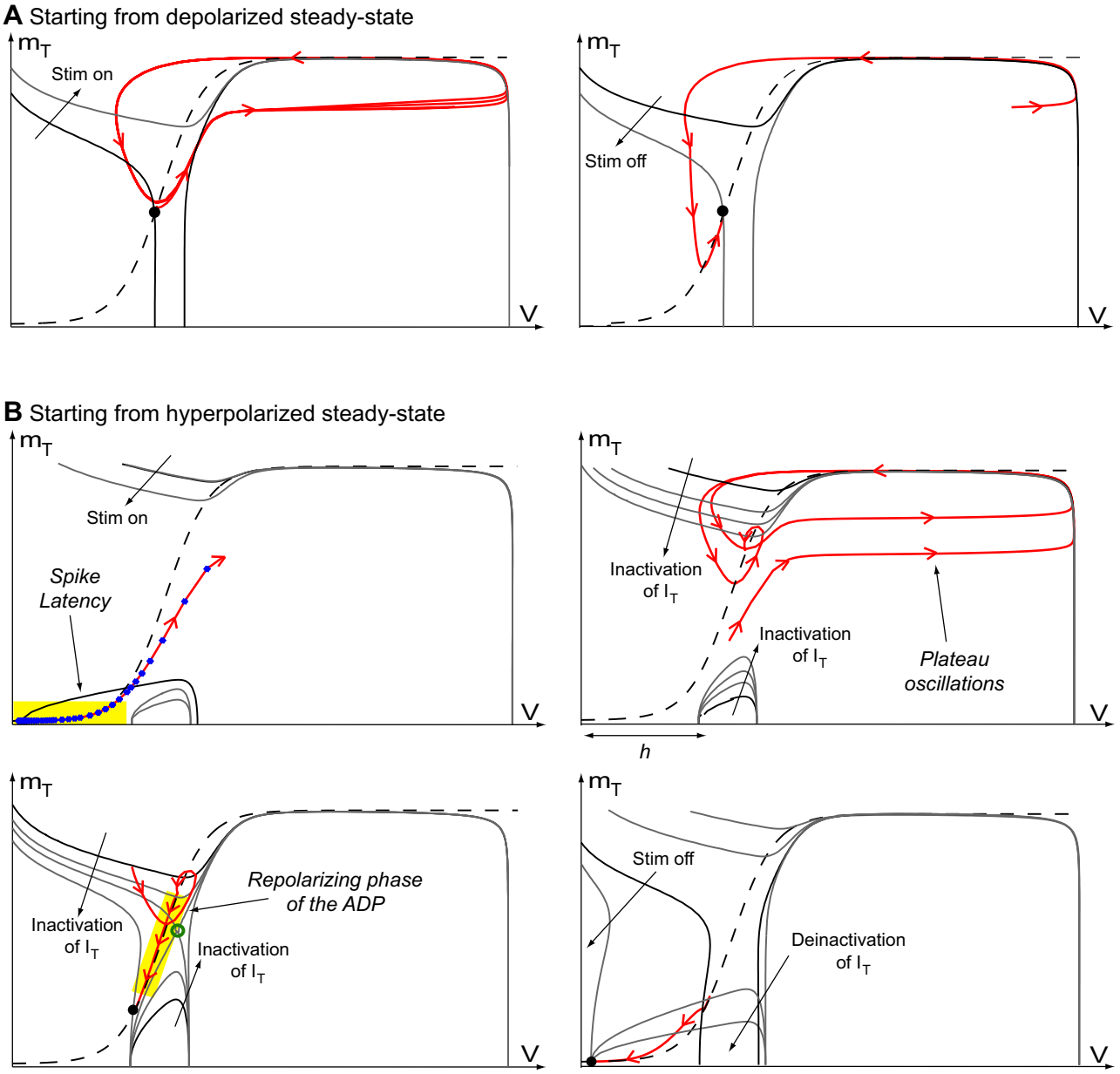

Figure 9.8 – Phase-portraits of the reduced conductance based TC model in low (A) and high calcium conductance modes (B). The v- and m_T-nullclines are drawn as full and dashed lines, respectively, and the hyperpolarized state as a filled circle •. The trajectories are drawn as red oriented lines. In high calcium conductance mode, the phase portrait shows two v-nullclines branches which derives from a transcritical singularity.

ous experimental and modeling data [204]. Furthermore, the relative position of the hyperpolarized state (lower branch) with respect to spiking cycle (upper branch) clearly explains the generation mechanism of plateau oscillations.

These high frequency plateau oscillations continue until the T-type calcium channel inactivation dominates (Fig. 9.8B, upper-right). At the end of the burst, the system converges toward the hyperpolarized state, being attracted first by the upper part of the v-nullcline (depolarizing phase of the ADP), then by its lower part (repolarizing phase of the ADP) (Fig. 9.8B, lower-left). Note the presence of a transcritical bifurcation in the phase portrait for a particular value of T-type calcium channel inactivation (Fig. 9.8B, lower-left, green circle). Finally, when the stimulation is relaxed, the neuron recovers its initial hyperpolarized state and the inactivation of T-type calcium channels is released (Fig. 9.8B, lower-right).

This phase portrait analysis confirms that the transcritical singularity in indeed a key ruler of excitability in this reduced conductance based TC neuron model. As a consequence, our proposed transcritical hybrid model seems appropriate to capture the essence of its firing mechanisms.

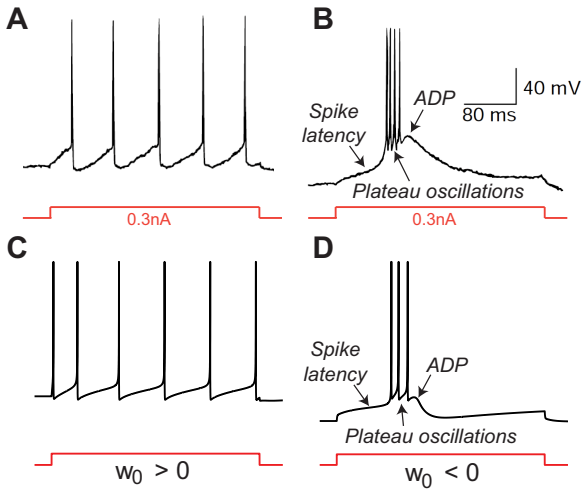

Figure 9.9 – Comparison of the experimental step response of a TC neuron in vitro[171] (top) and the step response of the proposed transcritical hybrid model (bottom) in low (left) and high calcium conductance modes (right). A. and **B.**: Membrane potential variations of the recorded TC neuron over time in both conditions. **C.** and **D.** Membrane potential variations of the modeled TC neuron over time in both conditions. A variation of w_0, which is an image of the calcium conductance, is sufficient to generate the switch of firing pattern physiologically observed in TC cells.

Transcritical hybrid modeling of a thalamocortical relay neuron

The phase portrait analysis in the previous section suggests the relevance of a reduced transcritical hybrid model to model TC relay neurons. We emphasize that our objective is not a fine tuned quantitative modeling of the TC neuron firing pattern. Rather, we attempt to provide a qualitative picture of how the proposed simple hybrid dynamics permits to reproduce and explain the behavior of TC neurons and, in particular, the role of calcium currents.

Fig. 9.9 compares the experimental step response of a TC neuron *in vitro* and the simulated step response of the transcritical hybrid model (12.1), both in the low and high calcium conductance modes. As discussed above, the small calcium conductance mode is obtained by choosing a positive w_0 (T-type calcium channels are inactivated), whereas the large calcium conductance mode is obtained by choosing a negative w_0 (T-type calcium channels are deinactivated), all the other parameters being identical in the two modes. An additional variable z accounts for the slow adaptation mechanisms, such as e.g. T-type calcium channels inactivation and variations of intracellular calcium concentration. The hybrid model reproduces the experimental observation: in the low-calcium mode, it responds with a slow regular train of action potentials; in the high-calcium mode, it responds with a long spike latency, plateau oscillations, and an ADP.

Fig. 9.10 shows the phase-portraits of the transcritical hybrid model in the two modes. Note the great similarity with these phase portraits and the ones of the reduced conductance-based TC neuron model. When $w_0 > 0$ (Fig. 9.10, left), the hyperpolarized state belongs to the upper branch of the v-nullcline. Application of a depolarizing current step lifts the voltage nullcline above the resting state, thus generating a transient non-delayed action potential (marked with a $*$ in Fig. 9.10A, left). When the hyperpolarized state belongs to the upper branch of the v-nullcline, no plateau oscillations are possible (Fig. 9.10A, left). Furthermore, the relaxation toward the hyperpolarized state is necessarily monotone (*i.e.* no ADP), as stressed in Fig. 9.10B, left.

At the generation of the first spike, z increases, which reduces the excitability of the cell (calcium accumulates in the intracellular space for instance, which activates hyperpolarizing calcium pumps), and the v-nullcline upper branch falls. As the neuron remains polarized, z decreases (the intracellular calcium is expelled), calcium pump currents slowly deactivate and the cell slowly depolarizes (interspike period), until the spiking threshold is reached and a new action potential is fired (Fig. 9.10**B**, left).

When $w_0 < 0$ (Fig. 9.10, right), the hyperpolarized

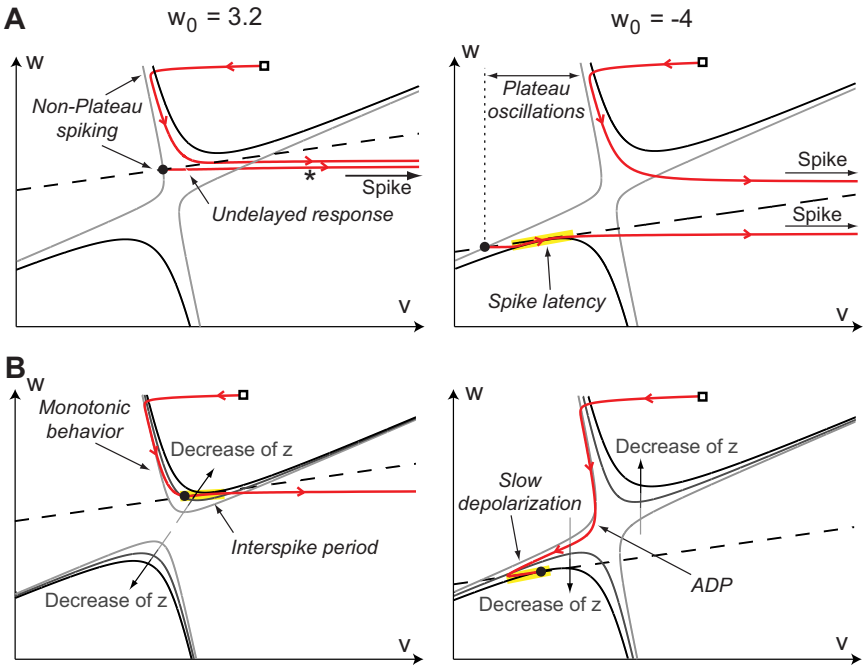

Figure 9.10 – Phase-portrait of the transcritical hybrid model of a TC cell in the low ($w_0 = 3.2$, left) and high calcium conductance modes ($w_0 = -4$, right). Trajectories are depicted as solid oriented red lines. The reset point is depicted as a square □, while the (instantaneous) hyperpolarized state as a filled circle •. The w-nullcline is depicted as a dashed line. In (**A**), the gray (black) thin solid line is the v-nullcline when the current step in off (on). In (**B**), the v-nullcline is depicted as gray thin lines of different darkness. As sketched in the figure, light gray correspond to large values of z, whereas dark gray to small.

state belongs to the lower branch of the v-nullcline, and is more hyperpolarized than for $w_0 > 0$, as in experiments. When a depolarizing current step is applied, this branch falls below the w-nullcline (Fig. 9.10A, right). In order to generate the first spike, the state travels in the narrow region between the two nullclines, resulting in a pronounced latency. Furthermore, the relative position of the hyperpolarized state (lower branch) with respect to (hybrid) spiking cycle (upper branch) clearly explains the generation mechanism of plateau oscillations, as in the reduced TC model. These high frequency plateau oscillations (burst) continue until z is sufficiently large (T-type calcium channels are inactivated and calcium accumulates in the cytoplasm). Plateau oscillations then terminate in a (hybrid) saddle-homoclinic bifurcation (Fig. 9.10A, right).

At the end of the burst, the system converges toward the hyperpolarized state following the left branch of the v-nullcline, thus generating a marked ADP at the passage near the nullcline funnel. The subsequent slow phase is mainly ruled by the variations of the intracellular calcium. With the adopted simple dynamics it consists in a slow depolarization that follows the decrease of the intracellular calcium (Fig. 9.10B, right). A finer and more physiological modeling of the intracellular calcium dynamics could reproduce *in vitro* recordings with a higher degree of fidelity. Note that the ADP trajectories are slightly different in the reduced conductance based and the transcritical hybrid models. This minor difference is due to a lower time-scale separation in the reduced TC model for low values of V, but the generating mechanisms are similar. We discuss the impact of this difference in the next section.

In order to further verify the physiological consistence of the transcritical model, we compare its behavior with the simulated step response of another quantitative one compartment model [83, 124], a quantitative 200-compartments model [37] (simulations were run in the *Neuron* environment, based on the configuration files freely available at `http://cns.iaf.cnrs-gif.fr/alain_demos.htML81`) and a fold hybrid model [89] of a TC relay cell in the large conductance mode (Supplementary Fig. S9.3). For the quantitative models, we plot the trajectory projection on the $V - m_T$ plane, where V and m_T denotes the somatic membrane potential and the activation gating variable of the somatic T-type calcium current, respectively.

There is a striking similarity between the projection of the trajectories between both quantitative models and the phase portrait of the second-order transcritical model. In both cases, the ADP is generated during a decrease of the activation variable, and plateau oscillations are exhibited far from the resting state. Moreover, the spike latency is a robust property of the transcritical model because the trajectory must visit the neighborhood of both the nullclines $\dot{V} = 0$ and $\dot{w} = 0$ before converging to the spiking limit cycle. It should be stressed that there are no comparable ways to reproduce this behavior in a fold hybrid model. Indeed, as highlighted above, reproducing this behavior with the standard reduced HH model necessitates a non physiological alteration of the

reset rule (Supplementary Fig. S9.3 [89, 182]). This underlines the relevance of the revisited model to capture the richness of neuronal excitability.

Robust generation of after depolarization periods

For a neuron model to be biologically relevant, it should be robust to exogenous disturbances (small synaptic inputs, thermal noise, etc.). The firing pattern, in particular, should remain unchanged. Fig. 9.11 compares the perturbation robustness of three TC neuron models to small current impulses. It suggests that the fold hybrid model is less robust than the transcritical model, because a tiny pulse is sufficient to generate an extra action potential at the ADP apex.

The difference in robustness is explained by the different ADP generation mechanisms, as illustrated in Figure 9.12. In the fold model, ADPs are generated when trajectories cross the v-nullcline from below (Fig. 9.12, see also Supplementary Fig. S9.3). The absence of any robust attractor in the ADP generation region makes the ADP height and shape heavily dependent on the exact reset point. Moreover, when small current pulses are applied, the ADP generation is disrupted, and the model fires an extra (non-physiological) spike.

Conversely, ADP generation in the transcritical hybrid model is robustly governed by the attractor S_a^ϵ that steers the trajectories through the ADP apex and toward the resting point. That is the reason why the ADP height and shape barely depend on chosen reset point. At the same time, the persistence to small perturbations of this invariant manifold [79] ensures, as required in biologically meaningful conditions, the robustness of the ADP generation mechanism to small inputs.

The ADP apex is the most excitable part of the trajectory. A physiologically relevant external stimulation can easily generate a spike during this small period, whereas the neuron is barely excitable in the preceding and following periods. This suggests a major role for this ADP in the modulation of external inputs by neuron endogenous rhythm. This excitability can be finely tuned through variations of channel kinetics. For instance, the presence of a "buckle" in the ADP trajectory of the reduced conductance based model in Fig. 9.8 (compare to Supplementary Fig S9.3) is an artifact that illustrates the sensitivity trajectories around the ADP apex, a mathematical illustration of the neuron excitability at this particular instant.

Discussion

Calcium channels physiologically unmask the physiological relevance of a global view of the reduced Hodgkin-Huxley phase portrait

The inclusion of calcium channels in Hodgkin-Huxley model has a dramatic impact on its mathematical reduction: the firing mechanisms are governed by the local normal form of a transcritical rather than fold bifurcation. It results in the presence of a new voltage nullcline branch in the phase portrait, which lies below the classical inverted N-shaped one. When the calcium channel density is high, neuronal excitability is governed by this lower branch, which accounts for the physiological signature of these currents: spike latency, plateau oscillations and afterdepolarization potential.

Interestingly, it is not the phase portrait of the reduced HH model that is affected by calcium, but only the subregion of the plane where it is physiologically relevant. Indeed, the transcritical singularity is the core mechanism of the classical Hodgkin-Huxley model as well, and the well known fold bifurcation derives from it. As a consequence, the classical FitzHugh Nagumo phase portrait is a particular (because localized) view of the more complete picture studied in the present paper. This complete picture and its dynamical consequences are brought to live by any slowly activating depolarizing current, calcium currents being the most representative. Note that it may be generated by a slowly activating persistent sodium current as well.

The proposed planar model differs from earlier planar models that include calcium channels

The proposed planar model is distinctively different from earlier reduced models that include calcium channels in that its slow variable (n or w) aggregates in the same time scale the antagonistic activation of potassium and calcium channels, thereby capturing the non monotonicity of the total ionic current (Fig. 9.2, right). This property is lost when the activation of calcium channels is treated as a fast variable, that is, set at steady-state in the reduction such as, for instance, in the popular Morris-Lecar model [132]. A classical reference such as [78] nevertheless suggests that the time constant of calcium and potassium activations are comparable, motivating the reduction adopted in the present paper.

The richness of neuronal excitability is captured in a two dimensional transcritical hybrid model

Although this enlarged phase portrait is the source of rich and diverse forms of excitability, its essence is captured in a simple and physiologically grounded hybrid model.

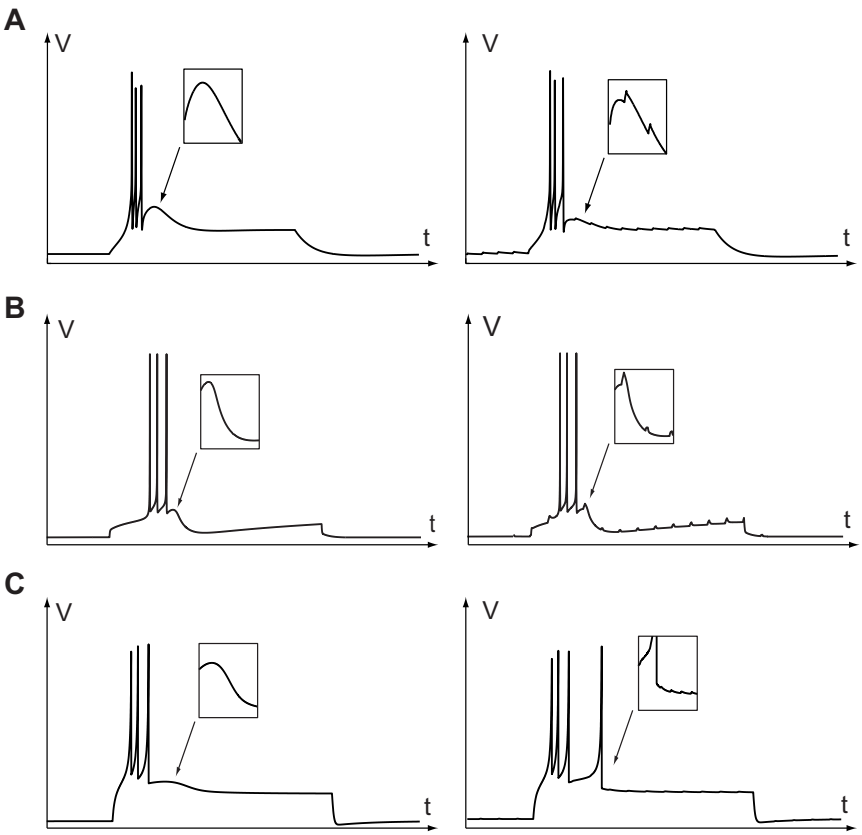

Figure 9.11 – Nominal step response (left) and step response in the presence of small current pulses in the 200 compartments TC neuron model (A), the transcritical hybrid model (B), and the fold hybrid model of TC neuron [91] (C).

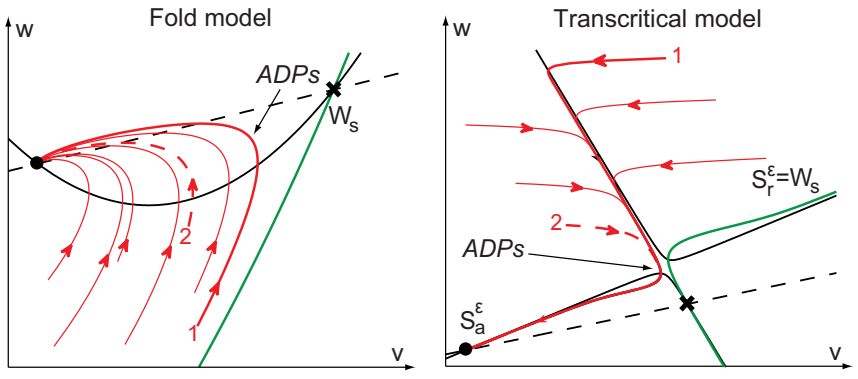

Figure 9.12 – Comparison of the ADP generation mechanisms in the fold (left) and in the transcritical hybrid models (right). The stable manifold of the saddle ($\times$) is depicted in green. In the fold hybrid model, ADPs are generated by sliding near the stable manifold of the saddle and crossing the v-nullcline from below. In the transcritical hybrid model, ADPs are robustly generated along the attractor S_a^ε.

The illustration of its modeling power on the thalamocortical neuron excitability shows the impact of revisiting the classical view. Indeed, whereas tonic spiking of these cells is well captured by classical models based on the fold normal form, the generation of burst firing needs non physiological alterations of the phase portrait and the reset rule of these models. On the other hand, both firing patterns can be generated in the transcritical hybrid model through a change in one parameter, which reflects the proportion of calcium channels which are not inactivated.

This illustration is just the top of the iceberg because the same principle will apply to many important families of neurons that are thoroughly studied and that have so far largely resisted reduced modeling. The proposed model will impact the understanding of excitability of e.g. dopaminergic, serotonergic, and subthalamic nucleus neurons, whose various firing patterns have a direct and critical impact in physiology and diseases, such as Parkinson's disease and depression.

Chapter 10

The Novel Phase Portrait uncovers two New Types of Excitability

In the early days of experimental neurophysiology, Hodgkin identified three distinct types of excitability (nowadays called Type I, II, and III) by stimulating crustacean nerves with constant current stimuli [80]. The three types of excitability have long been associated to three distinct mathematical signatures in conductance-based models. They all can be described in planar models of the FitzHugh type [50], which can be rigorously associated to the mathematical reduction of high-dimensional models (see for instance the planar reduction of Hodgkin-Huxley model in [148] and the excitability analysis in [150]). Reduced models have proven central to the understanding of excitability and closely related mechanisms such as bursting. However, understanding excitability in detailed conductance-based models remains a challenge, especially for neurons that exhibit transition between distinctively different firing types depending on environmental conditions. The present paper proposes a generalization of FitzHugh-Nagumo model that provides novel insights in the simple classification of excitability types.

The proposed model is a "mirrored" version of FitzHugh-Nagumo model, motivated by the mathematical reduction of conductance-based models including calcium channels proposed in Chapter 9 [42]. A central observation of Chapter 9 is that the electrophysiological signature of excitability is strongly affected by a local property of the recovery variable at the resting equilibrium: if the recovery variable is slow restorative, that is, provides a negative feedback on membrane potential variations such as in all planar reductions of Hodgkin-Huxley model, the qualitative properties of excitability are well captured by the classical Fitzugh-Nagumo model. In contrast, if the recovery variable is slow regenerative, that is, provides a positive feedback on membrane potential variations, then the electrophysiological signature is distinctively different. This is for instance observed in a planar reduction of Hodgkin-Huxley model augmented with an activating calcium current (see Chapter 9). The chief difference between the restorative or regenerative nature of the recovery variable is responsible for an alteration of the phase portrait that cannot be reproduced in FitzHugh-Nagumo model and that calls for a generalized model that motivates the present chapter.

We construct a highly degenerate pitchfork bifurcation (co-dimension 3) that is shown to organize excitability in five different types. The three first types correspond to the types of excitability extensively studied in the literature. They are all restorative, in the sense that they only involve a region of the phase plane where the model recovery variable is purely restorative. In addition, the model reveals two new types of excitability (Type IV and V) that match the distinct electrophysiological signatures of conductance-based models of high density calcium channels. We prove that these two new types of excitability cannot be observed in a purely restorative model, such as FitzHugh-Nagumo model. In addition, an important result of the analysis is that Type IV and V excitable models exhibit a bistable range that persists in the singular limit of the model. This, in sharp contrast to the Type I, II, and III. The result suggests the potential importance of Type IV and V excitability in bursting mechanisms associated to regenerative ion channels, as discussed in Chapters 11 and 12.

Results

A mirrored FitzHugh-Nagumo model and its physiological interpretation

The chapter studies the excitability properties of the planar model

$$\dot{V} = V - \frac{V^3}{3} - n^2 + I_{app} \tag{10.1a}$$

$$\dot{n} = \epsilon(n_\infty(V - V_0) + n_0 - n) \tag{10.1b}$$

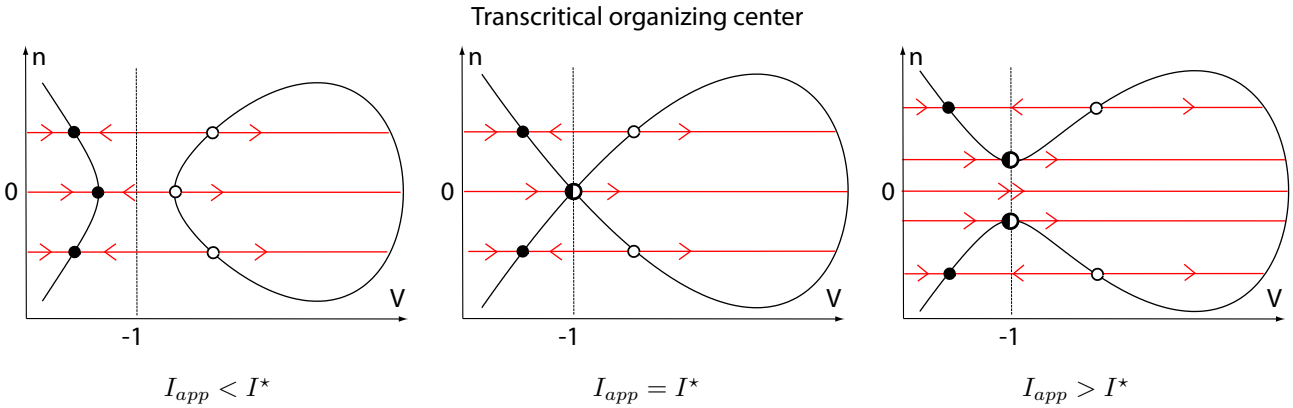

$I_{app} < I^\star$ $I_{app} = I^\star$ $I_{app} > I^\star$

Figure 10.1 – V-nullcline (in black) and singular, *i.e.* $\epsilon = 0$, vector field (in red) of system (10.1) for different values of I_{app}. Stable fixed points are depicted as filled circles, unstable as circles, and bifurcations as half filled circles

where $n_\infty(V)$ is the standard Boltzman activation function

$$n_\infty(V) := \frac{2}{1+e^{-5V}}, \tag{10.2}$$

The model is reminiscent of the popular FitzHugh-Nagumo model of neuronal excitability: Eq. (10.1a) describes the fast dynamics of the membrane potential V, whereas Eq. (10.1b) describes the slow dynamics of the "recovery variable" n that aggregates the gating of various ionic channels.

The voltage dynamics Eq. (10.1a) are identical to the FitzHugh-Nagumo model, except that the quadratic term n^2 replaces the linear term n. The resulting nullcline $\dot{V} = 0$ "mirrors" along the V-axis the classical inverse N-shaped nullcline of FitzHugh-Nagumo model, as illustrated in Fig. 10.1. The figure illustrates the phase portrait of the model in the singular limit $\epsilon = 0$. The left and right phase-portraits are the unfolding of the transcritical bifurcation organizing center (see e.g. [166, Pages 104-105]) obtained for $I_{app} = I^\star := \frac{2}{3}$. This particular value will help understanding excitability mechanisms at work in the situation $I_{app} > I^\star$, illustrated in the right figure.

The recovery dynamics Eq. (10.1b) exhibit the familiar first-order relaxation of ionic current to the static sigmoid curve illustrated in Fig. 10.2. For quantitative purposes, the numerator in the right hand side of Eq. (10.2) can be picked larger or equal than 2 without changing the underlying qualitative analysis. The parameters (V_0, n_0) locate the relative position of the nullclines in the phase portrait. In particular, the region

$$S_{n_0} := \{(V,n) \in \mathbb{R}^2 :\ n \in (n_0,\ n_0+2)\} \tag{10.3}$$

is attractive and invariant for the dynamics of system (10.1). The parameter n_0 slides up and down the "physiological window" of the recovery variable, whereas, V_0 is the half-activation potential. The potential $V^\star < V_0$ is defined as the voltage at which $n_\infty(V - V_0)$ has unitary slope. We adopt the conventional notation n for the recovery variable but will allow $n_0 < 0$, which makes the range of n include negative values. This is purely for mathematical convenience and should not confuse the reader used to the physiological interpretation of a gating variable with range $[0,\ 1]$. For any value of n_0, the mathematical range $[n_0,\ n_0+2]$ of the recovery variable n can be mapped to the physiological range $[0,\ 1]$ of a gating variable $\tilde{n}$ via the affine change of coordinate $\tilde{n} = \frac{n-n_0}{2}$.

Restorative and regenerative excitability

The recovery variable n of model (10.1) is restorative in the half plane $n > 0$, that is it provides a negative feedback on membrane potential variations, because

$$\frac{\partial \dot{V}}{\partial n}\frac{\partial \dot{n}}{\partial V} < 0.$$

In contrast, it is regenerative in the half plane $n < 0$, that is it provides a positive feedback on membrane potential variations, because

$$\frac{\partial \dot{V}}{\partial n}\frac{\partial \dot{n}}{\partial V} > 0.$$

A consequence of that observation is that the recovery variable of model (10.1) is always restorative when $n_0 > 0$. The corresponding phase portrait is illustrated in Fig. 10.3A. It is reminiscent of FitzHugh-Nagumo model and will recover known types of excitability. In contrast, n is either restorative or regenerative when $n_0 < 0$. The corresponding phase portrait (Fig. 10.3B) is distinctly different from FitzHugh-Nagumo model and it will lead to the novel types of excitability studied in this paper. The role of the proposed mirrored FitzHugh-Nagumo model is to study the transition from a purely restorative model

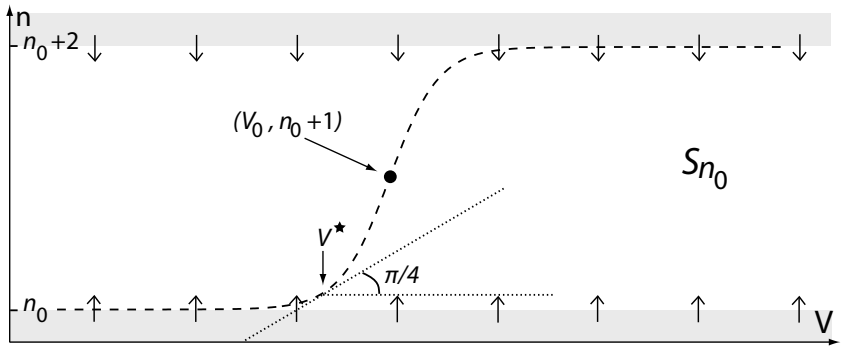

Figure 10.2 – Dependence of the n-nullclines (dashed line) of (10.1) on the parameters n_0 and V_0. The location of the nullcline in the phase plane determines an attractive invariant region S_{n_0}. At the voltage $V^\star$, the nullcline has unitary slope.

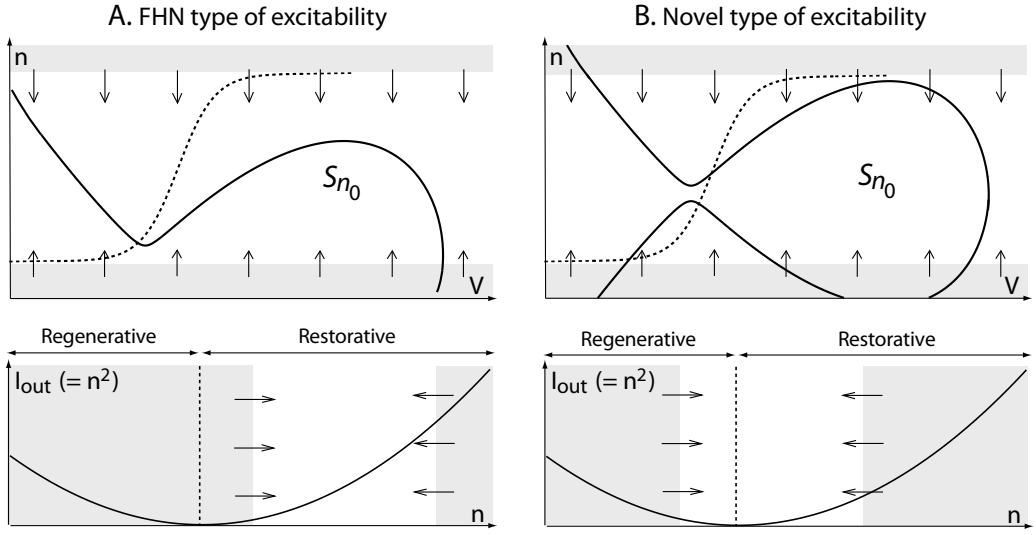

Figure 10.3 – Nullclines (top) and outward ionic current $I_{out} = n^2$ (bottom) for different positions of the n-nullcline and the associated invariant region S_{n_0}. A) When S_{n_0} is fully contained in the half-plane $n > 0$ the phase portrait is reminiscent of original FitzHugh-Nagumo model and the outward ionic current is monotone increasing. The recovery variable has a purely restorative role. B) When S_{n_0} extends to the half-plane $n < 0$, the phase portrait exhibits new characteristics. The outward ionic current is not monotone, corresponding to two anti-synergistic (restorative and regenerative) roles of the recovery variable.

to a model that is neither regenerative nor restorative through a single parameter n_0.

The physiology behind restorative and regenerative behaviors

Restorative and regenerative behaviors model different types of (in)activation gating variables in conductance-based models. When the recovery variable is purely restorative (Fig. 10.3A), it models the activation (resp. inactivation) of an outward (resp. inward) ionic current: a positive variation of V induces a positive variation of n and thus an *increase* of the total outward ionic current, *i.e.* n^2, which is monotone increasing in S_{n_0}. By contrast, when the recovery variable becomes regenerative (Fig. 10.3B), its role is reversed: it models the activation (resp. inactivation) of an inward (resp. outward) ionic current: a positive variation of V induces a positive variation of n and thus a *decrease* of the total outward ionic current, which is now monotone decreasing.

The seminal model of Hodgkin-Huxley only includes restorative slow gating variables: inactivation of sodium current and activation of potassium current. That is why the classical reduction of the Hodgkin-Huxley model leads to a FitzHugh-Nagumo type of phase portrait (Fig. 10.3A). However, conductance-based models often include slow regenerative gating variables. An example of the latter is the activation of calcium currents included in many bursting conductance-based models (e.g. R15 neuron of Aplysia's abdominal ganglion [140], thalamocortical relay and reticular neurons [36, 124], CA3 hippocampal pyramidal neuron [183]). Adding a calcium current in the Hodgkin-Huxley model is one natural way to obtain a reduced phase portrait as in Fig. 10.3B (see Chapter 9 and [42]).

A pitchfork bifurcation organizes different excitability types

The model (10.1) has three free geometrical parameters (I_{app}, n_0, V_0). The parameter n_0 is an additional parameter with respect to FitzHugh-Nagumo dynamics. The three parameters can be adjusted to create a codimension three pitchfork bifurcation that will provide an organizing center for excitability.

The degenerate bifurcation is illustrated in Fig. 10.4 and is constructed as follows (see [52] for mathematical details):

1. The applied current is fixed at $I_{app} = I^\star$, imposing the existence of the singularly perturbed transcritical bifurcation at the V-nullcline self-intersection (cf. Fig. 10.1 center).

2. We fix $n_0 = n_0^\star(V_0) := -n_\infty(-1 - V_0)$ to force a nullcline intersection at the transcritical singularity at $(-1, 0)$.

3. We fix $V^\star = -1$, or, equivalently, $V_0 = V_0^\star := -1 + \frac{1}{5}\log\left(-6 + \sqrt{35}\right)$, so that the n-nullcline is tangent to the V-nullcline at the intersection.

Fig. 10.4 also shows the presence of codimension two transcritical bifurcations for $I_{app} = I^\star$, $n_0 = n_0^\star$ and $V_0 \neq V_0^\star$.

Unfolding in the plane $I_{app} = I^\star$

The parameter chart in Fig. 10.5 unfolds the pitchfork bifurcation in the plane (V_0, n_0) for the fixed critical value $I^\star$. This bifurcation analysis reveals four qualitatively distinct regions denoted by I, II, IV, and V. The transition from Region I to Region II is through a saddle-node bifurcation at which the n-nullcline is tangent to the V-nullcline. See how the top right phase portrait is continuously deformed to the top left phase portrait in Fig. 10.5. The transition from Region I to Region IV is through a transcritical bifurcation at which a saddle and a node exchange their stability. See how the top right phase portrait is continuously deformed to the bottom right phase portrait in Fig. 10.5. A similar transition occur from Region IV to Region V. See how the bottom right phase portrait is continuously deformed to the bottom left phase portrait in Fig. 10.5. Finally, the transition from Region V to Region II is through a saddle-node bifurcation. See how the bottom left phase portrait is continuously deformed to the top left phase portrait in Fig. 10.5.

Region III in Fig. 10.5 is illustrated for future reference in the next section, but it should not be differentiated from Region II in the plane $I = I^\star$, *i.e.* there is no bifurcation associated to the transition from Region II to Region III.

The pitchfork bifurcation organizes excitability

The relevance of the unfolding in Fig. 10.5 for excitability is that the different regions correspond to different types of excitability for $I_{app} > I^\star$. Regions I, II, and III correspond to Types I, II, and III excitability identified in the early work of Hodgkin [80] and extensively studied in the literature since then. Those are the only types of excitability that can be associated to purely restorative models (*i.e.* $n_0 > 0$) and they all have been studied in FitzHugh-Nagumo type phase portraits. In contrast, Region IV and V correspond to new types of excitability that require the co-existence of restorative and regenerative ionic currents.

Our analysis assumes a timescale separation $\epsilon \ll 1$, reflecting the accepted strong separation between the *fast*

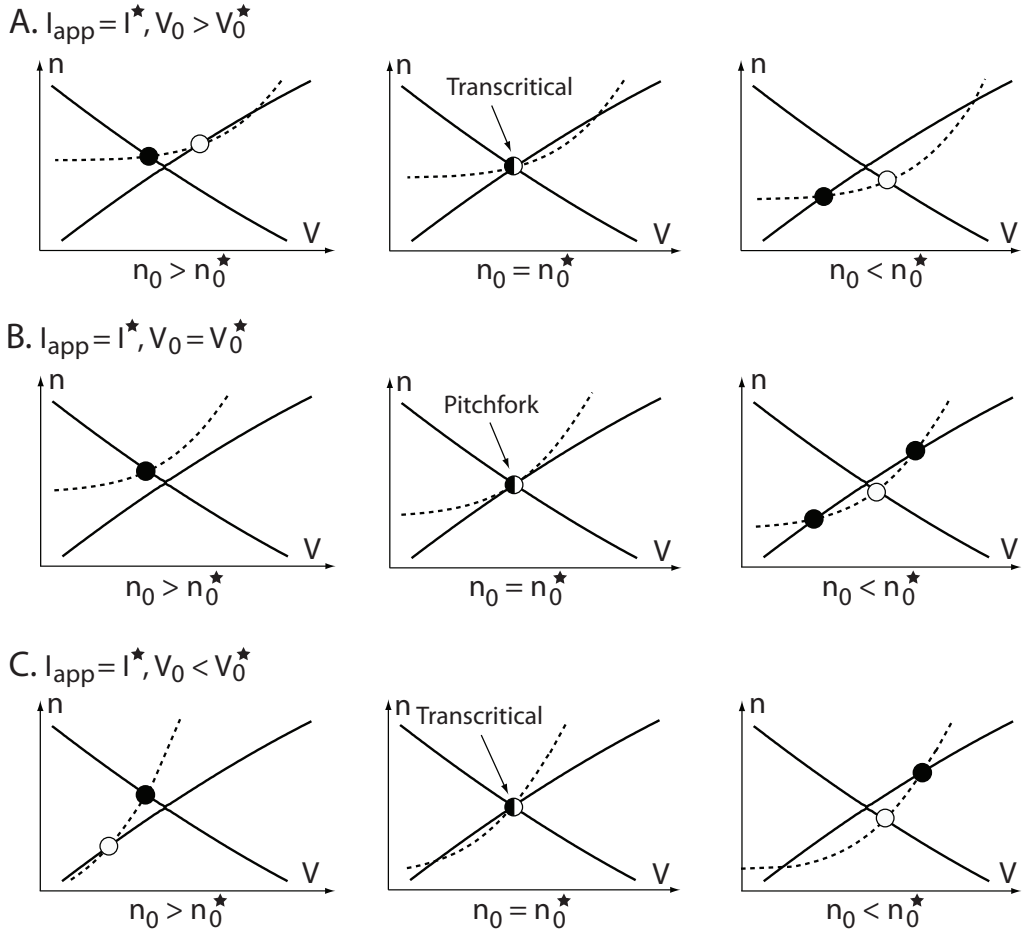

Figure 10.4 – Nullclines and fixed points of (10.1) for $I_{app} = I^\star$, different values of V_0, and with n_0 as the bifurcation parameter. Stable fixed points are drawn as filled circle, unstable as circle, and bifurcations as half-filled circle. **A,C**: When $V_0 < V_0^\star$ or $V_0 > V_0^\star$ as n_0 decreases below $n_0^\star(V_0)$ a stable and an unstable fixed points exchange their stability in a codimension 2 transcritical singularity. **B:** When $V_0 = V_0^\star$ the bifurcation degenerates in codimension 3 pitchfork at which a stable fixed point splits in two stable fixed points (outer) and an unstable fixed point (inner).

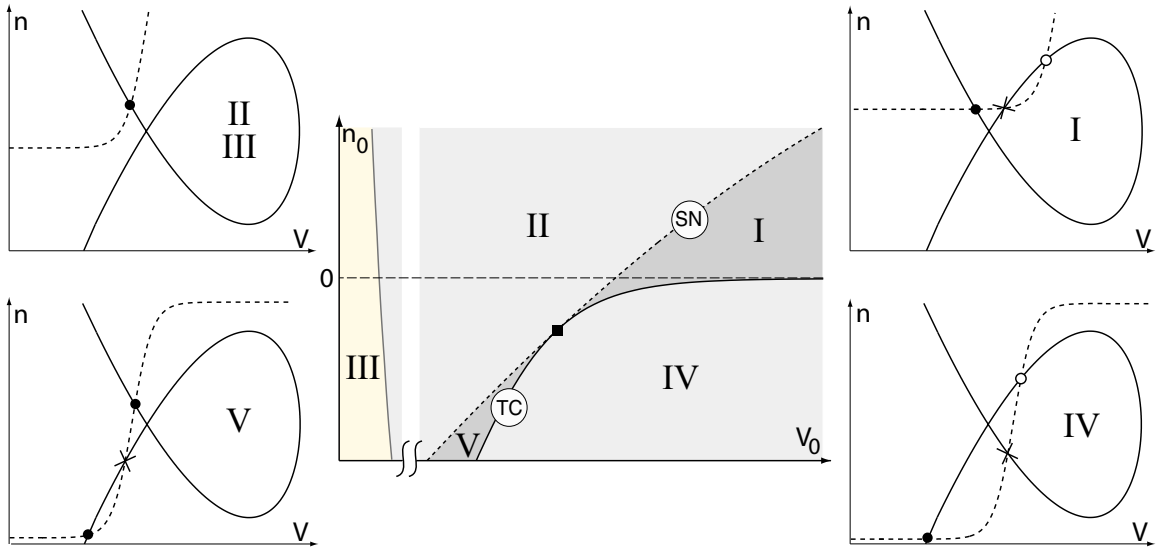

Figure 10.5 – Unfolding of the degenerate pitchfork bifurcation in the plane $I_{app} = I^\star$ and associated nullclines and fixed points. Stable fixed points are depicted as filled circles, whereas unstable as circles. Saddle points are depicted as crosses. ■: pitchfork bifurcation. TC: transcritical bifurcation. SN: saddle-node bifurcation.

voltage dynamics and sodium activation kinetics and the remaining *slow* gating kinetics. We focus on those bifurcations that persist in the singular limit $\epsilon \to 0$.

Fig. 10.6 summarizes the different types of excitability studied in the next section and their main electrophysiological signatures.

The case $I_{app} < I^\star$ is less relevant for excitability models and therefore not studied in details: for $I_{app} < I^\star$, there always exists a stable fixed point and the only possible bifurcations are the two "vertical" saddle-nodes ($I_{SN,up}$ in Fig.s 10.7-10.9) in which the unstable fixed point of Type IV excitable systems and the up stable steady state of Type V excitable systems disappear, respectively. In this sense, this case corresponds to a condition of reduced excitability.

Three types of restorative excitability

Type I (SNIC)

Fixing the parameters (V_0, n_0) in Region I of the parameter chart in Fig. 10.5, the node and the saddle approach each other as the applied current $I_{app} > I^\star$ increases and eventually collide in a saddle-node bifurcation at the critical value $I_{app} = I_{SNIC}$, as depicted in Fig. 10.6 (top right). Under the timescale separation assumption (*i.e.* $\epsilon \ll 1$), the center manifold of the bifurcation forms a homoclinic loop, as sketched in the figure. This bifurcation is commonly identified as saddle-node on invariant circle (SNIC). As I_{app} is further increased, the fixed point disappears and the system generates a periodic train of action potentials. The excitability properties of model (10.1) near a SNIC bifurcation are commonly referred to as Type I excitability (see e.g. [46, Section 3.4.4], [150], and [89, Section 7.1.3] and references therein). The main electrophysiological signatures associated to Type I excitability are as follows:

> **All-or-none spike.** The model has a well defined threshold (*i.e.* $I_{app} = I_{SNIC}$) to generate action potentials. Above the threshold, the amplitude of the action potentials does not depend on the stimulus intensity.
>
> **Low frequency spiking.** The frequency of the limit cycle decreases to zero as $I_{app} \searrow I_{SNIC}$. From a computational point of view, this property permits to encode the stimulus intensity in the oscillation frequency.

Examples of neurons exhibiting the electrophysiological signature of Type I excitability include: thalamocortical neurons with inactivated T-type calcium current (depolarized steady-state) [204, Figure 3], isolated axons from Carcinus maenas [80, Class 1], regular spiking neurons in somatosensory cortex [179], molluscan neurons [162].

Type II (Hopf)

In Region II of the parameter chart in Fig. 10.5, the nullclines intersect only once at a stable fixed point. As I_{app} is increased, this fixed point looses stability in a

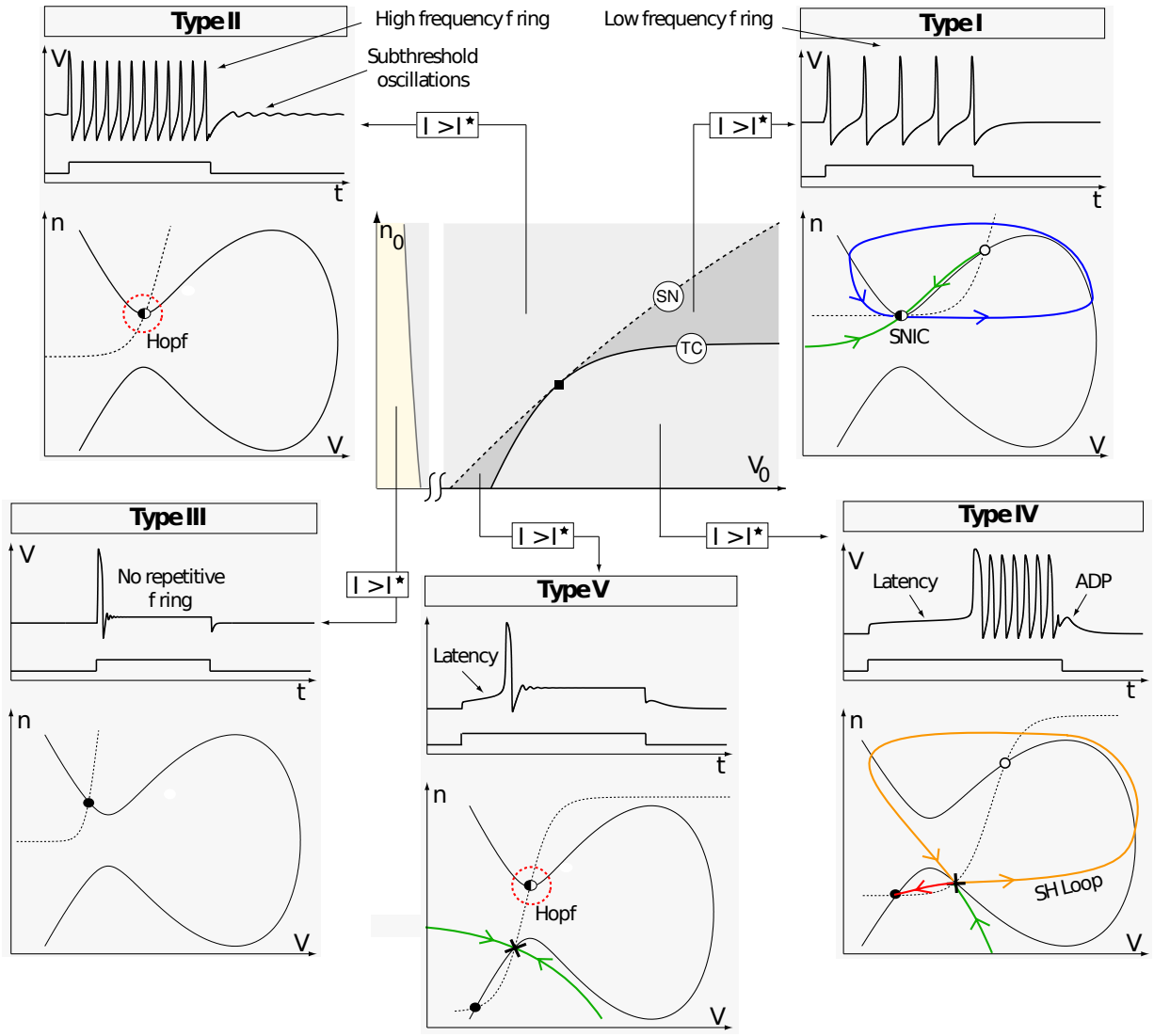

Figure 10.6 – Sketch of different types of excitable behaviors in the unfolding of the degenerate pitchfork bifurcation (■ in the central parameter chart) for $I_{app} > I^\star$ and $\epsilon \ll 1$. For each type, the typical voltage time course and the phase portrait are sketched. The abbreviation SNIC denotes the saddle-node on invariant circle bifurcation. Stable fixed points are depicted as filled circles, unstable as circles, saddles as cross, and bifurcations as half-filled circles. The stable manifold of saddle points is depicted in green. The center manifold of the SNIC bifurcation is depicted in blue. The saddle homoclinic loop in Type IV is depicted in orange.

Hopf bifurcation at $I_{app} = I_{Hopf}$, as illustrated in Fig. 10.6 (top left). Above this critical input current, the system possesses a stable limit cycle surrounding the unstable fixed point.

Excitability properties associated to a Hopf bifurcation are well known and define Type II excitability (see e.g. [46, Section 3.4.4], [150], and [89, Section 7.1.3] and references therein). Fundamental electrophysiological signatures of Type II excitable systems include:

No threshold. When the bifurcation is supercritical, the amplitude of the limit cycle decreases to zero as $I_{app} \searrow I_{Hopf}$, which makes it hard to define a threshold for the generation of an action potential. Canard trajectories [192] are sometime considered as "soft" threshold manifolds between small and large amplitude action potentials.

Subthreshold oscillations. When the applied current is slightly below the bifurcation values (*i.e.* $I_{app} \lesssim I_{Hopf}$) the system trajectory relaxes to the fixed point with damped oscillations at the natural frequency of the Hopf bifurcation (*i.e.* the imaginary part of the eigenvalues at the bifurcation).

No low frequency firing. The oscillation frequency is (almost) independent of the injected current and is equal to or larger than the natural frequency of the Hopf bifurcation.

Frequency preference. Trains of small ($< I_{Hopf}$) amplitude inputs can induce spike if the intra stimulus frequency is resonant with the natural frequency of the Hopf bifurcation. This phenomenon is tightly linked to the presence of subthreshold oscillations and permits to detect the presence of resonant harmonics in the stimulus.

Post-inhibitory spike. Transient negative current can induce an action potential in Type II excitable systems.

Examples of neurons exhibiting the electrophysiological signature of Type II excitability include: isolated axons from Carcinus maenas [80, Class 2], fast spiking neurons in somatosensory cortex [179], alpha moto-neurons [127].

Type III

Type III excitability was only recently studied [57]. It can be thought as a less excitable variant of Type II excitability. In Region III of Fig. 10.5, the half-activation voltage V_0 is so negative that the stable focus never looses its stability as the applied current is increased. Nevertheless, the model is still excitable. For instance, as depicted in Fig. 10.6 (bottom left), a positive current step instantaneously shifts the stable fixed point upright and an originally resting trajectory is attracted toward the right branch of the V-nullcline before relaxing back to rest. On the contrary, if the applied current varies slowly no action potential is generated.

Specific neurocomputational properties of Type III excitable systems have recently been highlighted in [57]:

Slope detection. Because a brutal variation of the applied current is necessary to excite the model, Type III excitable neurons acts as slope detectors with a high temporal precision

Slope based stochastic resonance. In the presence of noise, Type III excitable models are most sensitive to the stimulus slope and frequency, rather than to its amplitude. The associated stochastic resonance phenomenon (slope based stochastic resonance) exhibits distinctly different filtering properties with respect to the classical stochastic resonance in Type I/II excitable models.

Examples of neurons exhibiting the electrophysiological signature of Type III excitability include: squid giant axons (revised model) [28], auditory brain stem [57], isolated axons from Carcinus maenas [80, Class 3].

Two novel types of regenerative excitability

Type IV (singularly perturbed saddle-homoclinic)

As illustrated in the bottom right phase portrait of Fig. 10.5, Type IV excitability is the first excitability type that involves the "mirrored" shape of the voltage nullcline in (10.1): the stable node and the saddle lie on the lower regenerative branch of the V-nullcline. In particular, the hyperpolarized stable steady state of Type IV excitable models lies in the regenerative region of the phase portrait, *i.e.* where

$$\frac{\partial \dot{V}}{\partial n}\frac{\partial \dot{n}}{\partial V} > 0.$$

As a consequence, excitability properties of this phase portrait cannot be studied in FitzHugh-Nagumo like models.

Fixing the pair (V_0, n_0) in Region IV of Fig. 10.5, we obtain the bifurcation diagram illustrated in Fig. 10.7 together with the associated phase portraits. The stable node looses stability in a saddle-node bifurcation at the critical value $I_{app} = I_{SN,down} > I^\star$. For $I_{app} > I_{SN,down}$, the model possesses a stable limit cycle that attracts all solutions (but the unstable focus). The

spiking limit cycle disappears in a (singularly perturbed) saddle-homoclinic bifurcation at $I_{app} = I_{SH}$. The stable node attracts all solutions (but those on the stable manifold of the saddle) for $I_{app} < I_{SH}$. Further decreasing I_{app} below $I_{SN,up}$, the unstable focus disappear in a saddle-node, letting the stable node globally asymptotically stable.
The chief electrophysiological signatures of Type IV excitable systems are:

Bistability. Type IV excitable models are bistable in the parameter range $I_{SH} < I_{app} < I_{SN,down}$: a limit cycle attractor coexists with a stable fixed point.

Spike-latency. When the applied current is abruptly increased slightly above I_{SN}, the trajectory necessarily travels the narrow region between the nullclines. Since the vector field is small in that region, the first action potential is fired with a large latency.

After-depolarization potential. After the limit cycle has disappeared in the homoclinic bifurcation, the trajectory converges to rest by following the attractive branches of the voltage nullcline, thus generating robust ADPs (see [42]).

We stress that bistability, spike-latency, and ADPs are all direct consequences of the presence of a saddle point on the regenerative branch of the voltage nullcline: the basin of attraction of the stable node and the limit cycle are separated by the stable manifold of the saddle; spike-latency reveals the "ghost" of the center manifold of the saddle-node bifurcation; ADPs are generated along the hyperbolic invariant structure provided by the saddle stable and unstable manifolds.

Examples of neurons exhibiting the electrophysiological signature of Type IV excitability include: subthalamic nucleus neurons [72], thalamo-cortical reticular and relay neurons with deinactivated T-type calcium current (hyperpolarized state) [82, 125], dopaminergic neurons [63, 98], superficial pyramidal neurons [64].

Type V (saddle-saddle)

Type V excitability relates to Type IV as Type III does to Type II: similarly to Type IV, the hyperpolarized stable steady state of Type V excitable models lies in regenerative region of the phase plane. The distinct feature of the bottom left phase portrait of Fig. 10.5 is the co-existence of two stable fixed points, a "down-state" and an "up-state". The saddle stable manifold separates the two attractors. As I_{app} is decreased below $I^\star$, the up-state eventually looses its stability in a saddle-node bifurcation at $I_{SN,up}$, leaving the down-state globally asymptotically stable. Similarly, as I_{app} is increased above $I^\star$, the down-state eventually disappears in a saddle-node bifurcation at $I = I_{SN,down}$. But the up-state itself eventually looses its stability in a Hopf bifurcation at $I_{app} = I_{Hopf}$. The Hopf bifurcation can either take place beyond the bistable range $[I_{SN,up}, I_{SN,down}]$, a situation illustrated in Fig. 10.8, or it can take place within the bistable range $[I_{SN,up}, I_{SN,down}]$, in which case, depending on I_{app}, the stable down-state coexists with either a limit cycle attractor or a stable fixed point, a situation illustrated in Fig. 10.9.
The main electrophysiological signatures of Type V excitable models are similar to those of Type IV and can be summarized as follows:

Bistability Type V excitable models are bistable in the range $I_{SN,up} < I_{app} < I_{SN,down}$: a stable down-state coexists with an up-state attractor that can be either a stable fixed point or a stable limit cycle.

Spike latency. Similarly to Type IV, the down-state looses stability in a saddle-node bifurcation on the lower (regenerative) branch of V-nullcline, leading to a long latency before the convergence to the up-state.

Plateau potentials. The up-state having a higher voltage with respect to the down-state, the transition between the two gives rise to plateau potentials either with or without spikes.

Examples of neurons exhibiting the electrophysiological signature of Type V excitability include: olfactory bulb mitral cells [77] and striatal medium spiny neurons [195]. More examples are listed at Scholarpedia journal article [197].

Discussion

Mirroring the FitzHugh-Nagumo equation accounts for regenerative slow gating variables

Mirroring the FitzHugh-Nagumo equation was motivated by the inclusion, in a simple model of neuronal excitability, of the transcritical bifurcation observed in a planar reduction of the Hodgkin-Huxley model augmented with an activating calcium current (Chapter 9). This heuristic geometrical construction is actually tightly linked with the underlying electrophysiology: in the upper FitzHugh-Nagumo like part of the phase portrait the model recovery variable is restorative, as it is in all reduced models derived from Hodgkin-Huxley dynamics; in the mirrored part it is regenerative, accounting for regenerative slow gating variables, such as the activation of calcium current. To the best of our knowledge, this unified picture

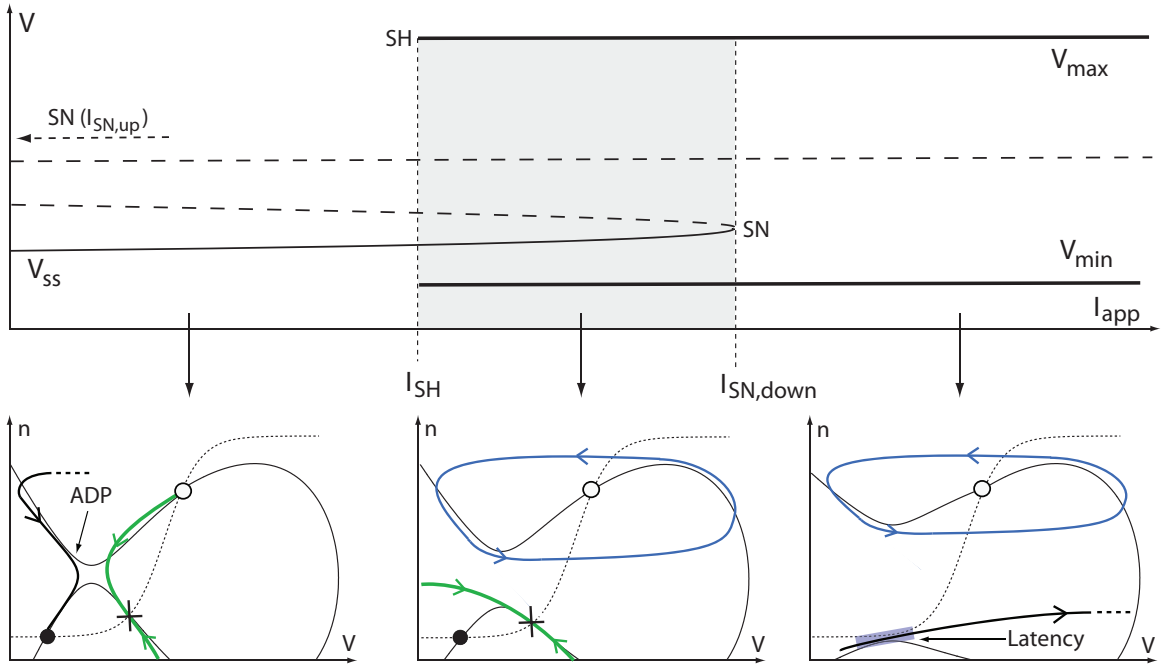

Figure 10.7 – Bifurcations in Types IV excitable systems. Top: bifurcation diagram. Branches of stable fixed points are drawn as solid lines, of unstable fixed points as dashed lines, and of stable limit cycles as thick lines. SH denotes the saddle-homoclinic bifurcation, SN the saddle-node bifurcation. Bottom: phase portraits. The stable manifold of saddle points is depicted in green. Unstable fixed point are depicted as circles, saddles as crosses, and stable fixed points as filled circles. Limit cycle attractors are depicted in blue. Sample trajectories are depicted as black oriented lines.

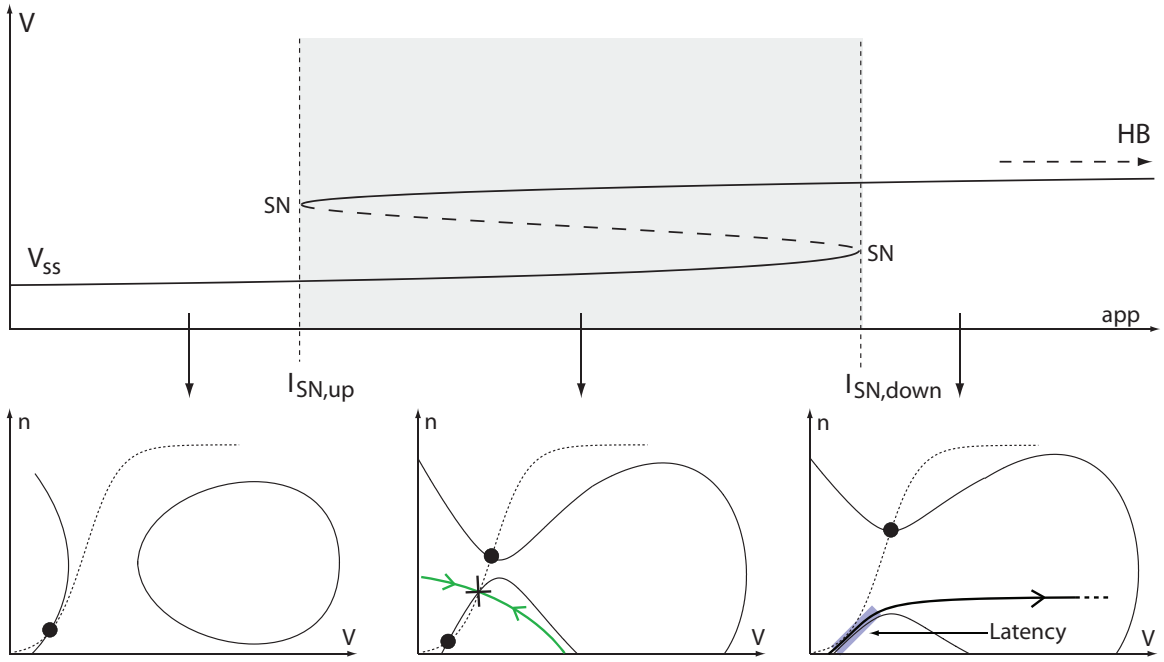

Figure 10.8 – Bifurcations in Types V excitable systems. Legend as in Figure 10.7, except HB denoting the Hopf bifurcation.

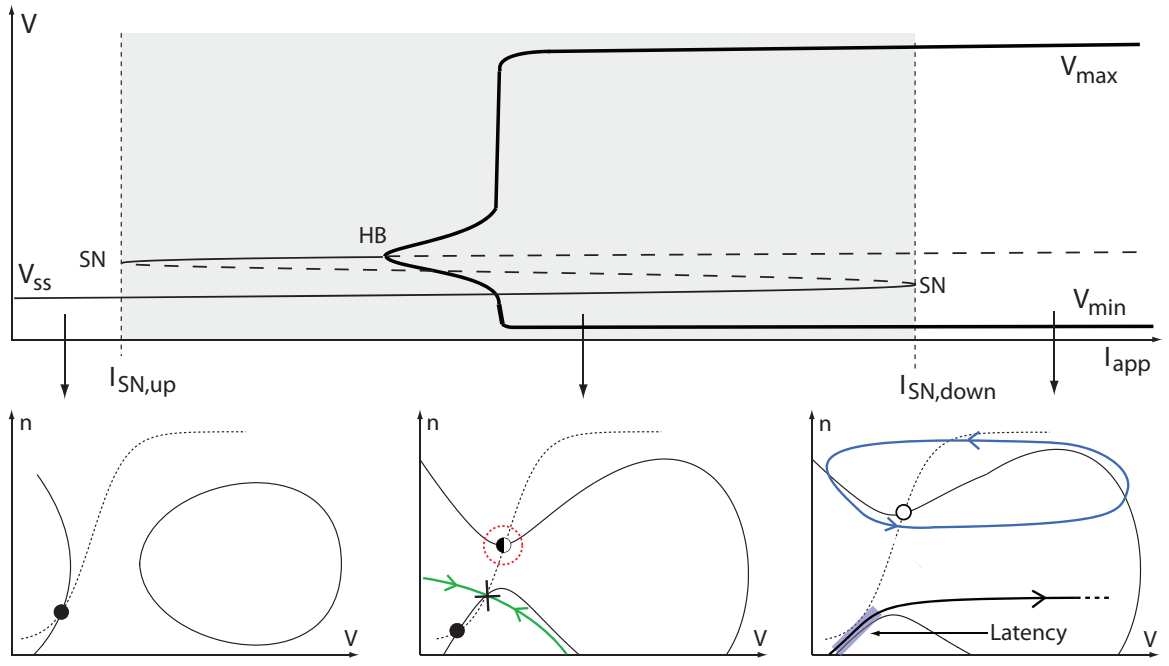

Figure 10.9 – Bifurcations in Types V excitable systems. Legend as in Figure 10.7, except HB denoting the Hopf bifurcation. The same bifurcation is depicted in the phase portrait a half-filled circle.

is not present in existing planar models of neuronal excitability, that are purely restorative.

Regeneracy unravels a pitchfork bifurcation organizing old and new types of excitability

The distinctive effects of regenerative gating variables on neuronal excitability are widely studied in high dimensional conductance-based models and in *in vitro* recordings. However, these same signatures can not be reproduced in restorative models and the underlying dynamical mechanisms have remained obscure to date.

The unfolding of a pitchfork bifurcation organizing the proposed model reveals how the inclusion of regenerative variables changes neuronal excitability. The obtained parameter chart recovers the three known types of (restorative) excitability and unmasks two novel types that we naturally defined as Types IV and V. The defining condition of Types IV and V excitability is regeneracy, *i.e.*

$$\frac{\partial \dot{V}}{\partial n}\frac{\partial \dot{n}}{\partial V} > 0,$$

at the hyperpolarized stable steady state. This sole condition ensures the presence of the electrophysiological signatures of regenerative slow gating variables, in particular, bistability.

Restorative and regenerative excitability in higher dimensional conductance based models

The planar model discussed in the present paper qualitatively captures an important switch from restorative to regenerative excitability. Electrophysiological recordings suggest that this switch actually occurs in the physiological range of many neurons. In Chapter 11, we show that the switch indeed occurs in a number of published higher-dimensional conductance based-models. A qualitatively identical parameter chart to that in Fig. 10.5 is found in those models and the switch from restorative to regenerative excitability is traced through a transcritical bifurcation in the parameter space. In this sense, the planar model studied in the present paper is thought to capture a normal form reduction associated to a transcritical bifurcation that occurs in many quantitative conductance-based models of neurons.

Bistability and bursting in singularly perturbed excitable models

A distinct feature of Types IV and V excitable models with respect to the three other types is the existence of a finite range of bistability. Bistability has been described in the context of Types I and II excitability as well (see e.g. [150]), but, in all these situations, the bistability range shrinks to zero as the timescale separation is increased [52]. In contrast, the stable manifold of the

saddle point that separates the two basin of attraction in Types IV and V excitability is a robust (hyperbolic) geometric object that persists in the singular limit. Because neurons do exhibit a pronounced timescale separation, the robustness of the bistable range in Types IV and V is thought to be an important feature of excitable models that are not purely restorative.

The relevance of bistability in excitable models lies in its relevance for model bursting. Bursting is typically the result of a slow adaptation variable that modulates the applied current across the bistability range, creating a hysteresis loop between the stable down-state and the up-state attractor. An important conjecture derived from our analysis is that bursting will persist near the singularly perturbed limit of model (10.1) only in Type IV and V excitability, that is only in the presence of regenerative ionic channels. In other words, Types IV and V excitability would be the essential sources of bursting in singularly perturbed models, as shown in Chapter 12.

Chapter 11

A Balance Equation Determines a Switch in Neuronal Excitability

Detailed computational conductance-based models have long demonstrated their ability to faithfully reproduce the variety of electrophysiological signatures that can be recorded from a same neuron in varying physiological or pharmacological conditions. But the predictive value of a computational model is limited unless its analysis sheds light on the core mechanisms at play behind a computer simulation. Because conductance-based models are nonlinear dynamical models, their analysis often requires a drastic reduction of dimension. The reduced model is amenable to the geometric methods of dynamical systems theory, but the mathematical insight is often gained at the expense of physiological interpretability; hence the need for methodological tools that can relate mathematical predictions of low-dimensional models to physiological predictions in detailed conductance based models.

In Chapter 10, we used phase plane analysis and dynamical bifurcation theory to characterize in *reduced-order* neurodynamics models a switch of excitability that is consistent with many physiological observations. More precisely, a transcritical bifurcation governed by a single parameter was shown to organize a switch from restorative excitability, extensively studied in most models inspired from the Hodgkin-Huxley model, to regenerative excitability whose distinct electrophysiological signature include spike latency, plateau oscillations, and afterdepolarizeation potentials..

The main contribution of the present chapter is to show that this transcritical bifurcation, and the associated excitability switch, exist in a number of *high-dimensional* conductance-based models and that the resulting mathematical predictions have physiological relevance. More precisely, we provide an algorithm to trace the transcritical bifurcation in arbitrary conductance-based models. Although purely mathematical in nature, the detection of the transcritical bifurcation is based on an ansatz that leads to a simple physiological interpretation: the switch of excitability is determined by a balance between restorative (those providing a negative feedback) and regenerative (those providing a positive feedback) ion channels at the resting potential. Because this simple tuning rule can take many different physiological forms, it is potentially shared by very different neurons. We apply the algorithm to detailed conductance-based models of six neurons known to exhibit drastic changes in their electrophysiological signatures depending on environmental conditions: the squid giant axon [81], the dopaminergic neuron [40], the thalamic relay neuron [37], the thalamic reticular neuron [36], the aplysia R15 model [149], and the cerebellar granular cell [33]. In each case, the algorithm identifies a transcritical bifurcation that occurs close to the nominal model parameters and its predictions are consistent with experimental observations.

After defining a novel classification of ion channels based on their restorative or regenerative nature, we briefly review the planar model presented in Chapter 10 and how its transcritical bifurcation qualitatively captures the switch between restorative and regenerative excitability. As a generalization of this low-dimensional case, we mathematically construct the same bifurcation in generic conductance based models and derive the balance condition determining the regenerative or restorative nature of the model. This construction and its electrophysiological predictions are firstly illustrated on the squid giant axon. An algorithm for generic conductance-based models is subsequently derived and different models analyzed. In particular, we revisit, using a TC neuron model as an insightful example, how neuronal signaling can rely on the dynamic regulation of the balancing between restorative and regenerative ion channels. Finally, we illustrate our results in an experiment on midbrain dopaminergic neurons.

Results

Restorative and regenerative ion channels

The gating of ion channels occurs on many different timescales. However, gating timescales can be grouped in three families, according to their influence on neuronal excitability [78]:

(i) **Fast gating variables**: These variables have a time-constant in the millisecond range. They generate the rapid regenerative upstroke of an action potential. Prominent representatives of this family are the activation gating variables of fast voltage-gated sodium channels ($Na_V1.1$ to $Na_V1.9$).

(ii) **Slow gating variables**: These variables have a time constant 5 to 10 times larger than fast gating variables. They influence the spike initiation, downstroke, and the afterspike period. They are key players of neuronal excitability. Prominent representatives of this family are the activation gating variables of delayed rectifier potassium channels ($K_V1.1$ to $K_V1.3$, $K_V1.5$ to $K_V1.8$, $K_V2.1$, $K_V2.2$, $K_V3.1$, $K_V3.2$, $K_V7.1$ to $K_V7.5$, $K_V10.1$) and the activation gating variables of all calcium channels ($Ca_V1.x$, $Ca_V2.x$, $Ca_V3.x$).

(iii) **Ultra-Slow (adaptation) variables**: These variables gate too slowly to be strongly activated by single action potentials. They modulate neuronal excitability only over periods of many action potentials. Prominent representative of this family are the inactivation gating variables of transient calcium channels ($Ca_V2.x$, $Ca_V3.x$). Ultra-slow variables might also include non gating variables. For instance, the intracellular calcium concentration $[Ca^{2+}]_{in}$, which modulates the conductance of calcium-regulated channels.

In view of their importance for neuronal excitability (see Chapter 10), we focus only on slow gating variables to classify ion channels: when the slow channel provides negative feedback to the membrane potential variation, we term the associated channel a restorative ion channel. When the slow variable instead enhances a voltage variation by positive feedback, the associated ion channel is termed regenerative (a characterization in terms of partial derivatives is postponed to the next sections). Ion channels that do not possess a slow gating variable are neither restorative nor regenerative and are called neutral. Neutral ion channels solely regulate the "quantity" of excitability without affecting its "quality".

Tab. 11.1 shows a classification of many known ion channels according to this criterion. Not surprisingly, potassium channels are the main representatives of restorative ion channels. By increasing the total outward current, their activation induces a negative feedback on membrane voltage variations that is responsible for neuron repolarization. On the other hand, physiologically described calcium channels are all regenerative. Their activation induces an increase of the total post-spike inward current, in contrast to potassium channels. This is the source, for instance, of afterdepolarization potentials (ADP's). Interestingly, sodium channels can be either restorative, regenerative, or neutral according to their fast transient, resurgent, or persistent behavior, respectively.

It is important to observe that the restorative (resp. regenerative) nature of channels is not solely linked to the outward (resp. inward) nature of the current. For instance, transient sodium channels (although responsible for the regenerative spike upstroke) are restorative, because their slow variable inactivates an inward current, inducing a negative-feedback on membrane potential variations. Similarly, potassium channels can be regenerative when their slow inactivation massively decreases the outward current, like in the case of A-type potassium channels.

Although elementary, the classification above seems novel. It is motivated by the central message of this paper, that the balance between regenerative and restorative ion channels in slow timescale determines its neuronal excitability type.

Restorative and regenerative excitability in planar models

Motivated by the phase portrait of an empirical reduction of the Hodgkin-Huxley model augmented with a calcium channel (Chapter 9) [42], Chapter 10 [52] explores the neuronal excitability of the planar model

$$\dot{V} = V - \frac{V^3}{3} - n^2 + I_{app} \tag{11.1a}$$

$$\dot{n} = \varepsilon(n_\infty(V - V_0) + n_0 - n) \tag{11.1b}$$

whose phase portraits are reproduced in Fig. 11.1 for two distinct values of the parameter n_0 (an indirect image of the calcium conductance in the high-dimensional model). The parameter $\varepsilon > 0$ is an image of the timescale separation between V and n. The function $n_\infty(\cdot)$ has the standard sigmoid shape of conductance-based models and V_0 is the half-activation potential. Typical phase portraits and step responses of (11.1) are reproduced in Fig. 11.1.

The phase portrait in Fig. 11.1 left is the qualitative phase portrait of FitzHugh-Nagumo model. It is associated to a reversible and sudden switch from rest to firing and has extensively been studied, with finer distinctions depending on the mathematical nature of the underlying bifurcation. See [46, 89, 150] and reference therein.

Ion Channel	Gating Kinetics	Classification
Sodium Channels		
Transient	FA, SI - Negative feedback via SI	Restorative
Persistent	FA - No slow gating variable	Neutral
Resurgent	SA, USI - Positive feedback via SA	Regenerative
Calcium Channels		
L-type	SA - Positive feedback via SA	Regenerative
T-type	SA, USI - Positive feedback via SA	Regenerative
N, P/Q, R-type	SA, USI - Positive feedback via SA	Regenerative
Potassium Channels		
Delayed Rectifiers	SA - Negative feedback via SA	Restorative
KCNQ	USA - No slow gating variable	Neutral
eag/erg	USA - No slow gating variable	Neutral
A-type	FA, SI - Positive feedback via SI	Regenerative
BK	SA - Negative feedback via SA	Restorative
HCN	SA - Negative feedback via SA	Restorative

FA: fast activation, FI: fast inactivation, SA: slow activation, SI: slow inactivation, USA: utraslow activation, USI: ultraslow inactivation

Table 11.1 – Classification of ion channels according to their gating kinetics. Activation and inactivation variables are distributed in three groups: fast, slow, and ultra-slow (adaptation). Slow variables are defined as restorative (resp. regenerative) if they induce a negative (resp. positive) feedback on membrane potential variations. An ion channel that posses a restorative variable is called "restorative channel", and similarly for regenerative channels. Channels that do not posses a slow variable are called "neutral channels". This classification might change for a given channel for some channel subtypes.

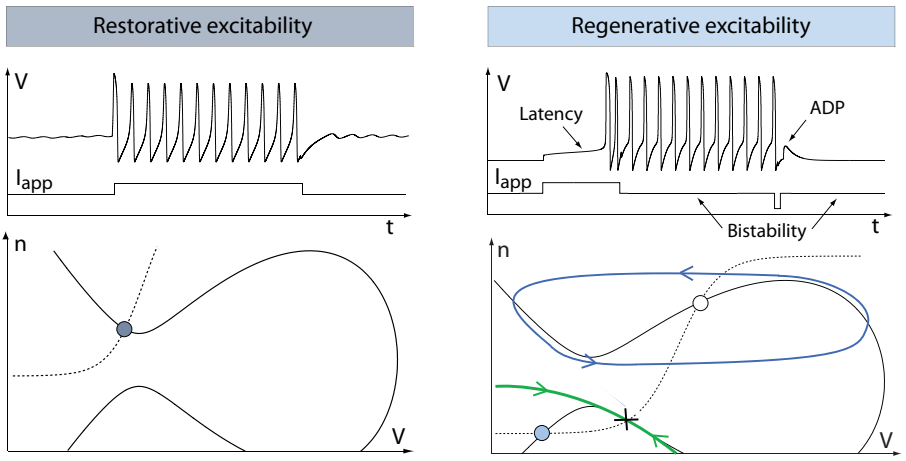

Figure 11.1 – Typical step responses (top) and phase portraits (bottom) of (11.1). The dark (resp. light) blue circle denotes a stable restorative (resp. regenerative) steady state $(\bar{V}, \bar{n})$. The full (resp. dashed) line is the voltage (resp. slow variable) nullcline. The saddle point in the right phase portrait is represented as the cross and its separatrix as the green oriented line. The stable limit cycle surrounding the unstable fixed point (represented as a circle) is represented by the blue oriented line.

The phase portrait in Fig. 11.1 right is in sharp contrast in that the electrophysiological response to a current input exhibits spike latency, plateau oscillations, and after depolarization potential (ADP). This specific signature, experimentally observed in many families of neurons, is fundamentally associated to the bistability illustrated in the phase portrait: namely, the robust coexistence of two stable attractors (a hyperpolarized resting potential and a limit cycle of periodic action potentials) and a saddle-separatrix that sharply separates their basins of attraction. The time evolution shown in the top figure is a consequence of this phase portrait and cannot be observed in FitzHugh-Nagumo like phase portraits. The distinction between the two phase portraits is further discussed in a later section on bistability.

A simple mathematical distinction between the two phase portraits shown in Fig. 11.1 is drawn from the Jacobian linearization of the model at the stable resting point $(\bar{V}, \bar{n})$:

$$J = \begin{pmatrix} 1 - \bar{V}^2 & -2\bar{n} \\ \underbrace{\varepsilon \frac{\partial n_\infty}{\partial V}(\bar{V} - V_0)}_{>0} & -\varepsilon \end{pmatrix}.$$

The product of the partial derivatives $\frac{\partial \dot{V}}{\partial n}\frac{\partial \dot{n}}{\partial V} = -2\bar{n}\,\varepsilon\frac{\partial n_\infty}{\partial V}(\bar{V} - V_0)$ is negative on the left phase portrait, capturing the restorative nature of the gating variable, whereas it is positive on the right phase portrait, translating the regenerative nature of the gating variable. This difference is schematized in the block diagrams of Fig. 11.2.

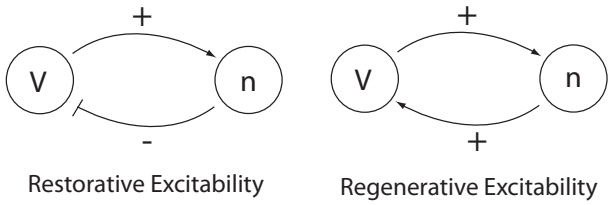

Figure 11.2 – Block diagrams representation of restorative and regenerative excitability in planar models.

Accordingly, excitability in planar models is called restorative (resp. regenerative) when the gating variable provides negative (resp. positive) feedback close to the resting point:

Planar restorative excitability

The model is said to be restorative at steady state if:

$$\left.\frac{\partial \dot{V}}{\partial n}\frac{\partial n_\infty}{\partial V}\right|_{SS} < 0$$

Planar regenerative excitability

The model is said to be regenerative at steady state if:

$$\left.\frac{\partial \dot{V}}{\partial n}\frac{\partial n_\infty}{\partial V}\right|_{SS} > 0$$

The planar model (11.1) can smoothly switch from restorative to regenerative excitability, with a transition occurring for $\bar{n} = 0$, or, in algebraic terms,

$$\frac{\partial \dot{V}}{\partial n}\frac{\partial n_\infty}{\partial V} = 0 \tag{11.2}$$

A convenient way to algorithmically track this excitability switch is to use bifurcation analysis and to impose that the critical condition (11.2) coincides with a bifurcation of the model, which imposes the additional algebraic condition

$$\begin{aligned} \det J = & -\varepsilon\left(\frac{\partial \dot{V}}{\partial V} + \frac{\partial \dot{V}}{\partial n}\frac{\partial n_\infty}{\partial V}\right) \\ & = 0. \end{aligned} \tag{11.3}$$

Simultaneously imposing (11.2) and (11.3) implies

$$\frac{\partial \dot{V}}{\partial V} = 0, \tag{11.4}$$

which, in geometrical terms, corresponds to the transcritical bifurcation obtained for $I_{app} = \frac{2}{3}$ and illustrated in Fig. 11.3.

The theory of bifurcation unfolding is further exploited in [52] in order to classify all excitability types associated to the planar model in Fig. 11.1. This analysis results in five different types of excitability obtained by varying the two parameters (V_0, n_0) around the singular phase portrait of Fig. 11.3, center (Chapter 10). The parameter n_0 acts in particular as the sole regulator of the balance between regenerative and restorative excitability by shifting the n-nullcline up and down: a positive n_0 corresponds to a phase portrait as in Fig. 11.3 left, whereas the phase portrait of Fig. 11.3 right is obtained for sufficiently negative n_0. The associated parameter chart is reproduced in Figure 11.4. It contains the two types of excitability discussed above. The transition from restorative to regenerative excitability is always through

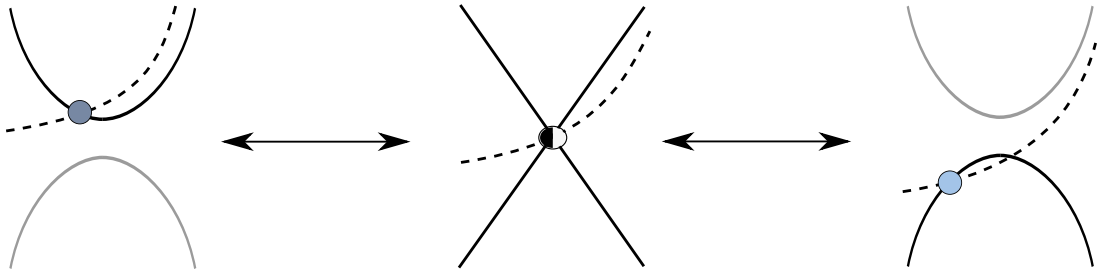

Figure 11.3 – Smooth switch from restorative to regenerative excitability in planar models. A continuous deformation from the restorative phase portrait of Fig. 11.1 left to the regenerative phase portrait of Fig. 11.1 right involving a transcritical bifurcation determined by the algebraic conditions (11.2) and (11.3). The dark blue circle represents a restorative stable steady-state, the light blue circle a regenerative stable steady-state, and the half-filled circle represents the transcritical bifurcation which separates the restorative and regenerative regimes.

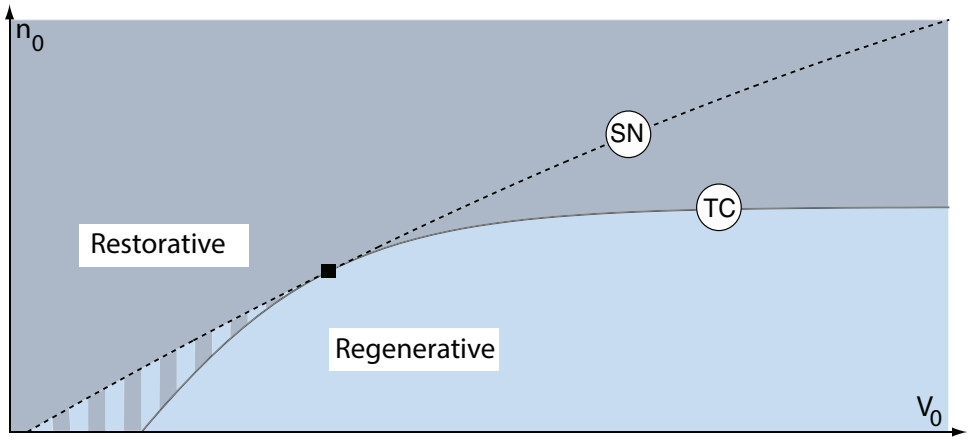

Figure 11.4 – Excitability types in model (11.1). SN denotes the saddle-node bifurcation, TC the transcritical bifurcation. ■: Pitchfork bifurcation organizing center. Varying n_0 and V_0 the model switches between excitability types.

a transcritical bifurcation. In addition, some paths traverse a small hybrid region where a down regenerative steady state and an up restorative steady state coexist.

The main contribution of the present chapter is to show that the analysis of Chapter 10 (Fig. 11.4) is not an artifact of planar reduction but captures excitability transitions that can algorithmically be tracked in conductance-based models of arbitrary dimension.

Restorative and regenerative excitability in conductance based models

We start by grouping gating variables of a given conductance-based model according to their time scales. The family $\mathcal{G}_F = \{m_{Na,f},\ m_{Na,p},\ m_{K,A},\ldots\}$ collects fast gating variables. The gating variable $x^f \in [0,1]$ denotes a generic member of this family. Similarly, the family $\mathcal{G}_S = \{h_{Na,f},\ m_{K,DR},\ m_{Ca,L},\ldots\}$ collects slow gating variables x^s, whereas $\mathcal{G}_A = \{h_{Ca,T},\ h_{Na,R},\ m_{K,M},\ldots\}$ collects adaptation variables x^a. For a given ion channel type i, the standard notation m_i (resp. h_i) is adopted for the activation (resp. inactivation) gating variable of the associated ionic current I_i. With these notations, a general neuron conductance-based model reads

$$C_m\dot{V} = -\sum_i \bar{g}_i m_i^{a_i} h_i^{b_i}(V-E_i) + I_{app}, \tag{11.5a}$$

$$\tau_{x^f}(V)\dot{x}^f = (x^f_\infty(V) - x^f), \tag{11.5b}$$

$$\tau_{x^s}(V)\dot{x}^s = (x^s_\infty(V) - x^s), \tag{11.5c}$$

$$\tau_{x^a}(V)\dot{x}^a = (x^a_\infty(V) - x^a), \tag{11.5d}$$

where the sum in (11.5a) is over all ion channels in the model, and (11.5b),(11.5c),(11.5d) hold for all the associated fast, slow, and adaptation variables, respectively. The activation (resp. inactivation) functions x^f_∞, x^s_∞ are strictly monotone increasing (resp. decreasing) sigmoids. In the forthcoming analysis, all adaptation variables are treated as constant parameter, that is their slow evolution is neglected.

We will detect a switch from restorative to regenerative excitability by mimicking the two-dimensional algorithm of the previous section. We first impose the bifurcation condition $\det J = 0$, where J denotes the Jacobian of the subsystem (11.5a),(11.5b),(11.5c). The algebraic condition writes

$$\det J_f + \sum_{x^s} \frac{\partial \dot{V}}{\partial x^s}\frac{\partial x^s_\infty}{\partial V} = 0 \tag{11.6}$$

where J_f denotes the Jacobian of the fast subsystem (11.5a),(11.5b) and the sum is over all slow variables. The particular form of equation (11.6) is a direct consequence of the specific structure of conductance-based models, that is, parallel interconnection of two-dimensional feedback loops involving the voltage dynamics (11.5a) and one of the gating variable dynamics (11.5b),(11.5c).

As for the planar model (11.1), we track the switch between restorative and regenerative excitability by imposing the high-dimensional equivalent of the balance condition (11.2). We therefore look for solutions of (11.6) satisfying the ansatz

$$\sum_{x^s} \frac{\partial \dot{V}}{\partial x^s}\frac{\partial x^s_\infty}{\partial V} = 0. \tag{11.7}$$

The two conditions (11.6),(11.7) now imply

$$\det J_f = 0. \tag{11.8}$$

The corresponding bifurcation is transcritical [53].

The singularity (11.8) is the high-dimensional counterpart of the V-nullcline self-intersection in the planar model. It reflects the geometric nature of the transcritical bifurcation, that is, a robust geometrical object that exists independently of the timescale separation and persists in the singular limit of an infinite timescale separation, regardless of the system dimension. Our ansatz makes the proposed analysis completely robust against the model time constants. The time constants are only used to classify the gating variables in the three physiological groups.

We split $\mathcal{G}_S$ in the two subfamilies $\mathcal{G}_{S+}$, which contains *regenerative* slow gating variables x^{s+}, and $\mathcal{G}_{S-}$, which contains *restorative* slow gating variables x^{s-}. The balance condition (11.7) is then rewritten as

$$\underbrace{\sum_{x^{s+}} \overbrace{\frac{\partial \dot{V}}{\partial x^{s+}}\frac{\partial x^{s+}_\infty}{\partial V}\Big|_{TC}}^{>0}}_{\text{regenerative gates}} + \underbrace{\sum_{x^{s-}} \overbrace{\frac{\partial \dot{V}}{\partial x^{s-}}\frac{\partial x^{s-}_\infty}{\partial V}\Big|_{TC}}^{<0}}_{\text{restorative gates}} = 0 \tag{11.9}$$

to express a balance between restorative and regenerative ion channels. It is the high-dimensional counterpart of (11.2) and it provides a rigorous high-dimensional generalization of restorative and regenerative excitability:

Restorative excitability

The model is said to be restorative at steady state if:

$$\left(\sum_{x^{s+}} \frac{\partial \dot{V}}{\partial x^{s+}} \frac{\partial x^{s+}_{\infty}}{\partial V} + \sum_{x^{s-}} \frac{\partial \dot{V}}{\partial x^{s-}} \frac{\partial x^{s-}_{\infty}}{\partial V} \right) \Bigg|_{SS} < 0$$

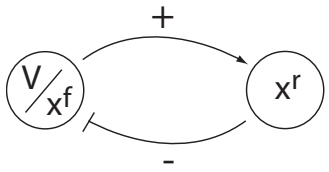

Regenerative excitability

The model is said to be regenerative at steady state if:

$$\left(\sum_{x^{s+}} \frac{\partial \dot{V}}{\partial x^{s+}} \frac{\partial x^{s+}_{\infty}}{\partial V} + \sum_{x^{s-}} \frac{\partial \dot{V}}{\partial x^{s-}} \frac{\partial x^{s-}_{\infty}}{\partial V} \right) \Bigg|_{SS} > 0$$

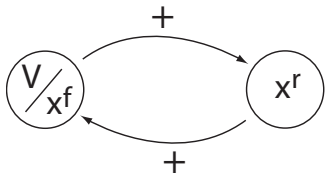

The insight provided by the planar model of the previous section predicts that the switch of excitability detected by the balance equation (11.9) will lead to the accompanying distinct electrophysiological signatures of Fig. 11.1.

Tracking excitability switches in the squid giant axon

The Hodgkin-Huxley (HH) model [81] provides a non-physiological, but historical and experimentally verified tutorial for tracking a switch of excitability in conductance based models. The model reads

$$\begin{aligned} C\dot{V} &= -g_l(V - V_l) - \bar{g}_{Na} m^3 h (V - V_{Na}) \\ &\quad - \bar{g}_K n^4 (V - V_K) + I_{app}, && \text{(11.10a)} \\ \tau_m(V)\dot{m} &= (m_\infty(V) - m), && \text{(11.10b)} \\ \tau_h(V)\dot{h} &= (h_\infty(V) - h), && \text{(11.10c)} \\ \tau_n(V)\dot{n} &= (n_\infty(V) - n), && \text{(11.10d)} \end{aligned}$$

where m is the fast sodium channel activation while the sodium channel inactivation h and the potassium channel activation n are the slow gating variables. We set all time constants to one, because this simplification has no effects on the algebraic conditions (11.7) and (11.8). The Jacobian of (11.10) reads

$$J = \left[\begin{array}{cc|cc} \frac{\partial \dot{V}}{\partial V} & \frac{\partial \dot{V}}{\partial m} & \frac{\partial \dot{V}}{\partial h} & \frac{\partial \dot{V}}{\partial n} \\ \frac{\partial m_\infty}{\partial V} & -1 & 0 & 0 \\ \hline \frac{\partial h_\infty}{\partial V} & 0 & -1 & 0 \\ \frac{\partial n_\infty}{\partial V} & 0 & 0 & -1 \end{array} \right]. \qquad \text{(11.11)}$$

The upper-left block is the Jacobian of the fast (V, m) subsystem. Imposing the singularity condition (11.8) yields

$$\frac{\partial \dot{V}}{\partial V}\bigg|_{TC} + \frac{\partial \dot{V}}{\partial m} \frac{\partial m_\infty}{\partial V}\bigg|_{TC} = 0, \qquad \text{(11.12a)}$$

while the balance equation (11.9) reads

$$\frac{\partial \dot{V}}{\partial n} \frac{\partial n_\infty}{\partial V}\bigg|_{TC} + \frac{\partial \dot{V}}{\partial h} \frac{\partial h_\infty}{\partial V}\bigg|_{TC} = 0 \qquad \text{(11.13a)}$$

Note that (11.12) and (11.13) imply the bifurcation condition $\det J = 0$ in (11.11).

At first sight, the balance condition (11.13) cannot be satisfied because both sodium and potassium channels are restorative channels according to their corresponding kinetics in the model, and in agreement with our proposed classification. This is consistent with the fact that the excitability of the HH model is always restorative in physiological conditions.

However, it was long recognized [131] that potassium channels can generate an inward current at steady-state if the extracellular K^+ concentration is sufficiently large. Indeed, any change in extracellular potassium concentration induces a change in the potassium reversal potential, as expressed by the Nernst equation. This suggests to use the potassium reversal potential V_K as a bifurcation parameter in HH model in order to satisfy the balance equation

$$\overbrace{\frac{\partial \dot{V}}{\partial n} \frac{\partial n_\infty}{\partial V}\bigg|_{TC}}^{!>0} + \overbrace{\frac{\partial \dot{V}}{\partial h} \frac{\partial h_\infty}{\partial V}\bigg|_{TC}}^{<0} = 0$$

n: regenerative gating — h: restorative gating

(11.14)

where potassium now acts as a regenerative gating variable provided that $V_K > V_{SS}$. Physiologically, condition (11.14) imposes that the potassium Nernst potential is large enough for the cooperativity of the potassium activation to balance the restorative effects of the sodium current inactivation.

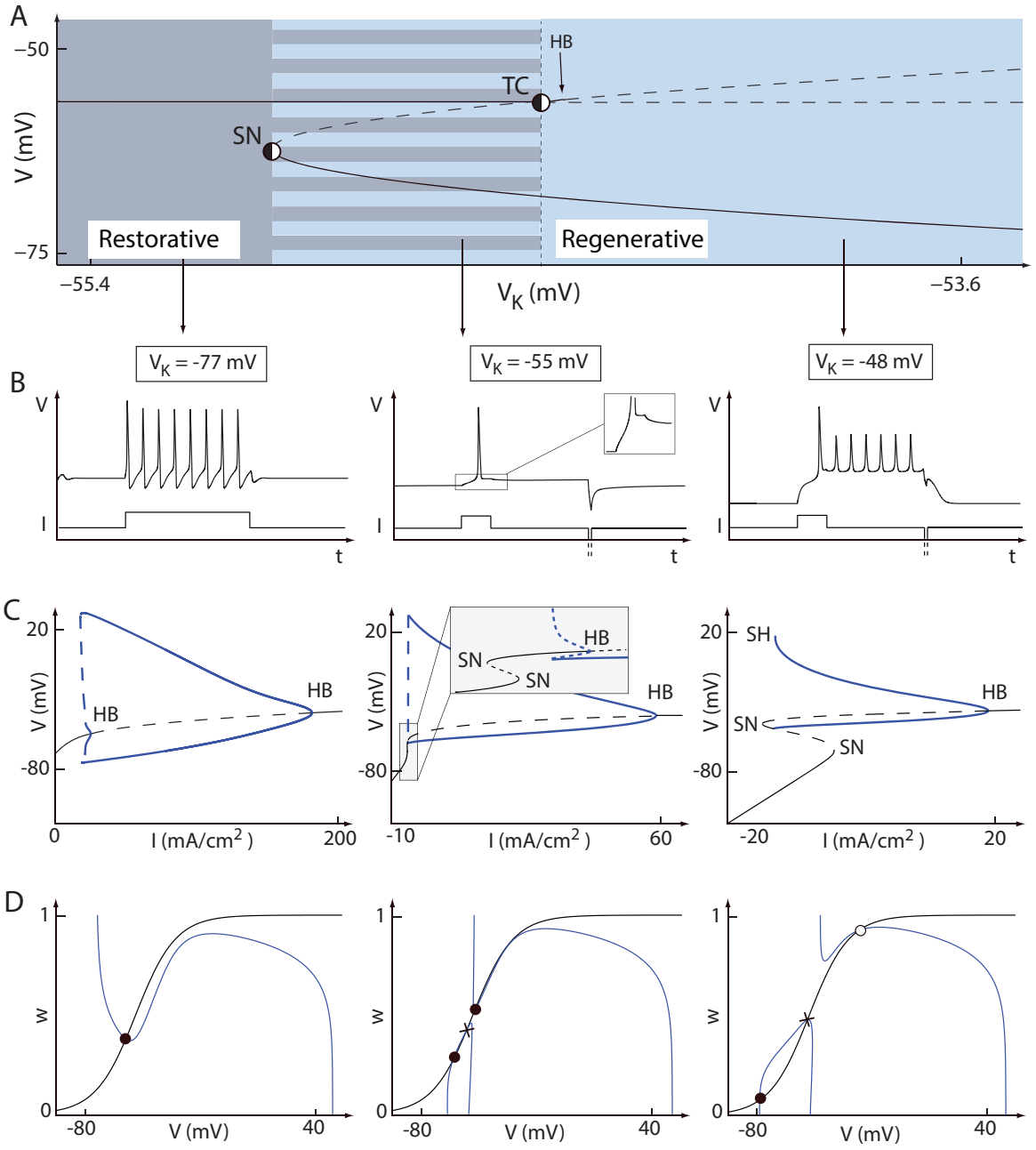

Figure 11.5 – Variations of the potassium reversal potential V_K induce excitability switches in the Hodgkin-Huxley model. **A.** Bifurcation diagram of the HH model with V_K as the bifurcation parameter. TC denotes a transcritical bifurcation, SN a saddle-node bifurcation, HB a Hopf bifurcation. Branches of stable fixed points are represented as solid line, whereas branches of saddle points and unstable points as dashed lines. **B.** Electrophysiological responses of the model for three different values of V_K, corresponding to three different excitability types (restorative, hybrid, and regenerative, from left to right). **C.** Bifurcation diagrams with the applied current as the bifurcation parameter for the same three values of V_K as in **B**. Black (resp. blue) full lines represent branches of stable steady-states (resp. limit cycles), black dashed lines branches of saddle and unstable steady-states. Branches of unstable limit cycle are drawn as dashed blue lines. HB denotes a Hopf bifurcation, SN a saddle-node bifurcation, and SH a saddle-homoclinic bifurcation. **D.** Phase portraits of reduced HH model proposed by Rinzel in [148] for the same three values of V_K as in **B,C**. Blue full lines denote the V-nullclines and black full lines the w-nullclines, where w denotes the slow variable of the reduced model. Filled circles denote stable steady-states, crosses saddle points, and circles unstable steady-states.

The two conditions (11.12) and (11.14) can numerically be solved to determine the critical values V_K^c and V^c. The value of the applied current at the transcritical bifurcation is then determined from (11.10a), which gives

$$\begin{aligned} I_{app}^c &= g_l(V^c - V_l) + \bar{g}_K n_\infty^4(V^c)(V^c - V_K^c) \\ &+ \bar{g}_{Na} m_\infty^3(V^c) h_\infty(V^c)(V^c - V_{Na}) \end{aligned} \quad (11.15)$$

The numerical bifurcation diagram in Fig. 11.5A confirms the transcritical bifurcation at V_K^c. That bifurcation diagram is drawn by varying V_K together with applied current I_{app}, following the affine reparametrization described in Supplementary Material. More precisely,

$$I_{app}(V_K) = I_{app}^c - \bar{g}_K n_\infty^4(V^c)(V_K - V_K^c).$$

Mathematically, this reparametrization imposes one of the defining conditions of the transcritical bifurcation. Physiologically, its effect is to keep the net current constant at steady-state V^c (*i.e.* $I_{ion}(V_K) + I_{app}(V_K) = 0$): as V_K is varied, the observed switch in the excitability type does not rely on changes in the net current across the membrane, but solely on changes in its dynamical properties.

The bifurcation diagram in Fig. 11.5A provides informations on the model excitability also far from the transcritical values. For highly hyperpolarized V_K, the model is purely restorative and exhibits the typical excitable behavior of the original Hodgkin-Huxley model. As V_K is increased, a stable regenerative steady-state is born in a saddle-node bifurcation. At this transition, the system switches to a hybrid excitability type. Short current pulses let the system switch between the depolarized restorative steady state and the hyperpolarized regenerative stable steady state (Fig. 11.5B,middle). The associated bifurcation diagram and phase portrait are reproduced in Fig. 11.5C,D,middle. Finally, further increase of V_K let the restorative steady state exchanges its stability with a (regenerative) saddle at the transcritical bifurcation and the system switches to regenerative excitability. The regenerative steady state coexists in this case with the spiking limit cycle attractor. Current pulses switch the systems between the two attractors (Fig. 11.5B,right). The associated bifurcation diagram and phase portrait are reproduced in Fig. 11.5C,D,right.

The same qualitative excitability switch was described by Rinzel in [148], who linked the appearance of a bistable behavior to the inward nature of potassium current at steady-state for sufficiently depolarized V_K. *In vitro* recordings of the squid giant axon with isotonic extracellular K^+ concentration show the same transition [131]. Our interpretation of this phenomenon in terms of restorative and regenerative excitability is as follows: as the potassium Nernst potential is increased, the potassium current activation gating variable becomes less and less restorative and eventually becomes regenerative. Further increases of V_K causes its cooperativity to dominate the competitivity of the sodium current inactivation, providing an overall positive feedback on the fast subsystem composed by the membrane potential and the sodium current activation, leading to regenerative excitability, as sketched in Fig. 11.6.

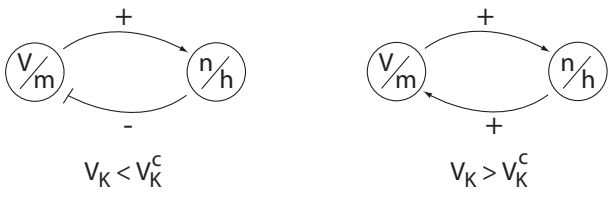

Figure 11.6 – Representation of HH model excitability as feedback interconnections. The membrane potential V and the sodium channel activation m are the fast variables, the potassium channel activation n and the sodium channel inactivation h are the slow variables. When V_K is below (resp. above) the critical value V_K^c, slow variables induce an overall negative (resp. positive) feedback on membrane potential variations, resulting in restorative (resp. regenerative) excitability.

Tracking excitability switches in conductance-based models

The mathematical analysis of the previous sections follows an algorithm that allows to detect a transcritical bifurcation in generic conductance based models of arbitrary dimension and to track associated excitability switches. The steps of the algorithm are summarized in Tab. 11.2. For simplicity and conciseness, we restrict our attention to the modulation of only one regenerative ionic current at a time. However, a similar algorithm can be written for an arbitrary modulation of ionic currents that brings the model to the balance expressed in (11.9).

We now apply this algorithm to a number of published conductance-based models and show that all these models can switch between restorative and regenerative excitability through a transcritical bifurcation, as sketched in Fig. 11.7. Figure 11.7 indicates two qualitatively distinct paths from restorative to regenerative excitability: one path traversing the hybrid excitability region just described with Hodgkin-Huxley model (Fig. 11.5A) and one path switching directly from restorative to regenerative excitability through the TC bifurcation that will be illustrated on the dopaminergic neuron model.

Dopaminergic (DA) neuron model

We first use the DA neuron model we developed in Chapter 4 [40].

(i) **Classification of gating variables as fast ($\mathcal{G}_F$), slow ($\mathcal{G}_S$), and adaptation ($\mathcal{G}_A$) variables**
(i-a) Following Tab. 11.1, group gating variables in the three groups $\mathcal{G}_F$, $\mathcal{G}_S$, and $\mathcal{G}_A$.
(i-b) Split $\mathcal{G}_S$ in regenerative $\mathcal{G}_{S,+}$ and restorative $\mathcal{G}_{S,-}$ slow gating variables.
(i-c) If adaptation variables are present, set them to constant physiologically relevant values.

(ii) **Balance equation and choice of the bifurcation parameter**
(ii-a) Select a regenerative ionic current I_{reg} and the associated regenerative slow gating variable x^{reg}.
(ii-b) Write the balance equation

$$\left.\frac{\partial \dot{V}}{\partial x^{reg}}\frac{\partial x_\infty^{reg}}{\partial V}\right|_{TC} = -\sum_{x^{r-}} \overbrace{\left.\frac{\partial \dot{V}}{\partial x^{s-}}\frac{\partial x_\infty^{s-}}{\partial V}\right|_{TC}}^{<0} - \sum_{x^{s+}\neq x^{reg}} \overbrace{\left.\frac{\partial \dot{V}}{\partial x^{s+}}\frac{\partial x_\infty^{s+}}{\partial V}\right|_{TC}}^{>0} \quad \text{(b.eq.)}$$

(ii-c) If I_{reg} has an adaptation variable x^a, pick it as the bifurcation parameter λ regulating the left hand side of (b.eq.), that is $\lambda = x^a$.
If I_{reg} has no adaptation variable, pick $\lambda = \bar{g}_{reg}$.

(iii) **Singularity condition and fixed point equation**
(iii-a) Solve (b.eq.) together with the singularity condition (11.8), in V and λ.
For numerical implementation, note that the left hand side of (11.8) can be written as

$$\det J_f = \frac{\partial}{\partial V}\left(\dot{V}\Big|_{x^f = x_\infty^f(V)}\right)$$

(iii-b) Plug the computed values V^c and λ^c into the fixed point equation $\dot{V}|_{TC} = 0$ to compute the value of the applied current at the transcritical bifurcation (I^c).

(iv) **Tracking of excitability switches**
Change the applied current according to the equation

$$I_{app} = I^c - \left.\frac{\partial \dot{V}}{\partial \lambda}\right|_{TC}(\lambda - \lambda^c),$$

and compute the model bifurcation diagram with V as the variable and λ as the bifurcation parameter.

Table 11.2 – Algorithm for the detection of a transcritical bifurcation in generic conductance-based models via modulation of a regenerative ionic current and computation of the excitability switch bifurcation diagram.

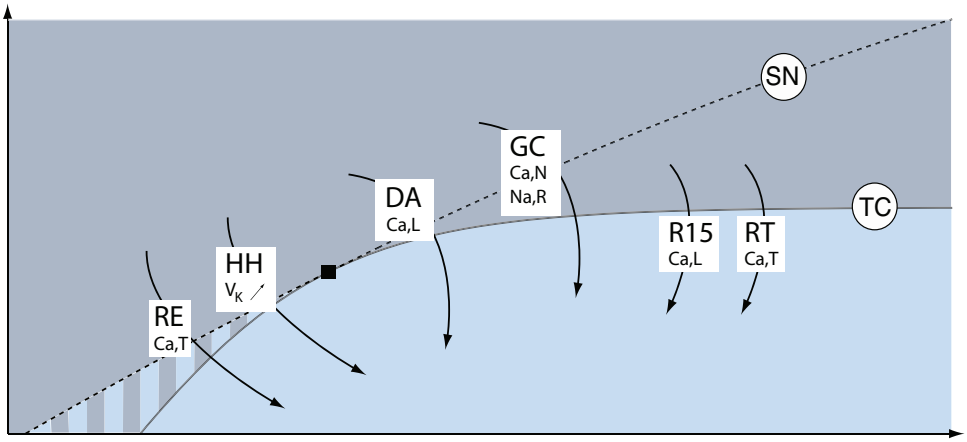

Figure 11.7 – Modifications in the balance between restorative and regenerative channels induce excitability switches in conductance-based models. The figure sketches excitability switches of the Hodgkin-Huxley (HH) model [81], Aplysia's R15 neuron (R15) model [149], a dopaminergic (DA) neuron model [40], thalamic reticular (RT) and relay (RE) neuron models [36, 37], and a cerebral granule cell (GC) model [33] on the excitability parameter map computed for the two-dimensional model of Chapter 10 [52]. All these conductance-based models can switch between restorative and regenerative excitability through the physiologically relevant regulation of specific ion channels.

(i) **Classification of gating variables as fast ($\mathcal{G}_F$), slow ($\mathcal{G}_S$), and adaptation ($\mathcal{G}_A$) variables**
The model includes fast sodium channels ($I_{Na,f}$), delayed-rectifier potassium channels ($I_{K,DR}$), L-type calcium channels ($I_{Ca,L}$), small conductance calcium-activated potassium (SK) channels ($I_{K,Ca}$), and calcium pumps ($I_{Ca,pump}$). We classify model variables as follows

- $\mathcal{G}_F = \{m_{Na,f}\}$
- $\mathcal{G}_{S,-} = \{h_{Na,f},\, m_{K,DR}\}$ and $\mathcal{G}_{S,+} = \{m_{Ca,L}\}$
- $\mathcal{G}_A = \{[Ca^{2+}]_{in}\}$

In order to unfold excitability switches, SK channel density is set to zero, since SK channels drastically attenuate DA neuron excitability by activating a strong calcium regulated potassium current [41, 95, 96, 191]. The intracellular calcium concentration is fixed at $[Ca^{2+}]_{in} = 300\,nM$.

(ii) **Balance equation and choice of the bifurcation parameter**
The only source of regenerative excitability is provided by L-type calcium channels. The balance equation reads

$$\left.\frac{\partial \dot{V}}{\partial m_{Ca,L}}\frac{\partial m_{Ca,L,\infty}}{\partial V}\right|_{TC} = -\left.\left(\frac{\partial \dot{V}}{\partial h_{Na,f}}\frac{\partial h_{Na,f,\infty}}{\partial V} + \frac{\partial \dot{V}}{\partial m_{K,DR}}\frac{\partial m_{K,DR,\infty}}{\partial V}\right)\right|_{TC}$$

We use the L-type calcium channel density $\bar{g}_{Ca,L}$ as the bifurcation parameter (*i.e.* $\lambda = \bar{g}_{Ca,L}$).

Solving Steps (iii) and (iv) of the algorithm above gives the following results (in this and the subsequent tables, the reported critical values are not exact, but rounded to the last significant digit):

V^c	$\bar{g}^c_{Ca,L}$	I^c
-64.92 mV	1.95 mS/cm^2	9.54 μA/cm^2

The critical value $\bar{g}^c_{Ca,L}$ is roughly 1.5 times smaller than the nominal parameter value in [40], which is consistent with the observation that the original model exhibits regenerative excitability during SK channel blockade.

The resulting bifurcation diagram is drawn in Fig. 11.8A. In addition to confirming the existence of a transcritical bifurcation for the computed values, it reveals the excitability switches induced by changes in L-type calcium channel density in this model: in the absence of L-type calcium channels, the model exhibits restorative excitability. As $\bar{g}_{Ca,L}$ increases, a saddle point and an unstable node emerge at a saddle-node bifurcation, which induces no excitability switch. Further increase of $\bar{g}_{Ca,L}$ causes a transcritical bifurcation, where the stable point and the saddle exchange their stability. At this point, the stable steady-state becomes regenerative, and the model switches to regenerative excitability.

These excitability switches induce the predicted changes in the electrophysiological signatures, as illustrated in Fig. 11.8B. Whereas the DA neuron model instantaneously reacts to a step input of depolarizing current for $\bar{g}_{Ca,L} < \bar{g}^c_{Ca,L}$, it exhibits electrophysiological signature of regenerative excitability such as spike latency, plateau oscillations and ADP as soon as $\bar{g}_{Ca,L}$ becomes higher than $\bar{g}^c_{Ca,L}$. In addition, the model becomes strongly bistable.

Thalamic relay (RE) neuron model

Model equations and parameters are taken from [37].

(i) **Classification of gating variables as fast ($\mathcal{G}_F$), slow ($\mathcal{G}_S$), and adaptation ($\mathcal{G}_A$) variables**
The model includes fast sodium channels $I_{Na,f}$, delayed-rectifier potassium channels $I_{K,DR}$ and T-type calcium channels $I_{Ca,T}$. We classify model variables as follows

- $\mathcal{G}_F = \{m_{Na,f}\}$
- $\mathcal{G}_{S,-} = \{h_{Na,f},\, m_{K,DR}\}$ and $\mathcal{G}_{S,+} = \{m_{Ca,T}\}$
- $\mathcal{G}_A = \{h_{Ca,T}\}$

(ii) **Balance equation and choice of the bifurcation parameter**
The only source of regenerative excitability is provided by T-type calcium channels. The associated balance equation reads

$$\left.\frac{\partial \dot{V}}{\partial m_{Ca,T}}\frac{\partial m_{Ca,T,\infty}}{\partial V}\right|_{TC} = -\left.\left(\frac{\partial \dot{V}}{\partial h_{Na,f}}\frac{\partial h_{Na,f,\infty}}{\partial V} + \frac{\partial \dot{V}}{\partial m_{K,DR}}\frac{\partial m_{K,DR,\infty}}{\partial V}\right)\right|_{TC}$$

T-type calcium channels are dynamically regulated by a (slow) voltage-gated inactivation $h_{Ca,T}$. We use this variable as the bifurcation parameter (*i.e.* $\lambda = h_{Ca,T}$).

Solving Steps (iii) and (iv) of the algorithm above gives the following results:

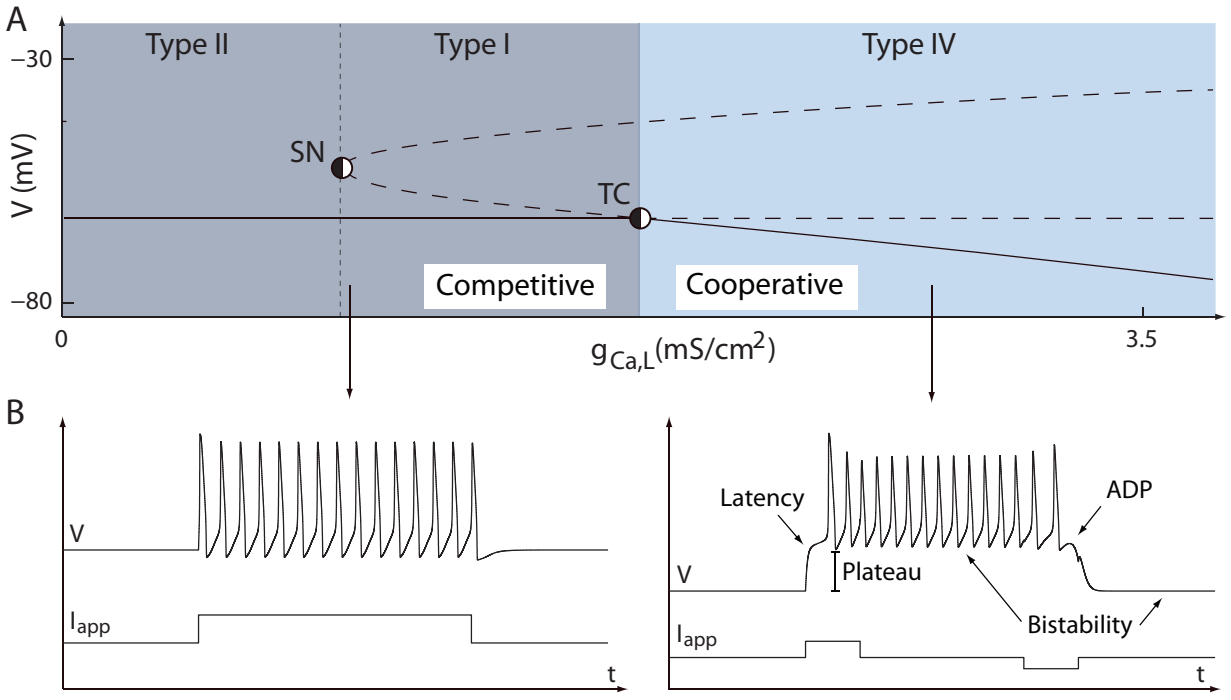

Figure 11.8 – Variations of L-type calcium channel density $\bar{g}_{Ca,L}$ induce excitability switches in the DA neuron model developed Chapter 4 [40]. **A.** Bifurcation diagram of the model with $\bar{g}_{Ca,L}$ as the bifurcation parameter. TC denotes a transcritical bifurcation, SN a saddle-node bifurcation. Branches of stable fixed points are represented as solid line, branches of saddle points and unstable points as dashed lines. **B.** Electrophysiological responses of the model to step inputs of excitatory/inhibitory current (the intracellular calcium concentration is fixed at $[Ca^{2+}]_{in} = 300\,nM$, which is within the physiological range). For $\bar{g}_{Ca,L}$ lower (resp. higher) than the critical value $\bar{g}^c_{Ca,L}$, the model exhibits typical electrophysiological signature of restorative (resp. regenerative) excitability. The low $\bar{g}_{Ca,L}$ configuration corresponds to $\bar{g}_{Ca,L} = 1mS/cm^2$, whereas the high $\bar{g}_{Ca,L}$ configuration corresponds to $\bar{g}_{Ca,L} = 3mS/cm^2$.

V^c	$\bar{h}^c_{Ca,T}$	I^c
-61.56 mV	0.004	0.91 nA/cm^2

Since $\bar{h}^c_{Ca,T} \in (0,\, 1)$, the model dynamically switches between restorative and regenerative excitability when $h_{Ca,T}$ crosses the critical value, and the electrophysiological signatures are consistent with the excitability switches. See Fig. 11.9.

Thalamic reticular (RT) neuron model

Model equations and parameters are taken from [36], maximal conductances are adapted as in Chapter 9 [42].

(i) **Classification of gating variables as fast ($\mathcal{G}_F$), slow ($\mathcal{G}_S$), and adaptation ($\mathcal{G}_A$) variables**
The model includes fast sodium channels $I_{Na,f}$, delayed-rectifier potassium channels $I_{K,DR}$ and T-type calcium channels $I_{Ca,T}$. We classify model variables as follows

- $\mathcal{G}_F = \{m_{Na,f}\}$
- $\mathcal{G}_{S,-} = \{h_{Na,f},\, m_{K,DR}\}$ and $\mathcal{G}_{S,+} = \{m_{Ca,T}\}$
- $\mathcal{G}_A = \{h_{Ca,T}\}$

(ii) **Balance equation and choice of the bifurcation parameter**
The only source of regenerative excitability is provided T-type calcium channels. The associated balance equation has the same structure as for the thalamic relay neuron model considered above. Along the same line, we choose the T-type calcium channel inactivation $h_{Ca,T}$ as the bifurcation parameter (*i.e.* $\lambda = h_T$).

Solving Steps (iii) and (iv) of the algorithm above gives the following results:

V^c	$\bar{h}^c_{Ca,T}$	I^c
-48.81 mV	0.18	-0.82 nA

As in the case of the thalamic relay neuron model, the T-type calcium channel inactivation generates a dynamical switch between restorative and regenerative excitability, significantly affecting neuron response to external inputs (Fig. 11.9).

Aplysia R15 neuron model

Model equations and parameters are taken from [149].

(i) **Classification of gating variables as fast ($\mathcal{G}_F$), slow ($\mathcal{G}_S$), and adaptation ($\mathcal{G}_A$) variables**
The model includes fast sodium channels $I_{Na,f}$, delayed-rectifier potassium channels $I_{K,DR}$, slow L-type calcium channels $I_{Ca,L}$ and calcium-activated potassium channels $I_{K,Ca}$. We classify model variables as follows

- $\mathcal{G}_F = \{m_{Na,f}\}$
- $\mathcal{G}_{S,-} = \{h_{Na,f},\, m_{K,DR}\}$ and $\mathcal{G}_{S,+} = \{m_{Ca,L}\}$
- $\mathcal{G}_A = \{[Ca^{2+}]_{in}\}$

The intracellular calcium conductance is fixed at $[Ca^{2+}]_{in} = 0.09nM$.

(ii) **Balance equation and choice of the bifurcation parameter**
As in the case of DA neurons, the source of regenerative excitability is provided by L-type calcium channels, and we take their maximal conductance $\bar{g}_{Ca,L}$ as the bifurcation parameter. The associated balance equation has the same structure as for the DA neuron model considered above.

Solving Steps (iii) and (iv) of the algorithm above gives the following results:

V^c	$\bar{g}^c_{Ca,L}$	I^c
-48.05 mV	$5.41\ 10^{-5}$ mS/cm^2	$-0.03\ \mu$A/cm^2

Comparing the critical value $\bar{g}^c_{Ca,L}$ with the original value $\bar{g}_{Ca,L} = 4\ 10^{-3}$ mS/cm^2 shows that the bursting model proposed in [149] exhibits strong regenerative excitability. Switches of electrophysiological signatures are illustrated in Fig. 11.9.

Cerebellar granular cell (GC) model

Model equations and parameters are taken from [33].

(i) **Classification of gating variables as fast ($\mathcal{G}_F$), slow ($\mathcal{G}_S$), and adaptation ($\mathcal{G}_A$) variables**
The model includes the following ion channels: fast ($I_{Na,f}$), persistent ($I_{Na,P}$) and resurgent sodium channels ($I_{Na,R}$) ; N-type calcium channels ($I_{Ca,N}$) ; delayed rectifier ($I_{K,DR)}$, A-type ($I_{K,A}$), inward rectifier ($I_{K,IR}$), calcium activated ($I_{K,Ca}$) and slow potassium channels ($I_{K,slow}$). We classify model variables as follows

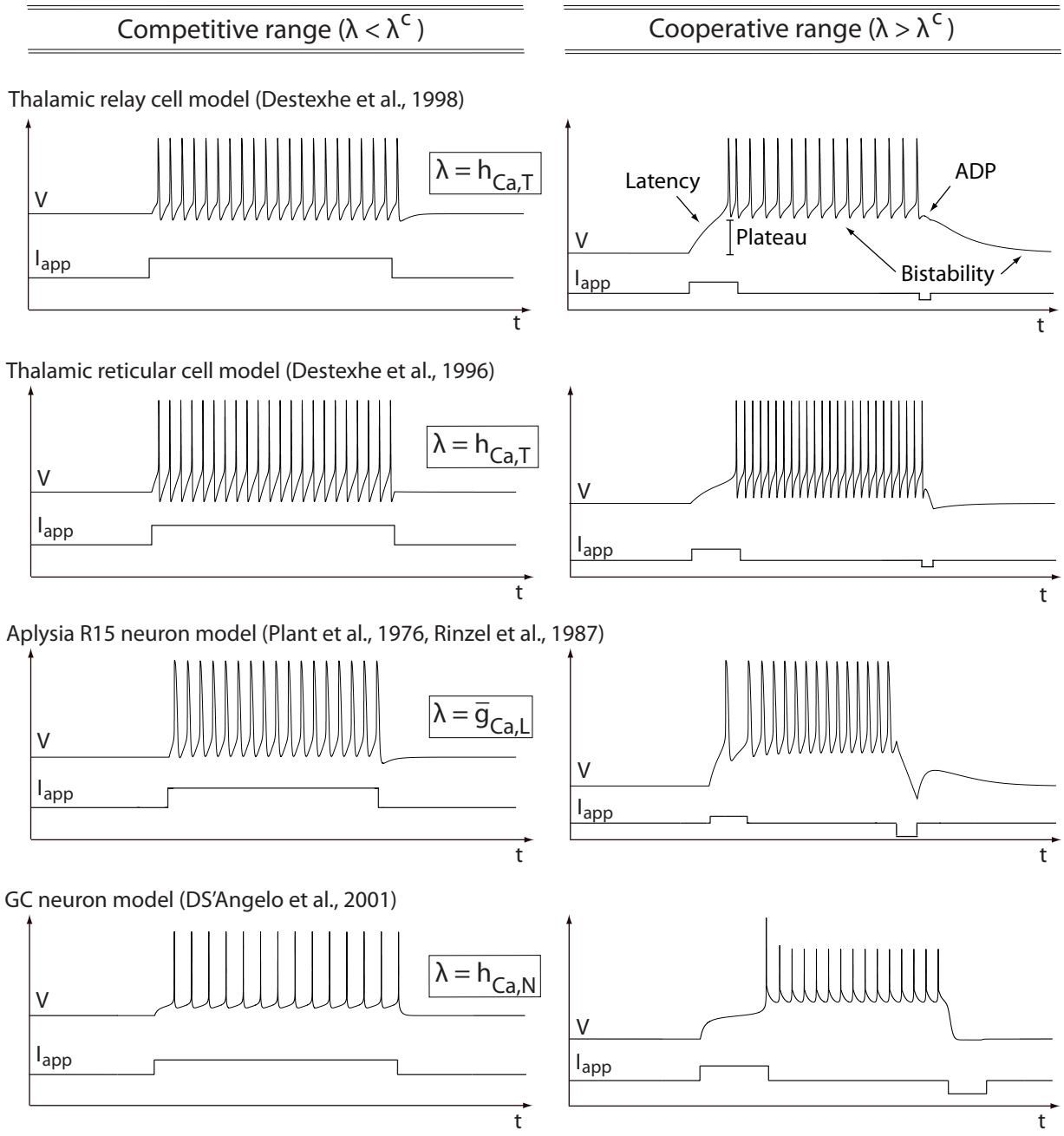

Figure 11.9 – The same mathematical bifurcation in different conductance-base models causes the same switch in electrophysiological signatures. The figure shows the electrophysiological responses of various conductance-based models to step inputs of excitatory/inhibitory current when the bifurcation parameter λ is lower (left) or higher (right) than the critical value λ^c. This bifurcation parameter can be either the density or the inactivation variable of a regenerative channel. Other adaptation variables are set to constant values chosen in physiological ranges (see text). For λ lower (resp. higher) than the critical value λ^c, all models exhibit electrophysiological signatures of restorative (resp. regenerative) excitability. Numerical values of the parameter λ in the different plots are as follows. Thalamic relay cell: left $h_{Ca,T} = 0$, right $h_{Ca,T} = 0.2$. Thalamic reticular cell: left $h_{Ca,T} = 0$, right $h_{Ca,T} = 0.4$. Aplysia R15 neuron: left $\bar{g}_{Ca,L} = 10^{-6} mS/cm^2$, right $\bar{g}_{Ca,L} = 0.004 mS/cm^2$. GC neuron: left $h_{Ca,N} = 0.01$, $h_{Na,R} = 0.1$, right $h_{Ca,N} = 0.3$, $h_{Na,R} = 0.1$.

- $\mathcal{G}_F = \{m_{Na,f},\, m_{Na,P}\}$
- $\mathcal{G}_{S,-} = \{h_{Na,f},\, m_{K,DR},\, m_{K,A},\, m_{K,IR}\}$ and $\mathcal{G}_{S,+} = \{m_{Na,R},\, m_{Ca,N}\}$
- $\mathcal{G}_A = \{h_{Na,R},\, h_{Ca,N},\, h_{K,A},\, m_{K,slow}\}$

We set the persistent and calcium-activated currents to zero (these two channels do not impact excitability type as anticipated by our classification and shown by D'Angelo and colleagues [33]). The inactivation of the A-type potassium current is fixed at $h_{K,A} = 0.02$ and the activation of the slow potassium current is fixed at $m_{K,slow} = 0.13$.

(ii) **Balance equation and choice of the bifurcation parameter**
The neuron model possesses two sources of regenerative excitability: resurgent sodium channels and N-type calcium channels. As in the case of T-type calcium channels mentioned above, these two channels possess an inactivation gate, which is used as the bifurcation parameter. We apply our algorithm by varying the parameter of one regenerative current while fixing the other at different values. This permits to draw an approximated hypersurface in the $(h_{Ca,N}, h_{Na,R})$ plane at which the balance equation is satisfied and the model undergoes the transcritical bifurcation and the associated excitability switch.

Solving Steps (iii) and (iv) of the algorithm one obtains the parameter chart in Fig. 11.10. These results show that both channels can induce a dynamical switch in excitability. However, the N-type calcium channel contributes much more to regenerative excitability than the resurgent sodium channel in this model: as soon as $h_{Ca,N} \gtrsim 0.03$ the model is in regenerative excitability for all values of $h_{Na,R}$. On the contrary, when $h_{Ca,N} = 0$ the inactivation of resurgent sodium channel should be more than a half deinactivated for the model to exhibit regenerative excitability.

The transcritical bifurcation determines a switch from restorative to regenerative excitability

As illustrated in Fig. 11.4, the significance of the transcritical bifurcation is that it delineates in the parameter space the boundary of a specific type of excitability and that this boundary is determined by a simple physiological balance between restorative and regenerative channels.

Specific to regenerative excitability is the bistable (right) phase portrait of Figure 11.1. For the five analyzed conductance-based models, our bifurcation analysis of the full model confirms the existence of a bistable range beyond the transcritical bifurcation, where a regenerative resting state and a spiking limit cycle coexist. In each case, the bistability range is obtained for the nominal time scales of the published model and is robust to a variation of time scales. In each case, the bistability range is also neuromodulated, that is, determined by conductance parameters that are known to vary in slower time scales and/or across neurons of a same type.

It is important to distinguish this robust and physiologically regulated bistability from other types of bistability that can be encountered in conductance-based models. Fig. 11.11 qualitatively illustrates three typical bistable phase portraits associated to the planar model (11.1) that exhibit the coexistence of a stable resting state and of a spiking limit cycle. The first two are associated to restorative excitability and are extensively studied in the literature. See, e.g., [89, 150] and references therein. Only the third one is associated to regenerative excitability.

The three bistable phase portraits share the common feature of "hard excitation": as the amplitude of a step input depolarizing current is increased, the response of the neuron abruptly switches from no oscillation to high frequency spiking. Following the historical classification of Hodgkin, the three situations correspond to Class II neurons, as opposed to Class I neurons for which the spiking frequency gradually increases with the depolarizing current amplitude.

Hard excitation can be a manifestation either of a switch-like monostable bifurcation diagram or of a hysteretic bistable bifurcation diagram. By definition, the three bistable phase portraits in Figure 11.11 give rise to hysteretic bifurcation diagrams. But for the two bistable phase portraits associated to restorative excitability, the hysteresis is highly dependent on the time scale separation, *i.e.*, the ratio ε between the slow and fast timescale. In the case of the first phase portrait (subcritical Hopf bifurcation), asymptotic analysis shows that the hysteresis vanishes as $\mathcal{O}(e^{-1/\varepsilon})$. In the case of second phase portrait (SN homoclinic bifurcation), the situation is even worse because for small $\epsilon > 0$ the system necessarily undergoes a monostable saddle-node on invariant circle bifurcation. In fact, the second phase portrait is not physiological for conductance based-models. For instance, in the hypothetical $I_{Na,p} + I_K$ conductance-based model considered in [89, Fig. 6.44], the time constant of the potassium activation must be set to below $0.17ms$ to create a saddle-homoclinic bifurcation, which is roughly 40 times smaller than its physiological value and even smaller that the fast time constant. A geometric proof of the generality of this fact is provided in [52]. The conclusion is that hysteresis associated to restorative excitability is at best very small (if any) in physiologically plausible conductance based models, which makes their electrophysiological signatures similar to those associated to a switch-like monostable bifurcation diagram.

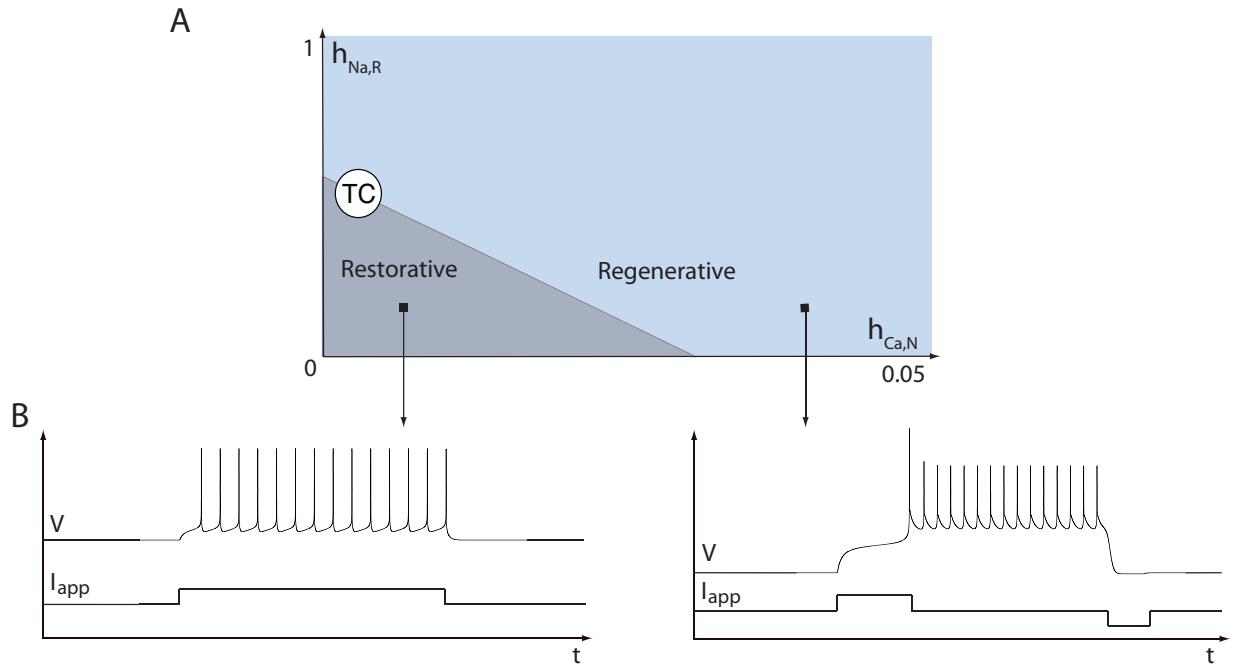

Figure 11.10 – Joint variations of the inactivation gates of N-type calcium channels and resurgent sodium channels induce excitability switches in cerebellar granular cells. A. Two parameter bifurcation diagram of the mode with $h_{Ca,N}$ and $h_{Na,R}$ as bifurcation parameters. TC denotes a branch of transcritical bifurcations detected following the algorithm in Tab. 11.2. **B.** Electrophysiological responses of the model to step inputs of excitatory/inhibitory current: left $h_{Ca,N} = 0.01$, $h_{Na,R} = 0.1$, right $h_{Ca,N} = 0.3$, $h_{Na,R} = 0.1$.

In sharp contrast, the hysteresis associated to regenerative excitability is barely affected by the time-scale separation. Instead it is regulated by conductance parameters whose modulation is physiological (for instance, an image of a regenerative ion channel density). The extended hysteresis is what determines the specific electrophysiological signature of regenerative excitability: a pronounced spike latency, a possible plateau oscillation, and an after depolarization potential. As a consequence, those features cannot be robustly reproduced in physiologically plausible conductance based models of restorative excitability. Because those features are important markers of modern electrophysiology [55, 100], the distinction between restorative and regenerative excitability seems physiologically relevant, beyond the possible shared feature of hard excitation.

In conclusion, the bistability associated to regenerative excitability is specific in that it produces a robust electrophysiological signature in physiologically plausible parameter ranges and consistent with many experimental observations. It is in that sense that the transcritical bifurcation delineates a switch of excitability of physiological relevance.

Discussion

A simple and robust balance equation identifies a transcritical bifurcation in arbitrary conductance based models

Motivated by a geometric analysis of a qualitative phase portrait, we have proposed an algorithm that easily detects a transcritical bifurcation in arbitrary conductance based models. Owing to the special structure of such models, the algorithm leads to solving an algebraic equation of remarkable simplicity and physiological relevance: a balance between slow restorative and slow regenerative ion channels. The condition is also robust because the balance is independent of the detailed kinetics. It only relies on a classification of variables in three well separated time-scales, in full accordance with what is known on ion channels kinetics [78].

The ubiquity of a transcritical bifurcation in conductance-based models

The detection of the transcritical bifurcation relies on the sole existence of a physiological balance between restorative and regenerative ion channels. Given that all neuronal models possess restorative sodium and potassium channels, this implies that a transcritical bifurcation ex-

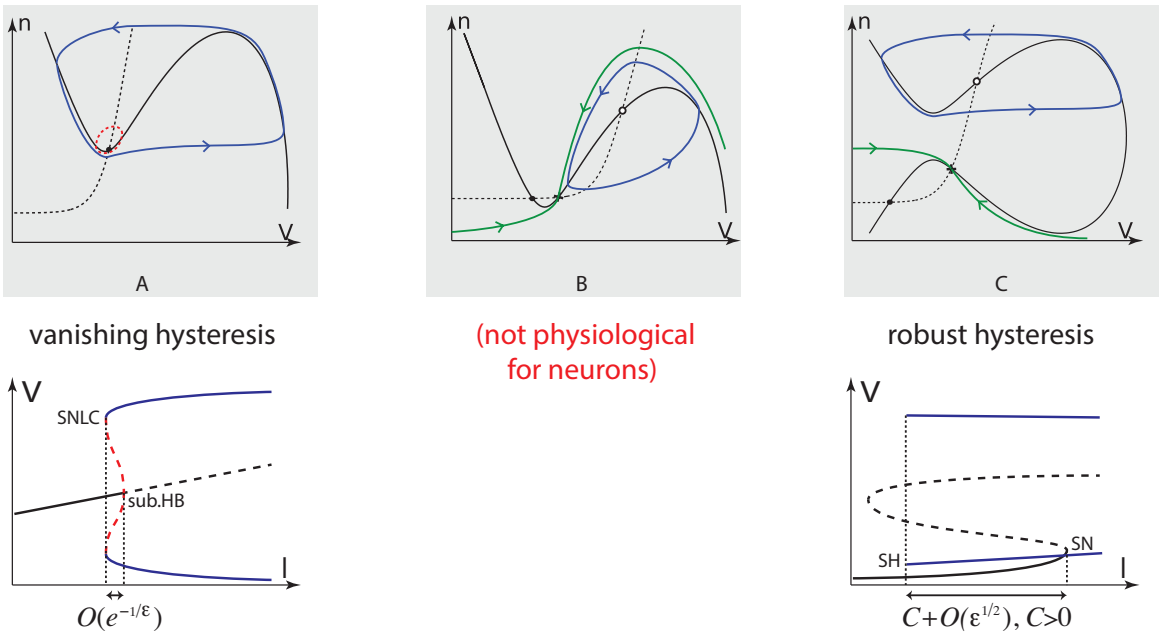

Figure 11.11 – Three bistable phase portraits of model (11.1) and cartoon of the associated hysteretic bifurcation diagrams. In the phase portraits, a solid line denotes the V-nullcline, whereas a dashed line denotes the n-nullcline. Stable fixed points are depicted as filled circles, whereas unstable as circles and saddle points as cross. Stable limit cycles are drawn as solid oriented blue curves, whereas unstable as red dashed curves. The stable manifolds of saddle points are depicted as green oriented curves. In bifurcation diagrams, a solid line denotes branches of stable fixed points, whereas a dashed line denotes branches of unstable or saddle points. Branches of stable limit cycles are depicted as blue lines, whereas branches of unstable limit cycles as red dashed lines. *sub.HB* denotes a subcritical Hopf bifurcation, *SNLC* a saddle-node limit cycles bifurcation, *SN* a saddle-node bifurcation, and *SH* a saddle-homoclinic bifurcation. **A-B.** Restorative bistability. **A.** Subcritical Hopf bifurcation. Hysteresis vanishes exponentially fast as timescale separation increases. **B.** Restorative saddle-homoclinic bifurcation. Not physiological because it violates the time scale separation between V and n. **C.** Regenerative bistability ruled by a regenerative saddle-homoclinic bifurcation. Hysteresis is barely affected by time-scale separation.

ists in every conductance-based model that possesses at least one regenerative ion channel. Moreover, the channel balance, and therefore the TC bifurcation, are readily detectable in a model of arbitrary dimension (both in the state and parameters): the balance (11.9) simply defines a hypersurface in the parameter space that can algebraically be tracked under arbitrary parameter variations, as illustrated with in the GC model above.

In spite of its ubiquity and of its physiological significance, we are not aware of an earlier reference to a transcritical bifurcation in conductance based models. A reason for this omission might be accidental: there are no regenerative channels in the seminal model of Hodgkin and Huxley (unless one modifies the potassium resting potential V_k) and this model has been the inspiration of most mathematical analyses of conductance-based models.

For the same reason, it seems physiologically relevant to distinguish between restorative and regenerative excitability beyond Hodgkin's classification in soft excitation (class I) and hard excitation (class II). Regenerative excitability faithfully captures specific electrophysiological signatures of modern electrophysiology such as spike latency, afterdepolarization potentials, or robust coexistence of resting state and repetitive spikes.

A same mathematical prediction applies to many distinct physiological observation

Although purely mathematical in nature, the transcritical bifurcation has a remarkable predictive value in several published conductance based models. In each of the six analysed models, the proposed algorithm identifies a physiological parameter that acts as a tuner of neuronal excitability in a physiologically plausible range and in full agreement with existing experimental data. At the same time, the distinct nature of the regulating parameter, which can be either the maximal conductance or the inactivation gating variable of a regenerative ion channel depending on the neuron model, is associated to distinctly different regulation mechanisms.

Reduced modeling should retain the balancing channel

The classification of gating variables in three distinct time scale is an essential modeling step both for the proposed algorithm and for the reduction of full conductance-based models to low-dimensional models that can be used in population studies [90]. When all slow ion channels are properly identified, they can be aggregated in a single slow variable to lead to a second order model of the type (11.1), where the single parameter n_0 captures the restorative or regenerative nature of the aggregated slow variable. Further reduction to a one-dimensional hybrid model with reset is possible thanks to the time-scale separation between the voltage V and the slow variable n. This reduction is illustrated in [42] on the thalamic TC neuron and the reduced model remarkably retains the switch of excitability of its high-dimensional counterpart. In contrast, a reduced model will loose the switch of excitability of the full conductance-based model when a regenerative ion channel is treated as a fast gating variable. This is for instance the case in the STN neuron model of [108]. The switch of excitability is well identified in experimental data [72] but cannot be reproduced in the model because the only source of cooperativity, the activation of T-type calcium channels, is treated as an (instantaneous) fast variable.

Neuronal excitability is regulated

In each of the analyzed conductance-based models, the balance equation responsible for the switch of excitability is satisfied for a set of parameters that is close to the published parameter values. This observation supports the hypothesis that neuronal excitability is tightly regulated by molecular mechanisms and that the influence of the channel balance condition on neuronal excitability might play a role in neuronal signaling.

Chapter 12

A Physiological Route to Neuronal Bursting

Neuronal bursting has been heavily investigated since the early days of neurodynamics, but the mechanisms underlying physiological routes to bursting have remained an open question to date. Most analyses agreed that endogenous bursting relies on the slow variation of an adaption variable over a bistable region, but the existence and possible regulation of such a robust bistable region in existing reduced models is elusive. Likewise, very few mechanisms of switch between single spike firing and bursting have been described, even though such a switch is a prevalent signaling component of many neurons.

In the previous chapters, we have described a novel type of excitability, taking the role of regenerative ion channels such as voltage-gated calcium channels into account. This excitability type, which we termed "regenerative excitability", is shown to be at the origin of a robust bistability between a resting state and a spiking state [52], this bistable region being regulable by a single parameter, that is the balance weight, both in planar models and in conductance based models.

In this chapter, we apply these concepts to propose a plausible route to neuronal bursting. This route relies on the regulated interaction between neuron excitability type and an ultraslow adaptation variable. In particular, we show that endogenous firing quality is determined by two parameters, that is the balance weight and the adaptation gain. These two parameters are physiologically regulated, as shown in Chapter 11.

We illustrate this phenomenon simply by adding an ultra-slow adaptation variable z to the transcritical hybrid model developed in Chapter 9. The model is able to switch from single-spike firing to bursting via a simple change in its balance weight, defined by the parameter w_0. The value of w_0 at which the neuron model switches to bursting mode depends on the value of another parameter, that is the adaptation gain k_z. The physiological correlate of this parameter is the maximal density of ion channels activating on an ultraslow timescale, such as SK channels, for instance. The simple hybrid model is also able to exhibit different bursting qualities, according to the values of w_0 and k_z, in contrast with the common view of neuronal bursting, where each bursting type is viewed as arising from a different underlying mechanism.

This bursting mechanism is shown to arise from the combination of four ion channel types, that is one fast depolarizing, one slow restorative, one slow regenerative and one ultraslow adaptation ion channel. These simple ingredients are the key components of most of bursting neurons and models, such as those involved in central pattern generators. Any regulation mechanism of one of these channel types therefore represents a potential physiological route to neuronal bursting.

Results

A Novel Bursting Model for Neurodynamics

Although there exists many types of bursting neurons, each expressing various ion channels and having different morphologies, the mechanisms underlying their firing behavior are strongly similar and can be simply modeled and reproduced in a reduced three-dimensional model. These three dimensions arise from the three sharply separated timescales that usually characterize neuronal dynamics [78]:

1. The fast activation is proper to membrane potential variations and to fast gating variables, such as activation of fast sodium channels. The rapid regenerative upstroke of the action potential is generated on this timescale.

2. The recovery (slow) timescale characterizes all gating variables that (in)activate during the action potential. They include the activation of the delayed rectifier potassium current, the inactivation of the fast sodium current, and the activation of all calcium currents. Recovery gating variables regulate neuronal excitability type via their regenera-

tive or restorative nature (see Chapters 9,10 and 11) [52, 53].

3. The adaptation (ultra-slow) timescale includes all the adaptation variables that varies only during long-lasting neuronal activity, such as the inactivation of calcium currents or activation of calcium-activated potassium channels through variations of the intracellular calcium concentration. Their effect is to modulate neuron excitability via slow changes in the net membrane current, as well as excitability type, through the indirect modulation of recovery gating variables.

In Chapters 9,10 and 11, we have shown that slow variables are responsible for neuron excitability type. Namely, when slow restorative variables, which provide a negative feedback to membrane potential variations, are dominant, the neuron exhibits restorative excitability, whose electrophysiological signatures are monostability, non-plateau firing and instantaneous response to external suprathreshold stimulations. Conversely, when slow regenerative variables, which provide a positive feedback to membrane potential variations, are dominant, the neuron exhibits regenerative excitability, whose electrophysiological signatures are robust bistability, plateau firing and spike latency. The degenerate case where the role of slow restorative and regenerative variables is exactly balanced corresponds to a transcritical bifurcation in arbitrary conductance-based models.

On the basis of these physiologically relevant results, we propose a reduced hybrid model of neuronal bursting based on the transcritical normal form (Chapter 9)

$$\begin{aligned} \dot{v} = v^2 + bvw - w^2 + \mathbf{I_{app}} - \mathbf{k_z}z \qquad & \text{if } \; v \geq v_{th}, \text{ then} \\ \dot{w} = \epsilon(av - w + \mathbf{w_0}) \qquad & v \leftarrow c, \; w \leftarrow d, \\ \dot{z} = -\epsilon_z z, \qquad & z \leftarrow z + d_z. \end{aligned}$$

where v merges the membrane potential and fast variables, w merges all recovery variables and z all adaptation variables .The only parameters are w_0 and k_z, I_{app} represents system input. Parameter w_0 represents the balance between restorative and regenerative channels: $w_0 > 0$ models the case where restorative channels are dominant, $w_0 < 0$ model the case where regenerative channels are dominant, and $w_0 = 0$ corresponds to the exact balance between both type of channels. Parameter k_z is the adaptation gain, which relates to the maximal conductance of all adaptation currents, such as calcium-activated potassium channels. These two parameters modulate excitability quality. They are physiologically regulated, as shown in Chapter 11, and will be the key players in tuning the quality of model firing pattern. I_{app} is the total applied current. It regulates excitability quantity. For our study, we set I_{app} to a particular value I_{SN} to normalize the value of z at which the neuron starts firing while w_0 is varying. All other parameters, such as reset values, are fixed to physiologically appropriate values and will not be modified in any case.

This simple hybrid model is able to reproduce single-spike (pacemaker) and bursting activities, as well as to continuously switch between these two states via changes in the balance weight w_0 (Fig. 12.1). In the restorative region, the model exhibits a very regular pacemaker activity, and variations of w_0 only slightly affect the shape of the interspike period. As the model becomes regenerative, the pacemaker activity first robustly persists and the neuron starts to exhibit after-depolarization potentials (ADPs) between spikes. Then, the neuron eventually reaches a bursting behavior as the balance weight increases (w_0 becomes more negative): the higher the balance weight, the longer the bursts and the higher the intraburst firing frequency, which is accompanied by a larger increase in z. Note that, as observed experimentally, the intra-burst firing rate is several times higher than the pacemaking rate. This physiological route to bursting is a peculiar feature of the proposed model and cannot be reproduced in existing reduced models, because all these models are exclusively restorative.

A Unique Bursting Model accounts for Different Bursting Qualities

Although regeneracy is a key to neuronal bursting, the figure shows that this firing pattern only occurs for a sufficiently large balance weight. Indeed, in the present case, the neuron bursts only for $w_0 < -3$. This highlights the presence of another key player in the regulation of pacemaker and bursting activities, that is the adaptation gain k_z. In fact, whereas the presence of a robust bistable region (a signature of regenerative excitability) is a critical component of neuronal bursting, transitions between spiking and quiescent periods are fully determined by the adaptation variable z. Any change in the adaptation gain k_z therefore strongly affects the firing pattern, and even generates switches from pacemaking to bursting and conversely.

The interaction between the balance weight and the adaptation gain in the regulation of neuronal firing pattern is illustrated in Fig. 12.2. As expected, restorative neurons ($w_0 > 0$, hatched area of Fig. 12.2) solely exhibit pacemaking for any value of k_z. In the regenerative region, a sufficient decrease in w_0 always leads to bursting whatever the value of k_z, suggesting that a regulation of the balance between restorative and regenerative ion channels is a robust regulator of neuron spiking behavior.

In addition, there exists many couple of parameters (w_0, k_z) for which the model can exhibit similar bursting patterns, with identical numbers of spikes in burst, for

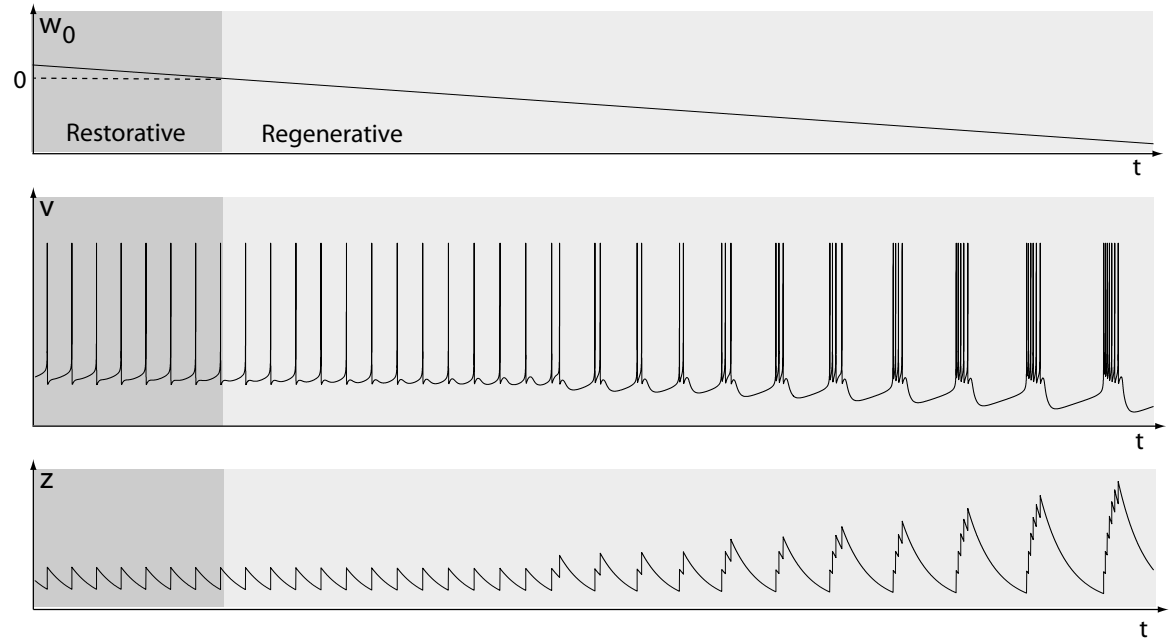

Figure 12.1 – Route into bursting in the transcritical hybrid model. The figure shows the evolution of the membrane potential v (middle) and the adaptation variable z (bottom) over time as the balance weight w_0 is decreased (top).

instance. However, the quality of bursting can strongly vary according to the considered couple (w_0, k_z), as illustrated by the inserts **A**, **B** and **C** of Fig. 12.2. These three inserts sketch membrane potential variations of the model for three different couple (w_0, k_z) at which the model exhibits bursts of four spikes. For low adaptation gain, bursting activity is reached at a low balance weight (Fig. 12.2, insert **A**), leading to non-plateau bursts of relatively low intra-burst frequency as compared to the inter-burst frequency. This bursting behavior, similar to the one exhibited by Aplysia's R15 neurons [140, 149], is usually referred as "parabolic bursting" [90, 149]. As the value of the adaptation gain increases, bursting activity is reached at a higher balance weight (Fig. 12.2, insert **B, C**), and the quality of bursting drastically changes, switching from a "parabolic" shape to a "square-wave" shape. Namely, bursts are generated on a depolarized plateau and are separated by hyperpolarized quiescent periods. In addition, the relative difference between the intra-burst and the inter-burst firing frequencies is much higher than in the previous case.

These results show that a common mechanism can generate different bursting types, the type being determined by two parameters: the balance weight and the adaptation gain. This is in sharp contrast with the classical view of neuronal bursting, where each bursting type is associated to a different generation mechanism [46, 90, 101]. This common mechanism of bursting can be found in many conductance-based models, where it is at the origin of a robust and physiological firing pattern regulation (see Chapter 11). The two parameters of bursting can be physiologically regulated via many different mechanisms in different neurons, giving rise to a great variety of bursting cells, although the underlying mechanisms are similar, as shown below.

A Minimal Set of Conductances modulate the three Parameters of Bursting

The abstract model described above is easily transposed to the physiology. As shown in the previous chapters, the balance weight w_0 is defined by the average feedback provided by all channels having a restorative or regenerative nature (see Tab. 1 of Chapter 10 for further details). In particular, this parameter is solely defined by the balance between restorative and regenerative ion channels, regardless of involved channel types. The adaptation gain k_z is set by the maximal conductances of all adaptation currents, namely that activate on an ultra-slow timescale. In addition to these channels, all other ion channels solely affect excitability quantity (action potential threshold, constant hyperpolarization/depolarization, etc.), which can be seen as changes in the parameter I_{app}.

As a consequence, very few ion channel types are necessary for the generation of the highly diverse firing patterns observed in physiology:

- One fast activating depolarizing channel, generally a transient sodium channel, for the generation of the

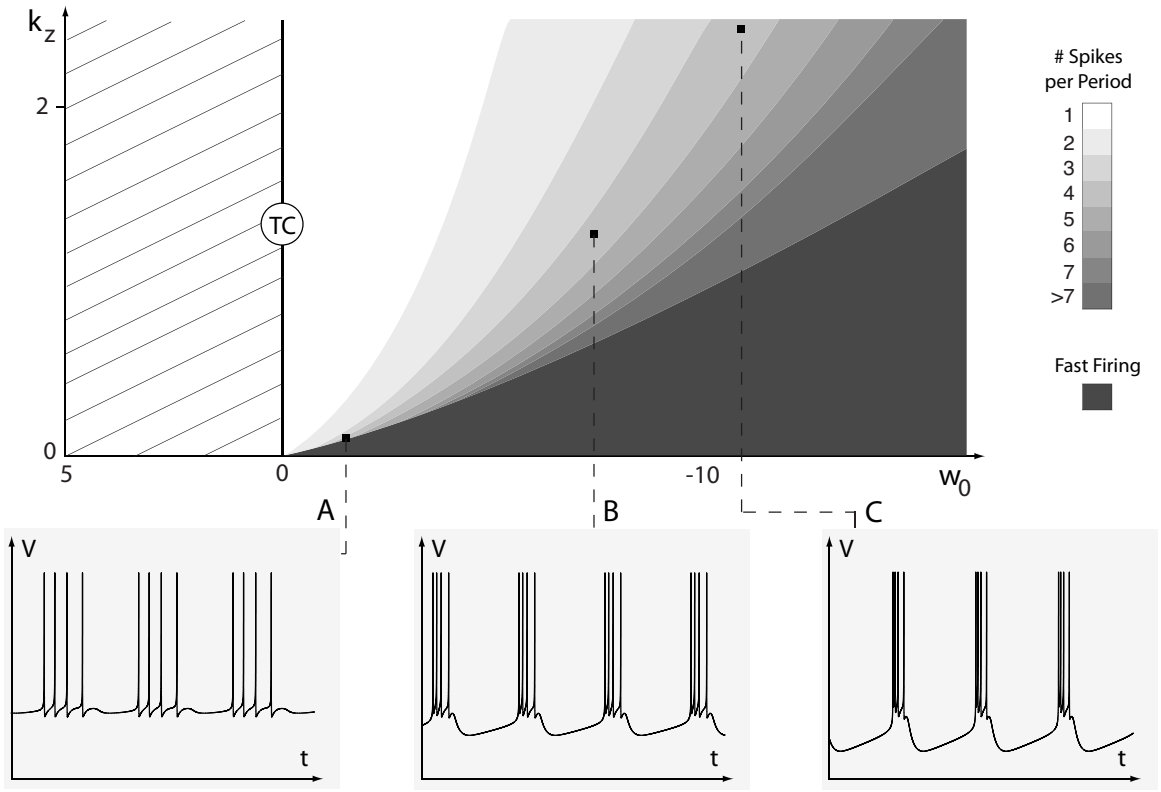

Figure 12.2 – The transcritical hybrid model is able to exhibit different bursting types. The central panel shows the behavior of the model for different balance weights and adaptation gains (the hatched area corresponds to the restorative parameter space). The inserts **A**, **B** and **C** show the time-course of the model for three different couples of w_0 and k_z. Although many different sets of parameters generate qualitatively similar firing patterns, their shape can strongly differ from one to the other.

regenerative upstroke of action potentials.

- One slow restorative ion channel, generally a delayed-rectifier potassium channel, for the action potential downstroke.
- One slow regenerative ion channel, generally a calcium channel, for the regulation of the balance.
- One ultraslow hyperpolarizing ion channel, such as calcium-activated potassium channels, for the adaptation of excitability during spiking.

These four simple ingredients are repetitively encountered in bursting neurons, such as molluscan bursting neurons (Aplysia's R15 neuron [140, 149], crab stomatogastric ganglion neuron [61], etc.), neurons involved in central pattern generators (CPGs), as well as many mammalian neurons (reticular and relay cells of the thalamus [36, 37], subthalamic nucleus neurons [72], dopaminergic neurons (see Part II), granule cells of the olfactory bulb [118], etc.). All these bursting neurons and models include at least one transient sodium channel, one delayed-rectifier potassium channel, one calcium channel and one calcium-activated (or slowly-activating) potassium channel.

In 1999, Wilson proposed a reduced model for mammalian neocortical neurons [198, 199]. He showed that, even if over 12 different ion channel types have been identified in these cells, their diverse firing activities could be reproduced in a simple conductance-based model composed of one fast variable V, one arbitrary (restorative) potassium current I_R, one arbitrary (regenerative) calcium current I_X and one arbitrary slow (adaptation) calcium-activated potassium current I_H [198, 199]. Those four states correspond directly to the four ingredients of our bursting model. Wilson model is indeed capable of generating the various firing patterns depending on the values of ion channel maximal conductances $\bar{g}_R$, $\bar{g}_X$ and $\bar{g}_H$ [145, 198, 199].

Following the procedure of the previous section, we analyze how Wilson model behaves for different balance weights and adaptation gains (Fig. 12.3). The former is varied through variations of the regenerative current maximal conductance $\bar{g}_X$ with $\bar{g}_R$ fixed. The latter is varied through variations of the adaptation current max-

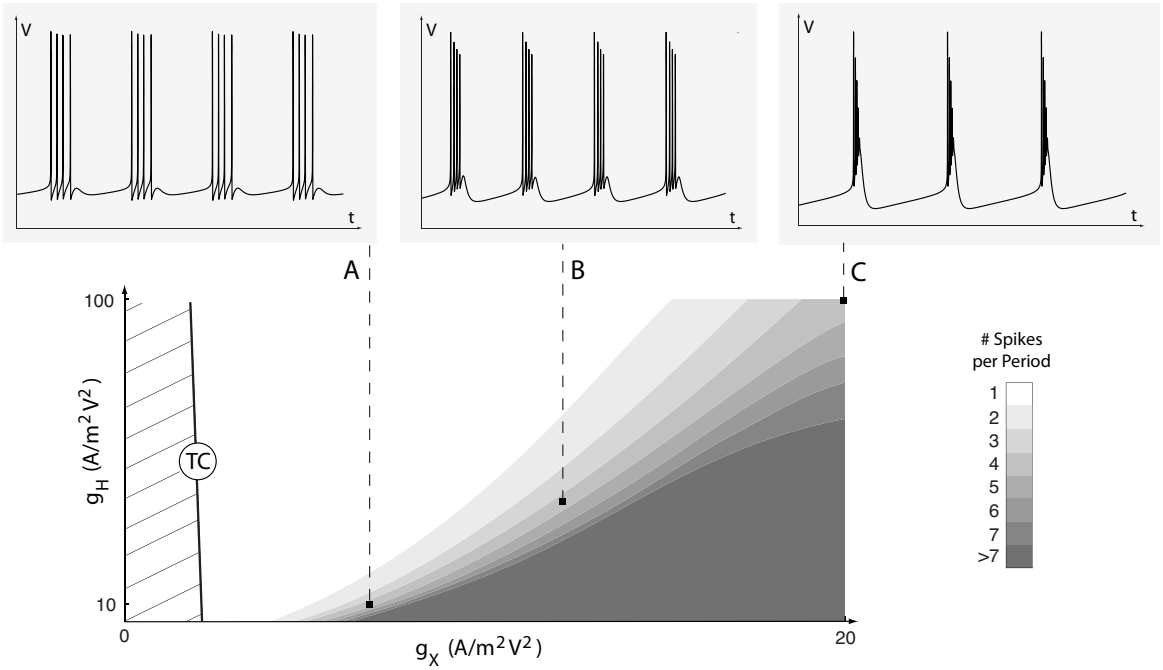

Figure 12.3 – Wilson model is able to exhibit different bursting types. The central panel shows the behavior of the model for different values of the regenerative current I_X and the adaptation current I_H maximal conductances ($\bar{g}_X$ and $\bar{g}_H$, respectively). The hatched area corresponds to the restorative parameter space. The inserts **A**, **B** and **C** show the time-course of the model for three different couples of $\bar{g}_X$ and $\bar{g}_H$. As it is the case for the transcritical hybrid model, many different sets of parameters generate qualitatively similar firing patterns, but their shape can strongly differ from one to the other.

imal conductance $\bar{g}_H$.

The similarity between hybrid model and conductance-based model behaviors is striking (compare Fig. 12.2 and Fig. 12.3). Indeed, a sufficient increase in $\bar{g}_X$ always leads to burst firing for any value of $\bar{g}_H$, and burst firing is solely reachable in the regenerative region. In addition, there also exists many couple of conductances $(\bar{g}_X, \bar{g}_H)$ at which the neuron exhibits comparable bursting activities in terms of number of spikes in bursts. For low values of $\bar{g}_H$, bursting can be reached at low values of $\bar{g}_X$. As in the hybrid model, bursting shape resembles parabolic bursting, that is non-plateau spiking and low intra-burst firing rate as compared to the inter-burst firing rate (Fig. 12.3, insert **A**). This is a typical bursting pattern defined by a low balance weight and a low adaptation gain. As $\bar{g}_H$ increases, bursting occurs for higher values of $\bar{g}_X$ and evolves towards a square-wave shape (Fig. 12.3, insert **B**), typical for intermediate balance weight and adaptation gain. The model even eventually converges towards a triangular shape as $(\bar{g}_X, \bar{g}_H)$ is further increased (Fig. 12.3, insert **C**). This phenomenon arises from the fact that a small part of I_X activates slowly during the spiking period, increasing the degree of membrane depolarization.

These results show that a small set of four channel types is sufficient to generate many of the different spiking behaviors observed in neurons, that is one fast, one restorative, one regenerative and one adaptation ion channel, regardless of their molecular properties. Based on this small set, neurons are able to switch between these different spiking behaviors through variations in channel properties such as maximal conductances, which directly and solely affect the balance weight and/or the adaptation gain of the neuron, together with excitability quantity. This phenomenon is at the basis of a great richness in neuron excitability, where even molecularly similar neurons can exhibit various firing activities.

A physiological route to bursting

The simple route to bursting is highly suggestive from a physiological viewpoint. The key parameters of neuronal bursting can indeed be physiologically regulated in many different ways, leading to a diversity of possible regulations mechanisms of neuronal excitability and firing pattern.

Fig. 12.4 shows some qualitative illustrations of such regulation mechanisms of physiological relevance. For each neuron, an experimental trace of a switch from tonic spiking to bursting is shown (top), and the switch is re-

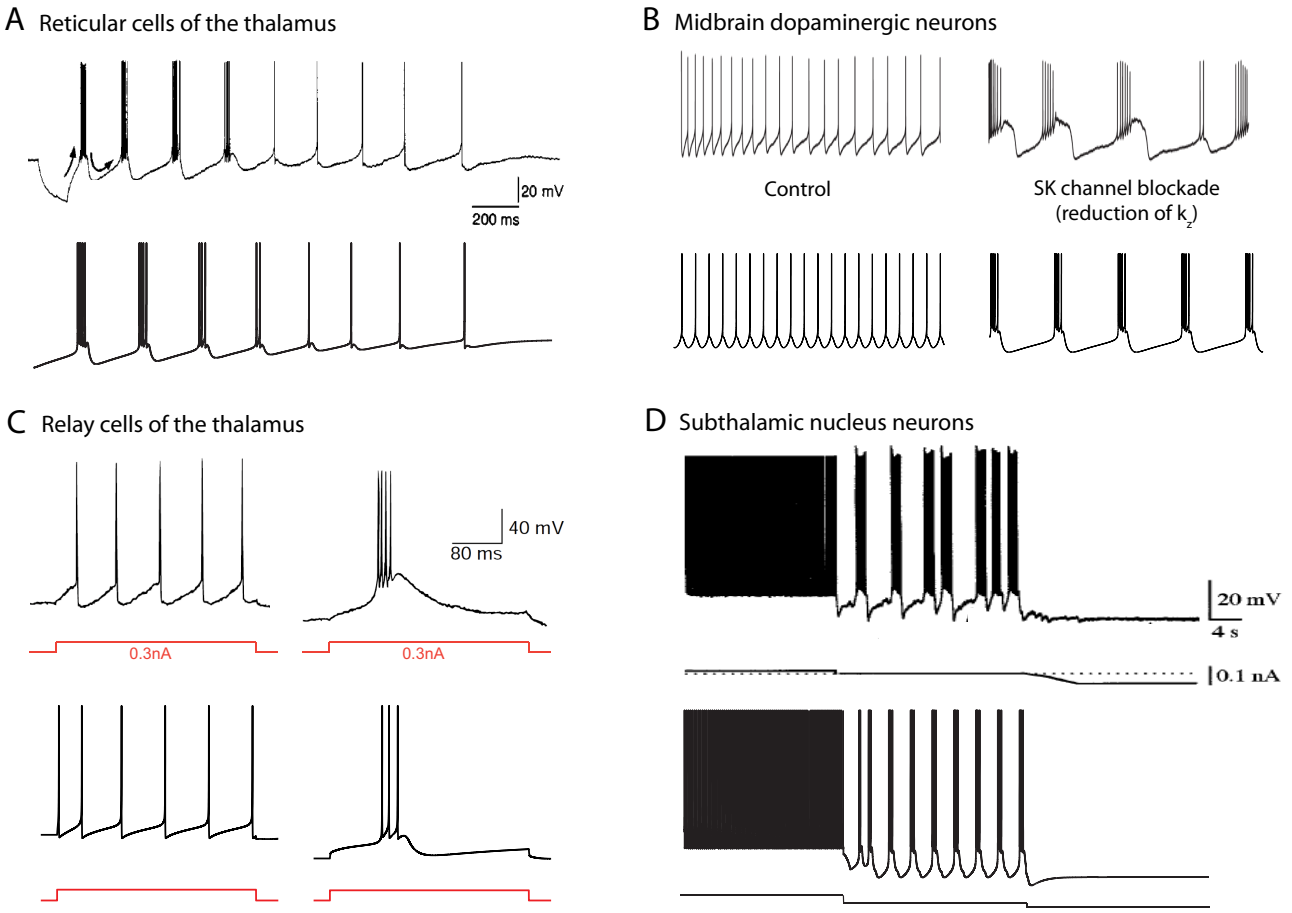

Figure 12.4 – Routes to bursting in different neuron types. The top traces show experimental data of thalamic reticular cells [125] (**A**), dopaminergic neurons of the thalamus [96] (**B**), relay cells of the thalamus [171] (**C**) and subthalamic nucleus neurons [9] (**D**). The bottom traces show qualitative reproductions of the experimental data using the transcritical hybrid model. The transcritical hybrid model is able to qualitatively reproduce the switch of firing pattern observed in different neuron types, via the physiologically relevant regulation of the balance weight and/or the adaptation gain.

produced in our hybrid model (bottom), through a simple variation of w_0 if the regulated channel is restorative or regenerative, or k_z if the regulated channel generates an ultraslow adaptation current. This figure shows how the simple route to bursting described above is able to qualitatively reproduce physiological switches of firing patterns observed in different neuronal populations.

The two parameters w_0 and k_z provide two distinct routes to bursting: the route to bursting via an increase of the balance weight, and the route to bursting via a decrease of the adaptation gain.

The route to bursting via an increase of the balance weight is observed in many neurons, and can potentially occur for any value of the adaptation gain, as shown above. This robust way of inducing bursting activity relies on the possible regulation of one restorative or one regenerative ion channel maximal conductance, the latter being more common. As shown in the previous chapters, the increase of the balance weight generates an increase of the robust bistable range, strengthening neuron endogenous activity and burstiness.

One example of this route to bursting is the manifestation of hyperpolarization-induced bursting in reticular and relay cells of the thalamus [36, 37, 125] and subthalamic nucleus neurons [9, 72], among others (Fig. 12.4A,C,D). This bursting activity has been related to the prominent presence of low-threshold inactivating T-type calcium channels in these cells. These regenerative channels inactivate on an ultraslow timescale, modulating the balance between restorative and regenerative ion channels, and in turn neuron excitability type (see Chapter 11). As a consequence, any modification of their inactivation state, which depends on neuron resting potential, affects the balance weight, the lower the inactivation, the higher the balance weight. Their action can therefore be modeled through a dependence of w_0 with the resting

potential, as for the modeling results of Fig. 12.4A,C and D.

The route to bursting via a decrease in the adaptation gain is also observed in many neurons, but can only occur if the neuron exhibits regenerative excitability. It relies on the possible regulation of one ultraslow ion channel generating an adaptation current. A reduction of the adaptation gain reduces amplitude variations of the adaptation current during spiking, leading to the generation of more spikes in a same bistable range.

One prominent example of this route to bursting is the SK channel blockade-induced bursting observed in many neurons, such as dopaminergic neurons [95, 191] and serotonergic neurons [151], among others. SK channels being solely activated by variations in intracellular calcium concentrations, which are several orders of magnitude slower than variations of membrane potential, they generate an adaptation current that mostly affects neuron adaptation gain. Their blockade reduces this adaptation gain, allowing neurons to exhibit bursting if their balance weight is large enough (Fig. 12.4B). A potential systemic role of this firing pattern regulation mechanism and implication of its dysregulation in discussed in Chapter 13.

Discussion

Switching from restorative to regenerative excitability: a simple yet robust physiological route to neuronal bursting

Robust bistability is a critical component of bursting. Such robust bistability is shown to arise from regenerative excitability. A consequence is that regulating neuron balance weight from restorative to regenerative dominance generates a switch from single-spike firing to bursting, regardless of the type of the neuron. This sole route to bursting, which relies on a switch from restorative to regenerative excitability, is sufficient to account for the switches of firing patterns physiologically observed in many neuron types.

This provides a very simple and robust dynamical mechanism of firing pattern regulation. Indeed, only two global parameters regulate neuron spiking activity, all ion channels cooperating to regulate the values of these parameters. It provides a great robustness to neuronal spiking, where the dysregulation of one channel, which affects the three parameters of bursting, can be easily overcome by another channel subtype, via the restoration of the three parameter values. Such an adaptation mechanism is often observed in neuroscience, and is generally referred as "intrinsic homeostasis".

One mechanism, many bursting qualities

It is often considered that each bursting type relies on a particular dynamical mechanism, differing in the bifurcations that occur at spiking initiation and termination [90]. The simple bursting mechanism proposed in this chapter exhibits many different bursting qualities, depending on the values of the balance weight and the adaptation gain. Namely, a slightly negative balance weight and a low adaptation gain results in a parabolic-like bursting shape, whereas a high adaptation gain leads to square-wave bursting for a sufficiently negative balance weight. These results suggest that one simple mechanism of bursting could be sufficient to account for the bursting activities physiologically observed in many neurons.

Bursting richness arises from the diversity of very few ingredients

Four ion channel types are shown to be sufficient to generate many bursting qualities, through the regulation of the three parameters of bursting, leading to a very simple and robust mechanism of firing pattern regulation. These four ingredients are repetitively encountered in bursting neurons.

On the other hand, a tremendous amount of different ion channel subtypes, differing in their quantitative kinetics, pharmacology, regulation mechanisms, etc., are potential regulators of the three proposed parameters of bursting. It allows a great richness in firing pattern regulation, leading to an enormous diversity in bursting cell types.

Discussion

Summary of Results

Part III of the dissertation attempts to integrate the role of regenerative ion channels in the dynamical picture of neuronal excitability. These channels, whose main representative are voltage-gated calcium channels, are depolarizing similarly to sodium channels, but activate on a slow timescale similarly to potassium channels.

We started by highlighting the role of voltage-gated calcium channels in DA neuron excitability and bursting (Chapter 8). We showed that an increase in L-type calcium channel maximal density increases neuronal excitability and burstiness both *in vitro* and *in vivo*, through the simulation of the minimal conductance-based model developed in chapter 4 and experimental recordings on rat brain slices. In addition, bifurcation analyses on the minimal model in low and high calcium configurations extracted two different dynamical mechanisms of action potential initiation, leading to the concepts of sodium and calcium pacemaking.

Integrating these channels into the Hodgkin-Huxley model before its reduction leads to a novel phase portrait that have been disregarded to date (Chapter 9). Namely, a specific part of the phase portrait lying out of the physiological region becomes physiological when the role of regenerative ion channels becomes sufficiently prominent. This specific part involves a transcritical bifurcation in the fast subsystem that is shown to organize neuronal excitability. It leads to the construction of a transcritical hybrid model in which a single parameter controls the neuron calcium conductance. As a basic illustration, the new model is shown to highlight a core dynamical mechanism by which calcium channels control the two distinct firing modes of thalamocortical neurons.

The results developed in Chapter 9 lead to the construction of a generalized FitzHugh-Nagumo model (Chapter 10). The model differs from the classical FitzHugh-Nagumo model in that it accounts for the effect of cooperative gating variables such as activation of calcium currents. Analyses on the model uncover two novel types of excitability whose peculiar electrophysiological signatures, that is first spike latency, after-depolarization potentials and plateau oscillations, apply to many neuron types.

The planar dynamical analyses are further extended to conductance-based models of arbitrary dimensions (Chapter 11). It shows the existence of a transcritical bifurcation in conductance-based models, which occurs at the balance between restorative and regenerative ion channels. Any modification of this balance affects model excitability types, generating switches from restorative to regenerative excitability. Such modification can be made through the regulation of regenerative ion channel properties, such as channel maximal conductance, for instance. These dynamical results are illustrated on seven published conductance-based models of neurons.

Finally, physiologically relevant switches from restorative to regenerative excitability are shown to provide a physiological route to bursting (Chapter 12). A transcritical hybrid model of bursting neurons is constructed by adding an ultraslow adaptation variable to the model of Chapter 9. This model is able to switch from single-spike firing to bursting via a sufficient decrease of the balance weight w_0. This model is also able to reproduce many bursting qualities, according to the values of two parameters, that is the balance weight and the adaptation gain. These two parameters are modulated in conductance-based models by four different ion channel types, these ion channels being the key ingredients of many bursting cells.

Limitations and Open Questions

The dynamical analyses proposed in Part III face some limitations and open questions that arise from the reduction approximation.

One source of approximation is the separation of model variables in three groups according to their timescale, in order to apply the algorithm described in Chapter 11. Indeed, such segregation might not be so clear in the differ-

ent models. For instance, the calcium current of Aplysia's R15 neuron model [140, 149] is significantly slower than the calcium currents used in the other models. Some of these currents might therefore play a significant role across several timescales, which is not taken into account in our analyses. Such approximations should not alter the underling qualitative mechanisms, but may affect some quantitative properties, such as the parabolic shape of intraburst firing frequencies observed in the R15 neuron model.

Many of the results discussed in this part call for further experimental validations. Some experimental protocols might be designed to highlight the role of the balance between restorative and regenerative ion channels in neuron excitability type and electrophysiological signatures. Similarly, the dynamical analyses provide predictions that might be tested experimentally on different neuron types, both *in vitro* and *in vivo*.

Part IV

Abnormal Timing of SK Channel Activation and Parkinson's Disease

Introduction

Mitochondrial dysfunction and metabolic issues are known to be strongly involved in the pathogenesis of Parkinson's disease (PD) [1, 11, 71, 120, 129, 138, 155, 156, 157, 177]. Indeed, since the first post-mortem description of complex I deficiency in the substantia nigra [120, 155, 156], platelets [120, 129, 138] and skeletal muscle [11, 120] of PD patients, many mitochondrial proteins or proteins associated with mitochondria have been associated with familial forms of PD, such as Parkin, PINK1 (PTEN-induced putative kinase 1), DJ-1 and HtrA2/Omi, inter alia [1]. Moreover, toxins used to create animal models of PD, and which are thought to increase the incidence of the disease in humans, are known to target mitochondria [8, 10, 20, 34, 94, 121].

One intriguing hallmark of PD is that, despite the fact that mitochondrial dysfunction and expression of PD associated genes is a general feature [177], the resulting neurodegeneration is highly specific: it is strongly localized and limited to particular areas, which are dispersed throughout the entire organism. The motor symptoms of PD primarily include the abnormal neuronal activity in the basal ganglia, through the degeneration of substantia nigra pars compacta (SNc) dopaminergic (DA) neurons and, to a lower extent, other basal ganglia/brainstem neurons [47, 135]. Other regions of the central nervous system are critically involved in the disease, such as the dorsal raphe (serotonergic (5-HT) neurons) [85, 141], the internal plexiform and mitral cell layers of the olfactory bulb (OB) [43], the anterior olfactory nucleus (AON) [43] and the dorsal motor nucleus of the vagal nerve [15]; neurodegeneration is even observed in the enteric nervous system, namely in the Meissner and Auerbach plexuses of the intestine [16]. In the remaining of this chapter, we will refer to these neurons as "PD affected neurons".

To date, the mechanisms by which metabolic and/or mitochondrial dysfunction trigger such a selective loss remain unclear [8, 20, 94], even if many modeling and experimental results have highlighted the enhanced vulnerability of SNc DA neurons [10, 34, 71, 121]. These results mainly suggest the involvement of cytoplasmic calcium accumulation in degeneration. Indeed, calcium accumulation induces mitochondrial stress, one role of the latter being to regulate the cytoplasmic concentration $[Ca^{2+}]_{in}$, through the pumping or release of calcium. In addition, an increasing body of experimental data highlights the involvement of endoplasmic reticulum (ER) stress in PD [47, 135, 136], the other intracellular source of calcium, which supports the previous idea.

In Parts II and III, we have highlighted the critical role of calcium channels in regenerative excitability, which underlines burst firing, for instance. We have also shown that $[Ca^{2+}]_{in}$ is a major regulator of cell excitability in DA neurons (Chapters 5 and 6), via the activation of small conductance calcium-activated (SK) potassium channels, among others. Despite their heterogeneous topography, neurochemistry and functions, other PD affected neurons share SNc DA neuron electrophysiological characteristics. Indeed, these neurons are all pacemakers and many of them have been shown to express SK channels (generally belonging to the SK3 subfamily). As it is the case for DA neurons (Part II), the blockade of these channels increases the excitability of the neurons *in vitro* and enhances bursting *in vivo*.

Finally, one recent and potentially critical finding is that the gating of SK channels is partially regulated by mitochondrial and endoplasmic reticulum calcium effluxes in SNc DA neurons. In addition, a deletion of two PD-associated genes coding for mitochondrial proteins, namely PINK1 or HtrA2/Omi, leads to a functional reduction in the activity of these potassium channels in SNc DA neurons, making them hyperexcitable, but not in VTA DA neurons or GABAergic interneurons, those neurons being spared in the disease [12].

These observations lead to our hypothesis that neurons in which SK channels regulate firing activity preferentially degenerate in Parkinson's Disease. This is well illustrated in the olfactory bulb, where neurodegeneration preferentially occurs in mitral cells, whose firing is regulated by SK channels, whereas granule cells, in which there is little SK channel activity, are barely affected [12]. This

observation is also valid for dopaminergic neurons of the SNc and the VTA, since SK channels express to a higher extent in SNc DA cells, the ones that degenerate in PD [154].

In this part, we discuss this hypothesis at the light of the results developed in Part II and Part III. We first propose a review of PD affected neurons that share this common electrophysiological signature, as well as an abstraction of the mechanisms underlying this spiking behavior. In particular, we show how SK channels affect in a similar way the excitability of neurons having very different morphological parameters and mean firing frequencies. On the basis of this abstraction, we discuss one potential impact of the intracellular calcium source dysfunction observed in PD on neuron electrophysiology and degeneration.

Although this part is purely hypothetical, it provides an illustration of the fact that only few parameters determine neuronal excitability and firing patterns, allowing one particular pathology to affect specifically but drastically different neurons. In Chapter 12, we underlined the role of the adaptation gain as a key regulator of neuronal excitability. In this part, we illustrate how a single dysfunction can affect the adaption gain of an heterogeneous population of neurons, affecting their firing in a similar way and leading to widespread pathological consequences.

Chapter 13

Parkinson's Disease Selective Neurodegeneration: Involvement of SK channel Dysregulation?

Neurons Affected in Parkinson's Disease Share Electrophysiological Characteristics

PD affected neurons are located in very different areas, and sustain highly different functions, such as the control of movement (SNc DA neurons and STN neurons), olfaction (mitral cells of the OB and the AON) or intestine motility (interstitial cells of Cajal (ICC) of the Meissner and Auerbach plexuses of the intestine). These excitable cells are also heterogeneous from an electrophysiological point of view. Indeed, whereas the spontaneous firing rate of DA cells is in the range of 0.5Hz to 5Hz [62], subthalamic nucleus neurons are able to fire at very high rate, up to 200Hz [72]. However, despite these differences, these neurons share several electrophysiological characteristics.

First of all, these PD affected neurons are pacemaker cells, i.e. they exhibit spontaneous firing *in vitro*, and intracellular calcium variations are a key element of their pacemaker activity [44, 70, 72, 190]. In other words, these neurons have a proper endogenous rhythm, which relies on the $[Ca^{2+}]_{in}$ variations. Moreover, they are able to exhibit two specific firing patterns *in vivo*, namely single-spike firing and burst firing [2, 48, 62, 63, 115, 116, 151, 191]. One important feature, as stated in Chapter 12, is that the intra-burst firing frequency is much higher than single-spike firing rate, although the absolute values of interspike intervals are quite different among these cells.

The firing pattern of these neurons is similarly regulated by a specific category of ion channels, the so-called small conductance calcium-activated (SK) potassium channels. The gating of SK channels is solely regulated by the intracellular calcium concentration at their vicinity. Indeed, these channels are tightly associated with the protein calmodulin, which accounts for their calcium sensitivity [122, 159]. On the other hand, their gating is insensitive to variations of the membrane potential, which makes these channels quite unique. As a consequence, their activity is an image of the $[Ca^{2+}]_{in}$ variations in their Nano-domain, and therefore linked to the endogenous rhythm of the cell. In addition, the EC50 for the activation by Ca^{2+} is rather low (about 300 nM [103]) meaning that, physiologically, these channels will operate during a large portion of the pacemaker cycle, contrary e.g. to BK channels, which are much less sensitive to calcium and therefore close at the end of the fast AHP (a few ms after the end of each action potential).

For many PD affected neurons, an inhibition of the SK current affects both the excitability and the firing pattern (Tab. 13.1). *In vitro*, SK channel blockade usually induces irregularities in the firing or even bursting and potentiates the response of the cell to excitatory stimuli. *In vivo*, the blockade also strongly affects the firing pattern. In particular, it causes several of those neurons to switch from low-frequency single spike firing to bursting, with a relatively high intra-burst firing frequency.

In addition, despite of the lack of electrophysiological studies on the role of SK channels on ICC of the myenteric plexus, immunohistochemical experiments have found that these cells are SK3 immunoreactive [56]. Knowing that the pacemaker activity of these cells strongly relies on $[Ca^{2+}]_{in}$ variations, which activate SK channels, it is reasonable to suggest that these channels have an important role in the regulation of ICC firing.

On the other hand, many neuronal types that are not affected in Parkinson's disease do not share these electrophysiological characteristics. This is for instance the case for granular cells (GC) of the olfactory bulb, the excitability of which is not controlled by SK channels [118]. Indeed, no Lewy bodies or neurodegeneration have been detected in the granular layer of the olfactory bulb in patients affected by PD [43].

To summarize, most of PD affected neurons are pacemaker neurons whose endogenous rhythm strongly relies on variations of intracellular calcium concentration. *In*

PD affected neuron	**Effect of SK channel blockade**
SNc Dopaminergic Neurons [59]	Increased irregularities *in vitro* [200] Increased bursting *in vivo* [95, 96, 191]
Serotonergic Neurons [85, 141]	Increased irregularities *in vitro* [151] Increased bursting *in vivo* [151]
Subthalamic Nucleus Neurons [174]	Increased irregularities *in vitro* [72] Increased bursting subjected to hyperpolarization [72]
Mitral Cells of the Olfactory Bulb [43]	Increased excitability [118]
Motoneurons of the Vagus [15]	Reduction of the after hyperpolarization period [152]
Locus coeruleus noradrenergic neurons [15]	Increased excitability [161]
Nucleus basalis of Meynert neurons [14]	Blockade of spontaneous miniature outward currents [5]
ICC of the gastrointestinal tract [16]	SK3 expression (no electrophysiological study) [56]

Table 13.1 – Effect of SK channel blockade on several PD affected neurons.

vivo, these neurons are able to exhibit two different firing patterns, namely low-frequency single-spike firing and burst firing. In addition, SK channels are key regulators of the excitability and firing pattern of those neurons. It is now important to understand the mechanisms by which these common electrophysiological characteristics might render these particular cells more sensitive to hyperactivity or neurodegeneration in PD.

SK Channels Dysregulation affects Calcium Homeostasis

The hybrid model developed in Chapter 12 provides a convenient abstraction of the shared electrophysiological characteristics of PD affected neurons. For many of these neurons, it has been shown that slow spiking follows calcium oscillations [44, 70, 72, 190], suggesting the intracellular calcium concentration $[Ca^{2+}]_{in}$ as an ultra-slow variable (resp. z in our hybrid model), whose adaptation gain k_z can be modulated through variations of SK channel density. The abstract model is therefore composed of the three timescales v, w and z. The only parameters that differentiate the control condition and the SK channel dysregulation state is the adaptation gain k_z, which is lowered in the latter case, as shown in Chapter 12.

The model suggests that a tenfold reduction of the adaptation gain has two possible consequences (Fig. 13.1): for endogenous bursters (i.e. neurons with a large balance weight), the SK dysregulation may switch the pacemaking activity to an endogenous bursting pattern (Fig. 13.1A). In contrast, for exogenous bursters (i.e. neurons with a relatively low balance weight), the SK dysregulation does not disrupt the pacemaking activity (Supplementary Fig. S13.1) but makes it much more sensitive to external excitatory inputs (Fig. 13.1B).

In both cases, a diminution of neuron adaptation gain increases the number of high frequency firing periods. High frequency firing induces high cytoplasmic calcium accumulation, the passive entry of calcium being much more rapid than its active removal during these periods. Therefore, mitochondrial and endoplasmic reticulum stress would be maximal when the neurons are in this pathological state, which might accelerate neurodegeneration, as discussed below.

SK channels equally affects vastly different neurons

PD affected neurons strongly differ in their endogenous firing rate, ranging from 0.5Hz to 5Hz for SNc DA neurons to more than 200Hz for STN neurons, and it is not obvious how SK channels may affect in a similar way such

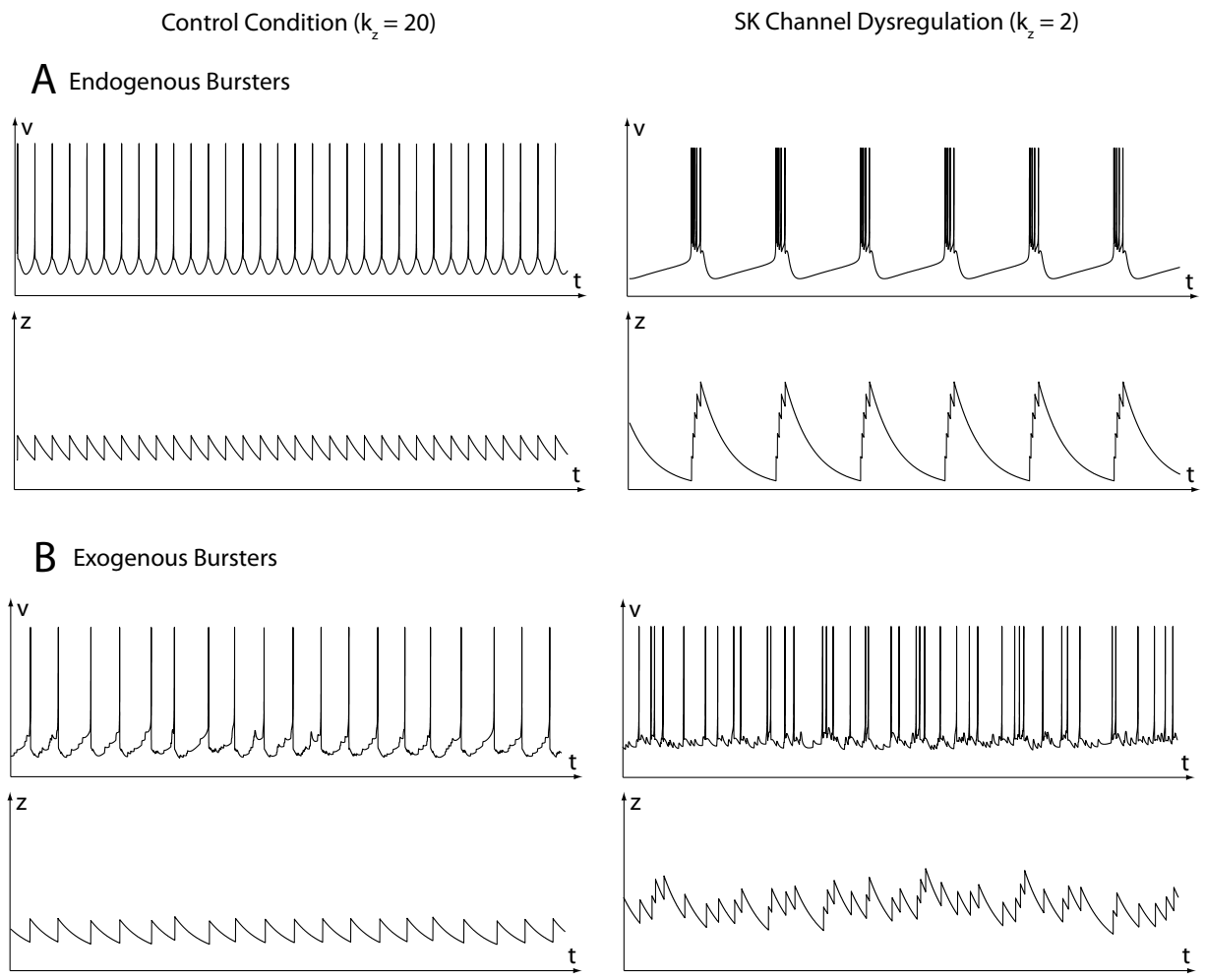

Figure 13.1 – Comparison of the firing patterns of two types of neurons in control condition (left) and during SK channel dysregulation (right). A. and **B.** Membrane potential (top) and calcium variations over time (bottom) in control condition (left) and during SK channel dysregulation (right). Note that a SK channel dysregulation affects calcium homeostasis in both cases, resulting in higher cytoplasmic calcium accumulation.

different neurons

The critical feature that makes SK channels so "adaptive" is that their gating is solely regulated by the intracellular calcium concentration in their nanodomain. Their gating is not affected by many parameters that vastly differ from one neuron to the other, such as the resting potential, the action potential amplitude and width, the presence of other ion channels, etc. In contrast, any of these differences would strongly affect a voltage-gated channel.

This specific feature of SK channels is illustrated in Fig. 13.2. This figure shows an *in vivo* simulation of the simple conductance-based model developed in Chapter 4 when SK channels are absent, present, or replaced by a voltage-gated potassium current (from top to bottom). As shown in Fig. 13.2A, the voltage-gated current is designed to play a similar role as SK channels in the simple model for one particular endogenous rhythm. In Fig. 13.2B, all time constants are modified similarly (except those of the SK current and the SK-like potassium current), in order to change the firing rate by a factor of 20 without affecting the behavior of the modeled neuron.

A comparison of Fig. 13.2A and Fig. 13.2B shows that SK channels play a similar role in both conditions, regardless of the timescale differences between the two neurons. In contrast, the role of the voltage-gated potassium current is completely altered by the timescale modification. Because of this, the kinetics of voltage-gated currents are specific to the neuron, whereas the properties of SK channels may remain constant.

Physiologically, the adaptability of SK channels to the endogenous rhythm is due to the fact that these channels are activated by intracellular calcium, and $[Ca^{2+}]_{in}$ varies several times slower than the kinetics of activation of SK channels. This activation can be considered as instantaneous compared to $[Ca^{2+}]_{in}$ variations, SK channel activation time constant being of few milliseconds. In addition, the gating might be controlled by the neuron itself, through the tight regulation of $[Ca^{2+}]_{in}$ in SK channel nanodomains ($[Ca^{2+}]_{in,SK}$) by intracellular calcium stores and sources, such as mitochondria and endoplasmic reticulum, as outlined below.

A Possible Interplay between Calcium Channels and Intracellular Calcium Sources in the Regulation of SK Channel Activation

Correlation between the intensity of neurodegeneration and the degree of expression of SK channels

As mentioned above, although mitochondrial dysfunction is global in PD, the degree of neurodegeneration is extremely variable within the brain. There is a wealth of studies that have tried to understand the mechanisms of this heterogeneity. Many potential mechanisms have been suggested, including a variable neuronal size, variable extent of axonal arborisation, etc. Recent in situ hybridization, electrophysiological and cell imaging data suggest another possibility based on the observations that SK channels are expressed to a much greater extent in sub-regions where neurodegeneration is very prominent [154].

In our opinion, a link can be made between these observations and the pathophysiology of PD. Indeed, we have shown that SK channels regulate cell entrainability, their inhibition inducing a hyperexcitability of the neuron. In particular, a SK channel blockade induces (synchronized) bursting *in vivo* in these cells. In addition, Bishop and colleagues analyzed the effect of the deletion of PD associated-genes encoding for mitochondrial proteins on the firing of SNc DA neurons, VTA DA neurons and GABAergic neurons of mouse brain slices [64]. They observed that the time to peak (TTP) of SK channel dependent after-hyperpolarization period (AHP) in PINK1- and HtrA2/Omi-Deficient Mouse SNc DA neurons was significantly reduced as compared to control conditions, whereas the maximum peak value was unaffected. As a consequence, SNc DA neurons displayed irregular firing patterns *in vitro* and were hyperexcitable in *ex vivo* brain slices and *in vivo* [64]. Moreover, they showed that an inhibition of ER Ca^{2+} release or mitochondrial Na^{+}/Ca^{2+} exchanger-mediated Ca^{2+} release reduces the amount of spike-generated SK currents in SNc DA neurons of mouse brain slices [64].

On the other hand, deletion of these genes did not affect either VTA DA neuron or GABAergic neuron electrophysiology [64]. The reason for VTA DA neuron unresponsiveness to these gene deletions is that SK channels do not play an important role in these cells, as mentioned above. By contrast, whereas SK channels play an important role in GABAergic neuron excitability [154], their activation does not rely on CICR [154]; an observation that may explain why they are spared in these conditions. Indeed, blockade of ER Ca^{2+} release does not affect SK channel activity in GABAergic neurons [154], whereas apamin, a SK channel blocker, strongly affects the firing of the latter [12, 154].

These observations highlight an important role for intracellular sources of calcium in the regulation of SK channels in SNc DA neurons, but not in GABAergic neurons. In addition, the idea that intermediates exist between the entry of calcium through calcium channels and the activation of SK channels is supported by various experimental observations. Namely, the SK channel-dependent AHP has strongly varying kinetics from one neuron to the other. For instance, the maximum time-to-peak of the AHP of SNc DA neurons, which express

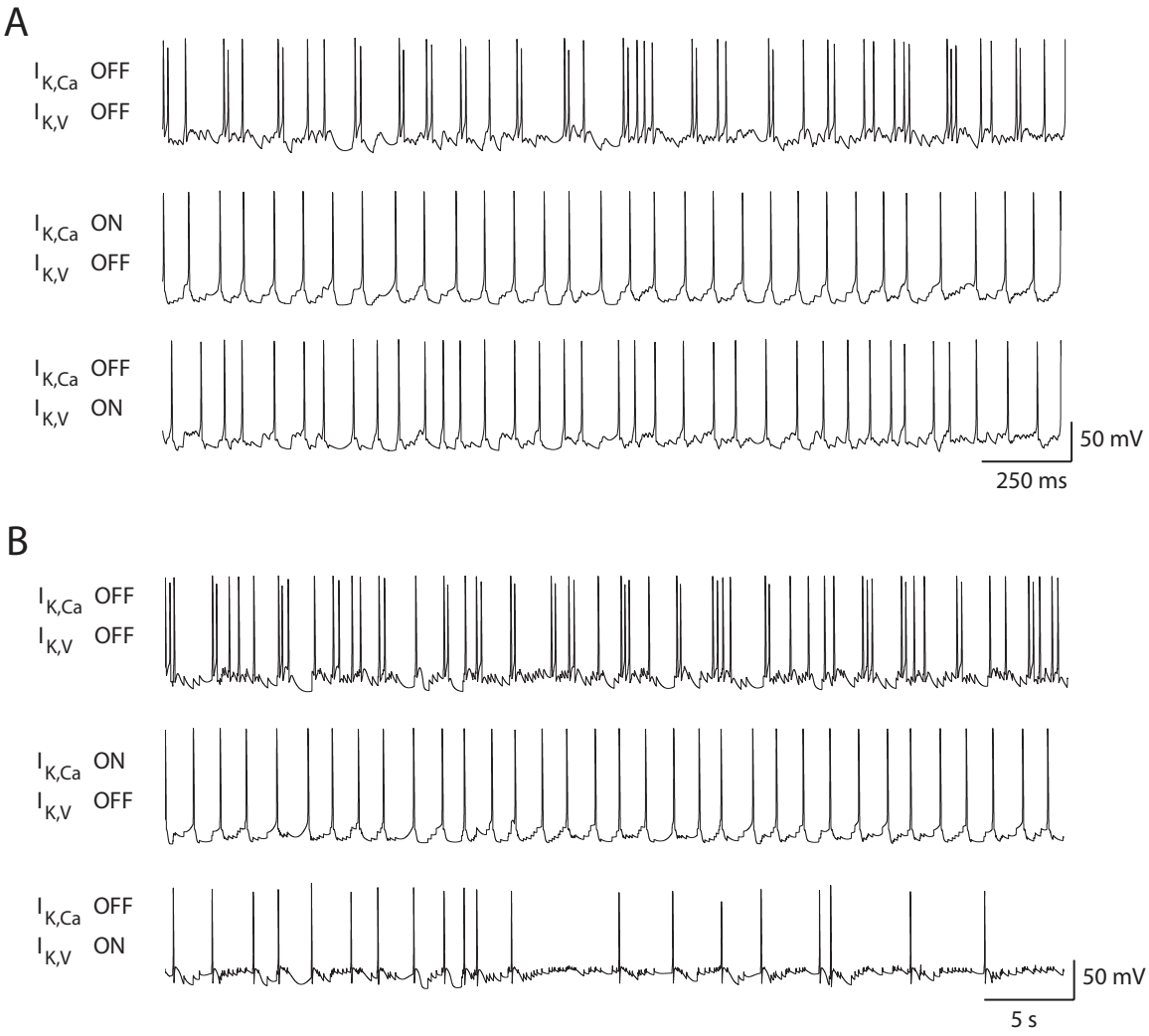

Figure 13.2 – Adaptation of SK channel activity to the endogenous rhythm of the cell. A. and **B.** From top to bottom: Membrane potential variations over time in the absence of $I_{K,Ca}$ and $I_{K,V}$, in the exclusive presence of $I_{K,Ca}$ and in the exclusive presence of $I_{K,V}$, respectively. Note that the time scale in (**B.**) is 20 times larger than in (**A.**). SK channels fully adapt to neuron endogenous rhythm, in contrast to voltage-gated channels.

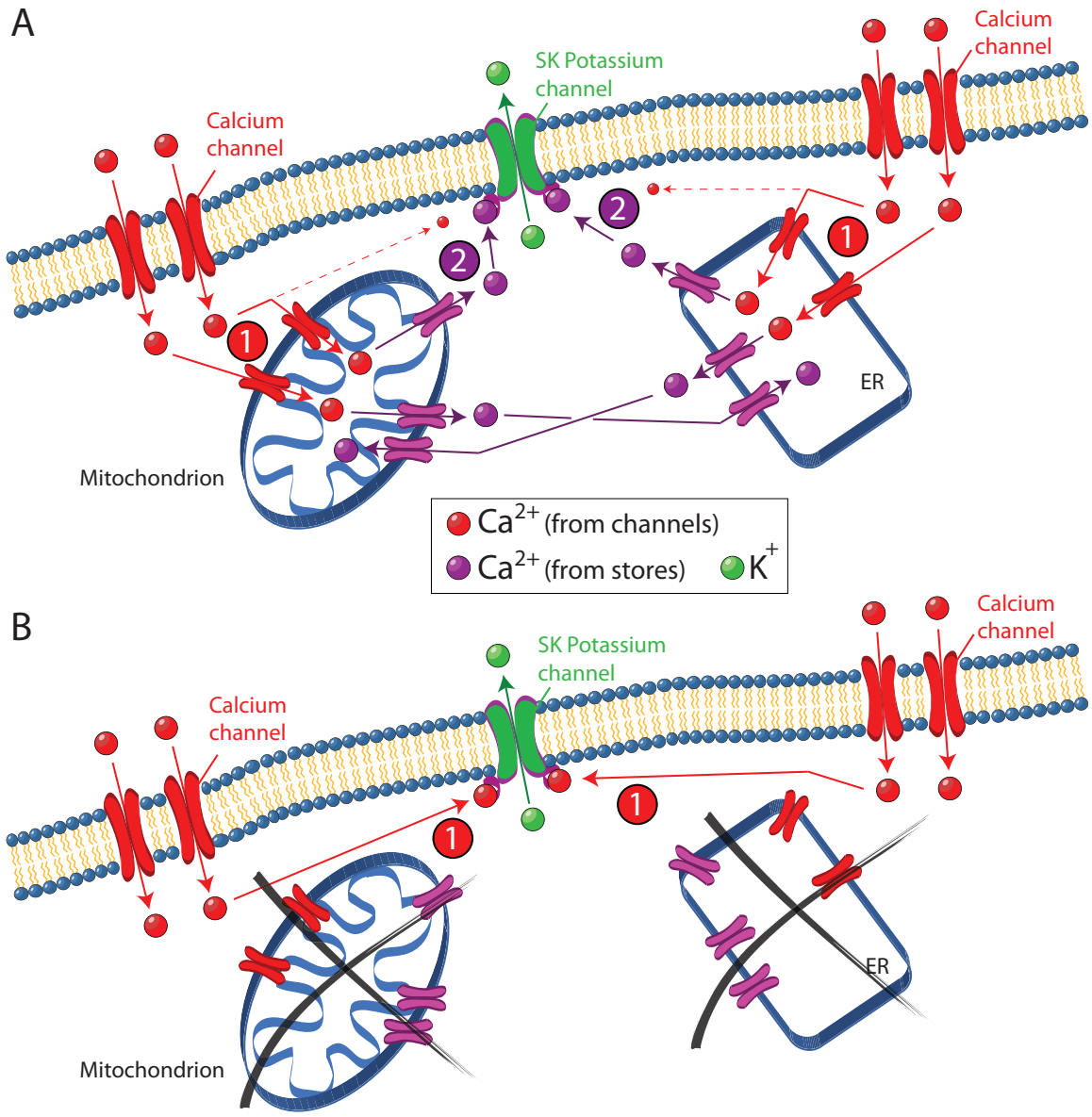

Figure 13.3 – Potential regulation mechanism of SK channel activity by mitochondria and ER. A. and **B.** The scheme illustrates a portion of neuron membrane and intracellular space, including a mitochondrion and the ER. A red dot represents a calcium ion entering into the cell through calcium channels (in red), a magenta dot a calcium ion released by intracellular sources, and a green dot a potassium ion passing through SK potassium channels (in green). Note that the scheme is very simplified, since, for example, ion channel pores are surrounded by accessory subunits and modulating proteins such as kinases and phosphatases.

the SK3 subunit [200], is significantly smaller to the one of substancia nigra pars reticulata (SNr) GABAergic neurons [154], which express the SK2 subunit [12]. However, the calcium-activation kinetics of these SK channel subunits are very similar [202]. Therefore, it is clear that the kinetics of $[Ca^{2+}]_{in,SK}$ are strongly different in these two neurons. This can probably not be explained specifically by a difference in calcium channel density.

A potential regulation mechanism of SK channel activity by mitochondria and ER

On the one hand, it is commonly accepted that activation of SK channels requires entries of calcium into the cell through voltage-gated calcium channels. Indeed, a substitution of calcium in the extracellular space, i.e. by cobalt or cadmium, has been shown to almost completely block the medium AHP in most of the SK expressing neurons [178], this AHP being generated by an activation of these SK channels [168].

On the other hand, the experimental and modeling results previously mentioned suggest an interaction between calcium channels and intracellular sources of calcium, such as mitochondria and ER, for the regulation of $[Ca^{2+}]_{in,SK}$. This hypothesis is illustrated in Fig. 13.3A. One could imagine that calcium entering through calcium channels is first taken up by mitochondria and ER. As a consequence, $[Ca^{2+}]_{in,SK}$ does not rise much at that time, and SK channels are not strongly activated yet. Subsequently, this accumulation of calcium into the stores induces a calcium-induced calcium release (CICR) in the SK nanodomain, which activates SK channels through the increase of $[Ca^{2+}]_{in,SK}$. In that configuration, SK channels would be activated after a delay, and their kinetic of activation would be controlled by mitochondria and ER. Strong arguments in favour of CICR exist in cardiac myocytes and in a number of other cell types, including neurons [29, 54, 112]. However, any dysregulation of CICR would affect neuron excitability.

Indeed, if the calcium entering through calcium channels is not collected by mitochondria and ER, this calcium immediately diffuses to the SK channel nanodomain (Fig. 13.3B). As a consequence, $[Ca^{2+}]_{in,SK}$ rises significantly at that time, and SK channels are strongly activated. This calcium subsequently diffuses, or is pumped, out of the SK nanodomain, and SK channels deactivate. In this configuration, SK channels are quickly activated and deactivated, in a way that generates a lower AHP TTP after the spike generation. As a consequence, the excitability of the cell is strongly enhanced during a large part of the interspike cycle, making it prone to excitotoxicity.

Mitochondrion- and endoplasmic reticulum-induced SK channel dysregulation as a potential origin of the selective neurodegeneration in PD

This phenomenon is of particular relevance in PD. Indeed, as mentioned above, it has recently been shown that deletion of two PD-associated genes, through their effect on the coupling between mitochondrial Na^+/Ca^{2+} exchanger and SK channels, affects the excitability of the PD affected SNc DA neurons, but not the PD-spared VTA DA neurons and GABAergic neurons [12]. These results suggest that this mitochondrion induced SK channel dysregulation might be a potential origin of the selective loss in PD.

Indeed, global dysfunctions of mitochondria and ER, which affect the metabolism of all cells, may specifically enhance the excitability of these particular pacemaker neurons. Once in a hyperexcited state, their metabolic demand is increased. In turn, this rise in metabolic demand increases mitochondrial and ER stress, which then affects their ability to regulate the intracellular calcium concentration even more [7], and amplifies neuron hyperexcitability. This is the beginning of a vicious circle that may lead to the selective degeneration observed in PD.

Discussion

Part IV highlights a potential systemic role for small conductance calcium-activated potassium channels in the excitability regulation of diverse neuronal populations. It shows how a same ion channel is capable to similarly affect vastly different neurons, and how ionic adaptation mechanism might involve neuron endogenous structures such as mitochondria and endoplasmic reticulum.

The implication of such a systemic role for SK channels is also discussed from a pathological point of view. In particular, a dysregulation of these channels is shown to increase excitability and burstiness of very heterogenous neuron populations. This increase in excitability leads to a dysregulation of cell signaling and calcium homeostasis, the latter being one potential cause of premature neurodegeneration. Interestingly, a review of the experimental literature concerning neurons whose firing patterns are tightly regulated by SK channels identifies precisely those neurons affected in Parkinson's disease, leading to the hypothesis that SK channel dysregulation is a potential cause of the selective neurodegeneration in this neurological disorder.

Our hypothesis is speculative and calls for extensive experimental validations. Nevertheless, it illustrates the interest of a system viewpoint on neurodynamics and electrophysiology when it comes to analyze their implications in neurological diseases.

Part V

Conclusion and Prospects

Summary

The present thesis is devoted to the understanding of the dynamical mechanisms underlying neuronal excitability and their physiological relevance. Starting from a concrete physiological question concerning a specific type of neuron of the midbrain, it attempts to extract a general dynamical picture of excitability, pacemaking and bursting as well as their potential regulation mechanisms.

Part II: Dopaminergic neuron electrophysiology

Part II focuses on the mechanisms underlying dopaminergic neuron excitability, both *in vitro* and *in vivo*, using experimental recordings, conductance-based modeling and dynamical analyses. In particular, it spotlights the qualitative mechanisms underlying DA neuron firing patterns and aims at extracting key players in the switches between these electrical activities.

Most of the analyses are performed via the use of a simplified conductance based model. This model is endowed with the minimal set of conductances that are necessary for the generation of DA neuron firing patterns. It contrasts with existing DA neuron models because its simplicity allows deeper mathematical analyses of the mechanisms underlying firing activities, at the expense of quantitative details, for which existing quantitative models are more successful.

The simple model is used to analyze the mechanisms of DA neuron spontaneous firing *in vitro*. Although much experimental work has been done in this field, the resulting conclusions are sometimes conflicting with each other. In particular, experimental analyses on the role of a particular type of calcium channels, called L-type calcium channels, lead to conflicting conclusions. Analyses on the simple model permit to highlight a potential origin for these discrepancies. It shows that several ion channels, including sodium and L-type calcium channels, cooperate to sustain this spontaneous activity, making it robust against variabilities in ion channel maximal density. However, these variabilities strongly affect neuronal response to experimental protocols, such as L-type calcium channel blockade, offering a possible explanation for the conflicting conclusions. *In vitro* extracellular recordings on substantia nigra pars compacta (SNc) dopaminergic neurons were performed to validate experimentally these modeling results.

In vivo entrainability mechanisms are analyzed subsequently, focusing on the mechanisms underlying irregular single-spike firing and bursting in DA neurons, and identifying small conductance calcium-activated (SK) potassium channels as potential key players in the regulation of the switch between these firing pattern. DA neuron entrainability is shown to be maximal during SK channel blockade, these channels acting as filters against excitatory inputs. While they protect the endogenous rhythm of the cell when present, a blockade of SK channels induces a switch from single-spike firing to bursting *in vivo* only, in agreement with experimental results. We suggest that this firing pattern is therefore exogenous, the neuron transmitting informations only in that state. In addition, we show that a similar mechanism might control the synchrony of neurons subjected to a common excitatory input, which would insure a concomitant switch towards bursting and synchrony.

Finally, analyses of the role of a particular type of potassium channels, called KCNQ potassium channels, in the regulation of DA neuron firing patterns are performed, combining *in vivo* extracellular recordings, *in vitro* intracellular recordings and quantitative mathematical modeling. These analyses show that these potassium channels selectively modulate the quantity of bursting without affecting the pacemaking behavior, their activity being masked by SK channels in the latter state. Analyses of experimental recordings and simulation results show that this current prevents the appearance of short interspike intervals during bursting. Knowing that these channels are often regulated by muscarinic receptors in neurons, it provides an endogenous mechanism by which bursting might be selectively regulated in dopaminergic neurons.

In summary, Part II attempts to bring some qualitative insights on the dynamical mechanisms underlying DA neuron electrophysiology. Only the mathematical results that are directly relevant to answer the physiological questions are considered. However, a further understanding of the role of calcium channels in neurodynamics motivates the analysis in Part III.

Part III: Restorative and regenerative excitability

Motivated by the observed effect of calcium channel variability on DA neuron excitability and pacemaking mechanisms, **Part III** attempts to capture and abstract the dynamical role of these channels on neuronal excitability.

A mathematical analysis of the effect L-type calcium channel variability on the behavior of the simple DA neuron model is firstly proposed. Bifurcation analysis shows that increasing L-type calcium channel maximal conductance induces a switch in the bifurcation responsible for the spike initiation during pacemaking, switching from a subcritical Hopf bifurcation to a saddle-node bifurcation, leading to the concepts of sodium and calcium pacemaking. Although the spontaneous activities are similar in both cases, the behavior of the model under SK channel blockade is strongly affected. In particular, modeling and experimental results show that calcium pacemakers are proner to bursting both *in vitro* and *in vivo* under the

blockade of SK channels. This analysis, which is very descriptive, raises questions concerning the effect of these calcium channels on the dynamics of neuronal excitability.

Mimicking the approach of FitzHugh in 1961, we then show that incorporating calcium channels in the HH model before its reduction leads to a significant revision of the traditional FitzHugh-Nagumo phase portrait. In particular, it uncovers the role of a transcritical bifurcation in the organization of neuronal excitability. This bifurcation has been absent from the neurodynamics literature to date. On the basis of this novel phase portrait, we develop a novel hybrid model of spiking neurons, in which a single parameter, termed w_0, is able to account for the calcium channel density. Modifying w_0 is shown to induce a switch in neuronal excitability, whose consequences are illustrated on thalamic relay neuron electrophysiology.

The properties of the novel phase portrait are further analyzed, through the study of the excitability properties of a mirrored FitzHugh-Nagumo model, in which the previously derived insights are incorporated. Excitability is explored by unfolding a pitchfork bifurcation that is shown to organize five different types of excitability. In addition to the three classical types of neuronal excitability, two novel types are described, whose main electrophysiological signatures are robust spike latency and robust bistability.

Given that these insights are for two dimensional reduced models, the generality of the results for arbitrary conductance-based models is further investigated. The presence of the transcritical bifurcation in arbitrary conductance-based models is proven, defining a frontier between *restorative excitability*, which includes the three previously described excitability types, and *regenerative excitability*, which includes the novel type of excitability described in planar models. From a physiological point of view, a neuron exhibits restorative (resp. regenerative) excitability when slow restorative (resp. regenerative) variables, i.e. providing a negative (resp. positive) feedback to membrane potential variations, are dominant, the exact balance between both variable types corresponding to a transcritical bifurcation. This physiological interpretation leads to a novel classification of ion channels as restorative, regenerative, or neutral, depending on their effect on neuronal excitability. For illustration purposes, the role of the transcritical bifurcation in the organization of excitability is analyzed in seven published conductance-based models.

Finally, the physiological relevance of these abstract results is examined. The regulation of the balance between restorative and regenerative ion channels is shown to provide a physiological route to bursting. Indeed, the main dynamical signature of regenerative excitability is robust bistability, a key component of neuronal bursting, this bistability being marginal or even absent in restorative excitability. In addition, although there exist many qualitatively different bursting types, they all arise from the same dynamical mechanisms, their qualitative properties being determined by two parameters, that is the balance weight and the adaptation gain. This statement is in sharp contrast with the current view of bursting in neurodynamics, each bursting type being linked to a particular dynamical mechanism.

To summarize, Part III incorporates the role of regenerative ion channels, such as calcium channels, in reduced models of neurodynamics. This inclusion leads to a novel global picture that permits to easily interpret a number of electrophysiological dynamical features of interest in contemporary electrophysiology, as well as to extract key players in the regulation of these electrophysiological properties. In addition, these results suggest that, although a large amount of different ion channels exist, spiking behavior is primarily governed by two parameters modulating excitability quality and quantity. One potential illustration of this property and its pathological consequences are discussed in Part IV.

Part IV: Abnormal Timing of SK Channel Activation and Parkinson's disease

Part IV proposes a novel hypothesis concerning a possible implication of the results described above for the genesis of Parkinson's disease. In particular, it highlights a common electrophysiological signature of neurons affected in Parkinson's disease: the firing of these neurons is commonly regulated by SK channels, these channels strongly affecting neuron adaptation gain, as shown in Part III. As a consequence, any global dysregulation of SK channel activity would strongly affect the adaptation gain of these neurons, increasing their entrainability and burstiness. This excitability dysregulation would affect calcium homeostasis, which would therefore render the neuron proner to degeneration. This hypothesis is shown to be consistent with the recent literature on the subject.

Although totally hypothetical, the discussion proposed in this part emphasizes the interest of a system viewpoint on neurodynamics for the investigation of global pathological processes, as in the case of neurodegenerative diseases.

Prospects

Systems analysis suggests novel experiments

The mathematical results discussed in this thesis suggest novel experiments. In particular, our results identify potential key players in excitability and firing pattern reg-

ulation, which can be correlated to specific physiological studies.

One potential application of the results is the investigation of the physiological mechanisms underlying burst firing in dopaminergic cells. Two key players have been identified: SK channels, which modulate the adaptation gain, and L-type calcium channels, which modulate the balance weight. One hypothesis is therefore that DA neuron firing pattern can be physiologically regulated via the modulation of these channels, as illustrated below.

SK channels are clearly important for regulating bursting *in vivo* [95, 191]. However, no physiological mechanism of SK channel regulation has been observed to date in DA neurons. The experimental exploration of such a mechanism would therefore spotlight a source for the regulation of DA neuron firing pattern, as well as a target for the pharmacological treatment of diseases whose symptoms correlate to a dysregulation of the dopaminergic system.

Concerning the role of L-type calcium channels, we show that their functionality can be heterogenous over a same population, leading to different responses to SK channel blockade *in vitro*. A physiological regulation of these channels might therefore also be a source of firing pattern modulation. For instance, knowing that L-type calcium channels can be activated only in their phosphorylated state, their activity might be modulated intracellularly via modifications in the level of protein kinase A (PKA), which can be controlled extracellularly by metabotropic receptor activation. This mechanism could be investigated by the use of patch clamp recordings on rat/mouse brain slices, for instance.

Using the dynamical results provided in Part III concerning the important role of regenerative ion channels in neuron excitability and bursting, such experimental strategies can be extended to other types of neurons, such as reticular and relay neurons of the thalamus, subthalamic nucleus neurons, etc.

Implications for intrinsic homeostasis

A promising application of our results concerns neuronal homeostasis. It has been shown that many neurons are able to robustly maintain neuronal and circuit excitability at a "target value" in responses to changes in their environment, via mechanisms known as synaptic and intrinsic plasticity, for instance [184]. In particular, intrinsic plasticity is mediated by changes in the expression level or biophysical properties of ion channels in the membrane [32], which affects ion channel kinetics and maximal conductances, for instance. In addition, very different neurons can reach a similar spiking behavior via the regulation of very different ion channel types. The mechanisms underlying this neuronal homeostasis are still poorly understood to date.

The dynamical properties we derive in Part III are of interest to investigate these mechanisms. In particular, the generalization of the concepts to conductance-based models provided in Chapters 11 and 12 suggests that neuron excitability is mainly determined by three parameters: the balance between restorative and regenerative ion channels, the adaptation gain and the net membrane current. Intrinsic homeostasis could therefore result from a tight regulation of these parameters only, which can be made via many different ion channel combinations, as illustrated in Fig. V.I.

In addition, our results show that many different sets of balance weight and adaptation gain can induce qualitatively similar endogenous behaviors, whereas sensitivity and robustness properties strongly differ between these sets of parameters (Chapter 12). This might provide a regulation mechanism by which neurons adapt their response to the environment while keeping their endogenous signaling behavior constant, to ensure the persistence of basic functions, as observed in central patterns generators. Similarly, although neurons would be able to adapt their intrinsic properties in pathological states to sustain their endogenous signaling, they might loose robustness against the environment, making these cells proner to degeneration, for instance. Such novel concepts, which derive from the proposed dynamical analysis, deserve further research.

Implications for network analyses

Finally, one natural extension of our single-neuron analysis is to explore its implications at the network level. In particular, the hybrid model developed in Chapter 12 contains all the dynamical properties extracted from conductance-based models in Chapter 11, yet is simple enough to allow large population simulations. This simple model differs from existing simple models because it integrates the role of regenerative ion channels, and is therefore able to express regenerative excitability from which robust endogenous bursting arises, as well as to switch between different excitability types.

One illustration of interest of this simple model at the network level is the analysis of the pathological rhythms observed in the basal ganglia during Parkinson's disease currently studied by Julie Dethier. It has been shown that a disruption of dopamine release into the striatum affects neuronal populations of the basal ganglia, including the external globus pallidus and the subthalamic nucleus [74, 174, 193]. These populations exhibit a pathological increase in their synchronized bursting activity, which correlates with the motor symptoms of PD [110].

One unsolved challenge is the extraction of the ionic mechanisms underlying this switch of firing activity. The

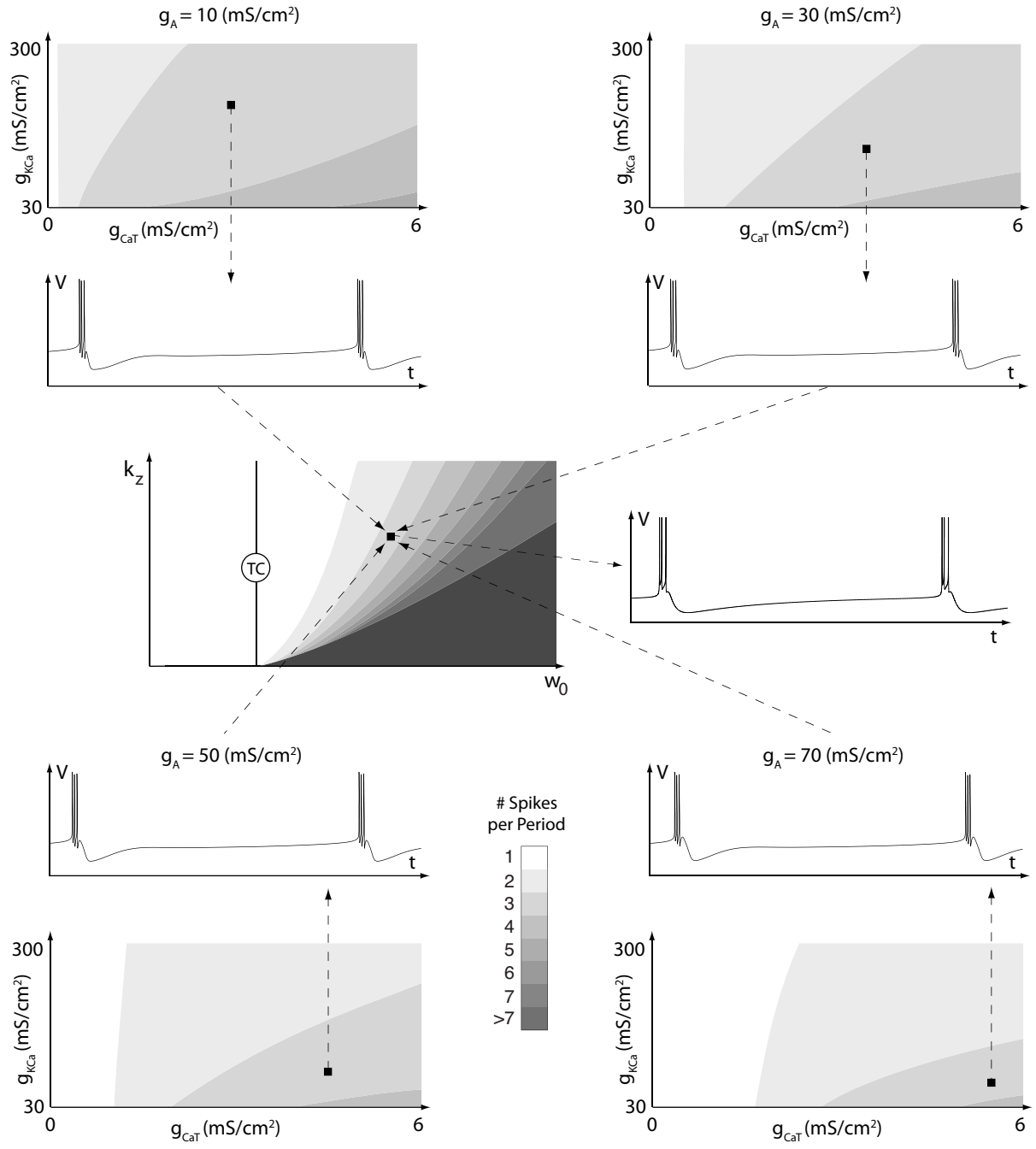

Figure V.I – Example of applications of our results to investigate the mechanisms underlying intrinsic homeostasis. The figure shows the behavior of a model of a stomatogastric ganglion neuron [61, 114] for different sets of parameters. These different sets of parameters define similar balance weight and adaptation gain, which leads to a similar spiking behavior, mimicked by our transcritical hybrid model.

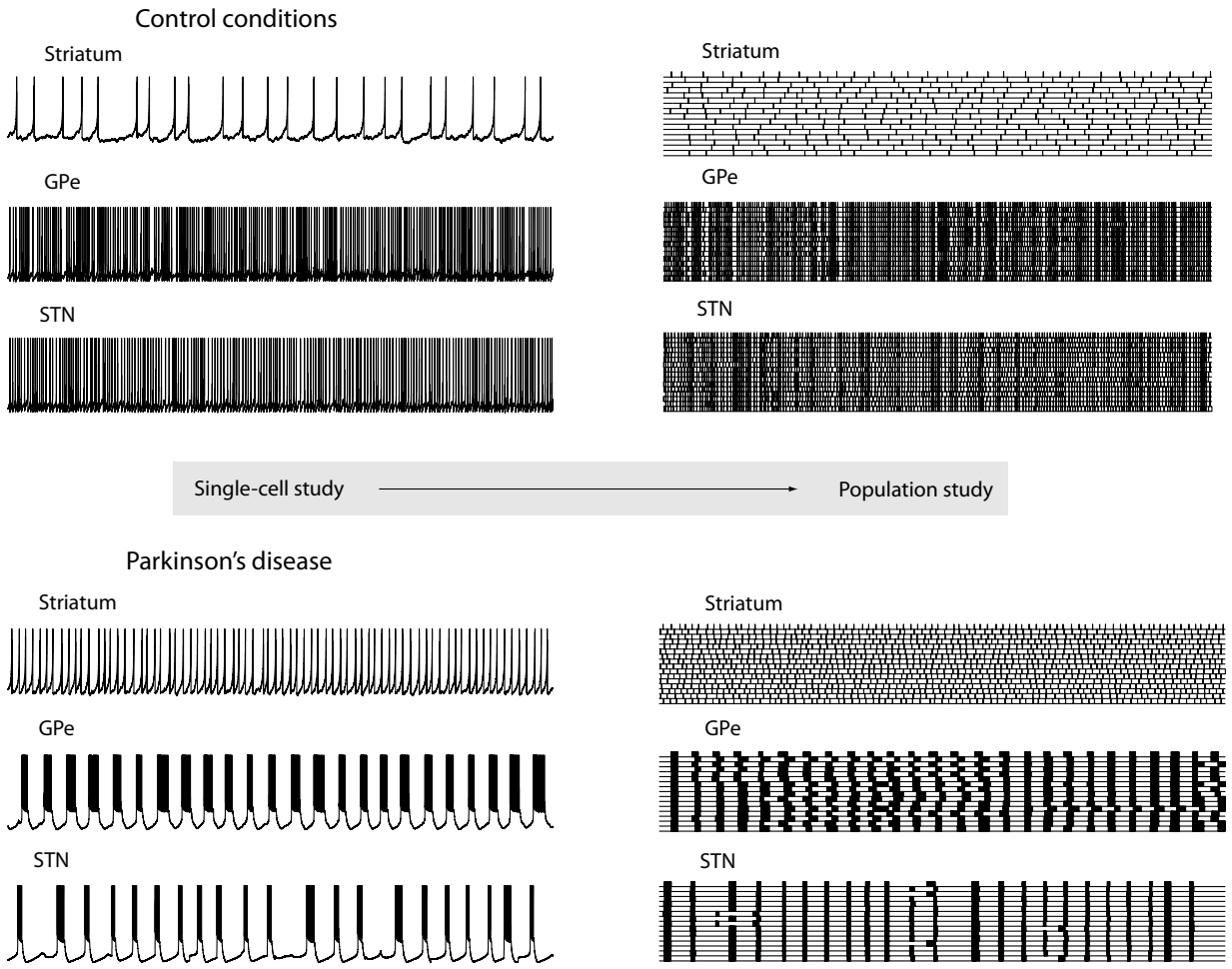

Figure V.II – Example of applications of our results at the network level. The figure shows the spiking behavior of three coupled neuron types of the basal ganglia, that is striatal medium spiny neuron, globus pallidus externus (GPe) and subthalamic nucleus (STN) neuron (provided by Julie Dethier from the University of Liege). Using the transcritical hybrid model described in Chapter 12, it is possible to reproduce the pathological switch in basal ganglia rhythms observed in Parkinson's disease both at the single cell level and at the network level, via a simple reduction of dopamine release in the striatum.

dynamical picture of neuronal excitability proposed in this thesis might be helpful to address this question, as illustrated in Fig. V.II. This figure shows how the simple hybrid model is able to reproduce the pathological switch in basal ganglia rhythms observed in Parkinson's disease both at the single cell level and at the network level, via a simple reduction of dopamine release in the striatum (data provided by Julie Dethier from the University of Liege). These promising data illustrate the potential role for the dynamical results provided in this dissertation in population studies.

To conclude. Working on the fascinating subject of neuron electrophysiology has been an exciting and surprising journey. Initially rooted in the investigation of a very concrete question, it has unexpectedly led to a broad revision of the dynamical picture of neuronal excitability, which we believe will enhance the interaction of neurodynamics with experimental electrophysiology and advance our understanding of neuronal excitability.

Part VI

Supplementary Figures

Supplementary Figures of Chapter 4

Parameter	Value	Parameter	Value
V_{Na}	$50\ mV$	$\bar{g}_{Na}$	$0.16\ S/cm^2$
V_K	$-95\ mV$	$\bar{g}_{K,DR}$	$0.024\ S/cm^2$
V_l	$-54.3\ mV$	g_l	$0.3\ 10^{-3}\ S/cm^2$
V_{Ca}	$120\ mV$	$\bar{g}_{Ca,L}$	$3.1\ 10^{-3}\ S/cm^2$
$K_{M,L}$	$0.00018\ mM$	$K_{M,P}$	$0.0001\ mM$
k_1	$0.1375\ 10^{-3}$	k_C	0
$\bar{g}_{Syn}$	$0.1\ 10^{-3}\ S/cm^2$	$I_{Ca,pump,max}$	$0.0156\ mA/cm^2$
$\bar{g}_{K,Ca}$	$5\ 10^{-3}\ S/cm^2$	K_D	$0.4\ 10^{-3}\ mM$
C_m	$1\ \mu F/cm^2$	k_2	$0.018\ 10^{-4}$

Table S4.1 – Parameters of the minimal model of DA neurons.

Supplementary Figures of Chapter 5

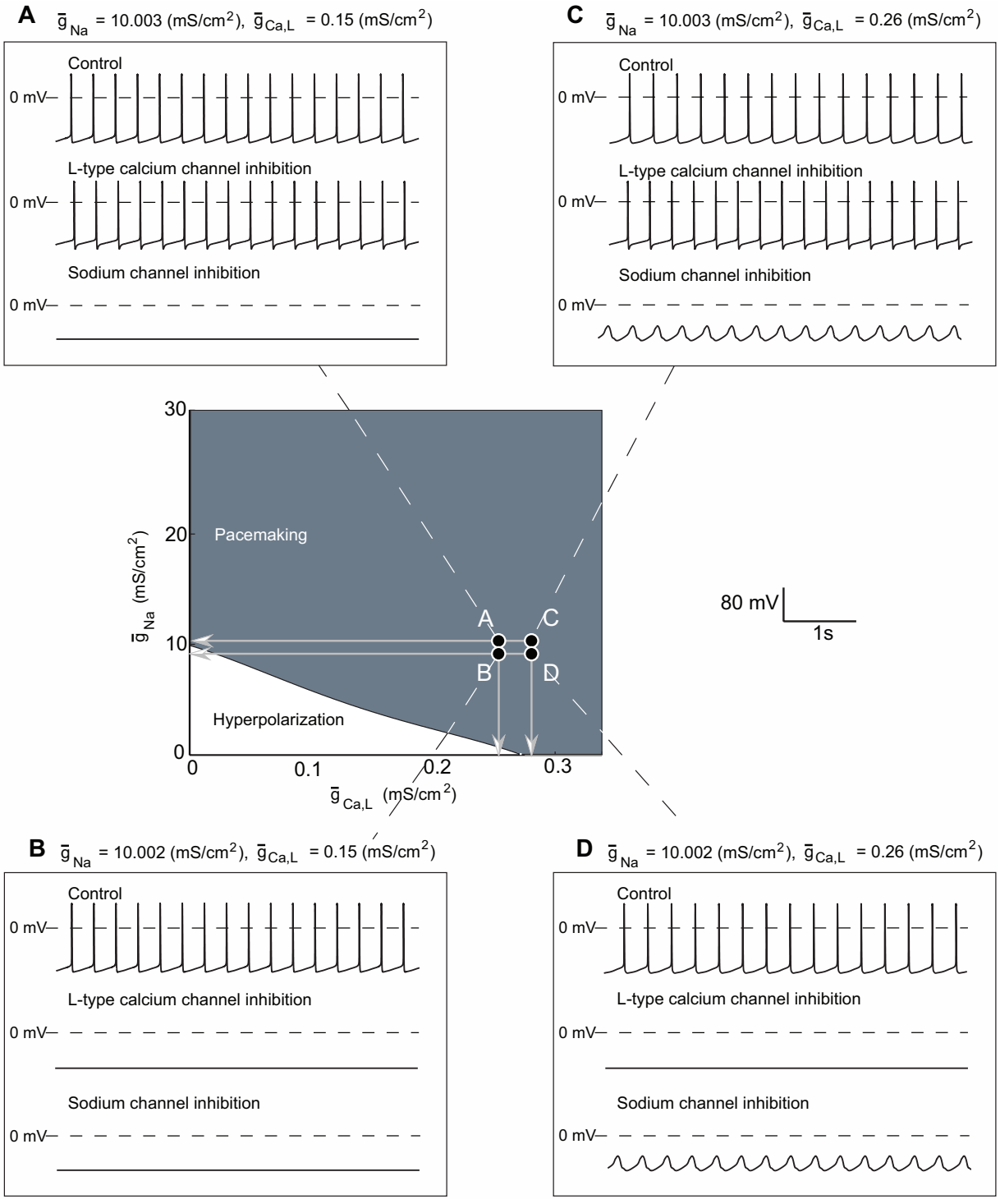

Figure S5.1 – Cooperation between sodium and calcium channels in the generation of spontaneous activity in the detailed model. The center pannel shows the type of pacemaker activity according to the sodium and L-type calcium conductances. The white zone represent the couples of conductances which results to a spontaneous hyperpolarization of the cell and the dark blue zone account for pacemaking. Each insert shows the behavior of the model in control condition and during a blockade of L-type calcium channels or sodium channels for a particular set of conductances, respectively. The pacemaker behavior of the model strongly relies on the values of both the sodium and the L-type calcium conductances.

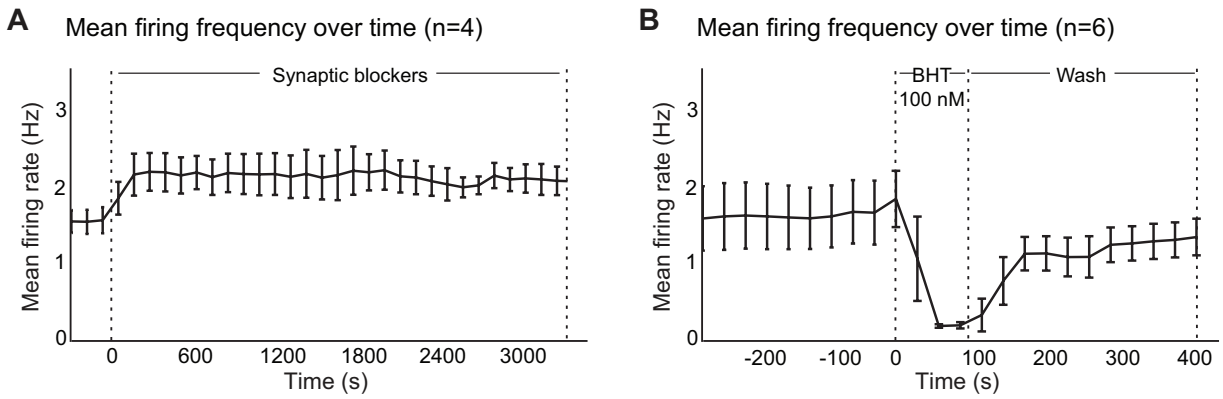

Figure S5.2 – Effect of synaptic blockers and a D2 receptor agonist on the firing rate of SNc DA neurons in brain slices. A. Mean firing frequency (samples of 2 minutes) of the recorded cells over time (mean ± sem, n=4). **B.** Mean firing frequency (samples of 30 seconds) of the recorded cells over time (mean ± sem, n=6). The application of synaptic blockers induces an increase in the firing rate which remains stable for at least one hour. The application of the D2 receptor agonist BHT 920 (100 nM) [33] strongly reduces the firing rate of the recorded cells.

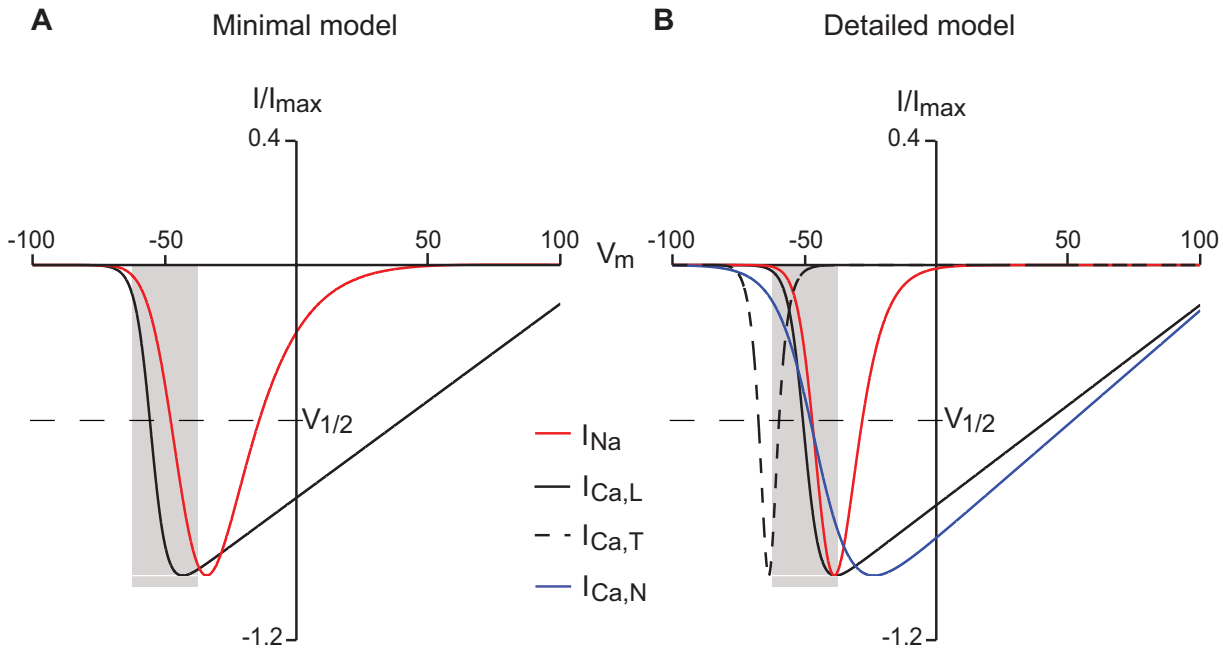

Figure S5.3 – I-V curves of various depolarizing currents in the two models. I-V curves of sodium channels (in black) and of L-type calcium channels (in red) of the minimal model **A.** and of the detailed model **B.**. For the detailed model, I-V curves of N-type (in blue) and T-type (in dotted black) calcium channels are also plotted. The only current which has a significantly different half-activation potential as compared to the L-type calcium current is the T-type calcium current.

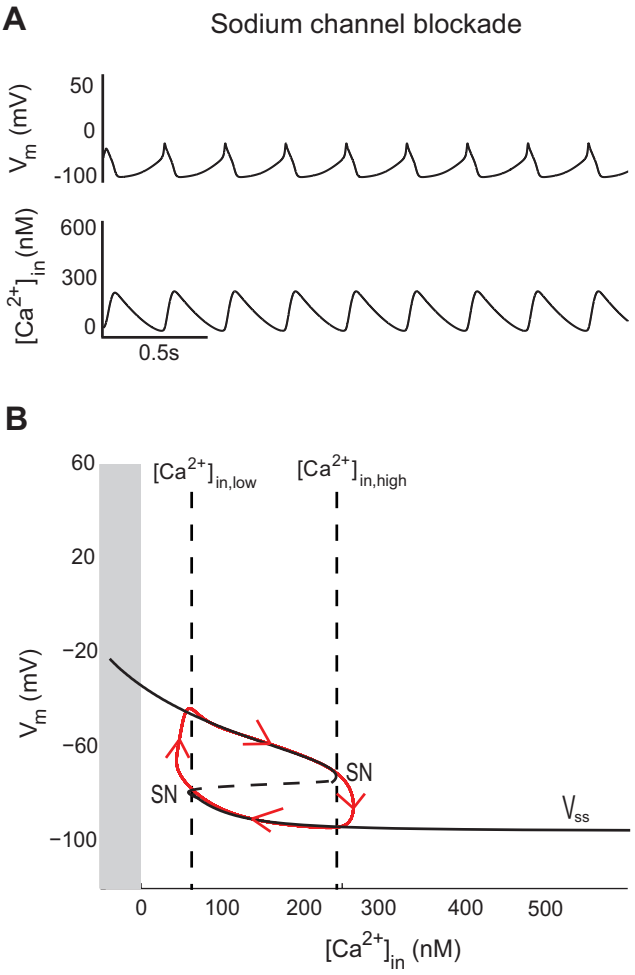

Figure S5.4 – Analysis of the slow oscillatory potentials of the minimal model. A. Variations of the membrane potential (top) and of the intracellular calcium concentration (bottom) over time. **B.** Sketch of the bifurcation diagram of the minimal model, with $[Ca^{2+}]_{in}$ as the bifurcation parameter. The gray part corresponds to negative values of $[Ca^{2+}]_{in}$, which are non physiological. V_{ss} denotes the steady-state curve for each value of the bifurcation parameters. The dotted part of V_{ss} shows its unstable part. SN denotes a saddle-node bifurcation. Trajectories of the membrane potentials are plotted in red.

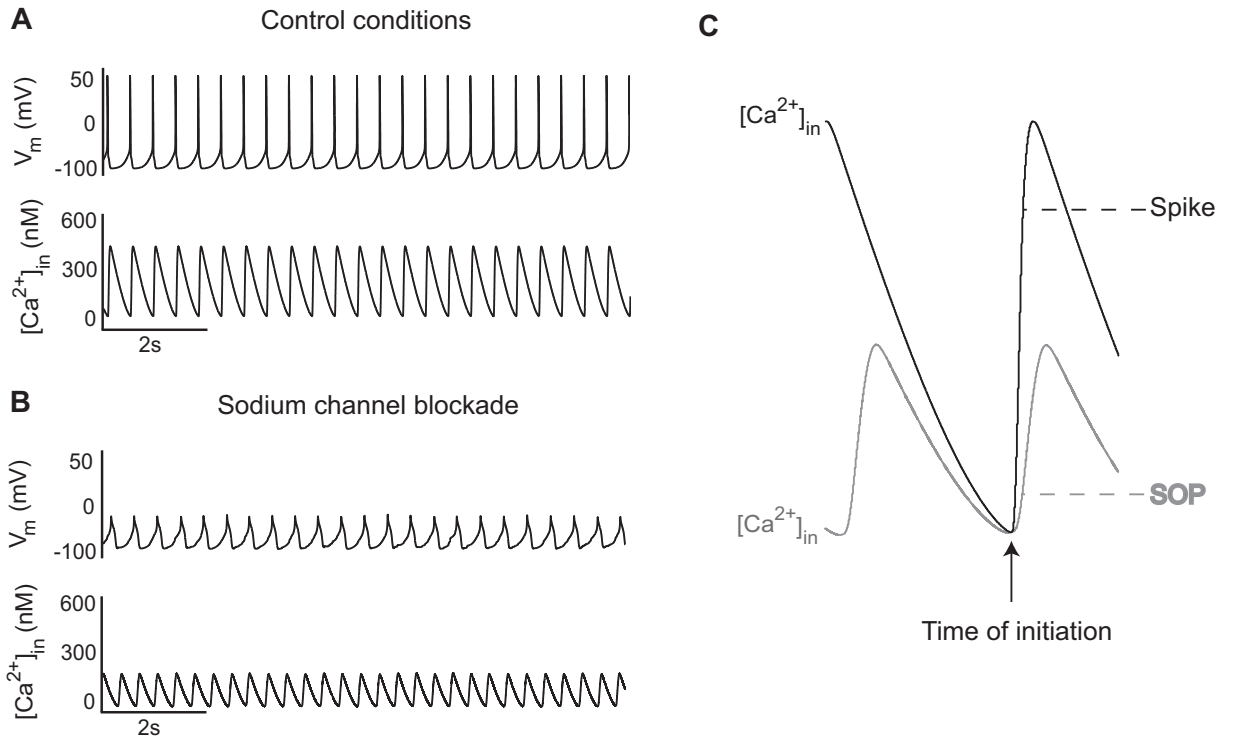

Figure S5.5 – Comparison of the calcium dynamics during pacemaking and slow oscillatory potentials. (a and **b)** Evolution of membrane potential (top) and calcium oscillations (bottom) over time in control conditions and during a sodium blockade, respectively. **C.** Variations of intracellular calcium concentrations during both oscillatory patterns.

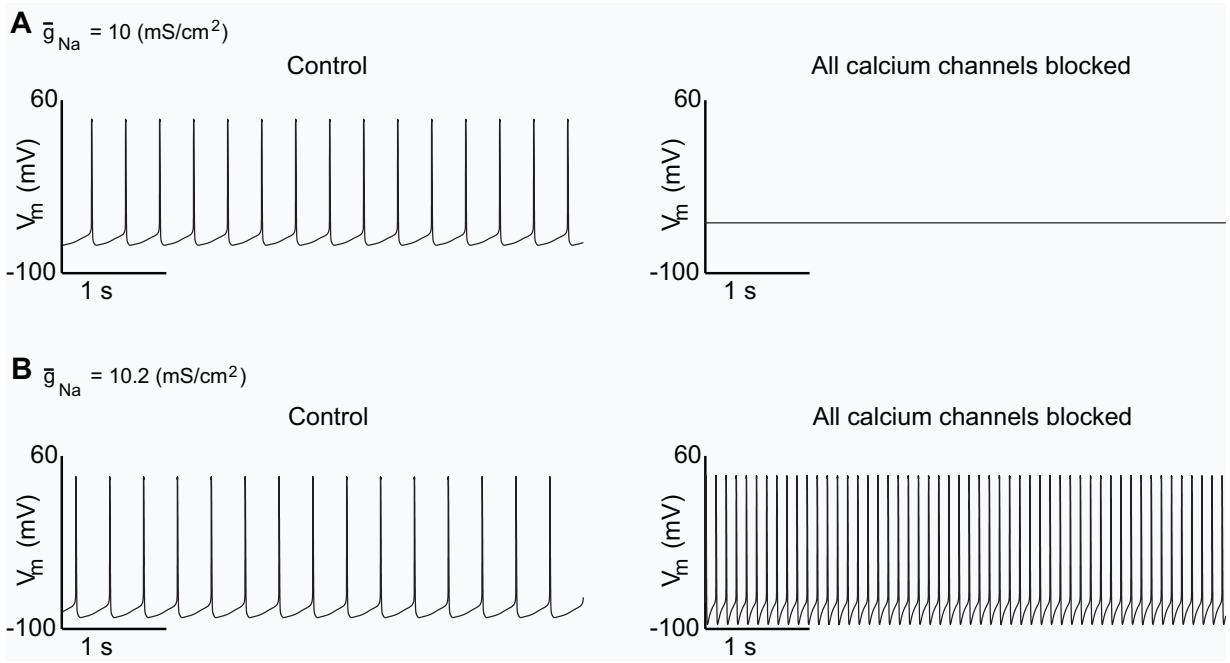

Figure S5.6 – Effect of sodium channel density on the response of the detailed model to calcium channel blockade. Response of the detailed model to an inhibition of all calcium channels for two slightly different values of sodium channel density. **(a** and **b)** Variations of the membrane potential over time in control conditions (left) and after the blockade of all calcium channels (right) for two different sodium conductances. Note how dramatically the value of $\bar{g}_{Na}$ influences the effect of calcium channel blockade.

Supplementary Figures of Chapter 6

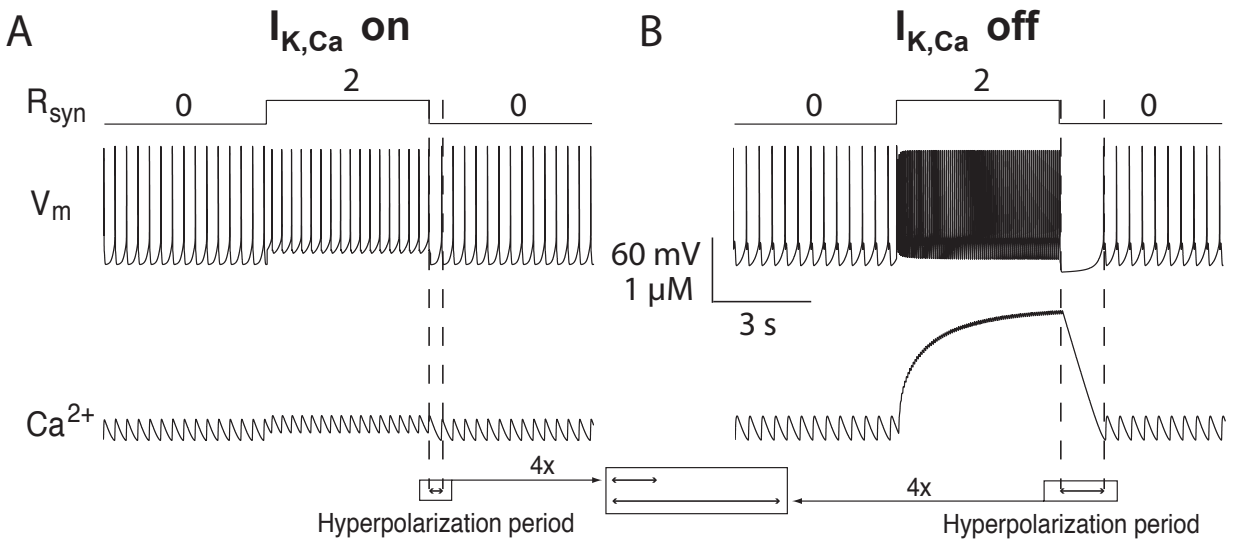

Figure S6.1 – Effect of a step input of synaptic current activation on the cell firing in the presence (left) and in the absence (right) of SK channels. (a and **b)** variations of synaptic input activation (top), the membrane potential (middle) and the intracellular calcium concentration (bottom) over time in the presence and in the absence of SK channels, respectively. The hyperpolarization period occurring after a downregulation of the step input is strongly longer in the absence of SK channels, due to the calcium accumulation during the period of excitation.

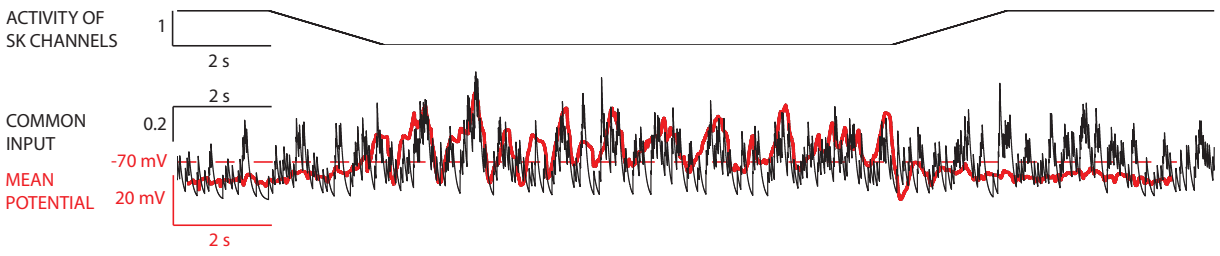

Figure S6.2 – Variations of neuronal firing pattern and synchrony during a down-regulation of SK channels. From top to bottom : variations of SK channels activity over time, merge of common activation of excitatory inputs variations and mean potential of the network. The mean potential of the network is correlated to synaptic inputs only in the absence of SK channels.

Supplementary Figures of Chapter 7

N=6; *, p<0.05	Control	GABA	SR95531	SR95531 + GABA
Firing frequency (Hz)	2.23 ± 0.40	0.92 ± 0.18	2.69 ± 0.32	2.44 ± 0.23

*

Table S7.1 – SR95531 blocks the inhibitory effect of GABA on the firing of DA neurons.

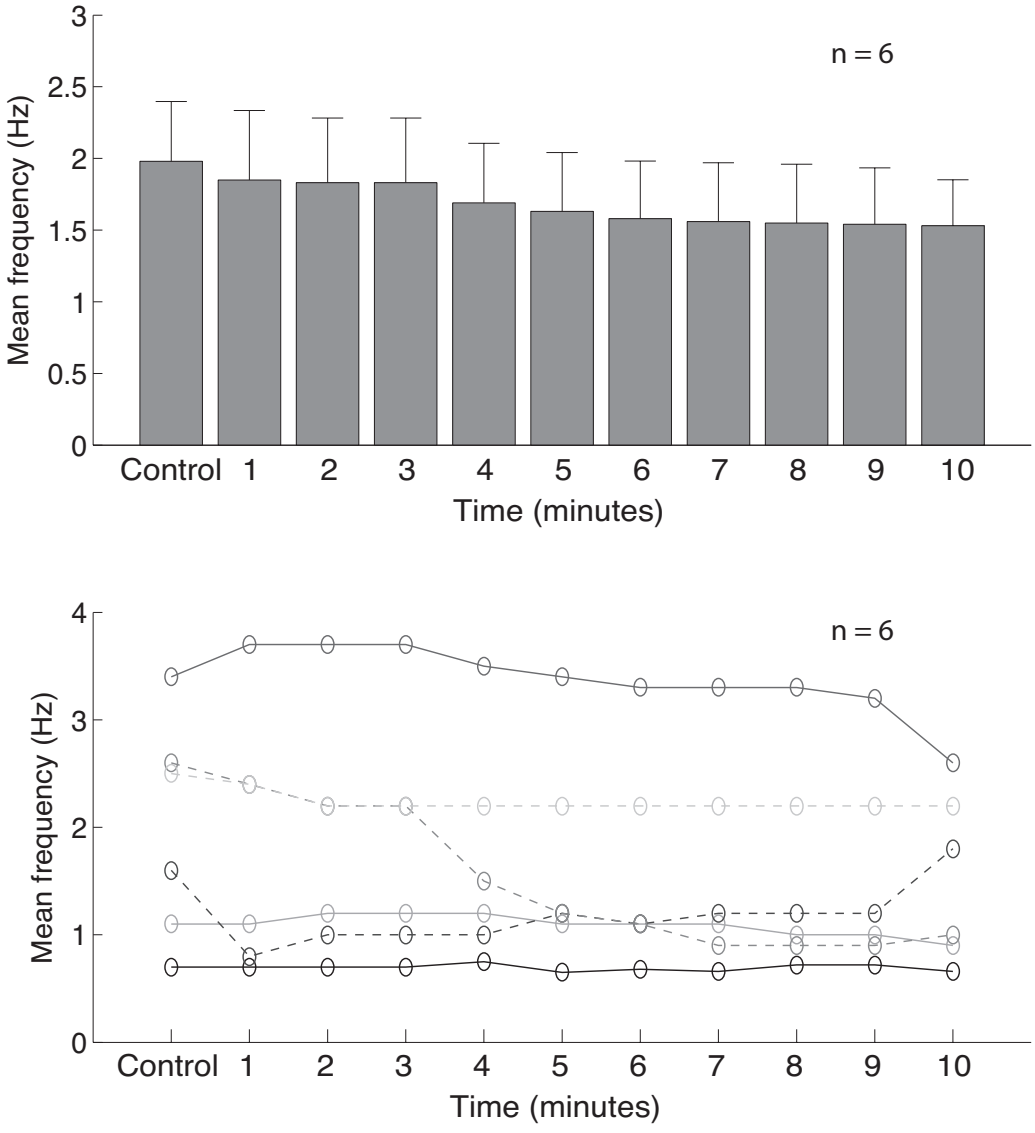

Figure S7.1 – Effect of the i.p. administration of XE991 on the firing rate of DA neurons in the absence of a GABA$_A$ antagonist. A variable effect was observed in these experiments, with some cells being inhibited (N=6). **A.** Mean frequency over time for the six cells. **B.** Single cell frequency over time.

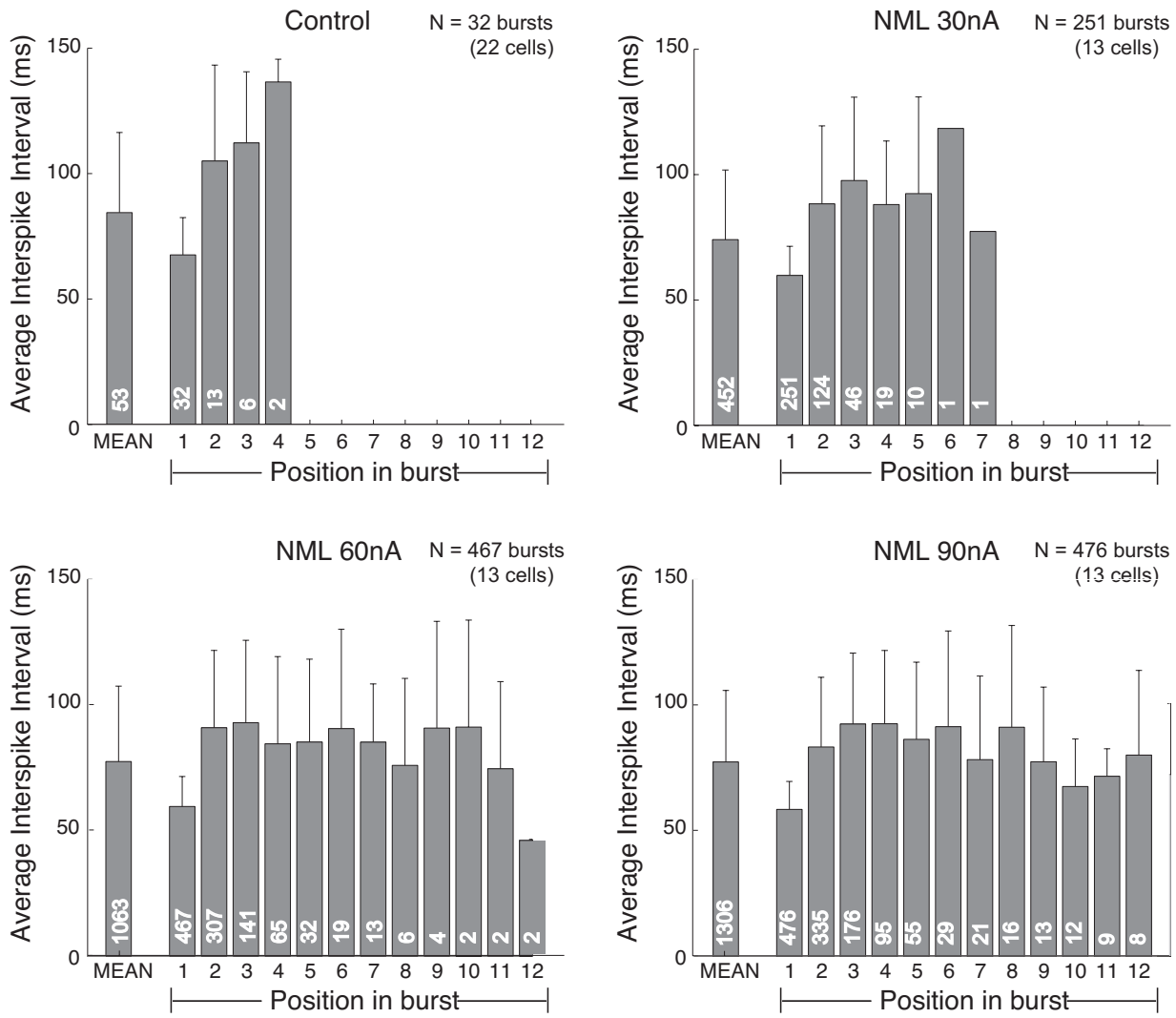

Figure S7.2 – Comparison of the interspike intervals. Both spontaneous bursts (control) and NML-induced bursts are represented. Note the similarity of all parameters in all cases. Means and SD's are shown in order to facilitate the comparison with data of [63] .

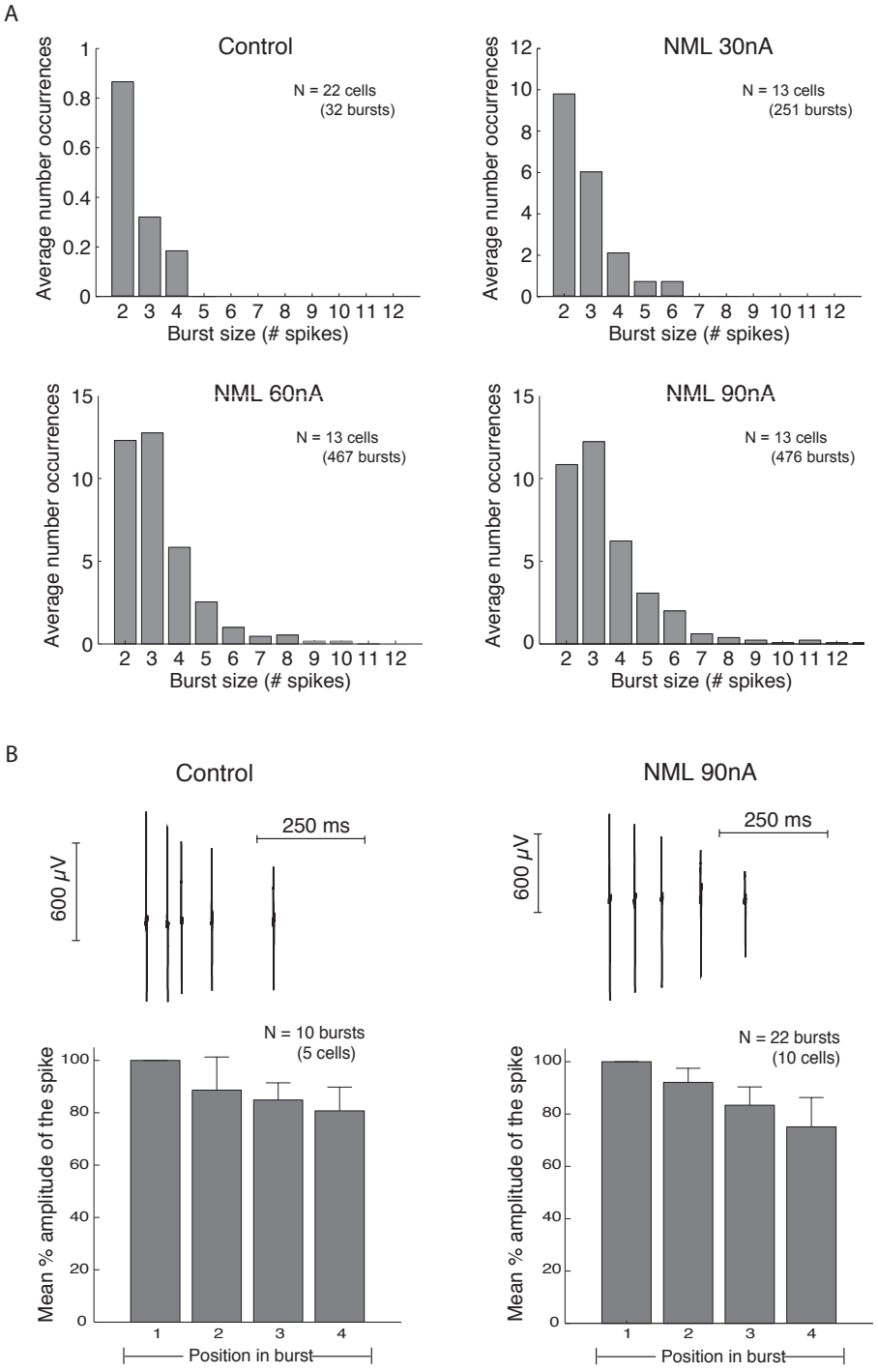

Figure S7.3 – A. Relative frequency of the bursts as a function of their number of spikes. Doublets are indicated as well. **B.** Changes in spike amplitude within bursts. One burst from our experiments (both spontaneous and NML-induced) is shown. Summary histograms for the four first ISI's are displayed. Means and SD's are shown in order to facilitate the comparison with data of [63], as in Supplementary Fig. S7.2.

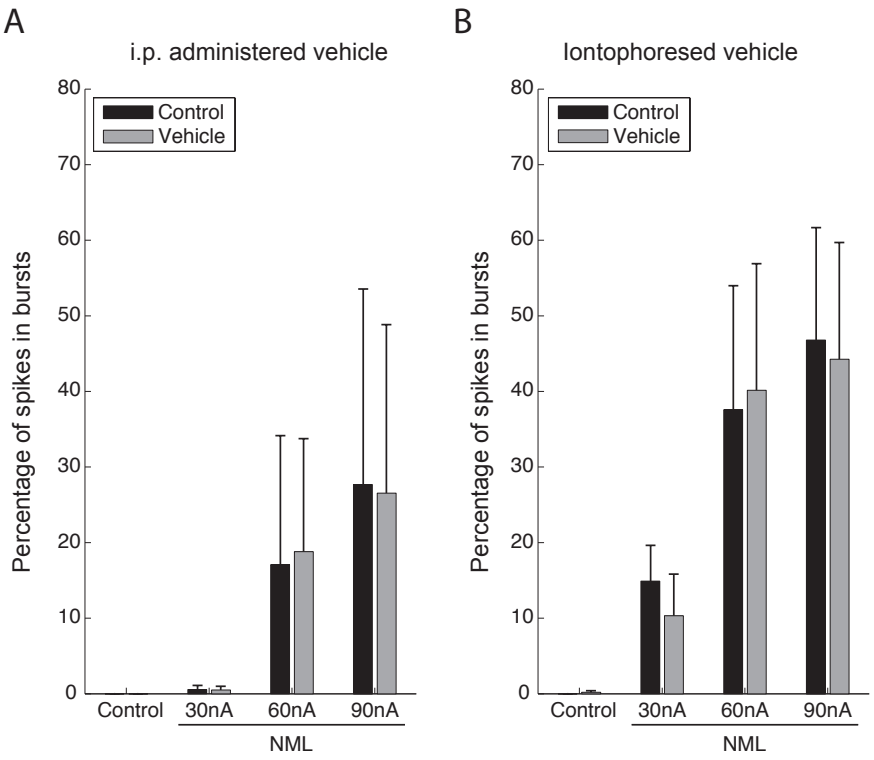

Figure S7.4 – Lack of effect of the vehicle on bursting in DA neurons. A. i.p. experiments (N=3). **B.** Iontophoresis experiments (100nA) (N=5). The vehicle had no effect on the percentage of spikes in bursts in either condition.

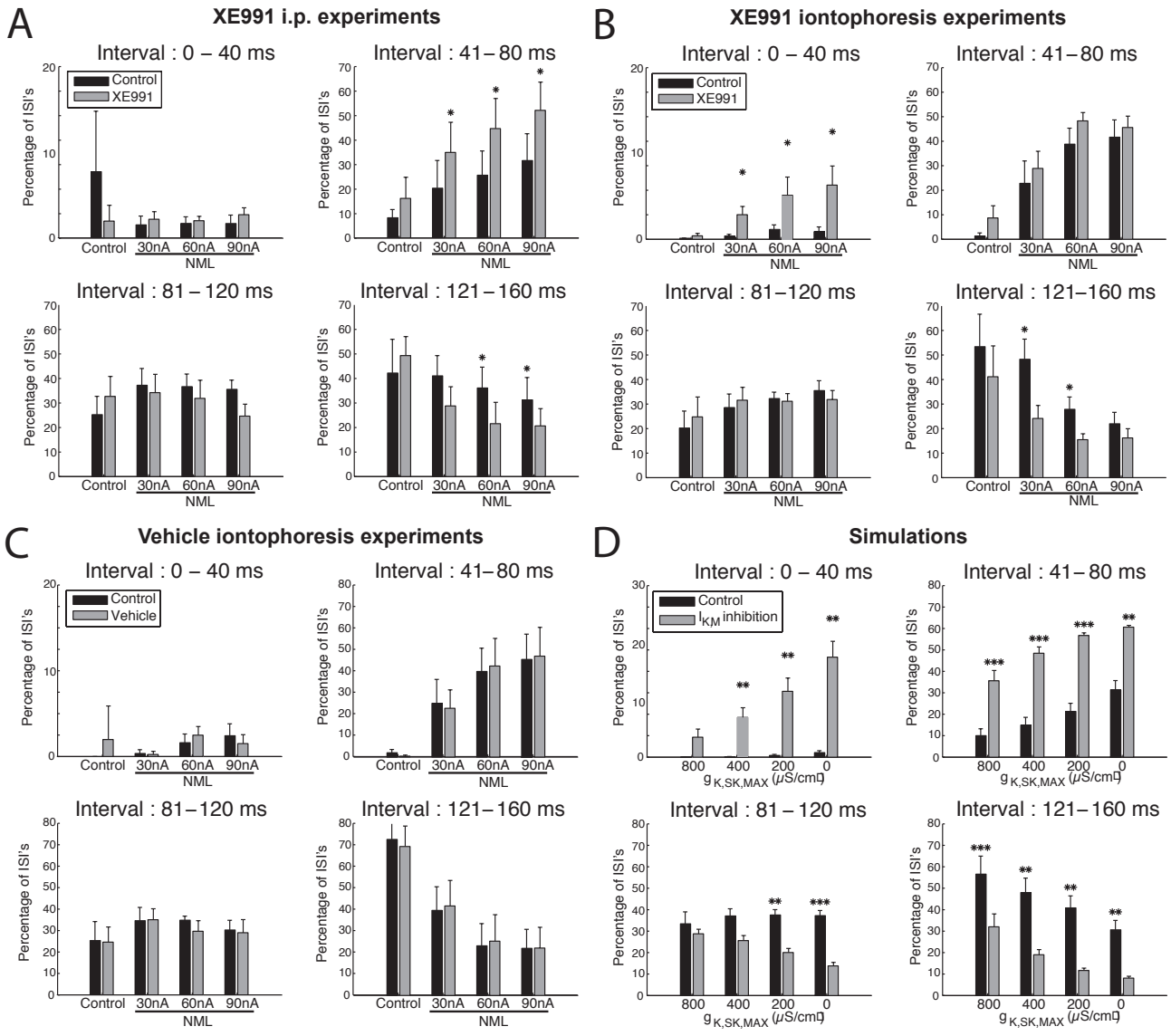

Figure S7.5 – Effect of M-channel blockade on the distribution of short interspike intervals. ISI's were classified into four categories (0-40, 41-80, 81-120 and 121-160 ms, respectively). Application of XE991 significatively increased the percentage of ISI's in the shorter intervals (**a**, intraperitoneal experiments; and **b**, iontophoresis experiments), whereas application of vehicle had no effect on this distribution **C.**. **D.** Simulations showed a qualitatively similar, but more robust effect. (*, $p < 0.05$; **, $p < 0.01$; ***, $p < 0.001$). Note that the ordinate scale is expanded in the upper left side of each panel.

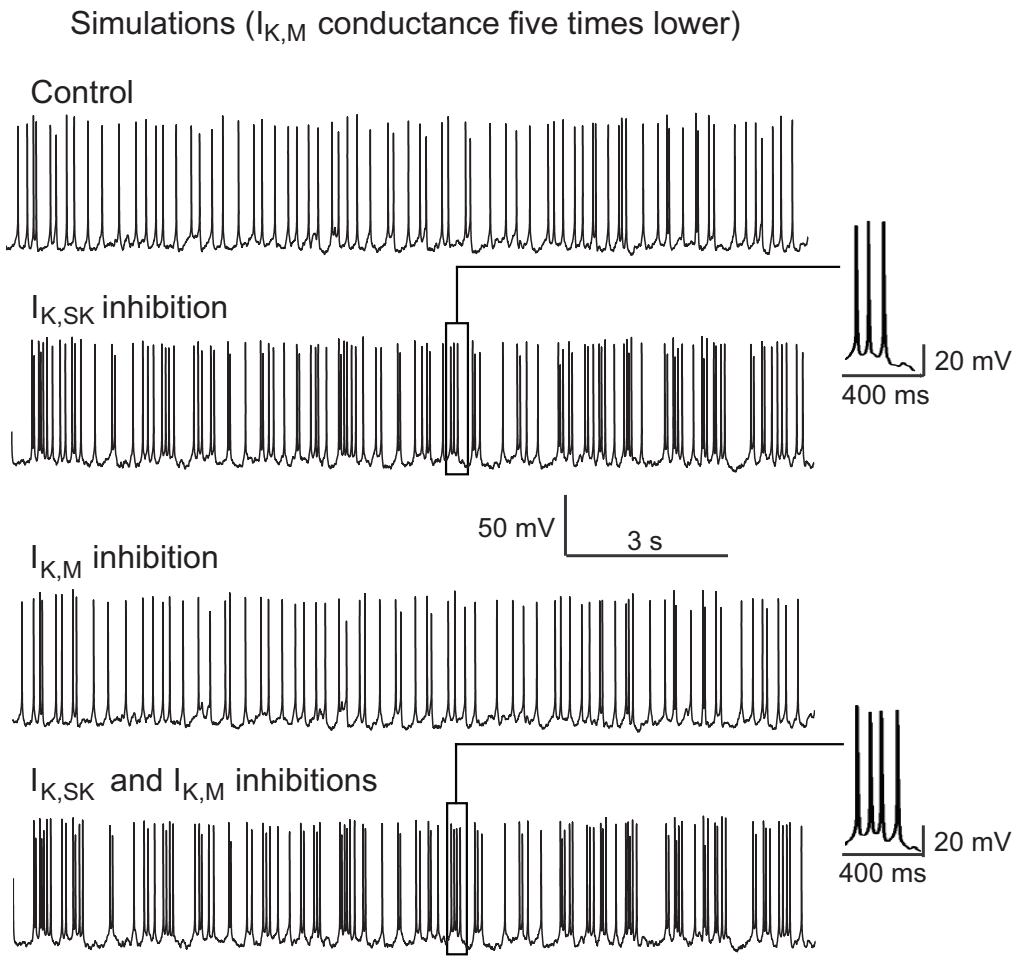

Figure S7.6 – Effect of M-current blockade on a DA neuron model when the M-current conductance was identical to the one reported experimentally [106].

Supplementary Figures of Chapter 8

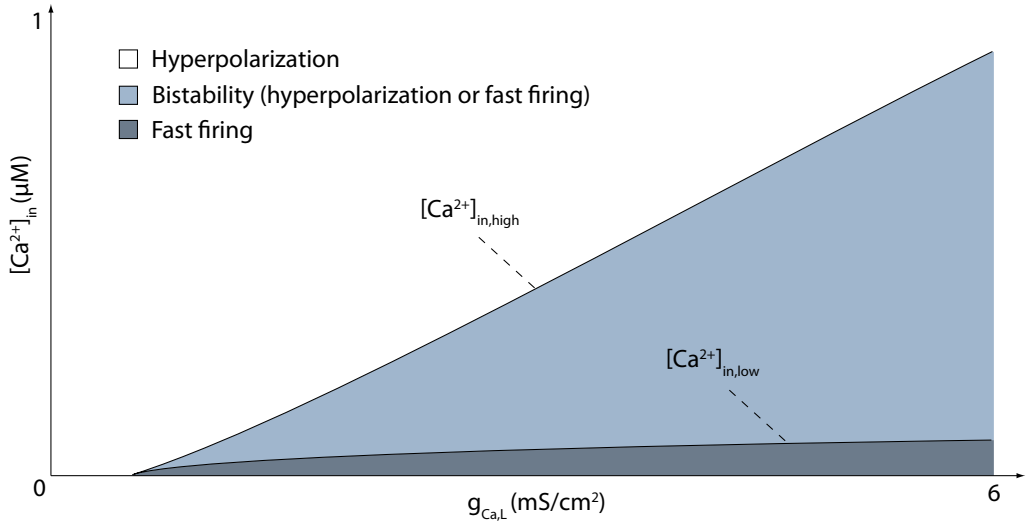

Figure S8.1 – Evolution of the calcium thresholds with an increase of L-type calcium channel maximal conductance $\bar{g}_{Ca,L}$ in the simple DA neuron model. The white part shows couple of values for which the model is hyperpolarized, the dark blue part shows couple of values for which the neuron is firing, and the light blue part correspond to a bistable region, where the model can both fire or be hyperpolarized. Note how the bistable zone increases with an increase in $\bar{g}_{Ca,L}$.

Supplementary Figures of Chapter 9

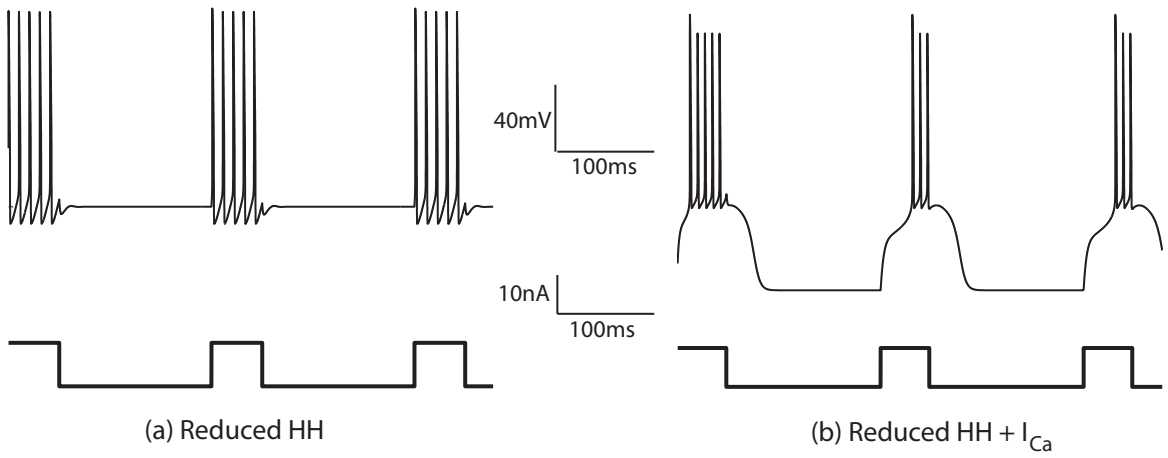

Figure S9.1 – Stimulation-induced bursting in the reduced Hodgkin-Huxley model without (left) and with calcium current (right).

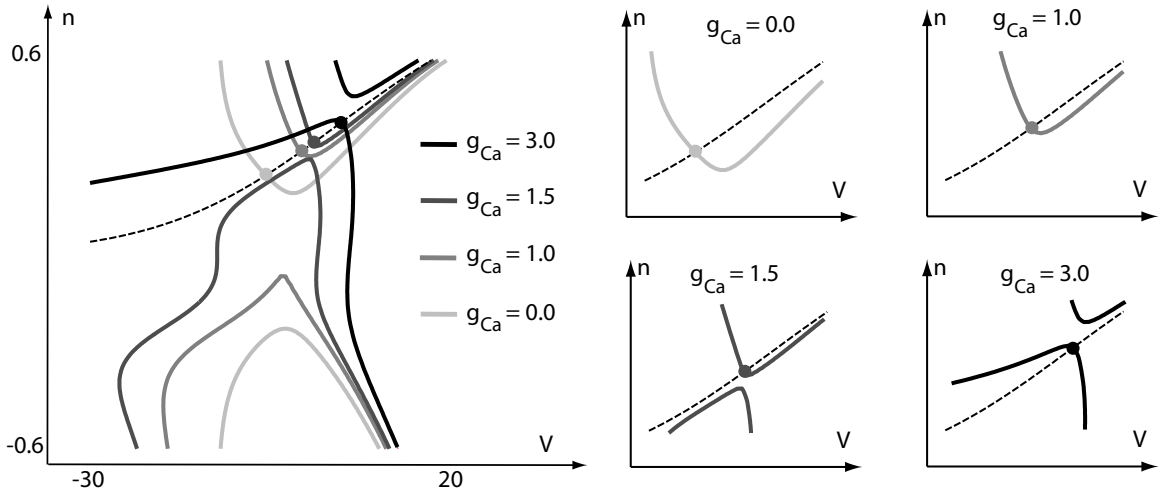

Figure S9.2 – Nullcline intersections in the reduced model (5) with calcium current for different values of the calcium conductance. The n-nullcline is depicted as a dashed line, the V -nullcline as a solid line. The associated calcium conductance is expressed via a gray scale, as indicated in the figure legend. The calcium pump currents is given by $I_{Ca,pump}$ = 0.0, -0.74, -2.78, -15.6 for, respectively, g_{Ca} = 0.0, 1.0, 1.5, 3.0.

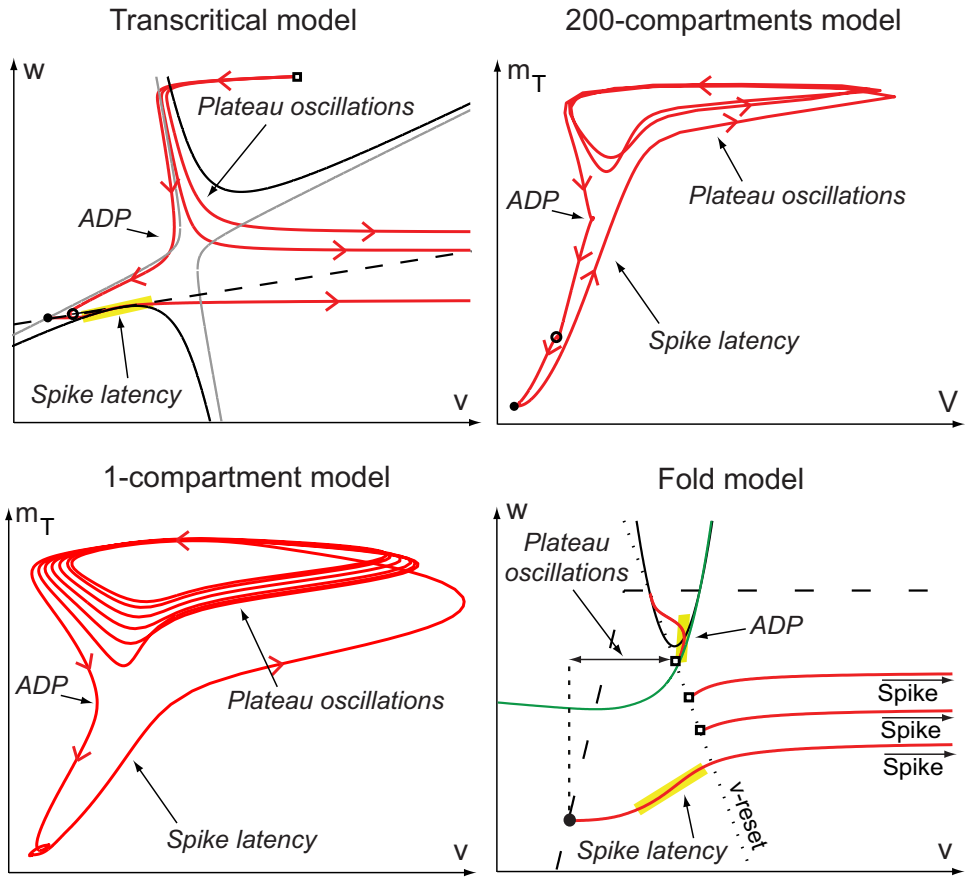

Figure S9.3 – Comparison of the step response and phase-portrait in the transcritical hybrid model, a quantitative one compartment model of TC neuron [83, 124], a 200-compartment model of TC neurons [37] and the fold hybrid model [89] in large calcium conductance mode. In the phase-portrait of the hybrid models, v- and w-nullclines are drawn as full and dashed lines, respectively, and trajectories are drawn as red oriented lines. The black full line represents the v-nullcline at the onset of the stimulation. The gray full line represents the v-nullcline at the end of the burst. The phase-portrait of the conductance based models depicts the trajectory projection on the $V - m_T$ plane, where V and m_T denotes the somatic membrane potential and the activation gating variable of the somatic T-type calcium current, respectively.

Supplementary Figures of Chapter 13

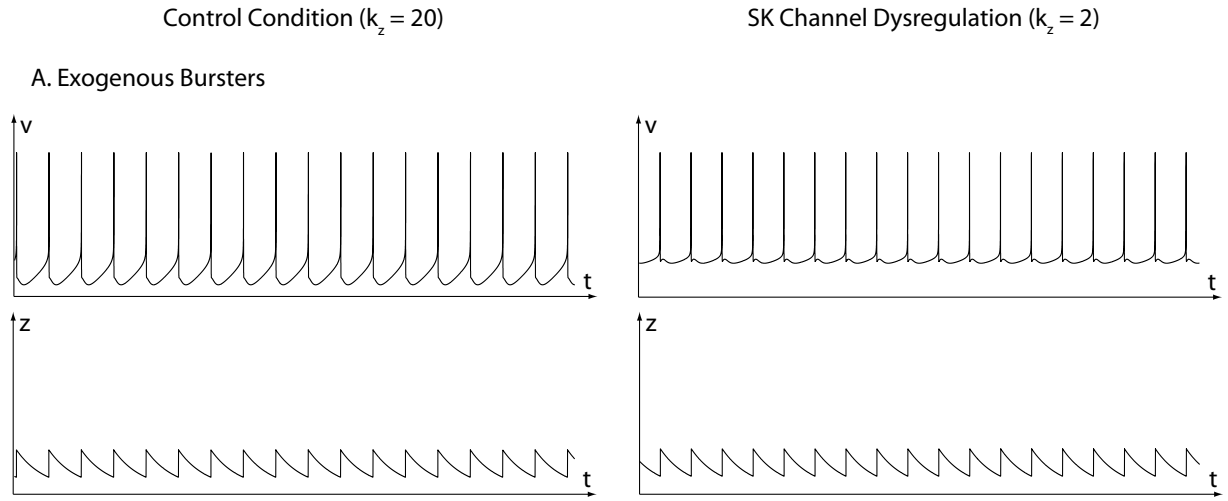

Figure S13.1 – Comparison of the firing patterns of two types of neurons in control condition (left) and during SK channel dysregulation (right). A. blabla. **B.** blabla. Note that a SK channel dysregulation affects calcium homeostasis in both cases, resulting in higher cytoplasmic calcium accumulation.

Bibliography

[1] Abou-Sleiman PM, Muqit MM, Wood NW (2006) Expanding insights of mitochondrial dysfunction in Parkinson's disease. Nat Rev Neurosci. 7:207-19.

[2] Akaike T (1982) Periodic bursting activities of locus coeruleus neurons in the rat. Brain Res. 239:629-33.

[3] Amini B, Clark JW Jr, Canavier CC (1999) Calcium dynamics underlying pacemaker-like and burst firing oscillations in midbrain dopaminergic neurons: a computational study. J Neurophysiol. 82:2249-61.

[4] Aragona BJ, Cleaveland NA, Stuber GD, Day JJ, Carelli RM, Wightman RM (2008) Preferential enhancement of dopamine transmission within the nucleus accumbens shell by cocaine is attributable to a direct increase in phasic dopamine release events. J Neurosci. 28:8821-31.

[5] Arima J, Matsumoto N, Kishimoto K, Akaike N (2001) Spontaneous miniature outward currents in mechanically dissociated rat Meynert neurons. J Physiol. 534:99-107.

[6] Azouz R, Jensen MS, Yaari Y (1996) Ionic basis of spike after-depolarization and burst generation in adult rat hippocampal CA1 pyramidal cells. J Physiol. 49: 211-223.

[7] Barsukova AG, Bourdette D, Forte M (2011) Mitochondrial calcium and its regulation in neurodegeneration induced by oxidative stress. Eur J Neurosci. 34:437-47

[8] Betarbet R, Sherer TB, MacKenzie G, Garcia-Osuna M, Panov AV, Greenamyre JT (2000) Chronic systemic pesticide exposure reproduces features of Parkinsons disease. Nat Neurosci. 3:1301-6.

[9] Beurrier C, Congar P, Bioulac B, Hammond C (1999) Subthalamic nucleus neurons switch from single-spike activity to burst firing mode. J Neurosci. 19: 599-609.

[10] Bezard E, Przedborski S (2011) A tale on animal models of Parkinson's disease. Mov Disord. 26:993-1002.

[11] Bindoff LA, Birch-Machin M, Cartlidge NE, Parker WD Jr, Turnbull DM (1989) Mitochondrial function in Parkinson's disease. Lancet. 2:49.

[12] Bishop MW, Chakraborty S, Matthews GA, Dougalis A, Wood NW, Festenstein R, Ungless MA (2010) Hyperexcitable Substantia Nigra Dopamine Neurons in PINK1- and HtrA2/Omi-Deficient Mice. J Neurophysiol. 104:3009-20.

[13] Blythe SN, Wokosin D, Atherton JF, Bevan MD (2009) Cellular mechanisms underlying burst firing in substantia nigra dopamine neurons. J Neurosci. 29:15531-41.

[14] Bohnen NI, Albin RL (2011) The cholinergic system and Parkinson disease. Behav Brain Res. 221:564-73.

[15] Braak H, Del Tredici K, Rb U, de Vos RA, Jansen Steur EN, Braak E (2002) Staging of brain pathology related to sporadic Parkinson's disease. Neurobiol Aging. 24:197-211.

[16] Braak H, de Vos RA, Bohl J, Del Tredici K (2005) Gastric alpha-synuclein immunoreactive inclusions in Meissner's and Auerbach's plexuses in cases staged for Parkinson's disease-related brain pathology. Neurosci Lett. 396:67-72.

[17] Brazhnik E, Shah F, Tepper JM (2008) GABAergic afferents activate both GABAA and GABAB receptors in mouse substantia nigra dopaminergic neurons in vivo. J. Neurosci., 28:10386-98.

[18] Brown DA, Adams PR (1980) Muscarinic suppression of a novel voltage-sensitive K+ current in a vertebrate neurone. Nature, 283:673-6.

[19] Buchanan KA, Petrovic MM, Chamberlain SE, Marrion NV, Mellor JR (2010) Facilitation of long-term potentiation by muscarinic M(1) receptors is mediated by inhibition of SK channels. Neuron. 68:948-63.

[20] Burns RS, Chiueh CC, Markey SP, Ebert MH, Jacobowitz DM, Kopin IJ (1983) A primate model of parkinsonism-selective destruction of dopaminergic-neurons in the pars compacta of the substantia nigra by n-methyl-4-phenyl-1,2,3,6-tetrahydropyridine. Proc Natl Acad Sci U S A. 80:4546-50.

[21] Byrne JH, Roberts JL (2009) From molecules to networks: an introduction to cellular and molecular neuroscience. Academic Press.

[22] Campbell RE, Gaidamaka G, Han SK, Herbison AE (2009) Dendro-dendritic bundling and shared synapses between gonadotropin-releasing hormone neurons. Proc Natl Acad Sci USA. 106:10835-40.

[23] Canavier CC and Landry RS (2006) An increase in AMPA and a decrease in SK conductance increase burst firing by different mechanisms in a model of a dopamine neuron in vivo. J Neurophysiol. 96:2549-63.

[24] Canavier CC, Oprisan SA, Callaway JC, Ji H, Shepard PD. (2008) Computational model predicts a role for ERG current in repolarizing plateau potentials in dopamine neurons: implications for modulation of neuronal activity. J Neurophysiol. 98:3006-22.

[25] Chan CS, Guzman JN, Ilijic E, Mercer JN, Rick C, Tkatch T, Meredith GE, Surmeier DJ (2007) 'Rejuvenation' protects neurons in mouse models of Parkinson's disease. Nature, 447:1081-6.

[26] Chen S, Yaari Y (2008) Spike Ca2+ influx upmodulates the spike afterdepolarization and bursting via intracellular inhibition of KV7/M channels. J Physiol. 586: 1351-1363.

[27] Chergui K, Suaud-Chagny MM, Gonon F (1994) Nonlinear relationship between impulse flow, dopamine release and dopamine elimination in the rat brain in vivo. Neuroscience, 62:641-5.

[28] Clay R, Paydarfar D, Forger DB (2008) A simple modification of the hodgkin and huxley equations explains type 3 excitability in squid giant axons. J R Soc Interface. 5:1421-8.

[29] Coulon P, Herr D, Kanyshkova T, Meuth P, Budde T, Pape HC (2009) Burst discharges in neurons of the thalamic reticular nucleus are shaped by calcium-induced calcium release. Cell Calcium. 46:333-46.

[30] Crick F (1984) Function of the thalamic reticular complex: the searchlight hypothesis. Proc Natl Acad Sci U S A. 81: 4586-4590.

[31] Crunelli V, Lightowler S, Pollard CE (1989) A T-type Ca2+ current underlies low-threshold Ca2+ potentials in cells of the cat and rat lateral geniculate nucleus. J Physiol. 413: 543-561.

[32] Cudmore RH, Desai NS (2008), Scholarpedia, 3:1363.

[33] D'Angelo E, Nieus T, Maffei A, Armano S, Rossi P, Taglietti V, Fontana A, Naldi G (2001) Theta-frequency bursting and resonance in cerebellar granule cells: experimental evidence and modeling of a slow K+-dependent mechanism. J Neurosci 21: 759-70.

[34] Dawson TM, Ko HS, Dawson VL (2010) Genetic animal models of Parkinson's disease. Neuron. 64:646-61.

[35] Delmas P, Brown DA (2005) Pathways modulating neural KCNQ/M (Kv7) potassium channels. Nat. Rev. Neurosci. 6:850-62.

[36] Destexhe A, Contreras D, Steriade M, Sejnowski TJ, Huguenard JR (1996) In vivo, in vitro, and computational analysis of dendritic calcium currents in thalamic reticular neurons. J Neurosci. 16:169-85.

[37] Destexhe A, Neubig M, Ulrich D, Huguenard J (1998) Dendritic low-threshold calcium currents in thalamic relay cells. J Neurosci. 18: 3574-3588.

[38] Dreyer JK, Herrik KF, Berg RW, Hounsgaard JD (2010) Influence of phasic and tonic dopamine release on receptor activation. J Neurosci. 30:14273-83.

[39] Drion G*, Bonjean M*, Waroux O*, Scuvée-Moreau J, Liégeois JF, Sejnowski J, Sepulchre R, Seutin V (2010) M-type channels selectively control bursting in rat dopaminergic neurons. Eur J Neurosci. 31:827-35.

[40] Drion G, Massotte L, Sepulchre R, Seutin V (2011) How modeling can reconcile apparently discrepant experimental results: The case of pacemaking in dopaminergic neurons. PLoS Comput. Biol. 7, e1002050.

[41] Drion G, Sepulchre R and Seutin V (2012) Mitochondrion- and endoplasmic reticulum-induced SK channel disregulation as a potential origin of the selective neurodegeneration in Parkinson's disease. The Systems Biology of Parkinson's Disease, Genetics and Systems Biology, Springer.

[42] Drion G*, Franci A*, Seutin V and Sepulchre R (2012) A novel phase portrait for neuronal excitability. PLoS One. 7:e41806.

[43] Duda JE (2009) Olfactory system pathology as a model of Lewy neurodegenerative disease. J Neurol Sci. 289:49-54.

[44] Egger V, Stroh O (2009) Calcium buffering in rodent olfactory bulb granule cells and mitral cells. J Physiol. 587:4467-79.

[45] Ermentrout GB (2002) Simulating, analyzing, and animating dynamical systems: a guide to XPPAUT for researchers and students. SIAM Press, Philadelphia, PA, USA.

[46] Ermentrout GB, Terman DH (2010) Mathematical Foundations of Neuroscience. Interdisciplinary Applied Mathematics. Springer.

[47] Fearnley JM, Lees AJ (1991) Ageing and Parkinson's disease: substantia nigra regional selectivity. Brain. 114:2283-301.

[48] Finlayson PG, Marshall KC (1988) Synchronous bursting of locus coeruleus neurons in tissue culture. Neuroscience. 24:217-25.

[49] Fiorillo CD, Williams JT (2000) Cholinergic inhibition of ventral midbrain dopamine neurons. J. Neurosci. 20:7855-60.

[50] FitzHugh R (1961) Impulses and physiological states in theoretical models of nerve membrane. Biophys J. 1:445-66.

[51] Franci A, Drion G, Seutin V, Sepulchre R (2011) A novel phase portrait to understand neuronal excitability. arXiv:1112.2588v1.

[52] Franci A*, Drion G* and Sepulchre R (2012) An organizing center in a planar model of neuronal excitability. SIAM J. Appl. Dyn. Syst., 11:1698-722.

[53] Franci A*, Drion G*, Seutin V and Sepulchre R (2013) A balance equation determines a switch in neuronal excitability. PLoS Comput. Biol. Under Revision.

[54] Friel D (2004) Interplay between ER Ca2+ uptake and release fluxes in neurons and its impact on [Ca2+] dynamics. Biol Res. 37:645-74.

[55] Fuentealba P, Timofeev I, Bazhenov M, Sejnowski TJ, Steriade M (2005) Membrane bistability in thalamic reticular neurons during spindle oscillations. J Neurophysiol. 93: 294-304.

[56] Fujita A, Takeuchi T, Saitoh N, Hanai J, Hata F (2001) Expression of Ca(2+)-activated K(+) channels, SK3, in the interstitial cells of Cajal in the gastrointestinal tract. Am J Physiol Cell Physiol. 281:C1727-33.

[57] Gai Y, Doiron B, Kotak V, Rinzel J (2009) Noise-gated encoding of slow inputs by auditory brain stem neurons with a low-threshold k+ current. J Neurophysiol. 102:3447-60.

[58] Ghazanfar AA, Nicolelis MA (1997) Nonlinear processing of tactile information in the thalamocortical loop. J Neurophysiol. 78: 506-510.

[59] Gibb WRG (1991) Neuropathology of the substantia nigra. Eur Neurol. 31:48-59.

[60] Giessel AJ, Sabatini BL (2010) M1 muscarinic receptors boost synaptic potentials and calcium influx in dendritic spines by inhibiting postsynaptic SK channels. Neuron. 68:936-47.

[61] Goldman MS, Golowasch J, Marder E, Abbott LF (2001) Global structure, robustness, and modulation of neuronal models. J Neurosci. 21:5229-38.

[62] Grace AA and Bunney BS (1984) The control of firing pattern in nigral dopamine neurons: single spike firing. J. Neurosci., 4:2866-76.

[63] Grace AA and Bunney BS (1984) The control of firing pattern in nigral dopamine neurons: burst firing. J. Neurosci., 4:2877-90.

[64] Gray CM, McCormick DA (1996) Chattering cells: superficial pyramidal neurons contributing to the generation of synchronous oscillations in the visual cortex. Science. 274:109-13.

[65] Gronier B, Rasmussen K (1998) Activation of midbrain presumed dopaminergic neurones by muscarinic cholinergic receptors: an in vivo electrophysiological study. Br. J. Pharmacol. 124:455-64.

[66] Guido W, Lu SM, Sherman SM (1992) Relative contributions of burst and tonic responses to the receptive field properties of lateral geniculate neurons in the cat. J Neurophysiol. 68: 2199-2211.

[67] Guido W, Lu SM, Vaughan JW, Godwin DW, Sherman SM (1995) Receiver operating characteristic (ROC) analysis of neurons in the cat's lateral geniculate nucleus during tonic and burst response mode. Vis Neurosci. 12: 723-741.

[68] Guido W, Weyand T (1995) Burst responses in thalamic relay cells of the awake behaving cat. J Neurophysiol. 74: 1782-1786.

[69] Gutman GA, Chandy KG, Adelman JP, Aiyar J, Bayliss DA, Clapham DE, Covarriubias M, Desir GV, Furuichi K, Ganetzky B, Garcia ML, Grissmer S, Jan LY, Karschin A, Kim D, Kuperschmidt S, Kurachi Y, Lazdunski M, Lesage F, Lester HA, McKinnon D, Nichols CG, O'Kelly I, Robbins J, Robertson GA, Rudy B, Sanguinetti M, Seino S, Stuehmer W, Tamkun MM, Vandenberg CA, Wei A, Wulff H, Wymore RS; International Union of Pharmacology (2003) International Union of Pharmacology. XLI. Compendium of voltage-gated ion channels: potassium channels. Pharmacol Rev. 55:583-6.

[70] Guzman JN, Sanchez-Padilla J, Chan CS and Surmeier DJ (2009) Robust pacemaking in substantia nigra dopaminergic neurons. J Neurosci. 29:11011-19.

[71] Guzman JN, Sanchez-Padilla J, Wokosin D, Kondapalli J, Ilijic E, Schumacker PT, Surmeier DJ (2010) Oxidant stress evoked by pacemaking in dopaminergic neurons is attenuated by DJ-1. Nature. 468:676-680.

[72] Hallworth NE, Wilson CJ, Bevan MD (2003) Apamin-sensitive small conductance calcium-activated potassium channels, through their selective coupling to voltage-gated calcium channels, are critical determinants of the precision, pace, and pattern of action potential generation in rat subthalamic nucleus neurons in vitro. J Neurosci. 23:7525-42.

[73] Halnes G, Augustinaite S, Heggelund P, Einevoll GT, Migliore M (2011) A multi-compartment model for interneurons in the dorsal lateral geniculate nucleus. PLoS Comput. Biol. 7:e1002160.

[74] Hammond C, Bergman H, Brown P (2007) Pathological synchronization in Parkinson's disease: networks, models and treatments. Trends Neurosci. 30:357-64.

[75] Hansen HH, Ebbesen C, Mathiesen C, Weikop P, Ronn LC, Waroux, O, Scuvée-Moreau J, Seutin V, Mikkelsen JD (2006) The KCNQ channel opener retigabine inhibits the activity of mesencephalic dopaminergic systems of the rat. J Pharmacol. Exp. Ther. 318:1006-19.

[76] Herrik KF, Christophersen P, Shepard PD (2010) Pharmacological Modulation of the Gating Properties of Small Conductance Ca2+-Activated K+ Channels Alters the Firing Pattern of Dopamine Neurons in vivo. J Neurophysiol. 104:1726-35.

[77] Heyward P, Ennis M, Keller A, Shipley MT (2001) Membrane bistability in olfactory bulb mitral cells. J Neurosci. 21:5311-20.

[78] Hille, B (2001) Ion Channels of Excitable Membranes (Sinauer, Sunderland, MA).

[79] Hirsh M, Pugh C, Shub M (1977) Invariant Manifolds. Lecture Notes in Mathematics. Springer-Verlag, Berlin, Germany.

[80] Hodgkin AL (1948) The local electric changes associated with repetitive action in a non-medullated axon. J. Physiol. 107:165-8.

[81] Hodgkin AL, Huxley AF (1952) A quantitative description of membrane current and its application to conduction and excitation in nerve. J Physiol., London, 177:500-544.

[82] Huguenard JR, Prince DA (1992) A novel T-type current underlies prolonged Ca(2+)-dependent burst firing in GABAergic neurons of rat thalamic reticular nucleus. J Neurosci. 12:3804-17.

[83] Huguenard JR, McCormick DA (1992) Simulation of the currents involved in rhythmic oscillations in thalamic relay neurons. J Neurophysiol. 68: 1373-1383.

[84] Huguenard JR (1999) Neuronal circuitry of thalamocortical epilepsy and mechanisms of antiabsence drug action. Adv Neurol. 79: 991-999.

[85] Huot P, Fox SH, Brotchie JM (2011) The serotonergic system in Parkinson's disease. Prog Neurobiol. 95:163-212.

[86] Ilijic E, Guzman JN, Surmeier DJ (2011) The L-type channel antagonist isradipine is neuroprotective in a mouse model of Parkinson's disease. Neurobiol Dis. 43:364-71.

[87] Iversen SD and Iversen LL (2007) Dopamine : 50 years in perspective. Trends Neurosci., 30:188-93.

[88] Izhikevich EM (2003) A simple model of spiking neurons. IEEE Trans Neural Netw. 14: 1569-1572.

[89] Izhikevich EM (2007) Dynamical Systems in Neuroscience: The Geometry of Excitability and Bursting. MIT Press.

[90] Izhikevich E, Edelman G (2008) Large-scale model of mammalian thalamocortical systems. Proc Natl Acad Sci U S A. 105: 3593-3598.

[91] Izhikevich EM (2010) Hybrid spiking models. Phil. Trans. R. Soc. 368: 5061-5070.

[92] Jahnsen H, Llinas R (1984) Electrophysiological properties of guinea-pig thalamic neurones: an in vitro study. J Physiol. 349: 205-226.

[93] Jahnsen H, Llinas R (1984) Ionic basis for the electro-responsiveness and oscillatory properties of guinea-pig thalamic neurones in vitro. J Physiol. 349: 227-247.

[94] Javitch JA, DAmato RJ, Strittmatter SM, Snyder SH (1985) Parkinsonism-inducing neurotoxin, N-methyl-4-phenyl-1,2,3,6-tetrahydropyridine-uptake of the metabolite N-methyl-4-phenylpyridine by dopamine neurons explains selective toxicity. Proc Natl Acad Sci U S A. 82:2173-77.

[95] Ji H, Shepard PD (2006) SK Ca2+-activated K+ channel ligands alter the firing pattern of dopamine-containing neurons in vivo. Neuroscience. 140:623-33.

[96] Ji H, Hougaard C, Herrik KF, Strøbaek D, Christophersen P, Shepard PD (2009) Tuning the excitability of midbrain dopamine neurons by modulating the Ca2+ sensitivity of SK channels. Eur J Neurosci. 29:1883-95.

[97] Jin X, Costa RM (2010) Start/stop signals emerge in nigrostriatal circuits during sequence learning. Nature. 466:457-62.

[98] Johnson SW, North RA (1992) Two types of neurone in the rat ventral tegmental area and their synaptic inputs. J Physiol. 450:455-68.

[99] Johnson SW, Wu YN (2004) Multiple mechanisms underlie burst firing in rat midbrain dopamine neurons in vitro. Brain Res. 1019:293-6.

[100] Junek S, Kludt E, Wolf F, Schild D (2010) Olfactory coding with patterns of response latencies. Neuron. 67: 872-84.

[101] Keener J, Sneyd J (1998) in Mathematical Physiology, eds Marsden JE, Sirovich L, Wiggins S (Springer, Interdisciplinary Applied Mathematics, Volume 8), pp 188-213.

[102] Khaliq ZM and Bean BP (2010) Pacemaking in dopaminergic ventral tegmental area neurons: depolarizing drive from background and voltage-dependent sodium conductance. J Neurosci. 30:7401-13.

[103] Khler M, Hirschberg B, Bond CT, Kinzie JM, Marrion NV, Maylie J, Adelman JP (1996) Small-conductance, calcium-activated potassium channels from mammalian brain. Science. 273:1689-14.

[104] Kokoz IuM, Krinskii VI (1973) [Analysis of the equations of excitable membranes. II. Method of analysis of the electrophysiological characteristics of a Hodgkin-Huxley membrane from graphs of a 2d-order null-isocline system]. Biofizika. 18: 878-885.

[105] Komendantov AO, Komendantova OG, Johnson SW, Canavier CC (2004) A modeling study suggests complementary roles for GABAA and NMDA receptors and the SK channel in regulating the firing pattern in midbrain dopamine neurons. J Neurophysiol. 91:346-57.

[106] Koyama S, Appel SB (2006) Characterization of M-current in ventral tegmental area dopamine neurons. J. Neurophysiol. 96:535-43.

[107] Krinskii VI, Kokoz IuM (1973) [Analysis of the equations of excitable membranes. I. Reduction of the Hodgkins-Huxley equations to a 2d order system]. Biofizika. 18: 506-511.

[108] Kubota S, Rubin J (2011) NMDA-induced burst firing in a model subthalamic nucleus neuron. J Neurophysiol. 106:527-37.

[109] Kuffler SW, Sejnowski TJ (1983) Peptidergic and muscarinic excitation at amphibian sympathetic synapses. J. Physiol. 341:257-78.

[110] Kuhn AA, Tsui A, Aziz T, Ray N, Brucke C, Kupsch A, Schneider GH, Brown P (2009) Pathological synchronization in the subthalamic nucleus of patients with Parkinson's disease relates to both bradykinesia and rigidity. Exp Neurol. 215:380-7.

[111] Kuznetsov AS, Kopell NJ, Wilson CJ (2006) Transient high-frequency firing in a coupled-oscillator model of the mesencephalic dopaminergic neuron. J Neurophysiol. 95:932-47.

[112] Lee KH, Cho JH, Choi IS, Park HM, Lee MG, Choi BJ, Jang IS (2010) Pregnenolone sul-fate enhances spontaneous glutamate release by inducing presynaptic Ca2+-induced Ca2+ re-lease. Neuroscience. 169:106-16.

[113] Li YX, Bertram R, Rinzel J (1996) Modeling N-methyl-D-aspartate-induced bursting in dopamine neurons. Neuroscience. 71:397-410.

[114] Liu Z, Golowasch J, Marder E, Abbott LF (1998) A model neuron with activity-dependent conductances regulated by multiple calcium sensors. J Neurosci. 18:2309-20.

[115] Liu S, Shipley MT (2008) Multiple conductances cooperatively regulate spontaneous bursting in mouse olfactory bulb external tufted cells. J Neurosci. 28:1625-39.

[116] Livingston CA, Berger AJ (1993) Response of neurons in the dorsal motor nucleus of the vagus to thyrotropin-releasing hormone. Brain Res. 621:97-105.

[117] Magee JC, Johnston D (1995) Synaptic Activation of Voltage-Gated Channels in the Dendrites of Hippocampal Pyramidal Neurons. Science 268:301-4.

[118] Maher BJ and Westbrook GL (2005) SK Channel Regulation of Dendritic Excitability and Dendrodendritic Inhibition in the Olfactory Bulb. J Neurophysiol 94:3743-50.

[119] Maingret F, Coste B, Hao J, Giamarchi A, Allen D, Crest M, Litchfield DW, Adelman JP, Delmas P (2009) Neurotransmitter modulation of small-conductance Ca2+-activated K+ channels by regulaton of Ca2+ gating. Neuron. 59:439-49.

[120] Mann VM, Cooper JM, Krige D, Daniel SE, Schapira AH, Marsden CD (1992) Brain, skeletal muscle and platelet homogenate mitochondrial function in Parkinson's disease. Brain. 115:333-42.

[121] Martinez TN, Greenamyre JT (2011) Toxin Models of Mitochondrial Dysfunction in Parkinson's Disease. Antioxid Redox Signal.

[122] Maylie J, Bond CT, Herson PS, Lee WS, Adelman JP (2004) Small conductance Ca2+-activated K+ channels and calmodulin. J Physiol. 554:255-61.

[123] Maylie J, Adelman JP (2010) Cholinergic signaling through synaptic SK channels: it's a protein kinase but which one? Neuron. 68:809-11.

[124] McCormick DA, Huguenard JR (1992) A model of the electrophysiological properties of thalamocortical relay neurons. J Neurophysiol. 68: 1384-1400.

[125] McCormick DA, Bal T (1997) Sleep and arousal: thalamocortical mechanisms. Annu Rev Neurosci. 20: 185-215.

[126] Mercuri NB, Bonci A, Calabresi P, Stratta F, Stefani A, Bernardi G (1994) Effects of dihydropyridine calcium antagonists on rat midbrain dopaminergic neurones. Br J Pharmacol.,113:831-8.

[127] Messina C, Cotrufo R (1976) Different excitability of type 1 and type 2 alpha-motoneurones: The recruitment curve of h- and m-responses in slow and fast muscles of rabbits. J Neurol Sci. 28:57-63.

[128] Miller AD, Blaha CD (2005) Midbrain muscarinic receptor mechanisms underlying regulation of mesoaccumbens and nigrostriatal dopaminergic transmission in the rat. Eur. J. Neurosci. 21:1837-46.

[129] Mizuno Y, Ohta S, Tanaka M, Takamiya S, Suzuki K, Sato T, Oya H, Ozawa T, Kagawa Y (1989) Deficiencies in complex I subunits of the respiratory chain in Parkinson's disease. Bi-ochem Biophys Res Commun. 163:1450-5.

[130] Molineux ML, Fernandez FR, Mehaey WH, Turner RW (2005) A-Type and T-Type currents interact to produce a novel spike latency-voltage relationship in cerebellar stellate cells. J Neurosci. 25: 10863-10873.

[131] Moore J (1959) Excitation of the squid axon membrane in isosmotic potassium chloride. Nature. 183:265-6.

[132] Morris C, Lecar H (1981) Voltage oscillations in the barnacle giant muscle fiber. Biophys J. 35: 193-213.

[133] Nedergaard S, Flatman JA, Engberg I (1993) Nifedipine- and omega-conotoxin-sensitive Ca2+ conductances in guinea-pig substantia nigra pars compacta neurones. J. Physiol., 466:727-47.

[134] Ngo-Anh TJ, Bloodgood BL, Lin M, Sabatini BL, Maylie J, Adelman, JP (2005) SK channels and NMDA receptors form a Ca2+-mediated feedback loop in dendritic spines. Nat Neurosci. 8:550.

[135] Obeso JA, Rodrguez-Oroz MC, Benitez-Temino B, Blesa FJ, Guridi J, Marin C, Rodriguez M (2008) Functional organization of the basal ganglia: therapeutic implications for Parkinson's disease. Mov Disord. 23 Suppl 3:S548-59.

[136] Obeso JA, Rodriguez-Oroz MC, Goetz CG, Marin C, Kordower JH, Rodriguez M, Hirsch EC, Farrer M, Schapira AH, Halliday G (2010) Missing pieces in the Parkinson's disease puzzle. Nat Med. 16:663-61.

[137] Overton PG, Clark D (1997) Burst firing in midbrain dopaminergic neurons. Brain Res. Rev. 25:312-34.

[138] Parker WD Jr, Boyson SJ, Parks JK (1989) Abnormalities of the electron transport chain in idiopathic Parkinson's disease. Ann Neurol. 26:699-23.

[139] Ping HX and Shepard PD (1996) Apamin-sensitive Ca^{2+}-activated K^+ channels regulate pacemaker activity in nigral dopamine neurons. NeuroReport, 7:809-14.

[140] Plant RE, Kim M (1976) Mathematical description of a bursting pacemaker neuron by a modification of the hodgkin-huxley equations. Biophys. J. 16:227-44.

[141] Politis M, Loane C (2011) Serotonergic dysfunction in Parkinson's disease and its relevance to disability. ScientificWorldJournal. 11:1726-34.

[142] Pospischil M, Piwkowska Z, Bal T, Destexhe A (2011) Comparison of different neuron models to conductance-based post-stimulus time histograms obtained in cortical pyramidal cells using dynamic-clamp in vitro. Biol Cybern. 105: 167-180.

[143] Puopolo M, Raviola E, and Bean BP (2007) Roles of subthreshold calcium current and sodium current in spontaneous firing of mouse midbrain dopamine neurons. J Neurosci. 27:645-56.

[144] Putzier I, Kullmann PHM, Horn JP and Levitan ES (2009) Cav1.3 channel voltage dependence, not Ca(2+) selectivity, drives pacemaker activity and amplifies bursts in nigral dopamine neurons. J Neurosci. 29:15414-19.

[145] Qi Y, Watts AL, Kim JW, Robinson PA (2012) Firing patterns in a conductance-based neuron model: bifurcation, phase diagram, and chaos. Biol Cybern. [Epub ahead of print].

[146] Rekling JC, Feldman JL (1997) Calcium-dependent plateau potentials in rostral ambiguus neurons in the newborn mouse brain stem in vitro. J Neurophysiol. 78: 2483-2492.

[147] Richert M, Nageswaran J, Dutt N, Krichmar J (2011) An efficient simulation environment for modeling large-cale cortical processing. Front Neuroinform. 5: 19.

[148] Rinzel J (1985) Excitation dynamics: insights from simplified membrane models. Fed Proc. 44: 2944-2946.

[149] Rinzel J, Lee Y (1987) Dissection of a model for neuronal parabolic bursting. J Math Biol. 25: 653-75.

[150] Rinzel J, Ermentrout GB (1989) Analysis of neural excitability and oscillations, 135-169. MIT Press, Cambridge, MA, USA.

[151] Rouchet N, Waroux O, Lamy C, Massotte L, Scuvée-Moreau J, Liégeois JF, Seutin V (2008) SK channel blockade promotes burst firing in dorsal raphe serotonergic neurons. Eur J Neurosci. 28:1108-15.

[152] Sah P, McLachlan EM (1992) Potassium currents contributing to action potential repolarization and the afterhyperpolarization in rat vagal motoneurons. J Neurophysiol. 68:1834-41.

[153] Salvador JM, Inesi G, Rigaud JL, Mata AM (1998) Ca^{2+} transport by reconstituted synaptosomal AT-Pase is associated with H^+ countertransport and net charge displacement. J Biol Chem. 273:18230-4

[154] Sarpal D, Koenig JI, Adelman JP, Brady D, Prendeville LC, Shepard PD (2004) Regional distribution of SK3 mRNA-containing neurons in the adult and adolescent rat ventral mid-brain and their relationship to dopamine-containing cells. Synapse. 53:104-13.

[155] Schapira AH, Cooper JM, Dexter D, Jenner P, Clark JB, Marsden CD (1989) Mitochondrial complex I deficiency in Parkinsons disease. Lancet. 1:1267.

[156] Schapira AH, Mann VM, Cooper JM, Dexter D, Daniel SE, Jenner P, Clark JB, Marsden CD (1990) Anatomic and disease specificity of NADH CoQ1 reductase (complex I) deficiency in Parkinson's disease. J Neurochem. 55:2142-5.

[157] Schapira AH (2008) Mitochondria in the aetiology and pathogenesis of Parkinsons disease. Lancet Neurol 7:97-109.

[158] Schultz W (2007) Behavioral dopamine signals. Trends Neurosci. 30:203-10.

[159] Schumacher MA, Rivard AF, Bchinger HP, Adelman JP (2001) Structure of the gating domain of a Ca2+-activated K+ channel complexed with Ca2+/calmodulin. Nature. 410:1120-4.

[160] Scuvée-Moreau J, Liégeois JF, Massotte L, Seutin V (2002) Methyl-laudanosine: A New Pharmacological Tool to Investigate the Function of Small-Conductance Ca(2+)-Activated K(+) Channels. J Pharmacol Exp Ther. 302:1176-83.

[161] Scuvée-Moreau J, Boland A, Graulich A, Van Overmeire L, D'hoedt D, Graulich-Lorge F, Thomas E, Abras A, Stocker M, Liégeois JF, Seutin V (2004) Electrophysiological characterization of the SK channel blockers methyl-laudanosine and methyl-noscapine in cell lines and rat brain slices. Br J Pharmacol. 143:753-64.

[162] Sessley S, Butera RJ (2002) Evidence for type i excitability in molluscan neurons. In Engineering in Medicine and Biology, 2002. 24th Annual Conference and the Annual Fall Meeting of the Biomedical Engineering Society, EMBS/BMES Conference, 2002. Proceedings of the Second Joint, volume 3, pages 1966-67.

[163] Seutin V, Scuve-Moreau J, Giesbers I, Massotte L, Dresse A (1990) Effect of BHT 920 on monoaminergic neurons of the rat brain: an electrophysiological in vivo and in vitro study. Naunyn Schmiedebergs Arch Pharmacol. 342:502-7.

[164] Seutin V, Johnson SW, North RA (1993) Apamin increases NMDA-induced burst-firing of rat mesencephalic dopamine neurons. Brain Res. 630:341-4.

[165] Seutin V, Engel D (2010) Differences in Na^+ conductance density and Na^+ channel functional properties between dopamine and GABA neurons of the rat substantia nigra. J Neurophysiol. 103:3099-114.

[166] Seydel R (1994) Practical bifurcation and stability analysis, volume 5 of Interdisciplinary Applied Mathematics. Springer-Verlag, New York, third edition.

[167] Shepard PD, Bunney BS (1988) Effect of apamin on the discharge properties of putative dopamine-containing neurons in vitro. Brain Res. 463:380-4.

[168] Shepard PD, Bunney BS (1991) Repetitive firing properties of putative dopamine-containing neurons in vitro: regulation by an apamin-sensitive Ca2+-activated K+ conductance. Exp. Brain Res. 86:141-50.

[169] Shepard PD, Stump D (1999) Nifedipine blocks apamin-induced bursting activity in nigral dopamine-containing neurons. Brain Res. 817:104-9.

[170] Sherman SM, Guillery RW (1996) The functional organization of thalamocortical relays. J. Neurophysiol. 76: 1367-1395.

[171] Sherman SM (2001) Tonic and burst firing: dual modes of thalamocortical relay. Trends Neurosci. 24: 122-126.

[172] Shin HS (2006) T-type Ca2+ channels and absence epilepsy. Cell Calcium. 40: 191-196.

[173] Sotty F, Damgaard T, Montezinho LP, Mork A, Olsen CK, Bundgaard C, Husum H (2009) Antipsychotic-like effect of retigabine [N-(2-Amino-4-(fluorobenzylamino)-phenyl)carbamic acid ester], a KCNQ potassium channel opener, via modulation of mesolimbic dopaminergic neurotransmission. J. Pharmacol. Exp. Ther. 328:951-62.

[174] Steigerwald F, Ptter M, Herzog J, Pinsker M, Kopper F, Mehdorn H, Deuschl G, Volkmann J (2008) Neuronal activity of the human subthalamic nucleus in the parkinsonian and nonpar-kinsonian state. J Neurophysiol. 100:2515-24.

[175] Steriade M, McCormick DA, Sejnowski TJ (1993) Thalamocortical oscillations in the sleeping and aroused brain. Science. 262: 679-685.

[176] Steriade M (2003) The corticothalamic system in sleep. Front Biosci. 8: 878-899.

[177] Sterky FH, Lee S, Wibom R, Olson L, Larsson NG (2011) Impaired mitochondrial transport and Parkin-independent degeneration of respiratory chain-deficient dopamine neurons in vivo. Proc Natl Acad Sci U S A. 108:12937-42.

[178] Stocker M (2004) Ca(2+)-activated K+ channels: molecular determinants and function of the SK family. Nat Rev Neurosci. 5:758-68.

[179] Tateno T, Harsch A, Robinson HPC (2004) Threshold firing frequency-current relationships of neurons in rat somatosensory cortex: type 1 and type 2 dynamics. J Neurophysiol. 92:2283-94.

[180] Tatulian L, Delmas P, Abogadie FC, Brown DA (2001) Activation of expressed KCNQ potassium currents and native neuronal M-type potassium currents by the anti-convulsant drug retigabine. J. Neurosci., 21:5535-45.

[181] Tepper JM, Lee CR (2007) GABAergic control of substantia nigra dopaminergic neurons. Prog. Brain Res. 160:189-208.

[182] Touboul J, Brette R (2009) Spiking Dynamics of Bidimensional Integrate-and-Fire Neurons. SIAM J. Appl. Dyn. Syst. 8: 1462-1506.

[183] Traub RD, Wong RK, Miles R, Michelson H (1991) A model of a ca3 hippocampal pyramidal neuron incorporating voltage-clamp data on intrinsic conductances. J Neurophysiol. 66:635-50.

[184] Turrigiano G (2011) Too many cooks? Intrinsic and synaptic homeostatic mechanisms in cortical circuit refinement. Annu Rev Neurosci. 34:89-103.

[185] Vandecasteele M, Glowinski J, Venance L (2005) Electrical synapses between dopaminergic neurons of the substantia nigra pars compacta. J Neurosci. 25:291-8.

[186] Vandecasteele M, Glowinski J, Deniau JM, Venance L (2008) Chemical transmission between dopaminergic neuron pairs. Proc Natl Acad Sci U S A. 105:4904-9.

[187] Vogalis F, Storm JF, Lancaster B (2003) SK channels and the varieties of slow after-hyperpolarizations in neurons. Eur J Neurosci. 18:3155-66.

[188] Wang HS, Pan Z, Shi W, Brown BS, Wymore RS, Cohen IS, Dixon JE, McKinnon D (1998) KCNQ2 and KCNQ3 potassium channel subunits: molecular correlates of the M-channel. Science, 282:1890-3.

[189] Wang XJ, Rinzel J, Rogawski MA (1991) A model of the T-type calcium current and the low-threshold spike in thalamic neurons. J Neurophysiol. 66: 839-850.

[190] Wang ZY, Han YF, Huang X, Zhao P, Lu HL, Kim YC, Xu WX (2010) Pacemaking activity is regulated by membrane stretch via the CICR pathway in cultured interstitial cells of Cajal from murine intestine. J Biomech. 43:2214-20.

[191] Waroux O, Massotte L, Alleva L, Graulich A, Thomas E, Liégeois JF, Scuvée-Moreau J, and Seutin V (2005) SK channel control the firing pattern of midbrain dopaminergic neurons in vivo. Eur J Neurosci. 22:3111-21.

[192] Wechselberger M (2007) Canards. Scholarpedia, 2:1356.

[193] Wichmann T, Dostrovsky JO (2011) Pathological basal ganglia activity in movement disorders. Neuroscience. 198:232-44.

[194] Williams SR, Toth TI, Turner JP, Hughes SW, Crunelli V (1997) The 'window' component of the low threshold Ca2+ current produces input signal amplification and bistability in cat and rat thalamocortical neurones. J Physiol. 505:689-705.

[195] Wilson CJ, Groves PM (1981) Spontaneous firing patterns of identified spiny neurons in the rat neostriatum. Brain Res. 220:67-80.

[196] Wilson CJ, Callaway JC (2000) Coupled oscillator model of the dopaminergic neuron of the substantia nigra. J Neurophysiol. 83:3084-100.

[197] Wilson CJ (2008) Up and down states. Scholarpedia journal. 3:1410.

[198] Wilson HR (1999) Simplified dynamics of human and mammalian neocortical neurons. J Theor Biol 200:375-88.

[199] Wilson HR (1999) Spikes, decisions, and actions. Oxford University Press, Oxford

[200] Wolfart J, Neuhoff H, Franz O, Roeper J (2001) Differential expression of the small-conductance, calcium-activated potassium channel SK3 is critical for pacemaker control in dopaminergic midbrain neurons. J Neurosci. 21:3443-56.

[201] Xu W, Lipscombe D (2001) Neuronal Ca(V)1.3alpha(1) L-type channels activate at relatively hyperpolarized membrane potentials and are incompletely inhibited by dihydropyridines. J Neurosci. 21:5944-51.

[202] Yanovsky Y, Zhang W, Misgeld U (2005) Two pathways for the activation of small-conductance potassium channels in neurons of substantia nigra pars reticulata. Neuroscience. 136:1027-36.

[203] Zaman T, Lee K, Park C, Paydar A, Choi JH, Cheong E, Lee CJ, Shin HS (2011) Cav2.3 channels are critical for oscillatory burst discharges in the reticular thalamus and absence epilepsy. Neuron. 70: 95-108.

[204] Zhan XJ, Cox CL, Rinzel J, Sherman SM (1999) Current clamp and modeling studies of low-threshold calcium spikes in cells of the cat's lateral geniculate nucleus. J Neurophysiol. 81: 2360-2373.

[205] Zhou Q, Godwin DW, O'Malley DM, Adams PR (1997) Visualization of calcium influx through channels that shape the burst and tonic firing modes of thalamic relay cells. J Neurophysiol. 77: 2816-2825.

[206] Zweifel LS, Parker JG, Lobb CJ, Rainwater A, Wall VZ, Fadok JP, Darvas M, Kim MJ, Mizumori SJ, Paladini CA, Phillips PE, Palmiter RD (2009) Disruption of NMDAR-dependent burst firing by dopamine neurons provides selective assessment of phasic dopamine-dependent behavior. Proc Natl Acad Sci U S A. 106:7281-8.